When estimating exposure to electric fields, the neck is a critical area, because current induced in the head flows through the neck into the trunk and the cross-section area in the neck is small compared with the trunk. Furthermore, the spinal cord as a part of the human central nervous system makes the neck an interesting area.

The Laboratory of Electrical Engineering and Health (LEEH) at Tampere University of Technology (TUT) has made several electric field measurements at Finnish 400 kV substations. At 75 % of the measured substations the action value 10 kV/m was exceeded already at the ground level. Higher values can be expected in maintenance situations, although live-line work tasks are not carried out in 400 kV level. Therefore further study of induced current densities was seen as necessary.

A study of induced current densities was done by using special measuring equipment which consists of a helmet coated with copper and having a transparent but conductive face shield, two commercial current recording ammeters, a commercial medical electrode and leads. The current induced in the helmet and shield was conducted away with a lead connected to the helmet. An ammeter was connected to the lead and the other end of the lead was connected to a medical electrode in test person's wrist. The test person wore insulated shoes and gloves and the medical electrode in the wrist was earthed with another insulated lead going along the body of the test person. Also the grounding lead had a recording ammeter. Hence, both the induced current in the helmet with face shield and in the whole body current could be measured. A schematic picture of the measuring arrangement is shown in Fig. 1.

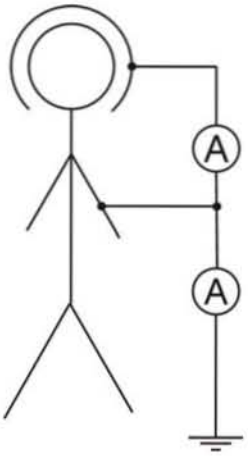


Fig. 1 Schematic picture of the measuring arrangement [2]

The current induced in the helmet and shield is called helmet current I_{helmet}. Because the helmet is slightly larger than head, current induced in the helmet is larger than the induced current in the head in normal conditions. This error was compensated for by multiplying the helmet current by empirically defined correction coefficient *k*, which is 0.819.

LEEH made induced current measurements at 7 different 400 kV air-insulated substations. Altogether 125 measurements were made in 12 different work tasks. The tasks consisted of normal walking in the substation, climbing in the maintenance and inspection platforms as well as maintenance work from ladders or from persons being lifted. The largest value for induced helmet current was 105.8 µA. This current causes current density 6.81 mA/m^2 in the neck area when the neck cross-sectional area is assumed to be a circle with circumference 40 cm (typical collar size for men is 40 cm).

Current density 6.81 mA/m^2 gives an obvious margin to the limit value 10 mA/m^2. However, individual variations in collar size may be rather considerable. Consequently, in order to get further analysis about 50 Hz currents and current densities in different tissues in the neck and especially in the central nervous system LEEH developed a model based on the cross-section of the neck.

2. Objectives and methods

2.1 Aim of the Study

The main aim of this study was to estimate with a developed model current densities in different tissues, especially in the spinal cord in the neck cross-sectional area. The purpose was to find current densities at 35 cm, 40 cm and 50 cm neck circumferences. Another aim of the study was to find out current percentages of induced head current in different tissues.

2.2 Description of the Model

The model is based on the anatomical picture of the cross-sectional area of neck. The anatomical picture was taken from source [3]. Each tissue in the anatomical picture was modeled by using circles, rings and half-rings as modeling shapes so that the shape fitted the anatomical picture of tissue as well as possible. The neck was also assumed to be a circular shape. A cross-sectional picture of the model is presented in Fig.2.

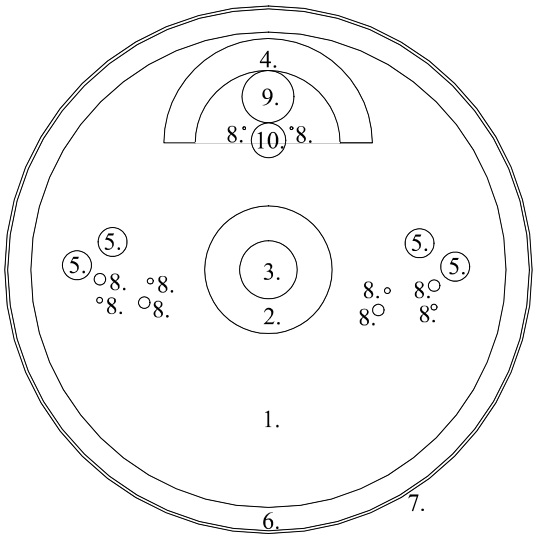


Fig. 2 Cross-sectional picture of the model

Tissue 5 includes arteries and veins, which are located on both sides of the model. Tissue 8 consists of five different nerves: spinal nerve, vagus nerve, phrenic nerve, sympathetic trunk and recurrent laryngeal nerve.

Windpipe (number 10) is assumed air with conductivity of 0 S/m. Muscle (number 1.) is a circle area, where tissues 2, 3, 4, 5, 8, 9, 10 create holes in.

Dimensions of the model are scaled when circumference of neck (collar size i.e. circumference of circle 7.) is changed. Dimensions of the tissues are presented in Table 1, when the diameter of the model is assumed *d*.

Table 1 Dimensions of the model, when the largest diameter is assumed as *d*.

Tissue	Dimensions	
1. Muscle	0.901*d*	
2. Bone trabecular	0.242*d*	
3. Spinal cord	0.110*d*	
4. Thyroid gland	0.396*d*	0.275*d*
5. Blood	0.055*d*	
6. Fat layer	0.989*d*	
7. Skin	*d*	
8. Nerves	constants	
9. Gullet	0.066*d*	
10. Windpipe	0.099*d*	

Nerves are the only tissue in model, which have constant dimensions at all collar sizes. Diameters are for spinal and vagus nerves 0.20 cm, phrenic nerve and sympathetic trunk 0.10 cm and recurrent laryngeal nerve 0.05 cm.

Each tissue has its own conductivity value. Tissues with conductivity values are presented in Table 2.

Table 2. Tissues used in the model and their conductivities at 50 Hz. [4], [5]

Tissue	Conductivity (S/m)
1. Muscle	0.3500
2. Bone trabecular	0.0700
3. Spinal cord	0.0300
4. Thyroid gland	0.5200
5. Blood	0.7000
6. Fat layer	0.0400
7. Skin	0.1000
8. Nerves	0.0274
9. Gullet	0.5200
10. Windpipe (air)	0

2.3 Induced Currents and Current Densities

All the tissues in the model are connected in parallel. In a resistive model the conductance value G_i for the tissue i can be calculated by using equation (1), when conductivity value σ_i and total area A_i of the tissue i are known. Length of the neck is l (constant).

$$G_i = \sigma_i \frac{A_i}{l}, \text{ where } i = 1\ldots9 \tag{1}$$

By using current distribution law in parallel connected circuit, currents I_i in tissues can be calculated by using equation (2).

$$I_i = k \cdot I_{helmet} \frac{G_i}{\sum_{i=1}^{9} G_i}, \text{ where } i = 1...9 \tag{2}$$

Current percentages of head current p_i in tissue i can be calculated by using equations (1) and (2). Hence, we get final equation (3) for current percentages of head current.

$$p_i = \frac{\sigma_i A_i}{\sum_{i=1}^{9} \sigma_i A_i} \cdot 100\%, \text{ where } i = 1\ldots9 \quad (3)$$

Current densities J_i in tissue i can be calculated by using equation (4).

$$J_i = \frac{I_i}{A_i} = k \cdot I_{helmet} \frac{\sigma_i}{\sum_{i=1}^{9} \sigma_i A_i} \quad (4)$$

3. Results

The model gives the current densities in various tissues in the neck area. Results were calculated with 35 cm, 40 cm and 50 cm collar sizes and maximum measured helmet current 105.8 µA by using equation (4). This helmet current corresponds to working in conditions where the local electrical field strength is highly non-uniform and clearly exceeds the action value limit. Induced current densities in each tissue are presented in Table 3. Average current densities in cross-sectional area of the neck are also presented.

The largest current densities in the neck area occur in blood (arteries and veins), thyroid gland, gullet and muscle. Current densities in bone, spinal cord, fat layer, skin and nerves stay below or near to 3 mA/m^2 even at 35 cm collar size.

Spinal cord is critical part in exposure because it is a part of the human central nervous system. According to the results current densities in central nervous system seem to stay below 1 mA/m^2 even at 35 cm collar size.

Table 3. Calculated current densities (mA/m^2) in different tissues at collar size 35 cm, 40 cm and 50 cm.

Tissue	**Collar size**		
	35 cm	**40 cm**	**50 cm**
1. Muscle	10.95	8.38	5.36
2. Bone trabecular	2.19	1.68	1.07
3. Spinal cord	0.94	0.72	0.46
4. Thyroid gland	16.27	12.45	7.97
5. Blood	21.90	16.76	10.72
6. Fat layer	1.25	0.96	0.61
7. Skin	3.13	2.39	1.53
8. Nerves	0.86	0.66	0.42
9. Gullet	16.27	12.45	7.97
Average current density in neck area	8.89	6.81	4.36

Current percentages in tissues were calculated by using equation (3). Results are presented in Table 4 at 40 cm collar size. Current distribution in tissues varies a bit depending on collar size. This results from nerves, which are not scaled as other tissues. However, the maximum variation is 0.1 % when varying collar size between 35 cm...50 cm.

Table 4. Current percentages in different tissues at collar size 40 cm.

Tissue	Percent of head current (p_i)
1. Muscle	84.43
2. Bone trabecular	1.14
3. Spinal cord	0.13
4. Thyroid gland	7.41
5. Blood	2.97
6. Fat layer	2.34
7. Skin	0.77
8. Nerves	0.01
9. Gullet	0.80

According to results most of induced current flows through muscle. This is due to its conductivity and a large area in cross-sectional area.

4. Discussion

The model gives a more specific estimation about current distribution in the neck area. According to results current densities in the central nervous system stay clearly under limit value 10 mA/m^2 even if the collar size is small (35 cm). Hence, it seems that substation workers in practical outdoor work situations in 400 kV substations are not exposed to current densities that exceed the limit value of the directive 2004/40/EC.

According to the model the collar size for neck should be 16.5 cm in order to exceed the limit value. Such a narrow neck circumference is extremely rare, if not undiscovered in the working age population.

There are some simplifications in the model that cause errors in calculations. Modeling shapes differ from real tissue shapes and so they do not fit into tissues perfectly. This difference relates also to the circumference of the neck cross-sectional area, which is not exactly circular in the anatomical picture. Another principal difference from reality in the model is that cross-sectional area of neck is assumed the same in every position of neck length *l*. In reality the proportions of tissues varies depending on the position of cross-sectional area on neck.

One limitation of the model is that it is purely resistive and it does not take account mutual inductances, which occur between different parallel-connected tissues. However, impedances of biological material are mostly resistive below 100 Hz and contribution on capacitive component is of the order of 10 % in most cases [5]. Hence, the error caused by this limitation does not seem to be large.

When comparing current densities to a study by Dimbylow, P. [4], we can notice that current densities in the spinal cord are larger than in our study. Our neck model is suited to a ballpark estimation. A three-dimensional model based on for example MRI scan gives us a more accurate estimation.

For further analysis of induced current densities it may be necessary to develop cross-sectional practical models also for other areas in the human body. Such areas could for example be the chest or stomach, because the spinal cord as a part of central nervous system is part of both cross-sectional areas.

References

[1] 2004/40/EC, 2004. Directive on the minimum health and safety requirements regarding the exposure of workers to the risk arising from physical agents (electromagnetic fields). The European parliament and the council. Official journal of the European Union, 159. 26 p.

[2] Långsjö, T., Latva-Teikari, J., et al. Occupational exposure to 50 Hz electric fields at substation. 16th World Congress on Ergonomics. Maastricht, Netherlands. 10. – 14.6.2006.

[3] Frank H. Netter, M.D. Atlas of Human Anatomy. Second Edition. East Hanover (N.J.): Novartis, 1997

[4] Dimbylow, P. Development of the female voxel phantom, NAOMI, and its application to calculations of induced current densities and electric fields from applied low frequency magnetic and electric fields. Physics in Medicine and Biology. 23 February 2005.

[5] Italian National Research Council, Institute for Applied Physics. Calculation of the Dielectric Properties of Body Tissues in the frequency range 10 Hz - 100 GHz. Available from: http://niremf.ifac.cnr.it/tissprop/ Referred 14.06.2006.

THERMODYNAMIC LAW AND THE PROBLEM OF STANDARDIZATION OF RADIOFREQUENCY ELECTROMAGNETIC RADIATION

YULIA CHUKOVA

Russian People's Academy of Science, Krasnopresnenskiy Ecological Fund. Moscow

Malaya Gruzinskaya St. 6 – 42, 123242, Moscow, Russian Federation

e-mail: y.Chukova@mtu-net.ru

Abstract

The problem of radiofrequency radiation standardization is the most important problem of up-to-date-ness because all frequencies of radiofrequency radiation are used in different technical and domestic devices. The sharpness of this problem was elucidated half a century ago, when the USSR standard for microwave radiation was 1000-fold lower than the USA standard. In the USA and in many other countries, a power density of 10 mW/cm^2 has been adopted as a standard safety level, but in the USSR a value of 10 $\mu W/cm^2$ was adopted.

This problem exists both for microwave radiation and other radiofrequencies at the present time.

The thermodynamic theory of systems under electromagnetic radiation gives the general law of electromagnetic energy conversion into energy of chemical bonds (the Helmholtz free energy). This law gives the dependence of bioeffects on absorbed power. The thermodynamic law shows that there are two regions of bioeffects of radiofrequency radiation: thermal effects and isothermal ones (endergonic + exergonic effects). The USA standard is good only for thermal effects, but the USSR standard is valid for thermal and isothermal effects.

It is discussed a role of a good social decision for conservation of public health.

Introduction. The general principle of hygienic standardization

The general principle of hygienic standardization is simple. Hygienic research begins with the most great influences. In these conditions, there is a hundred-per-cent adverse effect (death, illness etc). Then the influence decreases and the adverse effect decreases too. At last a hygienist does not see an adverse effect. This point is called the no-observed-adverse-effect level (NOAEL) or no-observed-effect dose. This point is the final one of natural research. The following decision (standard) is the social act because all levels and doses below the NOAEL or no-observed-effect dose are determined as safe levels or doses (Fig.1). This statement was the general paradigm of safety in 20th century. This paradigm prevails today.

Fig.1

The principle of radiofrequency radiation standardisation in the 20th century

During the second part of the 20th century, there was considerable development and increase in the number of devices that emit nonionizing radiofrequency radiation. For example, microwaves (MW) were used in all sectors of our society for military, industrial, telecommunications, medical and consumer applications. This is the frequency range receiving the most attention in terms of biological interaction. This is due to the widespread use of high MW energy densities in highly populated areas. High energy densities of MW radiation cause heating of the human body. This is a dangerous effect and the principle of 20th century standardization for radiofrequency radiation was simple and common [1]. It has needed to determine the no-observed- heating-effect level. Safe conditions must be lower than the no-observed-heating-effect level. This statement was the general paradigm of safety in the 20th century for radiofrequency radiation and prevails today. In the USA, a power density of 10 mW/cm^2 has been adopted as the standard safety level [2]. Standards in different countries are different because shifts from the no-observed-heating-effect level are not equal.

For a long time there was only one exception to this rule: it was the Soviet standard on adverse microwave radiation effects. This standard was 1000-fold lower than the USA standard. Such a huge difference in the representation of an adverse effect was a result of the great experimental programme in the USSR in the middle of the 20th century.

In the USSR, standardization for microwave radiation was begun in 1956. Soviet hygienists studied at first the thermal effects of high-intensity radiation and then they took an interest in low-intensity radiofrequency radiation. They revealed that changes resulting from chronic or repeated exposure to low intensities of radiation are specific, initially reversible and affect the nervous system, myocardium, kidneys etc. About 70 photos of those changes are in an English book [3]. The reversible changes disappear after some time, if the exposure is ended. In other cases, the changes are permanent. The results of these researches were published both in Russian and in English [3, 4].

In the end, the Doctor-hygienist Z.V. Gordon (head of the laboratory of radiofrequency electromagnetic waves of the Institute of Labour Hygiene and Occupational Diseases of the Academy of Medical Science of the USSR) proposed for the Soviet microwave hygienic standard a power density of 10 $\mu W/cm^2$. Her suggestion

was supported by Admiral A.I.Berg , Deputy Defence Minister for the USSR . So, in the USSR the value of 10 $\mu W/cm^2$ was adopted as the safety standard for microwave radiation. This led to the well-known difference of a factor of 1000 between the safety standards in the USSR and the USA. Thus, the Soviet standard was the most stringent standard in the world.

The Soviet standard has taken into account adverse non-thermal effects. It means that in the second part of the 20^{th} century in Russia, the other independent paradigm of hygienic standardization of radiofrequency radiation has been adopted. This confusing picture was indeed the beginning of a hygienic discussion which has been long and unsuccessful. The situation can be changed by the thermodynamic theory of systems under electromagnetic radiation.

Thermodynamics is free from the terms “adverse effect”, “hazard” etc. These terms are known in medicine and biology. Thermodynamics deals with thermal and isothermal processes, the endergonic and exergonic ones, but every process can be useful or adverse from a view of life and from a human standpoint. The method of thermodynamics of irreversible processes in systems under electromagnetic radiation yielded interesting results for up-to-date hygiene and physiology. One result is related to the radiofrequency safety problem.

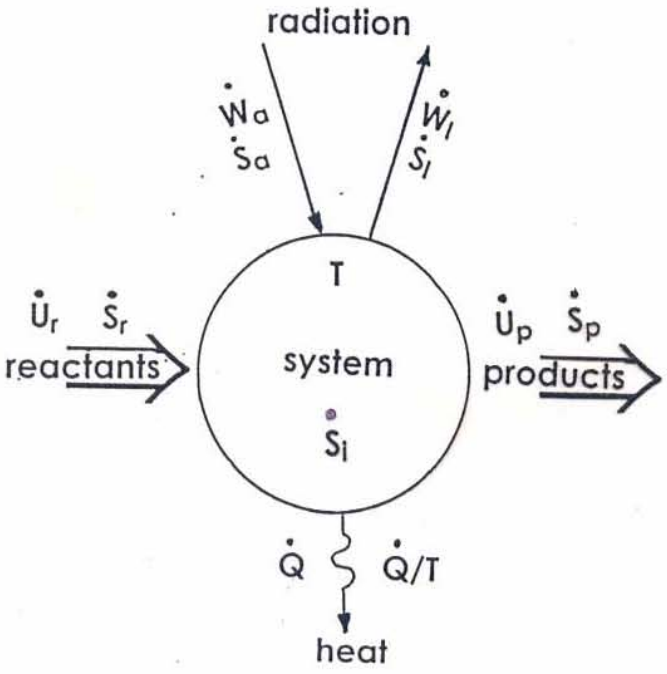
Resume of advances in the nonequilibrium thermodynamics of isothermal processes in systems under electromagnetic radiation

Thermodynamics deals with the energy of processes and the efficiency of energy conversion. It began with a study of technical systems under electromagnetic radiation (luminescent lamps and solar cells). The considered system is given in Fig.2, with the definitions. In this system, there are three kinds of energy conversion: radiation into radiation, radiation into Helmholtz free energy and radiation into heat.

The basic theoretical work was done by L. Landau in 1946 [5]. At that time, he was not yet a Nobel prize winner. Landau has estimated the first way – luminescence. The result for luminescence, which has been obtained by L. Landau, has struck scientists very much. Only some scientists can believe that optical cooling is possible. Optical heating is habituated for us. But during the 1970s the thermodynamically predicted result was obtained in many systems under laser light; and in 1997 the Royal Swedish Academy of Sciences decided to award the Nobel Prize in Physics jointly to Steven Chu (USA), Claude Cohen-Tannoudji (France) and William D. Phillips (USA) for the development of methods of cooling atoms with laser light.

It is foreseeable that in the future a device will be designed which combines the characteristics of a radiation-source and a refrigerator. Thermodynamics does not forbid a such device.

The second way is interesting for solar sells and bioeffects of electromagnetic radiation. For the second way of energy conversion, thermodynamics did not give any wonderful result [6], but the solar cell presented a possibility of direct numerical verification of the thermodynamic theory through a correlation with experimental data. This comparison became possible because theoretical physicists have gone from the thermodynamic limit efficiency estimation to the real efficiency calculation for processes with losses. The numerical correlation of experimental data with the theory was not only satisfactory, but the fit of theory and experiment was also quite good. Furthermore, the thermodynamic method may work even for living systems. It allowed understanding and explanation of many experimental results in living systems, which had not previously been exhaustively explained [7,8].



Simbols and Notations:

T - temperature

• time derivative sign

Energy	Corresponding entropy flux
U_r - internal energy of reactants	$\dot{S}_r$
U_p - internal energy of products	$\dot{S}_p$
$\dot{W}_a$ - absobed power	$\dot{S}_a$
$\dot{W}_l$ - power of luminescence	$\dot{S}_l$
$\dot{Q}$ - thermal flux	$\dot{Q}/T$

$\dot{S}_i$ - entropy generation rate in system

F - Helmholtz free energy $F = U - TS$ (1)

η - real efficiency $\eta = (F_p - F_r)/W_a = \Delta F/W_a$ (2)

$\Delta F > 0$ endoergonic process
$\Delta F < 0$ exoergonic process

FigFFFig.2

For bioeffects of electromagnetic radiation, there is a need to examine conversion of energy of electromagnetic radiation into energy of chemical bonds, i.e. into Helmholtz free energy. The efficiency of this conversion is given by formula (2). On the basis of the first and second equations of thermodynamics, for the steady state of a system, the efficiency η of MM radiation conversion at constant temperature is given by:

$$\eta = 1 - T\,(\dot{S}_a + \dot{S}_i)/\dot{W}_a \qquad (3)$$

From formula (3) it is obvious that the efficiency η is determined by two entropy terms. The first entropy term $\dot{S}_a$ (entropy flux of absorbed power) is dictated by the absorbed power characteristics and is defined by formula (4):

$$\dot{S}_a = 2\pi k c^{-2} \int \nu^2 (1 + \ln\rho)\, d\nu \qquad (4)$$

where c is the velocity of light, k is the Boltzmann constant, ν is a frequency and

$$\rho = c^2 E_\nu / 2\pi h \nu^3 \qquad (5)$$

E_ν is the spectral density of absorbed power $\dot{W}_a$

$$\dot{W}_a = \int E_\nu \, d\nu \qquad (6)$$

The second entropy term $\dot{S}_i$ (entropy generation rate) is determined as

$$\dot{S}_i = \alpha \dot{W}_a + \beta \dot{W}_a^{\,n} \qquad (7)$$

where α, β and $n \neq 1$ are constants connected with the system characteristics.

According to formulas (3 – 7), the dependence of efficiency on absorbed power $\dot{W}_a$ (or spectral density of absorbed power E_ν) is given by the left-hand curve of Fig.3

Fig.3 demonstrates two simple and important results:

1) A system at constant temperature can show three types of behaviour in response to energy absorption. In order increasing absorbed power, they are:

– exergonic isothermal processes
– endergonic isothermal processes
– endergonic nonthermal processes

2) Endergonic processes have a beginning and an end.

Fig.3

The rapid rise and the plateau of the left-hand curve of Fig.3 are determined by the entropy of absorbed power according to (4), but the position of the curve on the logarithm of absorbed power axis (the point of its intersection with the absorbed power axis, where the real endergonic processes are balanced out by exergonic processes) is dictated by the linear term of the entropy generation rate according to (7). The falling region of the left-hand curve is defined by the nonlinear term in the entropy generation rate. This is the second term in formula (7) for the condition $n > 1$.

A qualitative agreement between the thermodynamic theory of endergonic processes and experimental data was demonstrated in a series papers [9 –12] and in two books [7, 8]. That is why this aspect of the problem will be omitted in the present paper.

So, endergonic processes have a beginning and an end at some level of absorbed power, but an experimentalist can study the system not only at constant temperature, but also at increasing temperature for high absorbed power. According to thermodynamic theory in this case, we have two results: a system with no biological effects; and thermal processes in a system (right-hand curve in Fig.3).

Thermal effects of radiofrequency radiation have been studied for almost one hundred years and for thermal processes there is sufficient scientific clarity. That is why this aspect of the problem is omitted in the present paper. The interval without biological effects is poorly understood and it is therefore useful to recall a paper by scientists at the University of Utah (Salt Lake City, USA), who studied this interval [13]. They exposed monolayer cell cultures (for example BHK-21/C13 cells) to high levels of microwave radiation without significant microwave-induced heating ($\leq 0.1°$ C). They showed that for the frequency interval 38-48 GHz at a power density of 292 mW/cm^2 and for 65-75 GHz at a power density of 177 mW/cm^2 bioeffects of microwaves were absent [13].

Thermodynamic conclusions for hygienic standardization

The curves of Fig.3 are very important for the hygienic standardization of radiofrequency radiation. They show that the 20th paradigm of hygienic standardization takes into account only thermal processes in living systems under electromagnetic radiation. In the light of thermodynamic theory, it is clear that the experimentalists finished their research when they reached the interval between thermal and nonthermal effects. All current hygienic standards, except the Russian standards, lie in this interval (cross).

The standards of different countries are different because they are not equally close to the no-observed-heating level (the starting point for thermal processes). But they are all interposed between thermal effects and nonthermal endergonic ones.

From thermodynamics it is obvious that current international standards relate to thermal processes only.

The Soviet hygienic standard for radiofrequencies holds both for thermal and for isothermal processes. That is why it is 1000-fold more severe than the USA standard and all other standards.

It is obvious that in the future national and international standards will be changed. They will become more severe and, in the long run, isothermal effects will taken into account. Then the science of hygiene will have a theoretical basis as a third point of support, in parallel with the experimental and social ones. This is demonstrated schematically in Fig.4. But hygienists do not at present know the theoretical basis and the situation is therefore not simple.

Fig.4

Radiofrequency hygiene of the transitional period

The main current international documents, "Directive 2004/40/EC of the European Parliament and the Council of 29 April 2004 on the minimum health and safety requirements regarding the exposure of workers to the risk arising from physical agents" and "ICNIRP Guidelines for limiting exposure to time-varying electric, magnetic, and electromagnetic fields (up to 300 GHz)", take into account only thermal processes under radiofrequency radiation. How should hygienists deal with real situations today? There are two ways. One way is very simple: it is to wait for laboratory isothermal experiments to show scientifically what the standard of absorbed power must be. In this case, hygienists will leave the people without protection for a long time. But there is another way: a social resolution of the problem, i.e. a precautionary approach. Social decisions may vary, which means that national standardizations will be original, as is now indeed the case. Some examples are given below.

Poland

Polish hygienists understand that limits based on ICNIRP are not too liberal in the case of chronic occupational exposure, and the regulations established in Poland contain limits on permissible exposure which are more restrictive than the EC Directive and the ICNIRP Guidelines. The Polish standardization system allows harmonisation with the EC Directive/ICNIRP basic restrictions and, at the same time, the practical application of a precautionary approch in the occupational environment.

In Poland, there are three levels of exposure [14]:

- high-level and dangerous zone,
- medium-level and safety zone,
- low-level for outside the safety zone.

For pregnant women and young workers (below 18 years), the levels of restricted occupational exposure in Polish Standards (2002) are 2-3 times lower than international regulations. For thresholds of permissible environmental exposure, they are 10 times lower.

Sweden

It has long known that the Swedish occupational standards for personal computers are more severe than international ones.

Austria

The strictest precautionary approach has been established in Austria. It is the so-called "Salzburg Model" [15,16]. The "Salzburg Model" was created in the city of Salzburg in 1997- 1998, when the Department of Public Health of the Federal State of Salzburg was requested by the Salzburg Provincial Parliament, the director of the Department of Health and several mayors to provide a medical evaluation of the GSM fields emitted from mobile telecommunications base stations. The aim of the Salzburg Model is the implementation of a precautionary strategy for the protection of public health against electromagnetic fields.

The so-called "Salzburg precautionary value" is equal to $1 mW/m^2$ (or $0.1\ \mu W/cm^2$) for the bands of 900 MHz – 1800 MHz. This frequency band is used by GSM base stations. It is useful to compare the "Salzburg precautionary value" with the ICNIRP (1998) standard of $4 – 10\ W/m^2$, which is based on thermal effects in the same frequency range. The difference is 4 orders of magnitude. This difference accords well with theoretical estimates of the difference between the thresholds for thermal and isothermal processes.

Austrian hygienists understand that the Salzburg precautionary value is based on biological effects of low-intensity exposure (isothermal effects).

The decision of the Salzburg authority is a wise decision, and is in accordance with the WHO policy [23]. One can compare this decision with Napoleon's decision. As is known, Napoleon Bonaparte created a domestic code. According to Napoleon's code, the father of a child born in wedlock is the husband. In real situations, if the father is unknown, the husband is considered as the father. This decision is dictated by expediency, rather than truth. Napoleon's decision has been a wise decision, because it has saved the law-courts and the population from unnecessary trouble. Napoleon's decision has became a principle of legislation in many European countries for two centuries. Today, this problem is solved by scientific methods because science can establish paternity with high accuracy.

The "Salzburg Model" offers some advantages over Napoleon's decision, because the "Salzburg Model" corresponds to thermodynamic predictions. Thermodynamic law supports the Salzburg precautionary level.

It is now apparent that this work will be the subject of experimental investigation, as attested by the Austrian-Spanish paper [17].

Summary

Thermodynamic theory shows that there are two independent regions of biological effects of radiofrequency radiation: thermal and isothermal ones. Thermal effects are very simple, well studied and standardized. Isothermal effects are complicated to study and their standardisation is for the future.

The precedents of the Salzburg model and the Soviet (Russian) standard are the first steps in a new hygienic science and a new system of standardisation, which will be able to protect public health against adverse effects of radiation. These are real attempts to execute the WHO plans and intentions.

Acknowledgement

I wish to thank Prof. O.P. Gandhi (University of Utah, Salt Lake City, USA), who made available a complete set of his papers on this subject.
I thank the research workers of the University of Utah for a very difficult experiment, which is very important for thermodynamics and hygiene.

References

1. M.H. Repacholi Development of standards – Assessment of health hazards and other factors. Biological effects and dosimetry of nonionizing radiation. Ed. M. Grandolfo, S.M. Michaelson, A.Rindi v.49, 1983, Plenum Press, N.Y., London.

2. Johnson C.C., Guy W. - Nonionizing electromagnetic wave effects in biological materials and systems - Proceedings of the IEE, 1972, v.60, No 6 , pp.692-71

3. Tolgskaya M.S., Gordon Z.V. *Pathological effects of radio waves.* Consultants Bureau, N.Y., London, 1973

4. Biologic effects and health hazards of microwave radiation. Proceeding International Symposium, Warsaw. 1973. Polish Medical Publishers, 1974, pp.22-35, 289 -293

5. L. D. Landau,- On the thermodynamics of photoluminescence. J. Phys. USSR, 1946 ,v.10, p.503 -506

6. P.T. Landsberg , G.Tonge - Thermodynamic energy conversion efficiencies.- J. Appl. Phys. 1980, v.51, N7, p.R1 - R20

7. Yu.P. Chukova. Advances in nonequilibrium thermodynamics of the systems under electromagnetic radiation, 2001, Moscow, Khrizostom, ISBN 5-7508-0285-X

8. Yu.P. Chukova , Low-level influence effects. Thermodynamic, experimental (medical and biological), social, legislative, international and philosophical aspects of problem. Moscow, 2002, ISBN 5-89047-013-2.

9. Chukova Yu.P. Biological response to radiofrequency electromagnetic radiation.- Dokl. Biological Sciences.Proceedings of the Academy of Sciences of the USSR,1990, v.311,p.237-239

10. Yu.P. Chukova, Reasons of poor replicability of nonthermal bioeffects by millimetre waves, Bioelectrochemistry and bioenergetics, Vol. 48, 1999, pp. 349 – 353.

11. Yu.P. Chukova, Thermodynamics of isothermal processes of electromagnetic radiation and practical conclusions. Proceeding of the Millennium Workshop on Biological effects of electromagnetic fields. Crete, Greece, 2000, p. 338 - 341

12. Yu.P. Chukova, Bioeffects under electromagnetic radiation. Theory and experiment, Biological effects of EMFs. 2nd International workshop. Proceedings. Kos, Greece, 2004, Vol. 2, pp. 775 – 783

13. L.G. Bush, D.W. Hill, A Riazi, L.J. Stensaas, L.M. Partlow and O.P. Gandhi. Effects of millimeter-wave radiation on monolayer cell cultures.III. A search for frequency-specific athermal biological effects on protein synthesis. Bioelectromagnetics 1981,v. 2, pp.151-159.

14. Karpowicz J., Gryz K. – EMF exposure's occupational risk assessment – Approach implemented by EC directive 2004|40 and national regulations in Poland. Kos, 2004, v.2, p.1190 – 1195

15. G. Oberfeld, C. Konig , The Saltzburg Model: a precautionary strategy for sitting of base station. Biological effects of EMFs. 2nd International workshop. Proceedings. Rhodes, Greece, 2002, Vol..2, p.621-625

16. E. Marsalek. A possible regulatory framework for the erection of mobile phone base station within the European community, The "Round-table-consensus-Model" (So called "Saltzburg model"), Biological effects of EMFs. 2nd International workshop. Proceedings. Rhodes, Greece, 2002, Vol .2, pp. 611-620

17. Oberfeld G., Navarro A.E., Portoles M., Maestu C., Gomez-Perretta C. The microwave syndrome – further aspects of a Spanish study. Biological effects of EMFs. 3rd International workshop. Proceedings. Kos, Greece, 2004, v.2, p.728 – 735.

EFFECTS OF MOBILE PHONE EXPOSURE ON HUMAN COGNITIVE FUNCTION

ANDREW WOOD

CON STOUGH

RODNEY CROFT

VANESSA KEETLEY

DENISE HAMBLIN

SARAH LOUGHRAN

BRAIN SCIENCES INSTITUTE, SWINBURNE UNIVERSITY OF TECHNOLOGY, HAWTHORN, VICTORIA 3122, AUSTRALIA

Abstract

This presentation will summarize the results of several human volunteer studies carried out at Swinburne University over the last 7 years. The outcomes (significant unless otherwise stated) were:

- Tests of cognition (n = 120 subjects; battery of 8 tests): When adjusted for co-variables, worse performance in simple reaction time and choice reaction time; worse performance in some measures of information retrieval, but improved speed of processing of information held in memory.
- Event Related Potential pilot study (n = 12 subjects; auditory stimuli): Reduced N1 amplitude and latency to non-target and increased P3 latency to oddball target stimuli; worse reaction time performance.
- Event Related Potential main study (n = 120 subjects; auditory, visual and cognitive task stimuli): no significant changes in ERP-related parameters.
- Sleep study (n = 50; polysomnography): REM latency reduced by 16%. EEG alpha power enhanced by 8% during 1st non-REM period.
- Overnight melatonin (metabolite) output (n = 55): Overall no change, but 27% reduction in normalized output pre-bedtime.

These results will be compared for overall internal consistency and with studies from other laboratories. Part of the program of the Australian Centre for Radiofrequency Bioeffects Research is to extend some of the studies.

Introduction

The basic question our research program has sought to answer is: do the emissions from mobile phone handsets lead to an immediate change in a person's neuropsychological performance, such as ability to react to stimuli, recall information, perform tasks accurately, get a good night's sleep and so on? The specific hypotheses we formulated were on the basis of research available to us in the planning phase. An extensive literature review was taken at this time (Hamblin & Wood 2002). This identified EEG alpha power increase in response to radiofrequency (RF) exposure as being the most consistent observation

Methods

Exposure to RF was accomplished by the use of a popular handset, programmed into GSM pulsed mode (0.25 W average) using the manufacturer's software, giving a constant output over the time of the experiment, typically 1 – 2 hours. The output was checked in three ways: i) with dipole antenna; ii) direct connection to RF power meter and iii) by measurements in SAR phantom. The maximum 10g-averaged SAR value obtained was 0.11 W/kg (Hamblin et al 2006), with the phone attached to a cradle placing the handset in a normal position next to cheek. A number of checks were made: firstly, that the participants could not detect audible cues from the handset circuitry; secondly that ELF pickup in EEG electrode leads was not significant (Wood et al 2003) and thirdly that the SAR value was not affected by the presence of EEG lead wiring. In the case of auditory stimuli, an additional test ensured that the test tones (which were delivered by air-tube ear inserts) were uncontaminated by EMI from the phone handset.

A number of biological endpoints were assessed as follows: a) speed & accuracy in performing (mainly paper & pencil) cognitive tasks; b) Event-related potentials (ERPs): specific changes in EEG evoked by visual, auditory & cognitive stimuli; c) sleep architecture: quality and type of sleep following 30 min of phone exposure just prior to going to bed and d) the output of urinary melatonin metabolite: before and after sleep in both exposure conditions.

The basic procedure followed was of two types: for the cognition & ERP experiments, there were two testing sessions 1 week apart each with one of two exposure conditions: a random number generator determined which of exposure condition A (sham) or B (actual exposure) occurred first. To minimise practice effects alternate forms of the cognitive tests were given: the tests in each battery were given in random order (but in the same order between the two exposure conditions). The test were given twice at each session (4 times altogether), one before and once during the (real or sham) exposure. The outcomes were scored as a difference between performance before and performance during exposure, then score for weeks A & B were compared.

For the sleep study the procedure was somewhat different: participants stayed overnight for the Saturday and Sunday nights of two successive weekends. The Saturday nights were for adaptation to sleeping in the laboratory and on the Sunday nights the A or B type exposure was given for a period of 30 minutes prior to getting into bed. The monitoring electrodes were not attached until the exposure had finished. Polysomnography was carried out until 6 am the next morning. Urine was collected before getting into bed and at 6 am: urine volumes, creatinine and 6-hydroxy-melatonin sulphate (aMT6s) concentrations were measured.

In statistical analysis of results the potential confounding of multiple comparisons was recognised. Where possible we used prior hypotheses based on literature expectations: in these confirmatory hypotheses $p < 0.05$ was taken as the critical value for changes being regarded as significant. In hypothesis-generating comparisons, the critical p value was taken as 0.05 divided by an effective number of independent comparisons. For example, where the EEG was typically measured from 62 scalp sites: data from several sites were grouped and trends across the scalp studied (giving just 2 levels of laterality and 3 levels in the front/back direction).

Outcomes

1. Effects on Cognition (Keetley et al 2006)

In this study of 120 volunteers, a battery of 8 tasks were given, but task scores yield 18 measures of cognitive performance. The results were adjusted for co-variables: sex, age & educational level where there was literature evidence for this. It was found that participants scored worse in reaction time & information retrieval tests, but showed improvement in speed of processing of information held in memory. We concluded that basic memory tasks were impaired, but higher cortical functions improved

2(a). ERP pilot study (Hamblin et al 2004)

This was a small hypothesis-generating study of 12 volunteers. An auditory 'oddball' task was studied: responses to the 'oddball target' stimulus (t) and 'non-target' stimuli (nt) were considered separately. For the 'nt' responses, N1 amplitude was reduced (50%) and latency was 8.7% less with exposure. For 't' responses, P3 latency was 8% longer. Reaction Time (RT) was 10% worse.

2(b). ERP main study (Hamblin et al 2006)

This followed on from the above and was a study of 120 volunteers. For the auditory and visual 'oddball' tasks: 't' and 'nt' responses were considered separately. ERP amplitudes and latencies at specific sites were analysed, along with RT to 't' responses in both the auditory and visual tasks. No significant changes were found in relation to these parameters. Future analysis will concentrate on ERP changes from various scalp regions derived from factor analyses together with Event Related-Desynchronisation/Synchronisation (ERD/ERS) and Choice

Reaction Time (CRT) recorded during a cognitive task, which was a card-sorting task which was also conducted as part of the test battery. Psychological activation, as well as investigation into all above parameters by age, gender, previous mobile phone use, hemisphere exposed and laterality is also currently being undertaken.

3. Sleep study stages (Loughran et al 2005)
This was of a group of 55 volunteers (5 who had to be excluded because a sleep disorder was revealed during the subsequent sleep analysis). Ten standard sleep parameters were compared for RF effect: all were non-significant, except for rapid eye-movement (REM) sleep latency, which was reduced 16% by exposure (and which was a serendipitous finding). The EEG Alpha band power (range 11.5 – 12.25 Hz) was shown to be significantly enhanced (by 8%) in the 1st non-REM period (and this supported a prior hypothesis).

4. Sleep study melatonin (Wood et al 2006)
The urine melatonin metabolite (aMT6s) was measured in pre-and post bed-time samples in the same 55 volunteers involved in study 3. Overall, there was no change in total output (pre- + post-bedtime: 14.1 vs 14.6 µg). When values were normalised to urine creatinine concentration (which is considered to give a more precise estimate of aMT6s output), there was a significant reduction (by 27%) in pre-bedtime samples (Sham: 7.7; Exposed 5.6; units: ng aMT6s/mg creatinine). However, the distribution showed that 4 of the subjects were outlying the normal distribution (all in the same direction). If these were eliminated from the analysis the difference was not significant.

Summary
The results of these separate studies are currently being evaluated for internal consistency and for consistency with results from other laboratories. Under the program of the Australian Centre for Radiofrequency Bio-effects Research some of these studies are being replicated using some of the same cohort of subjects and using 3-G type exposures.

Grant Support
This research was supported by grants 78/3718 (Stough & Wood) and 154905 (Wood & Stough) from the National Health and Medical Research Council of Australia.

References

Hamblin DL, Croft RJ, Wood AW, Stough C, Spong J. 2006. The sensitivity of human event-related potentials and reaction time to mobile phone emitted electromagnetic fields. *Bioelectromagnetics* 27:265-73

Hamblin DL, Wood AW. 2002. Effects of mobile phone emissions on human brain activity and sleep variables. *Int J Radiat Biol* 78:659-69

Hamblin DL, Wood AW, Croft RJ, Stough C. 2004. Examining the effects of electromagnetic fields emitted by GSM mobile phones on human event-related potentials and performance during an auditory task. *Clin Neurophysiol* 115:171-8

Keetley V, Wood AW, Spong J, Stough C. 2006. Neuropsychological sequelae of digital mobile phone exposure in humans. *Neuropsychologia* 44:1843-8

Loughran SP, Wood AW, Barton JM, Croft RJ, Thompson B, Stough C. 2005. The effect of electromagnetic fields emitted by mobile phones on human sleep. *Neuroreport* 16:1973-6

Wood AW, Hamblin DL, Croft RJ. 2003. The use of a 'phantom scalp' to assess the possible direct pickup of mobile phone handset emissions by electroencephalogram electrode leads. *Med Biol Eng Comput* 41:470-2

Wood AW, Loughran SP, Stough C. 2006. Does evening exposure to mobile phone radiation affect subsequent melatonin production? *Int J Radiat Biol* 82:69-76

THE EFFECT OF A SPECIFIC PULSED MAGNETIC FIELD ON MICROCIRCULATION

MCKAY JC [1,2], TYML K [2], PRATO FS [1,2,3], THOMAS AW [1,2,3]

[1]BIOELECTROMAGNETICS, IMAGING PROGRAM, LAWSON HEALTH RESEARCH INSTITUTE, LONDON, ONTARIO, CANADA, N6A 4V2
[2]DEPARTMENT OF MEDICAL BIOPHYSICS, SCHULICH SCHOOL OF MEDICINE AND DENTISTRY, UNIVERSITY OF WESTERN ONTARIO, LONDON, ONTARIO, CANADA, N6A 5B8
[3]DEPARTMENT OF IMAGING AND NUCLEAR MEDICINE, ST. JOSEPH'S HOSPITAL, LONDON, ONTARIO, CANADA, N6A 4V2

ABSTRACT

The effect of magnetic field (MF) exposure on microvascular blood flow is controversial with no clear evidence of any one effect. In this study, we investigated the effect of a complex, low frequency, electromagnetic pulse (CNP) on microvascular blood flow when stimulated with acetylcholine (vasodilator). The effect of CNP exposure on blood flow (after 30 and 60 min) when stimulated by 3 concentrations of acetylcholine (Ach) was tested in the peripheral muscle microvasculature of a rat and measured using laser Doppler flowimetry. A mixed design ANOVA indicated that there was a main effect of time, and a main effect of Ach concentration (positive control). There was no significant interaction between time and exposure type due to the large variance created by the Ach concentration; however, a power analysis projection of the data suggests that with additional rats a significant effect would be present at the 0.1 mM Ach concentration. This data will further be analyzed using spectrographs to identify possible imprints of the CNP in the blood flow recordings, as well as any other frequency differences that are present between the sham- and CNP-exposed animals. In light of the present results, it would appear that the CNP modestly increases microvascular blood perfusion after 60 min of exposure in the rats that received 0.1 mM Ach compared to sham-exposed animals. These findings are important in that one potential 'side-effect' of MF exposure to this particular MF sequence has been investigated.

MICROCIRCULATION AND CNP

INTRODUCTION

The effect of magnetic field (MF) exposure on microvascular blood flow is controversial with no clear evidence of any one effect. Published literature is mixed, however, it could be suggested that results are mostly divided into 2 categories[1]: those studies that suggest that MFs lead to an increase in perfusion, and those studies that support a biphasic effect of MFs. The former group of studies indicates that when blood vessels are resting at a normal tone, MF exposure leads to an increase in perfusion (both during and after exposure) [2,3]; while the latter studies indicate that when vessel tone is either low or high, MF exposure alters vasomotion so that normal vessel tone is re-established[4]. The observed variation in published studies is likely attributed to the variation in tested parameters (duration of exposure, time-varying vs. static MF, localization of exposure, MF strength) and species (mice, rats, humans).

In this study, we investigated the effect of a specific pulsed MF sequence, a complex neuroelectromagnetic pulse (CNP), on microvascular blood flow when stimulated with a vasodilator (acetylcholine). The CNP has been shown by our lab to be effective in providing analgesia[5] for snails, mice, and humans, therefore we were interested in its potential effects on other biological systems, such as the microcirculatory system.

Numerous applications and benefits could be derived from locally manipulating microcirculatory blood flow. For instance, the ability to locally modify blood flow may be of benefit to wound healing, site-specific absorption of drugs, and re-perfusion of ischemic tissue. Conversely, if an individual was receiving MF therapy for a particular condition unrelated to blood flow, understanding other effects of that MF (e.g. microcirculatory effects) would be of importance.

According to previous research, results from this study should be explained by 1 of 2 theories: A.) The CNP will provide a homeostatic effect. That is, when acetylcholine (Ach) is administered, blood flow should increase, however, the CNP will cause resistance against this blood flow increase and no effect or a reduced effect on perfusion should be observed. B.) In agreement with our preliminary data[6] and other research showing that MFs increase perfusion, the CNP will in some way enhance the effects of Ach on blood flow leading to an increase in perfusion. It is proposed that nitric oxide may be involved in the potential interaction of Ach with the CNP.

OBJECTIVE

The objective of this experiment was to determine the effect of CNP exposure (after 30 and 60 min) on blood flow when stimulated by Ach in the peripheral muscle microvasculature of a rat.

METHOD

100 male Sprague-Dawley rats (210-290 g) were housed on a 12hr/12hr light/dark cycle and were provided with food and water *ad libitum*. All procedures were performed in accordance with the *Ethics Review Board* at the *University of Western Ontario*.

Rats were anesthetized using pentobarbital sodium (65mg/kg of mass) and surgery was performed on the left hind limb. The extensor digitorum longus (EDL) muscle was carefully exposed and allowed to stabilize for half an hour prior to the MF exposure. Individual rats were then placed within the set of Helmholtz-like coils and a laser Doppler flow meter probe was lowered directly on top of the EDL. Specifics of the coils and MF are as follows: 1.2 m diameter for the coil that generates the vertical low frequency (< 1000 Hz) MF with a 200 μT peak (400 mT/s). The sequence consists of 5 pulse segments (each 853 ms) with an average frequency of 72 Hz separated by an increasingly long refractory period (110-1200 ms).

A Time 0 (prior to MF exposure) measurement was taken for 8 min using PeriMed for Windows software. The MF (CNP) was then turned on. After 30 min had elapsed from the end of the Time 0 recording, a second measurement was taken (Time 30) for 8 min. After 60 min had elapsed from the end of

the Time 0 recording, a final (Time 60) measurement was made again for 8 min. For each recording, the same procedure was followed: 20 sec of un-stimulated blood flow was recorded to obtain a baseline and then Ach was dropped directly on top of the EDL. Three different concentrations of Ach were used: 0.1, 1, and 10 mM. Prior to each Ach injection, phosphate-buffered saline was injected on the EDL as a control measure.

At the end of the experiment, rats were euthanized via an intra-cardiac injection of pentobarbital. The Time 30 and Time 60 peak blood flow values were normalized to the Time 0 peak values and the results were analyzed using SPSS 12.0.

RESULTS

A mixed design analysis of variance was performed to test the effects of CNP exposure on blood flow, using time as a repeated measure. There was a significant difference in peak blood flow response across the 3 tested time points ($F(2, 179) = 18.15$, $p < 0.001$). The Time 60 values were lower that the Time 30 values. Also, as expected, there was a significant interaction between injection type (0.1, 1, or 10 mM Ach), our positive control, and time of exposure ($F(4, 184) = 3.92$, $p < 0.05$). There was no significant interaction between time and exposure type due to the large variance created by the Ach concentration; however, a power analysis projection of the data suggests that with additional rats a significant effect would be present at the 0.1 mM Ach concentration. Please refer to Figure 1 for the normalized peak blood flow response to Ach over time. Note that the greatest effect of the CNP appears to be occurring at the lowest concentration of Ach (0.1 mM). This is illustrated in Figure 2.

CONCLUSION

In light of the present results, it would appear that theory B – 'CNP increases microvascular blood perfusion' could possibly explain the obtained data. After 60 min of CNP exposure, the rats that received 0.1 mM Ach showed a modest increase (12 %) in peak blood flow response compared to sham-exposed animals. Analysis of a greater sample size is required to confirm this finding; however, these results are in support of preliminary data collected from our lab[6].

These findings are important in that one potential 'side-effect' of MF exposure to this particular MF sequence has been investigated. It would appear that MF exposure of this type modestly increases blood flow in the microvasculature after 60 min of exposure.

SUMMARY

The objective of this experiment was to determine the effect of 30 and 60 min exposure to a specific pulsed electromagnetic field (CNP) in the peripheral muscle microvasculature of a rat. Changes in blood flow, when stimulated by 3 different concentrations of acetylcholine (a vasodilator), were recorded using laser Doppler flowimetry. After 60 min of CNP exposure, the rats that received 0.1 mM acetylcholine (the lowest concentration) showed a modest increase (12 %) in peak blood flow response compared to sham-exposed animals. Analysis of a greater sample size is required to confirm this finding. These findings are important in that one potential 'side-effect' of MF exposure to this particular MF sequence has been investigated.

ACKNOWLEDGEMENTS

St. Joseph's Health Care (London) Foundation, The Lawson Health Research Institute Internal Research Fund, Natural Sciences and Engineering Research Council of Canada (NSERC), Canadian Institutes of Health Research (CIHR), the Ontario Research and Development Challenge Fund (ORDCF), Canada Foundation for Innovation (CFI), and the Ontario Innovation Trust (OIT).

REFERENCES

[1]McKay JC, Prato FS, Thomas AW. Bioelectromagnetics (accepted July 2006).
[2]Gmitrov J, Ohkubo C, Okano H. Bioelectromagnetics 23: 224-9, 2002.
[3]Xu S, Okano H, Ohkubo C. Bioelectrochemistry 53: 127-35. 2000
[4]Okano H, Ohkubo C. Bioelectromagnetics 22: 408-18, 2001.
[5]Thomas AW, Kavaliers M, Prato FS, Ossenkopp KP. Neurosci Lett 222: 107-10, 1997.
[6]Hensel JM, Bohnert R, Tyml K, Prato FS, Thomas AW. Bioelectromagnetics Soc Abstracts 25, 2003.

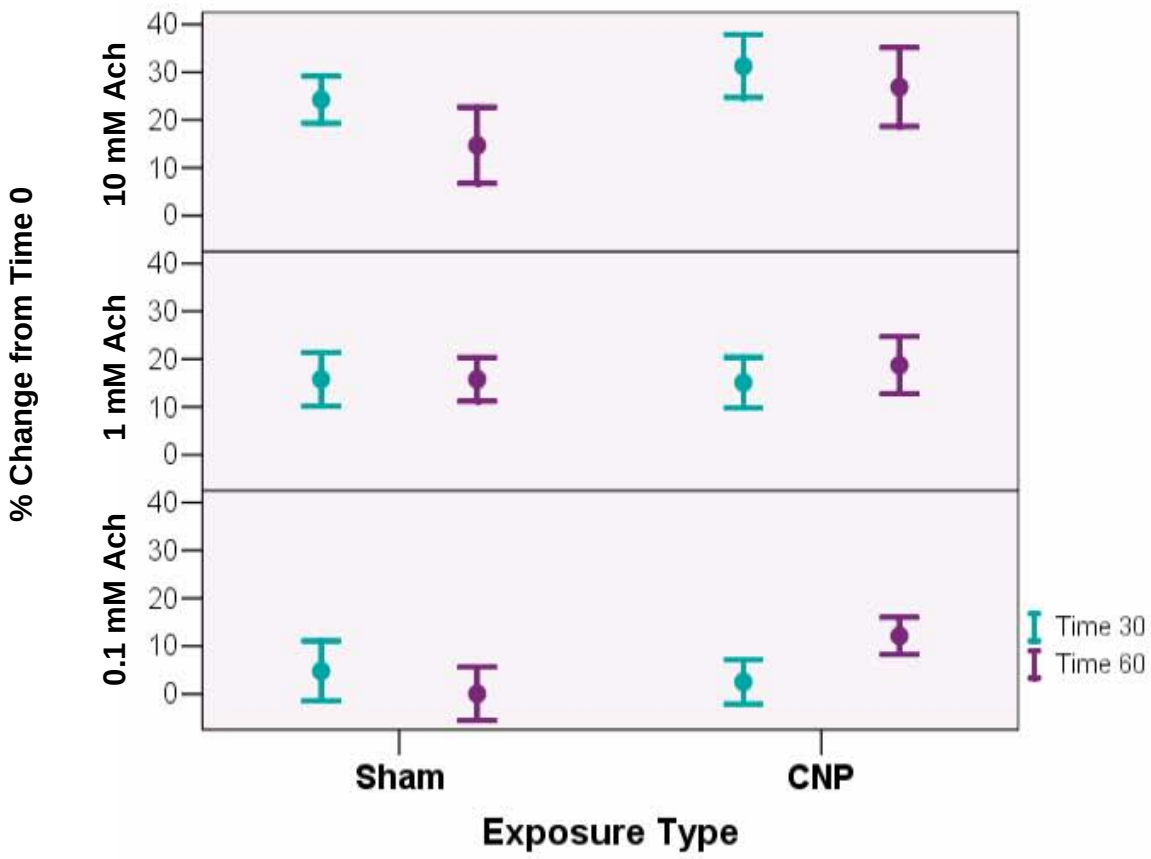


FIGURE 1. Change in microvascular blood flow after 30 and 60 min of exposure to the CNP relative to pre-exposure blood flow baseline. The line of reference at point 0 indicates 'no change' from the Time 0 blood flow values. The most noted difference in peak blood flow response between the sham- and CNP-exposed animals occurs at the lowest concentration of Ach (0.1 mM) after 60 min of exposure. Within each of the sham and CNP cells, the left hand points and error bars refer to the Time 30 measurements and the right hand points and error bars refer to the Time 60 measurements.

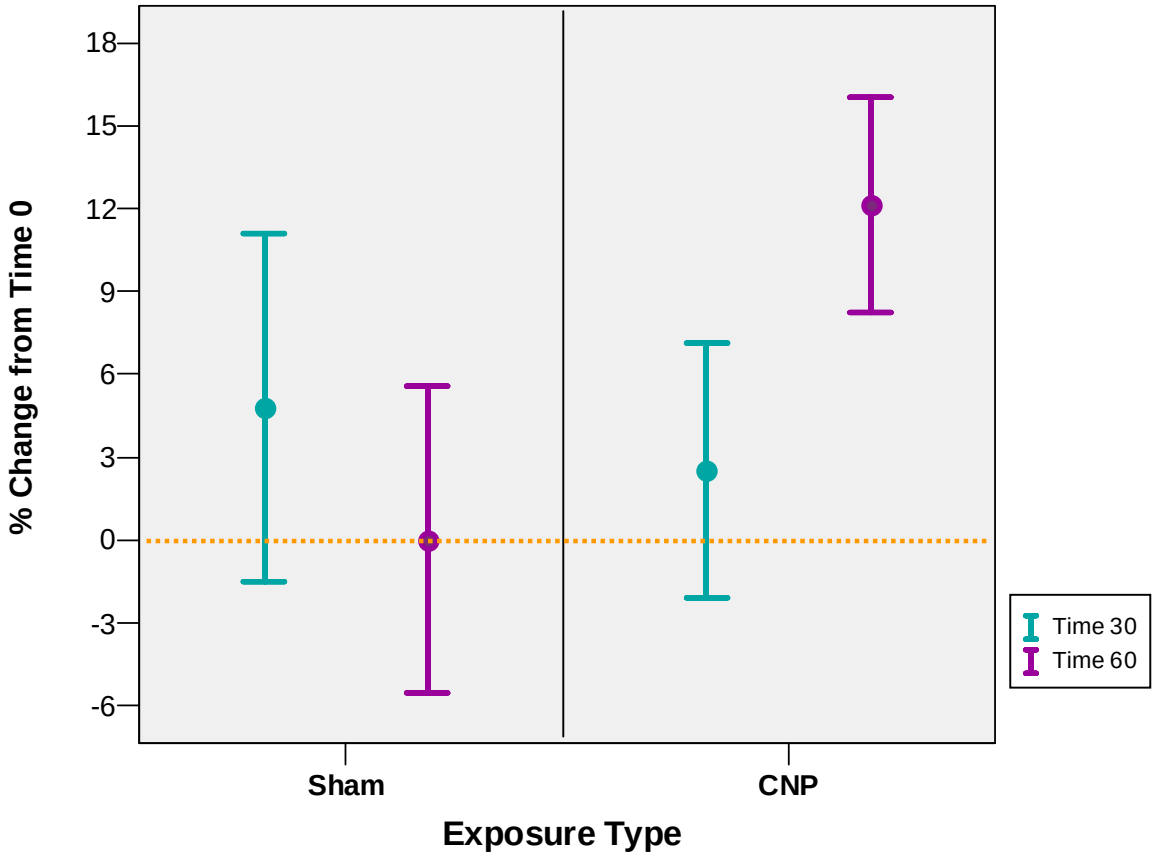


FIGURE 2. Percent change (from Time 0) in peak blood flow response to 0.1 mM Ach after 30 and 60 min of sham and CNP exposure. The line of reference at point 0 indicates 'no change' from the Time 0 blood flow values. Within each of the sham and CNP cells, the left hand points and error bars refer to the Time 30 measurements and the right hand points and error bars refer to the Time 60 measurements.

ABSENCE OF LINEAR CORRELATION BETWEEN BIOLOGICAL EFFECTS AND POWER DENSITY IN THE NON-THERMAL RF RADIATION RANGE

SIANETTE KWEE
DEPARTMENT OF MEDICAL BIOCHEMISTRY, UNIVERSITY OF AARHUS, BUILDING 170,
DK-8000 AARHUS C, DENMARK.

Abstract

During the past years many studies, including our own, have shown significant changes in various cellular processes caused by rates of adsorption at very low level of RF irradiated tissue.
In our investigations we found that MW-EMF exposure of cells down to SAR 0.0002 - 0.002 W/kg caused changes in the cell cycle, which could explain the resulting changes in cell proliferation. Therefore it can be assumed that the observed changes were due to non-thermal RF effects. This could also be concluded from our experiments at various temperatures, which showed that changes in cell proliferation were significantly higher in RF exposed cells than in non-exposed cells at the same temperature.
Nevertheless present safety levels are still based on thermal effects only.
Another argument in favour of non-thermal effects are the socalled "window" effects, i.e. only at specific power densities and/or frequencies, significant effects are seen. These "window" effects have only been observed in the non-thermal range. The same applies to the phenomenon of adaptation.
In this study it will be shown that, though changes in cell proliferation following RF exposure varied with the different SAR levels, they were not linearly proportional with increasing SAR levels, but exhibiting so- called "window" effects.
Effects also varied with the length of exposure time and after 24 h of exposure no changes in cell growth were detected any more. Moreover repeated exposure did no show any difference from results found at a single exposure. This can only be explained by adaptation of cell growth to RF exposure.
So a maximum increase in cell proliferation was only found at certain power densities and exposure times. This can be considered to be characteristic for non-thermal effects.

S.KWEE

Introduction

This study is part of our on-going work to find a mechanism for the biological effects of electromagnetic fields (EMF), in particular non-thermal effects.
From laboratory, clinical and epidemiological studies various effects have been reporterd after exposure to microwave electromagnetic fields. In course of time many theories have been proposed for these effects. On the other hand, very few experimental studies have appeared that offer an explanation for the reported effects.
At first it was assumed that biological effects of radiofrequency (RF) or microwave (MW) fields are solely the result of heat generation. Unfortunately the misconception still persists that all effects of MW-EMF are thermal. Even though we have started to talk about non-thermal effects of MW fields, they are being discussed in terms traditionally applied to heat effects. This is also reflected in the official standardlevels for safe exposure that are only based on heating and are based on average, whole-body irradiation of laboratory animals. However, a lot of tissue damage has been done long before a laboratory animal shows behaviour changes or dies from thermal effects.
At present we have enough experimental evidence to question the validity of standards based only on thermal effects. In particular fundamental research on cell tissue cultures has presented the strongest evidence. During the past years many studies, including our own, have shown significant changes in various cellular processes caused by rates of adsorption at very low level of RF irradiated tissue. At these levels it was also observed that the biological effects were not always linearly proportional with higher power densities or exposure times, but there were so-called "window effects". It also appeared that these window effects are characteristic for non-thermal effects.
We have chosen cell proliferation as the parameter to follow the changes in mammalian cell tissue cultures after exposure to EMF. Our experiments were all done at very low field strength, so the observed changes could be considered as non-thermal effects of EMF.

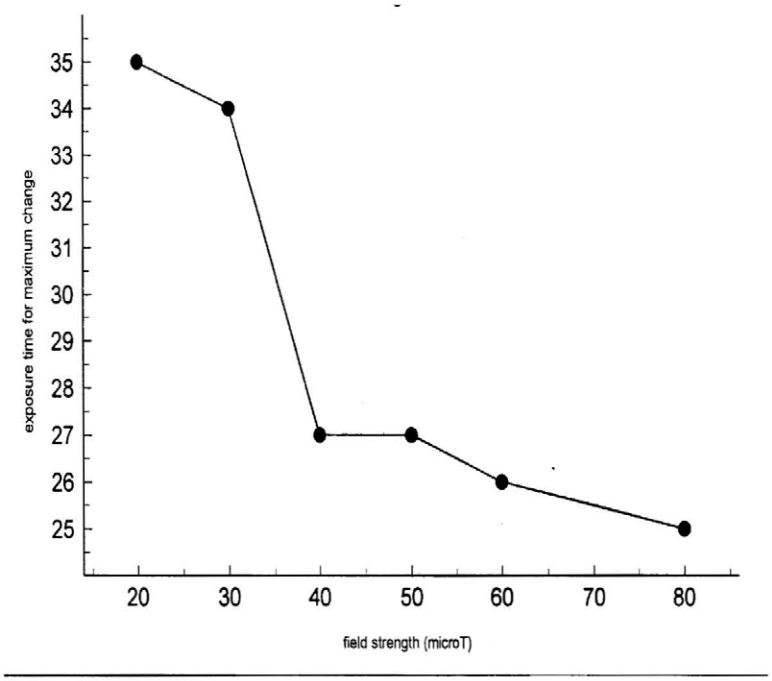


Figure 1:ELF electromagnetic fields: Dependance of maximum change in proliferation rate on exposure time and field strength.

Methods

Materials, cell cultures, EMF - MW exposure, experimental protocol and calculations have been described before [1-4].

Results and discussion

ELF magnetic fields

In previous work [3] we showed that in case of ELF-EMF exposure there was a linear correlation between field strength and the exposure time to obtain a maximum effect as shown in Fig. 1. However it can be seen that this proportionality is not present within a certain power range. As shown in Table 1 there is a plateau at 40-50 µT or a socalled " window".

TABLE 1

Dependance of maximum changes in proliferation rate on exposure time and ELF magnetic field strength in AMA cell cultures .

Field strength µT	Exposure time for maximum change in proliferation rate min
20	35
30	34
40	27
50	27
60	26
80	25

MW magnetic fields

The cell cultures were exposed to 960 MHz microwave fields at various power levels and exposure times. As shown in Table 2 and 3 this resulted in a significant change in cell growth, dependent on energy level and exposure time. Repeated periods of exposure did not seem to change the effects.

It is notable that increased energy levels are not proportional to an increased change in cell growth. At certain levels there is a negative change, while others show a positive change. Also linearity between exposure time and change in cell growth is different and dependent on energy levels. At varying energy levels the maximum change is seen at 20 or 30 or 40 min (Table 4).

At specific levels there is an increase and at others a decrease in growth change at longer exposure times. The latter could indicate adaptation. So adaptation is apparently also dependent on energy level, since at certain levels adaptation takes place already at shorter exposure times than at other levels.

TABLE 2

Percent change in proliferation rate in AMA cells after exposure to MW-EMF of varying energy levels and different exposure times.

Field strength SAR mW.kg^{-1}	**Exposure time min**	**Change in proliferation rate**		
		mean	95% confidence limit	
21	20	- 3.5*	-43	87
21	30	-75	-55	199
21	40	-120	14	219
52	10	70	-5	200
52	20	80	-17	204
52	30	645	-4	191
21	20	- 1.75*	-76	111
21	30	-90	-4	191
21	40	- 4.8*	-194	289
11	10	50	-5	223
11	20	230	-9	312
11	30	40	-99	126
21	20	1.3*	-99	126
21	30	-55	17	108
21	40	-103	58	148

* not significant. P value > 0.5 (paired t-test)

TABLE 3

Percent change in proliferation rate in AMA cells after **30 min** exposure to pulsed microwave fields of varying power levels.

Field strength SAR mW.kg^{-1}	**% change in proliferation rate**		
	mean	95% confidence limit	
6	665	-43	87
7	376	-55	199
12	-40	14	219
16	246	-3	160
21	-750	-55	190
23	-48	-220	105
4	924	-76	111
5	645	-4	191
8	832	-194	289
9	-752	-55	190
16	- 0.62*	-46	105
21	-90	-4	191
26	4.0*	-99	126
33	398	17	108
56	472	58	148
107	-38	-43	87
21	-55	17	108

* not significant. P value > 0.5 (paired t-test)

TABLE 4

Dependance of maximum changes in proliferation rate on exposure time and RF field strength.

Field strength SAR mW.kg^{-1}	**Exposure time for maximum change in proliferation rate min**
21	40
52	20
21	30
11	20
21	30

In conclusion it can be said that the same lineair correlation between power level, exposure time and growth change was not as clear in the case of RF exposure as it is for ELF exposure. As observed also by others the effects registered are not linear over the whole radiofrequency field density spectrum. This can be related to the oscillatory nature of cell growth. Apparently the interaction of microwave radiation with cellular oscillators contributes more to these effects than in case of ELF electromagnetic fields.

Summary

We have studied the effects of ELF and RF exposure on cell growth in cell tissue cultures. Our experiments were done at very low field strength and in case of RF fields corresponding to a SAR not exceeding 2.1 $mW.kg^{-1}$. So the changes observed can be considered as non-thermal effects.
In case of exposure to ELF we can see one specific window at a field strength of 40-50 μT.
In case of RF exposure the picture is more complicated: there are several windows or rather maxima and minima dependant not only on fieldstrength, but also on exposure times. This is certainly due to the different nature of RF radiation and also the modulating frequencies. It has been shown that at constant frequencies the biological effects are much less or even absent.
Longer exposure times and recording periods will result in adaptation and this might be the reason why under different experimental conditions no changes were observed. Due to the process of adaptation it may often no longer be possible to measure changes in cell proliferation when repeated exposures or and much longer exposure times are applied. It is known that under these conditions increasing Hsp concentrations are required to produce the effects as described above. So the Hsp mechanism is certainly also responsible for the resulting adaptation.
It is clear that these window and adaptation effects are crucial for long-term health effects of RF radiation [5] at non-thermal level.
In the thermal range these effects cannot be observed [6]. This is another reason to reconsider the present safety standard, which only applies to thermal effects of RF radiation.

Acknowledgements

The complete exposure system, including the SAR calculations, were designed and assembled by the late prof. Povl Raskmark.

References

[1] S. Kwee, P. Raskmark, Changes in cell proliferation due to environmental non-ionizing radiation. 1. ELF electromagnetic fields, Bioelectrochem. Bioenerg. 36: 109-114, 1995.
[2] S. Kwee, P. Raskmark, Changes in cell proliferation due to environmental non-ionizing radiation. 2. Microwave radiation, Bioelectrochem.Bioenerg. 44: 251-255, 1998.
[3] S. Kwee, P. Raskmark, Radiofrequency electromagnetic fields and cell proliferation, in Electricity and Magnetism in Biology and Medicine, F.Bersani, ed., Kluwer Academic/Plenum Publishers, New York, 187-190, 1999.
[4] S. Kwee, P. Raskmark, S. Velizarov, Changes in cellular proteins due to environmental non-ionizing radiation. 1. Heat-shock proteins, Electromagnetobiology 20(2):141-152, 2001.
[5] S. Kwee, Effects of concentration chances in certain cellular proteins due to microwave radiation, 3rd International Workshop on Biological effects of EMFs, Kos, Greece 2004.
[6] S. Velizarov, P. Raskmark, S. Kwee, The effects of radiofrequency fields on cell proliferation are non-thermal, Bioelectrochem. Bioenerg. 48:177-180, 1999.

MAGNETIC FIELD EXPOSURE METERING

TOMMI KEIKKO
TAMPERE UNIVERSITY OF TECHNOLOGY, P.O. BOX 692, FIN-33101 TAMPERE, FINLAND

REINO SEESVUORI
TAMPERE POWER DISTRIBUTION, P.O. BOX 175, FIN-33101 TAMPERE, FINLAND

SEPPO VALKEALAHTI
TAMPERE UNIVERSITY OF TECHNOLOGY, P.O. BOX 692, FIN-33101 TAMPERE, FINLAND

Abstract
A magnetic field exposure metering system has been developed to be utilized in indoor MV/LV substation measurements. The metering system follows the guidelines published by the International Commission on Non-Ionizing Radiation Protection (ICNIRP) and the EU directive of 2004 for public and occupational exposure. It can be used to measure magnetic field values, total harmonic distortion of the magnetic field, magnetic field exposure ratios for public and workers, load current values and total harmonic distortion of the load current. This paper presents the developed magnetic field exposure metering system, quantities to be measured by the system and exemplary measurements.

1. Introduction
Measurements of electric and magnetic fields in living and working environment have increased because the public concern on the fields has increased. Due to their possible health effects, the International Commission on Non-Ionizing Radiation Protection (ICNIRP) has published guidelines, in which upper limits for public and occupational exposures have been presented /1/. Based on these guidelines, European Parliament and Council have adapted a Directive on minimum health and safety requirements regarding the exposure of workers to electromagnetic fields in 2004 /2/. The European Parliament and Council Directive has to be nationally implemented in 2008. In Finland and in several other EU countries the legislation for occupational exposure to low frequency electric and magnetic fields is still missing. In addition to that common practices and standards have to be created for everyday measurements and estimation of magnetic field exposures.

Table 1 presents occupational exposure reference levels of the ICNIRP guidelines and the Directive. The limit for allowed public exposure to 50 Hz magnetic fields is 100 μT and for occupational exposure 500 μT.

Table 1. Public /1/ and occupational /1, 2/ magnetic field exposure reference values.

Frequency, f (Hz)	**Public allowed magnetic flux density, B (μT)**	**Occupational allowed magnetic flux density, B (μT)**
Up to 1	4×10^4	2×10^5
1-8	$4 f^{-2} \times 10^4$	$2 f^{-2} \times 10^5$
8-800	$5 f^{-1} \times 10^3$	$25 f^{-1} \times 10^3$
800-820	6.25	$25 f^{-1} \times 10^3$
$(0.82\text{-}65) \times 10^3$	6.25	30.7
$(0.065\text{-}0.15) \times 10^6$	6.25	$2 f^{-1} \times 10^6$
$(0.15\text{-}10) \times 10^6$	$0.92 f^{-1} \times 10^6$	$2 f^{-1} \times 10^6$
$(10\text{-}400) \times 10^6$	0.092	0.2
$(0.4\text{-}2) \times 10^9$	$4.6 f^{0.5} \times 10^{-6}$	$10 f^{0.5} \times 10^{-6}$
$(2\text{-}300) \times 10^9$	0.2	0.45

In 2003 ICNIRP expanded their guidelines by taking into account the harmonic components of the magnetic field with phase angles /3/. This statement provides accurate guidelines, in practice, to estimate the magnetic

field exposure due to harmonic components, but it has not been referenced widely. In the case of electricity transmission and distribution only frequencies from 50 Hz to 65 kHz contribute to magnetic field exposure. So far, there is only one commercial magnetic field exposure meter, which is able to consider this frequency range including the phases of the magnetic field components. Measurement method utilized in that meter seems to stands up to a close examination. However, the output of the results in this commercial meter is inadequate for advanced measurements.

Electromagnetic fields have been studied at the Tampere University of Technology (TUT) since the 1980's. In recent years, the research has concentrated on evaluating exposure to magnetic fields. Previously, measurement system at TUT was based on commercial magnetic field meters and power quality analyzers /4/. In that system, the exposure was calculated afterwards enabling advanced magnetic field exposure measurements considering the phases of the harmonic components. However, load current of the indoor MV/LV substation and magnetic field were measured with different equipments, thus not exactly simultaneous. There was a clear need for an improved measurement system providing directly simultaneous measurements of all physical quantities of interest. In this paper we will describe a magnetic field exposure metering system utilized in indoor MV/LV substation measurements meeting these requirements.

2. Measurement methods

In addition to magnetic field exposure measurements, the system measures synchronously load currents. The measurement system saves magnetic field values, total harmonic distortion of the magnetic field, magnetic field exposure ratios for public and workers, load current values and total harmonic distortion of the load current.

A conservative estimate of the cumulative magnetic field *K'* normalized to the measured 50 Hz magnetic field value B_1 is calculated according to the ICNIRP guidelines /1/ by

$$K' = 1 + \sum_{k=2}^{16} k \frac{B_k}{B_1} + \sum_{k=17}^{1300} 16 \frac{B_k}{B_1}, \tag{1}$$

where k is the index of harmonic frequency and B_k is the measured magnetic field of the harmonic component k /5/. According to the ICNIRP guidelines the magnetic field exposure ratio *R'* is

$$R' = \frac{B_1}{B_{L,1}} K', \tag{2}$$

where $B_{L,1}$ is the 50 Hz magnetic field reference level. The allowed upper limit for the magnetic field exposure ratio *R'* is 1. The method presented in equations 1 and 2 has been shown to overestimate the exposure ratio close to 50% in indoor distribution substation by /4/.

According to the ICNIRP statement /1/ and the anticipated implementation of the EU Directive /2/ the maximum cumulative magnetic field K normalized to the 50 Hz magnetic field component B_1 can be obtained as the maximum value of the sum of harmonic components inside a cycle time of 20 ms as follows

$$K = \left\{ 1 + \sum_{k=2}^{16} k \frac{B_k}{B_1} \cos(k\omega_1 \tau + \varphi_k + \phi_k) + \sum_{k=17}^{1300} 16 \frac{B_k}{B_1} \cos(k\omega_1 \tau + \varphi_k + \phi_k) \right\}_{\max}, \tag{3}$$

where ω_1 is $2\pi f_1$, φ_k is the phase angle of B_k, ϕ_k is the biological correction angle at frequency $k \times f_1$, f_1 is fundamental frequency of 50 Hz. Further, the magnetic field exposure ratio R is

$$R = \frac{B_1}{B_{L,1}} K. \tag{4}$$

The calculation procedure of equations 3 and 4 was presented by /6/ and also by /3/ and /7/. The calculation procedure of the magnetic field exposure ratio based on equations 3 and 4 was earlier used to study the validity of the method based on equations 1 and 2 in indoor distribution substation environment by /4/.

The maximum cumulative magnetic field K of equation 3 can be presented in a more general form as a function of time t for long term measurements as follows

$$K(t) = \left\{ \sum_{f=8Hz}^{800Hz} \frac{f}{f_1} \frac{B_f(t)}{B_1(t)} \cos\left[\omega\tau + \varphi_f(t) + \phi_f\right] + \sum_{f>800Hz}^{150kHz} 16 \frac{B_f(t)}{B_1(t)} \cos\left[\omega\tau + \varphi_f(t) + \phi_f\right] \right\}_{\max}. \tag{5}$$

This approach, in principle, is a continuous integration of the magnetic field spectrum corresponding closely to the weighted peak approach /3, 6/. In the weighted peak approach the waveform is weighted with a simple high-pass filter with a 3 dB cut-off frequency at 800 Hz. This approach has been used in the measurements of this paper. However, one must note that a discrete summation of equation 3 is quite adequate for power engineering applications and takes into account all essential frequencies.

3. Meters

In the measurements a 3-axial EnviroMentor BMM-3000 magnetic field meter (accuracy ±5%, RMS) was used. Measured signal was further processed and stored with data acquisition system NI-DAQPad-6015 by National Instruments. Measurement program is named as Keikko6 and created with LabView 7.1. Fig. 1 presents an exemplary screen from a magnetic field measurement.

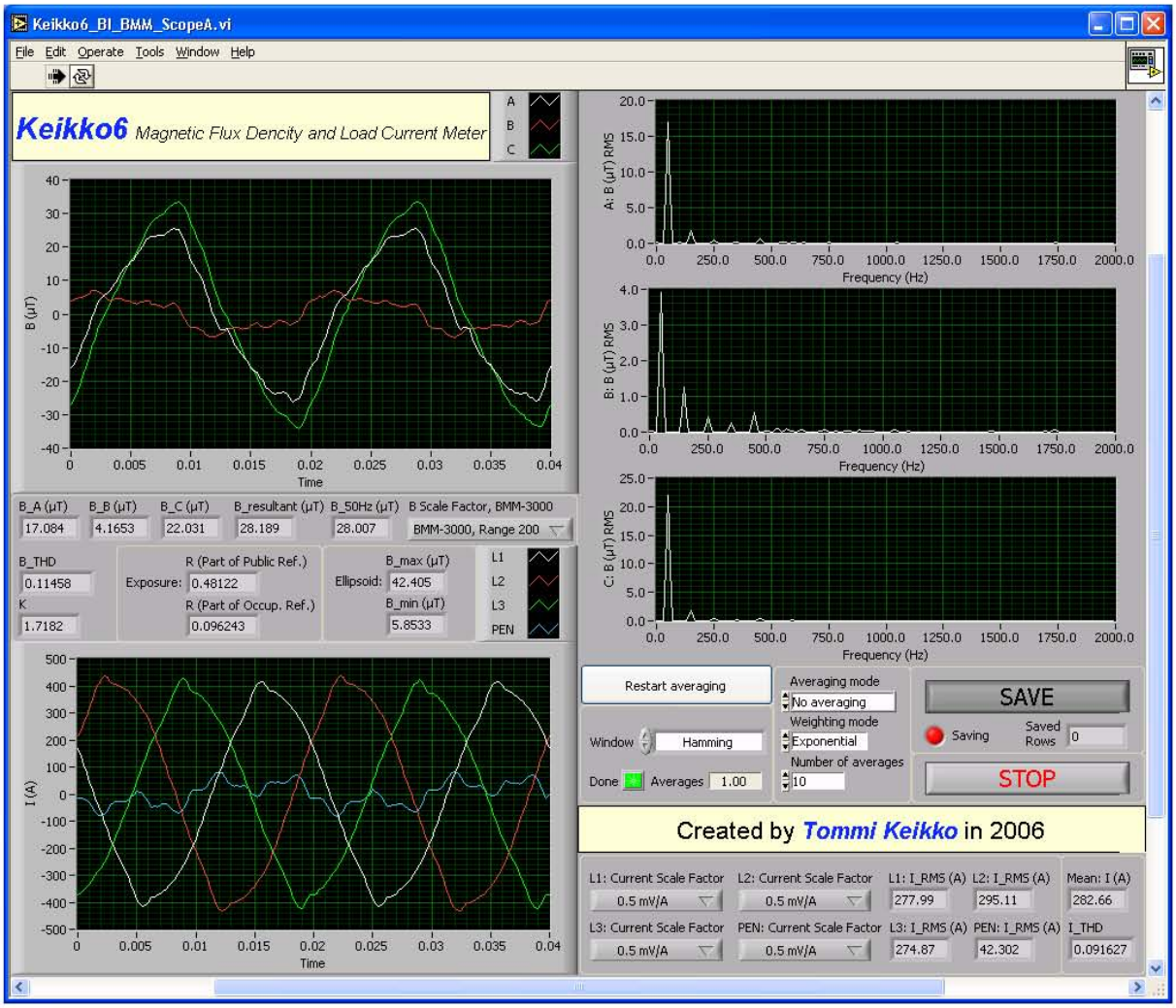


Figure 1. Output screen of the magnetic flux density and load current meter with exemplary measurement results.

The developed metering system saves magnetic field values, total harmonic distortion (THD) of the magnetic field, magnetic field exposure ratios for public and workers, load current values and total harmonic distortion of the load current. Magnetic field values *B_A*, *B_B*, and *B_C* in Fig. 1 are RMS components of the orthogonal magnetic flux density values B_x, B_y, and B_z. Also their resultant value and the resultant 50 Hz value are shown. Total harmonic distortion of the magnetic field B_{THD} is calculated, as follows

$$B_{THD} = \frac{\sum_{k=2}^{1300} \sum_{D=x,y,z} B_{k,D}^2}{\sum_{D=x,y,z} B_{1,D}^2}, \tag{6}$$

where D is the index of the orthogonal magnetic field component. Further, the cumulative magnetic field K normalized to 50 Hz, and public and occupational magnetic field exposures are saved as well.

In addition, elliptic polarization of the magnetic flux density is measured. Ellipsoid based on maximum and minimum magnetic field values during five 50 Hz cycles presents the polarization grade of the vibration.

Load current values *I_RMS* are RMS values for the three phase currents I_{L1}, I_{L2} and I_{L3} and the combined protective earth and neutral conductor current I_{PEN}. Mean current is the average value of the three phase currents.

Mean total harmonic distortion of the load current $I_{THD,Mean}$ (*I_THD* in Fig. 1) is determined and calculated from the load currents of the phases, as follows

$$I_{THD,Mean} = \frac{1}{3} \sum_{L=L1,L2,L3} \frac{\sum_{k=2}^{n} I_{k,L}^2}{I_{1,L}^2}, \quad (7)$$

where L is the index of phases.

4. Measurement set-up

Magnetic field and load current measurements were performed inside 12 indoor MV/LV substations. Fig. 2 presents a photo of an indoor distribution substation, its surroundings and the measurement set-up in one typical substation structure having the LV connection near the ceiling. The magnetic field measurement point nearby the LV connections was determined by considering public exposure in the residence above an indoor distribution substation. The structure of the substation and the building was examined before each measurement.

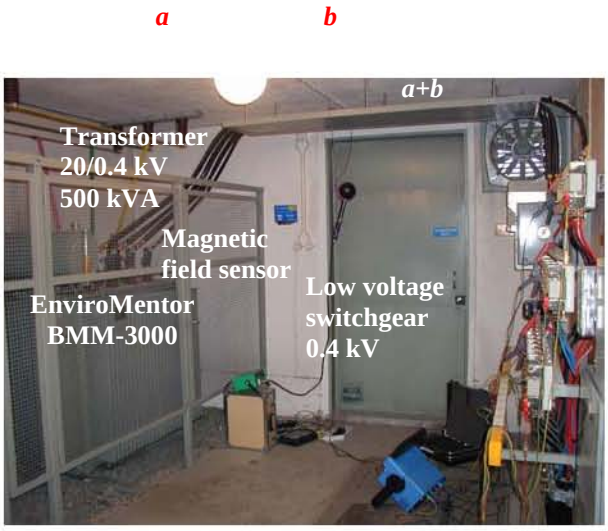


Figure 2. Measurement set-up in a typical indoor distribution substation having the LV connection near the ceiling. Dimension *a* is the thickness of the ceiling and dimension *b* is the distance between the LV connection and the ceiling. /4/

In cases, where the LV connection was not close to the ceiling, the magnetic field sensor was located in the ceiling of the substation above the LV connection or above the expected highest magnetic field source, if possible. Fig. 3 presents a typical measurement set-up, where the LV connection goes on the floor level. Low voltage switchgear can be seen in left-hand photo.



Figure 3. Photos of a measurement set-up in an indoor MV/LV distribution substation, where LV connection is located on the floor level.

Right-hand photo presents the MV/LV transformer. Meters and other measurement equipment are on the floor of the substation. What comes to the public exposure on magnetic fields in the residence above the substation, the space above the transformer is the interesting area to be measured. This area is rounded in the right-hand photo in Fig. 3 and is considered in this paper.

5. Measured magnetic field waveform exposures

Different types of indoor distribution substation structures were selected for measurements to obtain an overall picture on the public magnetic field exposure. Measurements were carried out during the spring 2006. Loads were apartment houses, office buildings or school buildings. The loads of the distribution substations were mostly heat loads, fluorescent and tungsten lamps, computers, and other electronic devices. These loads cause harmonics in the load current that increase the total magnetic field in the substation and decrease the allowed reference value of the 50 Hz magnetic field component. Measured locations and periods are presented in Table 2, where I_{max} is the highest 15 minutes average load current during the previous year and I_{Rated} is the rated load current.

Table 2. Measured indoor distribution substations in spring 2006.

Substation	Transformer		LV connection structure	Measurement period (h:min)
	I_{max} (A)	I_{Rated} (A)		
A	1000	1155	Cables near ceiling	21:35
B	1100	1155	Cables in floor	18:28
C	350	722	Cables near ceiling‡	Period 1: 69:57 Period 2: 28:55§
D	650	1443	Bus bars near ceiling	22:19
E	560	722	Cables near ceiling	18:08
F	730	722	Cables near ceiling	117:11
G	500	722	Cables in floor	21:55
H	T1: 500 T2: 300	T1: 722 T2: 433	Cables near ceiling	44:56
I	T1: 440 T2: 290	T1: 722 T2: 433	Cables near ceiling	73:18
J	450	722	Cables in floor	18:39
K	T1: 350 T2: 750	T1: 1155 T2: 722	Cables near ceiling	21:29
L	560	722	Bus bars near ceiling	66:34

‡ special structure: two × tree phase cables
§ measured in two periods and two locations, period 1 near LV switchgear and period 2 near transformer

Magnetic fields were measured during 1 to 5 day periods. Transformers in substations B, F and K were near their capacity limits. The other substations were clearly within the capacity of their transformers. More detailed results are presented for substation A to describe the advantages of our metering system. Long periods can be measured to consider varying load situations when metering exposure to magnetic field. Due to data handling purposes long measurements can be saved automatically to several files. We used a measurement interval of 1 s and saved 30 000 measurements in one output file i.e. a measurement of 8 hours and 20 minutes. In the following we present a set of measurements done during the first metering lot for substation A to demonstrate our metering systems. This substation has the same type of structure as in Fig. 2.

Fig. 4 presents 50 Hz magnetic field component and public exposure ratio during the first metering lot for substation A. The public exposure ratio correlates, on the average, well with the fundamental magnetic field component, which is in accordance with small variations of $K(t)$ as a function of time being close to 2 (Fig. 5). Thus, according to equation 4, the public exposure ratio has to be multiplied by a factor of 50 μT to obtain the 50 Hz magnetic field component in Fig. 4. This simply means, that the total magnetic field exposure including the harmonic components is, in practice, two times the exposure due to the fundament frequency.

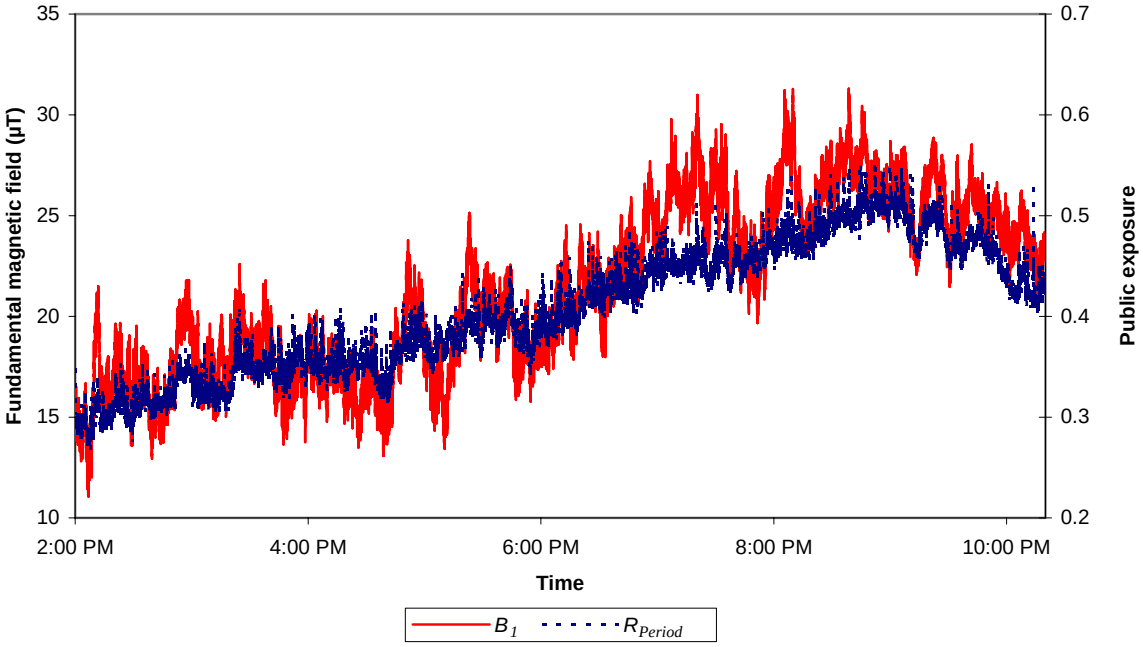


Figure 4. Measured 50 Hz magnetic field component and the public exposure ratio in substation A.

Candidates to explain varying *K(t)* are the total harmonic value for the magnetic field and the relative load current defined as load current divided by the rated current of the transformer (1155 A for substation A), which are presented in Fig. 5. There seems to be a slight negative correlation between the cumulative magnetic field normalized to 50 Hz and the relative load current in agreement with earlier observations /4/. The same negative correlation exists also between B_{THD} and the relative load current. A strong positive correlation is seen between *K(t)* and B_{THD}, as expected.

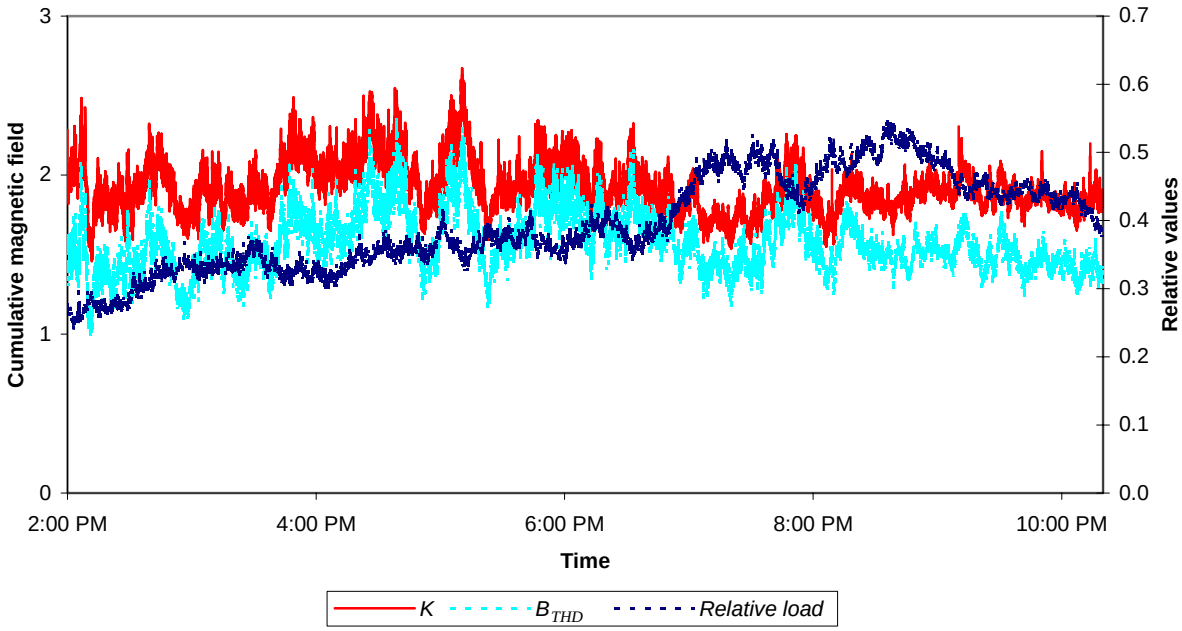


Figure 5. Measured *K(t)*, B_{THD} and relative load current as a function of time for substation A.

Based on Fig. 5 the correlation between *K(t)* and B_{THD} is clear. The shapes of the curves seem to be almost similar having only minor differences. Further, based on /4/ load current and magnetic field harmonics had correlation. The same was tested for substation A in Fig. 6. Correlation between the load current and the magnetic field total harmonic distortions is clear also in these measurements.

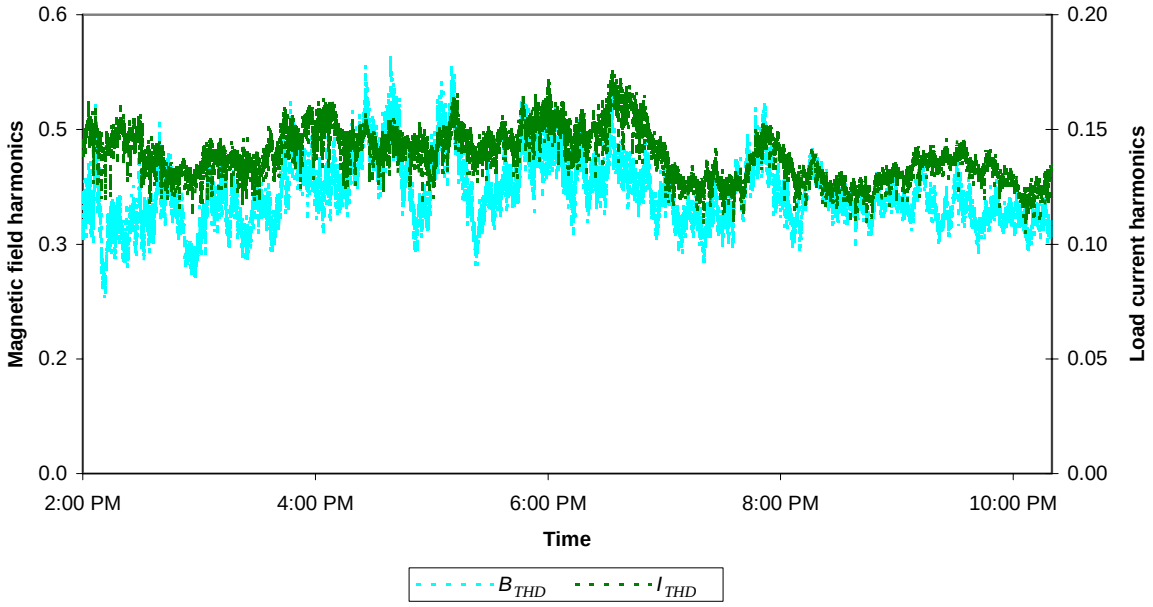


Figure 6. Load current and magnetic field harmonics for substation A.

The coefficient between I_{THD} and B_{THD} is close to 3 in this measurement. This coefficient is the same than in /4/, although the determination of the total harmonic distortion values differs. Previously the values were determined based on the highest load current and highest magnetic field component. The more advanced determinations in this paper were presented in equations 6 and 7.

Summary of the results for all measurement periods is presented in Table 3, where I_{load} is the highest load current, B_{period} is the highest magnetic field and R_{period} is the highest magnetic field public exposure ratio during the measurement period. Significance of the measurement result is determined based on congruence between the measured location and the possible public exposure so that ** means a significant result and * means a indicative result. R_{max} is the highest magnetic field public exposure ratio during the measurement period scaled to the rated load current.

Table 3. Key results for the measurement periods.

Substation	Significance	I_{load} (A)	B_{period} (µT)	R_{period} (%)	R_{max} (%)
A	**	633	32.7	0.73	1.33
B	*	851	120.8	1.57	2.13
C	**	Period 1: 326	Period 1: 7.90	Period 1: 0.17	Period 1: 0.37
	*	Period 2: 279	Period 2: 41.6	Period 2: 0.90	Period 2: 2.32
D	**	688	44.3	0.71	1.49
E	**	349	26.7	1.37	2.83
F	**	478	51.4	0.82	1.24
G	*	378	7.40	0.27	0.51
H	**	454	75.4	1.37	2.18
I	**	352	13.1	0.20	0.42
J	*	343	27.5	0.41	0.86
K	**	567	12.1	0.33	0.67
L	**	445	75.6	1.73	2.81

Significance is valuated based on the structure of the indoor MV/LV substation. For bus bars or cables near the ceiling the location of the magnetic field sensor corresponds to the floor of the space above the substation. If the sensor is located in the ceiling of the substation, the results of the measurement periods are indicative. In the Table 3 the public exposure ratio during the measurement period exceeded value one in 3 out of 9 significant measurement periods. When the exposure ratio is scaled with the rated load current the value one is exceeded in 6 out of 9 significant measurement periods. The exposure ratios exceeded one in 1 and 2 out of 4 indicative measurement periods, respectively.

6. Summary

Magnetic field exposures are presented considering harmonics for the case of 12 indoor MV/LV distribution substations. Based on the measurements, the public exposure often exceeded the reference value in rooms above indoor distribution substations. Further, this means that indoor distribution substations can cause public exposure. Another relevant question is do the structures of the present indoor MV/LV distribution substations produce too high magnetic fields considering the EU Directive /2/, which will be nationally implemented within the EU by 2008.

In this paper, magnetic fields were measured with a new and advance metering system. All important magnetic field and load current values were measured with a simultaneous measurement. This new metering system gave relevant results and made further analyses possible. Previous measurements and references supported results and analysis made with the new metering system. Furthermore, magnetic fields can cause disturbances in measurement or control systems and in electrical devices, and that is another possible use of this new metering system.

Based on the measurements of substation A, the load current is the primary cause for the magnetic field level. Fig. 7 presents the measured magnetic field generation defined as magnetic field divided by the load current for substation A.

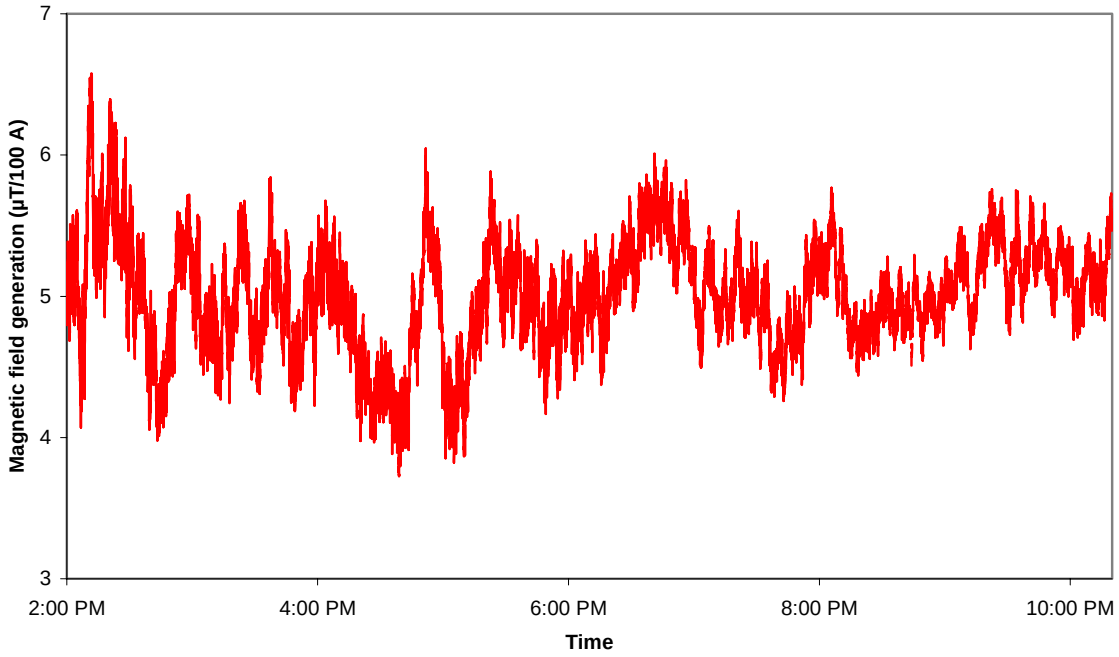


Figure 7. Measured magnetic field generation in substation A.

A generally accepted basic approximation is that the magnetic field is considered to be directly proportional to the load current. This seems to be roughly true for substation A. The average value for the magnetic field generation in Fig. 7 is around 5 µT/100 A. However, it varies most of the time between 4 and 6 µT/100 A. Because the curve in Fig. 7 is not linear, the phase angle differences of the currents have important role when estimating magnetic fields.

The structural differences between indoor distribution substations will have a significant impact on magnetic fields. Therefore, to create general magnetic field exposure estimates, a wider range of grouped structures of the indoor MV/LV distribution substations and with grouped load parameters should be analyzed.

References

1. ICNIRP. Guidelines for limiting exposure to time-varying electric, magnetic, and electromagnetic fields (up to 300 GHz). Health Phys 74:494-522; 1998.

2. Directive 2004/40/EC of the European Parliament and of the Council on the minimum health and safety requirements regarding the exposure of workers to the risks arising from physical agents (electromagnetic fields). Brussels; 2004.

3. ICNIRP. Guidance on determining compliance of exposure to pulsed and complex non-sinusoidal waveforms below 100 kHz with ICNIRP guidelines. Health Phys 84:383-387; 2003.

4. Keikko T, Seesvuori R, Valkealahti S. Exposure to magnetic field harmonics in the vicinity of indoor distribution substations. Health Phys 2006. (In press.)

5. Keikko T, Isokorpi J, Korpinen L, Elovaara J, Vanhala P. Considering electric and magnetic fields in electric power system design in Finland. In: Proceedings of a CIGRE, International Conference on Large High Voltage Electric Systems. Paris: CIGRE; ID 36-102; 2000.

6. Jokela K. Restricting exposure to pulsed and broadband magnetic fields, Health Phys 79: 373-388; 2000.

7. Keikko T. Technical management of the electric and magnetic fields in electric power system. Dr.Tech. dissertation, Dept. El. Eng. Tampere: Tampere University of Technology; 2003.

ALGORITHM FOR NOISE-DATA REDUCTION FOR LONG-TERM EMF MONITORING SYSTEMS

H. HAIDER[1], A. NÖHRER[1], G. NEUBAUER[1]

[1]*ARC SEIBERSDORF RESEARCH GmbH, A-2444 SEIBERSDORF, AUSTRIA*
HARALD.HAIDER@ARCS.AC.A T

Abstract
In addition to present popular 'in situ' EMF-measurements performed at critical locations like schools, hospitals or in front of base stations for one-time, long-term evaluations of RF-fields become more and more essential. This is especially because of the continuously increasing number of new applied technologies and even more emitting base stations. To perform such long-term investigation, fully automatic, stand alone EMF-monitoring stations are suited very well. Typically, several of such stations are connected to one environmental network, fully remote controlled by one server. To yield maximum of information, each station is continuously in operation, performing frequency selective measurements and generating an enormous amount of measurement data. The data communication often represents the bottleneck of such systems and therefore the reduction of these data becomes very essential. By implementing an intelligent algorithm for data reduction directly on the measurement station this problem could be reduced. Therefore we will provide in this paper a methodology suited for a considerable reduction of noise points without loosing any relevant signal information. The specific nature of this algorithm and his efficiency in data reduction will be discussed and explained, including how it works and what parameters are needed. The results which can be achieved with this technique are demonstrated with the existing monitoring system 'Field Nose' from ARC Seibersdorf research.

I. **Introduction**

Today more than 1 billion people are using mobile telephones world-wide, about 360 million people of them in Europe. Such wide use of this technology led to an increase in the environmental exposures to RF-fields and the introduction of new, additional technologies has intensified this process.

In the meantime most countries have national laws, regulations, guidelines or standards and more or less accurate defined measurement procedures and protocols how to handle RF-exposure. The ICNIRP guidelines [1] are used as reference in most European countries. However, many countries apply more restrictive limits, e.g. Switzerland and Italy [2]. Independent of the absolute values of limits, different measurement procedures are used in different countries. In general, the limit are frequency dependent and given over a wide frequency range. There are different concepts regarding the kind of exposed people and the considered areas, i.e. general public versus workers or controlled versus uncontrolled areas. For EMF-exposure evaluation, the contributions of all relevant RF-emitters for the whole body have to be investigated, considering individual signal form, frequency range, bandwidth, polarisation, direction and deviation over time. This leads to a lot of essential requirements for EMF measurement systems and especially also for the data evaluation procedures of such equipment. Another need for adequate measurement and evaluation techniques is the demand for epidemiological studies on the potential health effects caused by the numerous RF-emitters. In the frame of an international project the feasibility of epidemiological studies on potential health effects arising due to the exposure from mobile telephone base stations was jointly assessed by a team of RF experts and epidemiologists. A major outcome of this study was the need for reliable exposure assessment procedures [3]. Frequency selective, monitoring exposure assessment equipment is one of the best suited approaches to assess exposure in a reliable way. Also one COST 281 program activities are focusing at that topic.

II. EMF Measurement Systems

One of the most important requirements for EMF-measurement systems for exposure evaluation is an isotropic (receiving) radiation characteristic over the whole frequency range to add all contributes of different RF-emitters (technologies) in the same way, independent of their distance and direction in relation to the measurement point

and their polarisation. Further the sensitivity of the measurement systems have to be high enough to measure very small signals of modern communication technologies of a few mV/m as well as the dynamic range has to be large enough to consider signals close to the limit level, which is typical at 4 V/m to 60 V/m. Of course measurements have to consider the effective field strength or power flux density independent on the kind of signal or technology (e.g. modulation, pulsing or frequency hopping) and they should be fast, easy to handle, accurate and reliable. The instruments should be small, low cost, easily to operate and the requirement to enable long-term evaluation is essential for RF-dosimetry. Currently three different technical solutions are on the market to perform EMF measurements and each one has its individual assets and drawbacks in relation to the requirements mentioned above.

First there are the well known wideband field probes. They are low priced, easy to handle, have a wide frequency range typically from 100 kHz to 3 GHz, good isotropic characteristic and they are popular also for other kind of measurements e.g. for classical EMC. Some types also enable to select some frequency dependent limits and return the result in percentage of that limit. Unfortunately this is a global result without any information of the relative contribution of the considered transmitters. Also the sensitivity is limited at about 0.1 V/m. Therefore field probes are popular and well suited for preliminary measurements, e.g. to decide if and at what position frequency selective measurements should be performed.

A second group is represented by so called transmitter-selective or narrowband instruments. With these instruments, which are relatively new on the market, fixed or user definable frequency bands corresponding with the bands of transmitter-technologies are measured. Each narrowband is evaluated separately but of course there is, similar to field probes, no possibility to get any information about signal intensity within a band e.g. any differences in channels or for competitive providers. Depending on the system, data acquisition in the time domain is very flexible, from milliseconds to minutes for long-term evaluations. Typically 7 to 15 narrow-bands are measured together at each time cycle and therefore the resulting data amount is relatively easy to handle. Some systems are small enough to carry them on the body or in a rucksack and use these instruments for ‘live time’ RF-dosimetry during the whole day or to evaluate typical exposure at a working place. Typical limitations of those systems are given if signals occur out of the predefined narrow-bands because they were totally ignored. Another problem is caused by crosstalk of bands close together which is often used for up- and downlink of one technology, but could also affect different technologies, if their frequency bands are proximate to each other. Increasing the number of RF-technologies or even the number of bands which should be evaluated will increase that crosstalk problematic. The sensitivity of the systems is typically given at the data-sheets with 10 to 50 mV/m, which is suitable for most applications. Unfortunately the isotropic behaviour and measurement uncertainty are often not clearly specified especially if these data are needed for the individual bands.

The third group of systems is a more or less traditional method using a wideband antenna or field sensor in combination with a frequency selective measurement instrument like a spectrum analyser. Due to the fact that no antenna has an isotropic radiation characteristic by itself, one solution consists in the addition of the contributions of three measurements of an antenna with a dipole like radiation pattern to yield an isotropic receiving characteristics for the system. ARC Seibersdorf research developed small RF-antennas with a dipole like radiation pattern and established the so-called ‘Add3D Method’ [2] in 2002. An automatic positioner can be used to realize the three orthogonal antenna orientations. Figure 2 is showing a schematic drawing of the ARC Seibersdorf research system ‘Field Nose Complete’ and a picture of the real system (see also at http://www.seibersdorf-rf.com). This EMF-measuring and monitoring system is fully remote controlled by the software ‘Nose’, and enables the user to perform automatic measurements as well as many data evaluation procedures. The following examples and evaluations of that publication are based on this system.

Other manufacturers offer systems based on three small sensors with dipole characteristic and switch between them or combine them by an electrical network. In those cases there is the challenge to get an acceptable isotropic radiation pattern of the system because the three sensors interfere with each other. On the other hand such systems are faster, because they need no time to rotate the receiving antenna.

All these systems based on frequency selective spectrum analyser measurements enable individual RBW-settings, rms-, peek- or average signal detection, max-hold trace functionality, very high dynamic range and best sensitivity (low noise level) caused by the performance of state of the art spectrum analysers. The measurement time for a frequency scan is different and mainly depending on the trace speed, the analyser settings, the number

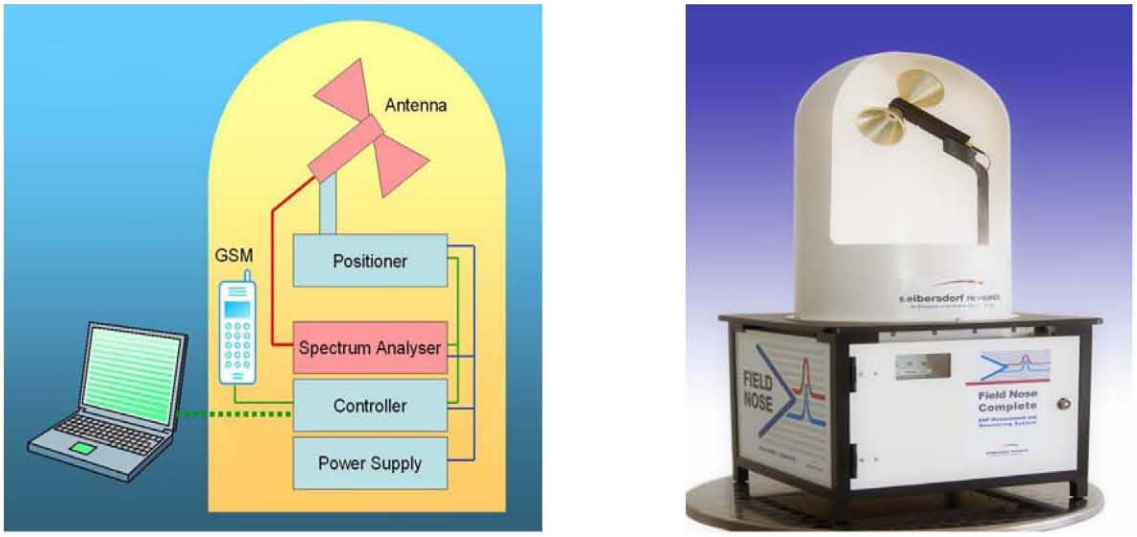


Figure 2: EMF-monitoring system Field Nose Complete (schema and picture)

of repetitions and the sensor type. Measurement cycles of a scan from e.g. 80 MHz to 2.5 GHz can be done within a minute or less. With these frequency selective measurements most information is generated and available for evaluation on the one hand. On the other hand especially that large amount of data can make problems. One possible way of the challenging task to reduce the amount of data without any loss of relevant information is presented in the next chapters.

III. Evaluation problematic of frequency selective systems

Figure 3 is showing a measurement trace and the corresponding data evaluation of a frequency selective, wideband EMF-measurement performed in the centre Vienna. Radio and TV signals as well as the typical downlink signals of mobile phone technologies (GSM 900, DCS 1800 and UMTS) can be seen. The frequency bands of those technologies are marked by coloured, vertical areas corresponding to technology bands as common for band-selective data evaluation. The measurement was done from 80 MHz up to 2.5 GHz using a Field Nose system with a PCD8250 antenna, a 5 m long RF-cable and an Anritsu MS 2711D spectrum analyser.

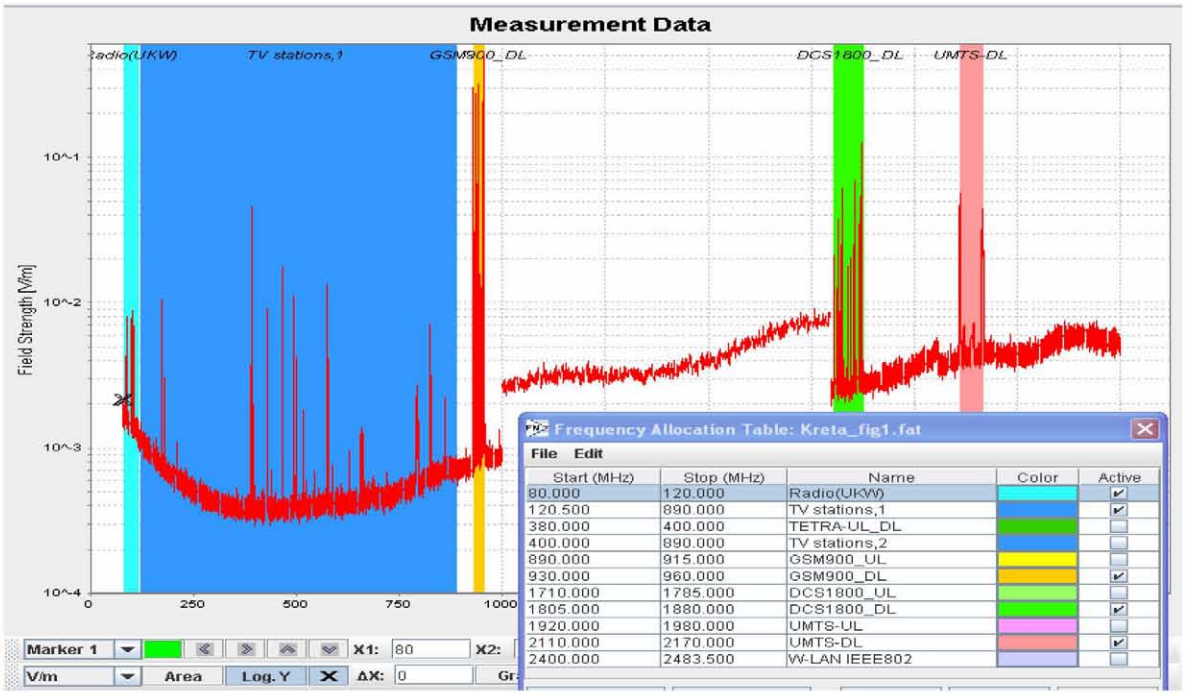


Figure 3: Frequency selective EMF-wideband measurement trace (overview measurement) from Vienna

The characteristic ‘bathtub’ noise floor for this frequency selective, wideband measurement trace can be seen very clearly because of the logarithmic scaling of the field strength axis. It is caused by the noise floor of the spectrum analyser itself (primary depending on its RBW setting, internal attenuator setting or an activated preamplifier), the cable- and connector losses and the antenna factor of the used PCD-antenna. Also caused by the logarithmic scaling and the high sensitivity of the system, the small signals from radio and TV-stations and less strong mobile technology signals with a few mV/m can be detected well. For the measurements from 80 MHz to 1 GHz and from 1.8 GHz to 2.5 GHz a RBW-setting of 100 kHz was used to get a good frequency resolution of the measured technologies. Between those bands we do not expect any signals. Therefore the RBW at that frequency range was set to 1 MHz to save time for the frequency scans and to reduce the number of measurement points too. The higher noise floor does not disturb in that case because of the lack of public communication technologies in that range.

Caused by the selected RBW-settings with 100 kHz respectively 1 MHz and the wide frequency range, 17.000 measurement points are needed for the one single scan according to Figure 3. For example if one scan should be performed each 5 minutes during one day, 288 scans respectively nearby 5 million measurement points are needed. To save that data including measurement information like settings, used antenna and cable factors, time and date, the Field Nose system needs approximately 15 MByte of memory, if the data was stored in a binary format. Even up-to-date computers need considerable time (from a few seconds to minutes) to process such big amount of data, e.g. to print them on screen, perform any data calculations, load and save them or to send them to a host system computer in case of a monitoring system consisting of several measurement stations. In practice measurement may differ to that example, but still a huge amount of data could be produced and the resulting time delay for data processing will not be accepted by the user. This would limit the application of frequency selective systems for long-term evaluation in a considerable way.

IV. Algorithm for noise-data reduction

Having a look to Figure 3, it can be seen that most of the measurement points are representing noise. The only important information of this noise floor is that all signals below that level could not be detected by the measurement system and not considered for any evaluation. On the other hand if the level of noise is deep enough, the signals below that do not affect the evaluation results in a significant way. This fact is the starting point to overcome the problem of extremely large amount of data for frequency selective measurements. Based on an effective signal detection method it should be possible to divide the signals from noise sequences and reduce or eliminate the noise data. Of course the efficiency of that process depends on the relation of signal and noise parts in a measurement scan but especially for wideband measurements it should reduce the number of data points in a considerable way and help to speed up the systems.

The simplest solution segmenting noise and signals is a user defined threshold line near above the noise. All values above that threshold will be accepted as signals. Unfortunately this works only for small frequency ranges because for wideband measurements the noise floor usually is frequency dependent and there is the question where to set the threshold limit. Another method is to select the largest signals by a peak detection algorithm. There of course is always the question of a proper predefinition of the number of relevant peaks as well as the problem that the highest signals not necessary are the one with most of energy because of different bandwidths. Approaches like they are typical in the noise reduction of sound signals were not applicable because of the fact that EMF signals sometimes look like noise to them. Other approaches which are used in image processing are not really applicable too.

Therefore we developed a specific algorithm for signal detection considering the unique requirements in the area of EMF signal processing. The processing of the data can be applied to measured data that is already available, but the main intention was to perform the reduction during measurements on the embedded system of the Field Nose Complete system. Therefore the reduction algorithm works completely automatically but it is also possible to set some parameters manually to improve the results for certain measurements. The noise data can be reduced so that the noise floor is still present or it is possible to remove the noise data completely. Signals are not affected by the algorithm in any way.

The noise data reduction algorithm itself works in the way that first the noise floor is detected and segmented from the signals. The next step is to calculate the new reduced noise floor with less data points and finally this new noise floor is merged with the original signal data. The most difficult part was to find a way how to distinguish very efficient between the noise floor and the signals because sometimes signals share many characteristics with the noise. For that purpose an upper and a lower envelope of the noise are calculated by

using a 'Noise Height' factor in dB. Based on this predefined noise-amplitude factor the decision is derived if the measured points are noise or not. If a Gaussian distribution function is assumed for the noise, this factor should be 2 sigma of the noise amplitude to catch approximately 99 % of noise by the envelope curves. For that process it is essential to consider not only the difference between adjacent measurement points, but also the amplitude differences of proximate points have to be considered.

Between the envelope curves of the noise a new noise curve is calculated with much less points in correlation to the original measured curve. The reduction of noise points for the calculated noise curve is predefined in the software or can be selected manually by a percentage value, which is typically around 90 % (this is an input value for the software and not correlating with exact 90 % of noise point reduction; see also Table 1). The resulting, data reduced measurement curve consists of the original signals matched with the sequences of reduced noise points. In Figure 4 an example of the signals is displayed. The thick (red) curve is the new calculated curve with reduced number of points in the noise sequences and unchanged points for all signals.

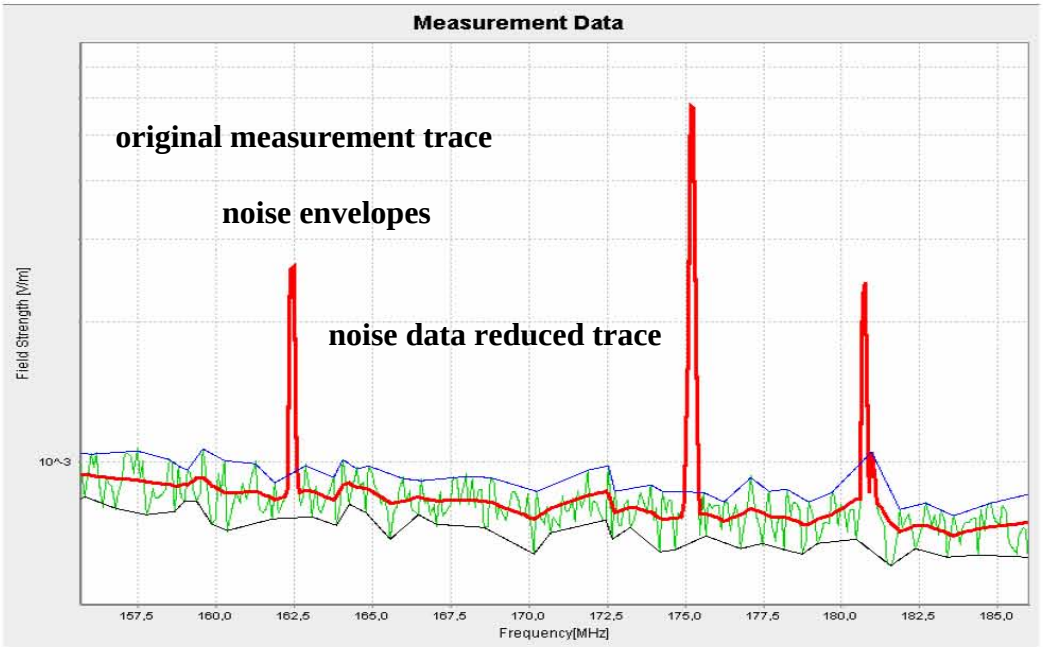


Figure 4: Noise points reduced measurement trace with noise envelopes

However there are still some kinds of signals making problems like typical UMTS signals. Because of their 5 MHZ bandwidth and the RBW-setting of 100 kHz these signals look like noise to the algorithm. This can be solved in a second signal check, where it is assumed that the noise floor is continuous. Jumps in the noise floor because of different analyser settings are handled by the evaluation of each measurement trace separately.

The next step to reduce the amount of data is to eliminate the noise sequences totally. Therefore simply all noise points are neglected and only the signals are still part of the data reduced, noise points excluding trace. In the graphic chart the flanks of signals are connected by a line. In Figure 5 the UMTS-DL band of the overview measurement from Vienna (Figure 3) is shown magnified. For the original measurement trace the noise data reduced trace and the trace with eliminated noise points were calculated and displayed together. The difference in the number of needed data points for these three signals is obvious.

Another powerful effect of the presented algorithm besides the data reduction is the possibility to evaluate the effective signal power without any incorrect additional integration of noise to the signals. To demonstrate that we have again a look at the UMTS band of Figure 5 respectively Figure 6 at left side. This time the vertical bands in Figure 6 are representing the DL-channels of the Austrian UMTS providers, which are used for data evaluation of the three UMTS-traces. On the right side of this figure the evaluation results are given. In all 3 diagrams the results for the active channels are identical because the algorithm does not affect the signal parts.

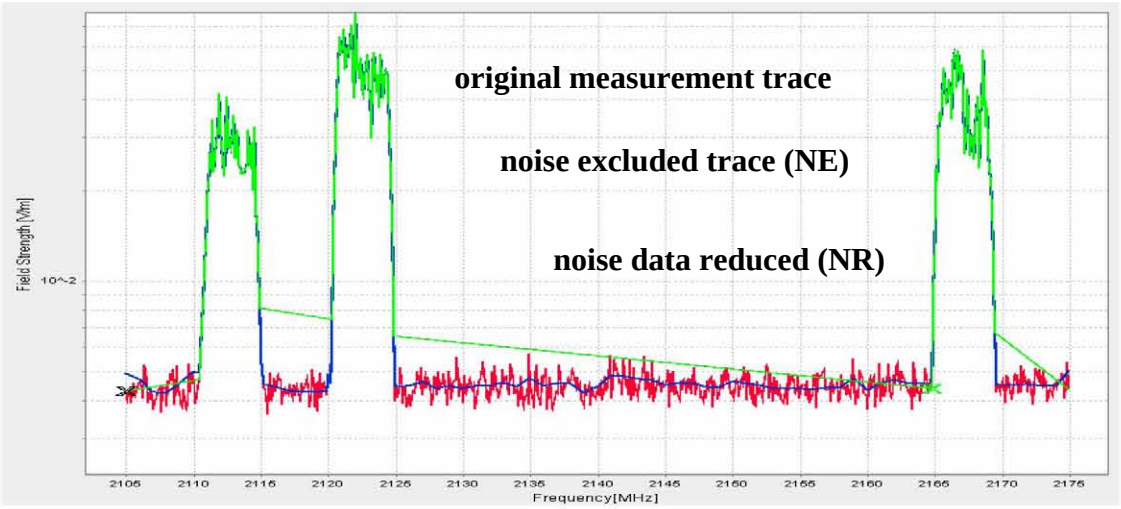


Figure 5: UMTS-DL traces after noise data reduction

Also the results of the other channels, representing the noise power, are very similar for the original trace and the noise data reduced trace. However for the trace without any noise points the evaluation result for inactive bands is zero. Therefore the presented algorithm enables the user to add only the power of measured signals to yield in fact EMF-field strength evaluation results without any disturbing noise contributes.

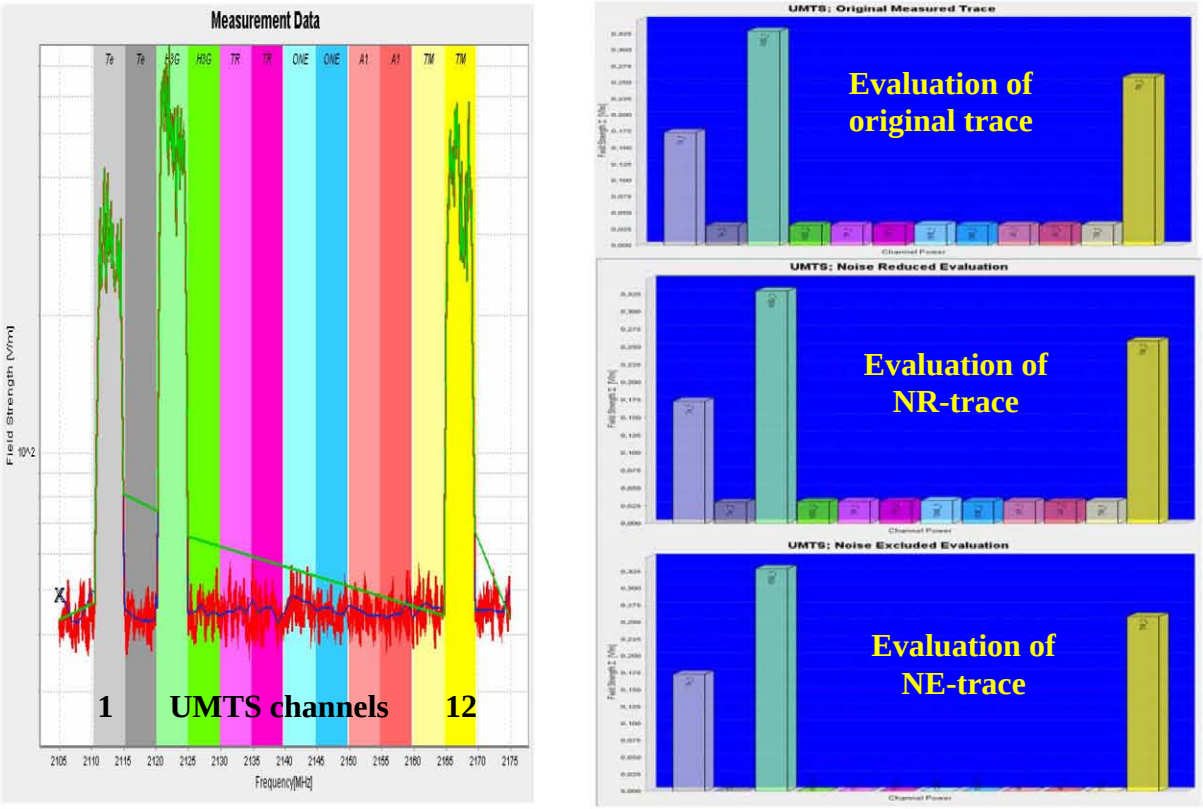


Figure 6: UMTS-DL traces and corresponding channel selective evaluation results

V. Results

Figure 7 is showing 4 original measurement traces and the noise excluded traces after implementation of the algorithm to the original measurement traces. At the top there are typical GSM900-DL measurements performed from 930 MHz to 960 MHz. The left one was made in the rural environment at Seibersdorf and the right during an EMC-exhibition at Stuttgart in 2005. Below them there are 2 of the overview measurements corresponding to

the measurements described in Figure 3. The left one is again from Seibersdorf and the other one from the centre of Vienna. These 4 pictures are showing typical traces which are used to investigate the efficiency in data reduction of the presented algorithm. The results are given in Table 1 for one, ten and fifty similar measurement traces (repetitions) for each of the 4 signal groups.

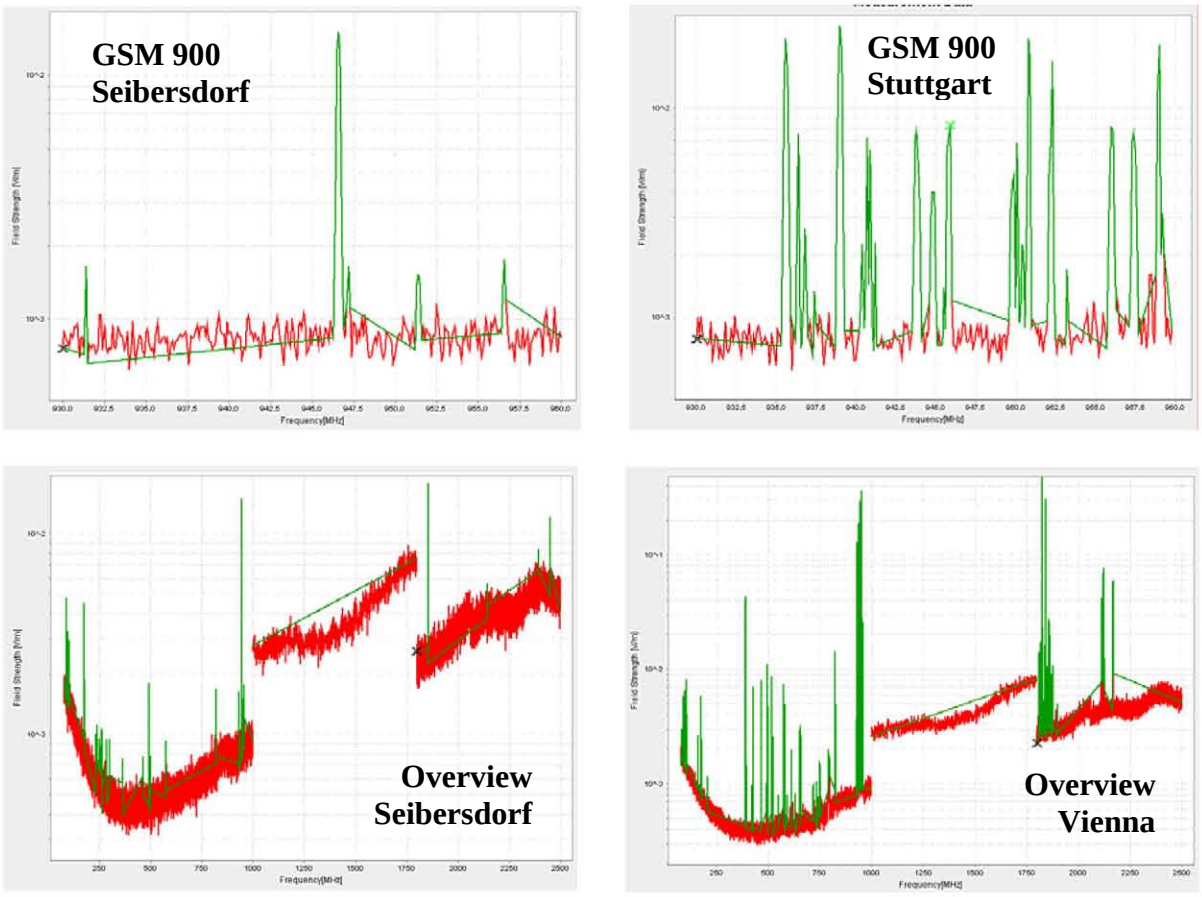


Figure 7: Example traces for the evaluation of Table 1

The values given in percentage are relating to the original measurement traces and give the amount of needed disk space after data reduction. That means a number of 30 % corresponds with a data reduction of 70 %. For the original measured traces the necessary disc space to save the measurement including all settings, factors and other useful information is given in kByte.

	Signal Group	GSM 900; Seibersdorf	GSM 900; Stuttgart	Overview; Vienna	Overview; Seibersdorf
1 Trace	Original Sig. [kB]	9	9	178	178
	NR [% of the original sig.]	77,8	77,8	19,7	14,6
	NE [% of the original sig.]	66,7	77,8	8,4	3,9
10 Traces	Original Sig. [kB]	34	34	1721	1721
	NR [% of the original sig.]	52,9	61,8	12,9	12,3
	NE [% of the original sig.]	32,4	44,1	1,8	1,6
50 Traces	Original Sig. [kB]	140	140	8515	8515
	NR [% of the original sig.]	54,3	59,3	12,3	12,1
	NE [% of the original sig.]	32,9	37,9	1,6	1,5

Table 1: Efficiency of the data reduction algorithm (Noise Height factor = 5dB and 90 % Reduction Value)

As expected the best results are given for overview measurements in a rural environment like Seibersdorf. There are only a few signals present and the noise reduction is very efficient with up to 87,9 % data reduction for the noise data reduced traces and up to 98,5 % for the noise excluded traces at 50 repetitions. That means that the needed disc space is reduced from about 8.5 MByte to less than 130 kByte. This is a data amount which can be processed easily within short time by computers. Also for the noise excluded wideband trace performed in the city of Vienna the reduction is quite similar with 1.6 % of remaining data instead of 1.5 % like Seibersdorf. For the scenario of 288 wideband traces during one day as assumed in chapter III including the evaluation problematic for frequency selective measurements, a total disc space of about 620 kByte would be generated if the presented algorithm is used. This data amount is still not a large problem to process at modern PCs and therefore in fact this algorithm supports frequency selective EMF-measurement systems to overcome the problematic of time delay caused by too much data generation. For a single overview trace the efficiency of the data reduction is a little bit less because of the data overhead necessary for each measurement job independent of its number of repetitions but with about 80 % to 95 % still excellent. For the GSM900 evaluations the reduction of data is from about 22 % for noise reduced signals for one single trace up to 77 % at the 50 noise excluded traces for the GSM900 band at Seibersdorf, but the absolute amount of data is much less than for the overview measurements and therefore not a problem in processing. In addition to that it is a big advantage of the algorithm too, that it is working automatically as a selector to differ between the existing signals and noise, which is not of interest. Only pure signal information is kept in opposite to other methods like band-selective methods or by wideband measurements using field probes where signal and noise is mixed without any possibility for differentiation.

VI. Conclusion

Recapitulating it was found that especially for wideband measurements with a lot of repetitions the presented algorithm has its best efficiency with typically more than 98 % of data reduction for the investigated traces and measurement settings. This enables frequency-selective measurements for sophisticated single investigations on site as well as for long-therm monitoring e.g. for dosimetry studies. Caused by the fact that the data reduction algorithm can automatically be applied in real-time to the measured data and it is not specific for any spectrum analyser, it could be used generally for data reduction purposes. Another big advantage of that data reduction process is the differentiation between signal and noise. This enables the user to define the pure signal power for EMF-evaluation instead of a mixture of signal and noise contributes. Furthermore the frequency selective measurement method is still the most sensitive procedure which allows best isotropic behaviour, sharp frequency differentiation and accurate uncertainty estimation. Drawbacks of those systems are the relatively high cost, large mechanical dimension of the some equipment and typically the engineer needs measurement expertise and experience to perform well suited settings that the advantages of frequency selective systems could be utilized.

References

[1] ICNIRP: "Guidelines for limiting exposure to time-varying electric, magnetic, and electromagnetic fields.", Health Physics 74 (4), pp 494 – 522, 1998.

[2] W. Müllner, G. Neubauer, H. Haider: "Add3D, a new technique for precise power flux density measurements at mobile communications base stations", 10. Internationale Fachmesse und Kongress für EMV, Düsseldorf, pp 305–312, 2002

[3] Neubauer, G.; Röösli, M.; Feychting, M.; Hamnerius, Y.; Kheifets, L.; Kuster, N.; Ruiz, I.; Schüz, J.; Wiart: „Feasibility of future epidemiological studies on possible health effects of mobile phone base stations", Platform Presentation at the BioEM 2005 (joint meeting of the Bioelectromagnetics Society and the European BioElectromagnetics Association), June 20.-24., 2005, Dublin, Ireland, Abstract Book pp. 102-103.

Long term effects of microwaves from GSM mobile phones on the rat brain

Jacob L. Eberhardt[1], Bertil R.R. Persson[1], Arne Brun[2], Lars Malmgren[4], Gustav Grafstrom[1], and Leif G. Salford[3]

Department of Radiation Physics[1], Neuropathology[2], Neurosurgery[3] and The MAX-lab national facility[4], University of Lund, Lund, Sweden.

1. INTRODUCTION

Our group has since 1988 studied the effects of different intensities and modulations of 915 MHz RF in a rat model. In series of more than 1600 animals, we have proven that subthermal energies from both pulse-modulated and continuous RF fields including those from real GSM mobile phones - have the potency to significantly open the BBB
for the animals own albumin (but not fibrinogen) to pass out into the brain and to accumulate in the neurons and glial cells surrounding the capillaries. These results are duplicated recently in another laboratory [1]. Similar results are found by others [2]. In a recent study, we found signs of neuronal damage in the rat 28 and 50 days after a 2 hours exposure for GSM microwaves at 900 MHz with SAR < 0.2 W/kg [3,4].

2. OBJECTIVE

To investigate in the rat the occurrence behavioral changes, leakage of the blood-brain barrier and of neuronal damage after a one year period of weekly 2 hour exposures to radiation from a GSM mobile phone at different intensities.

3. METHODS

48 male and female Fischer 344 rats were exposed or sham exposed for two hours once a week for 55 weeks in TEM-cells to radiation from a software programmable GSM-900 mobile telephone. The animals were awake during the exposure and could move and turn within the exposure chamber. The peak output power fed into the TEM cells were 5 or 500 mW, resulting into average whole body specific absorption rates of 1 or 100 mW/kg. A further 8 animals served as cage controls: The latter stayed ndisturbed in the animal facility during the whole period of the investigation. 3 weeks after the last exposure, all animals were subjected to two different behavioral test: (i) the Open Field
test for testing exploratory and motor behavior as well as anxiety, and (ii) the Episodic-like memory task for testing episodic memory and novelty preference [6]. After the behavioral testing period, the animals were anaesthetized and sacrificed by perfusion-fixation with 4% formaldehyde. Brain slices were stained for RNA/DNA with cresyl violet and HSP70 for heat shock protein. Applying albumin antibodies (Dakopatts), albumin in the brain tissue and albumin uptake into neurons is revealed.

4. ANALYSIS and RESULTS

The occurrence of blood-brain barrier leakage and damaged (dark) neurons in different parts of the brain were judged semi-quantitatively by the neuropathologist. No increased number of albumin foci or dark neurons were found in exposed animals as compared to sham-exposed. The Open Field test revealed no effect of exposure on exploratory and motor behavior. The episodic memory test revealed worse short-term memory for exposed animals as compared to sham exposed animals.

A grant from the Swedish Council for Working Life and Social Research is gratefully aknowledged.

1. F Tore, P-E Dulou, E Haro, B Veyret, P Aubineau. Two-hour exposure to 2 W/kg, 900 MHz GSM microwaves induces plasma protein extravasation in rat brain. In: Proceedings from the 5th International Congress of the European Bioelectromagnetics Association. (M Hietanen, K Jokela, J Juutilainen, eds) 2001, pp 43-45.

2. K Fritze, C Sommer, B Schmitz, G Mies, K Hossman, M Kiessling, et al. Effect of global system for mobile communication (GSM) microwave exposure on blood-brain barrier permeability in rat. Acta Neuropathology (Berlin) 1997, 94, pp 465-470.

3. LG Salford, AE Brun, JL Eberhardt, L Malmgren, BRR Persson. Nerve cell damage in mammalian brain after exposure to microwaves from GSM mobile phones. Environmental Health Perspectives, 2003, 11(7), pp 881-883.

4. JL Eberhardt, BRR Persson, LOG Malmgren, AE Brun and LG Salford. Blood-brain barrier permeability and nerve cell damage in the rat brain 14 and 28 days after exposure to microwaves from GSM mobile phones. Manuscript 2006.

5. FA Malek, K-U Moritz, J Fanghanel. Formaldehyd inhalation and open field behavior in rats. Indian Journal of Medical research 2003, 118, pp 90-96.

6. E Dere, JP Huston, MA De Souza Silva. Integrated memory for objects, places, and temporal order: Evidence for episodic-like memory in mice. Neurobiology of Learning and Memory 2005, 84, pp 214-221.

THE TREATMENT OF PERIPHERAL NERVE TRANSECTION INJURY UNDER 50 HZ ELECTRIC FIELD EXPOSURE

*OZLEM ULUKUT

*SELCUK COMLEKCI

**SÜLEYMAN DEMİREL UNIVERSITY, FACULTY OF ENGINEERING, DEPARTMENT OF ELECTRICAL & COMMUNICATIONS ENGINEERING, 32260, ÇÜNÜR, ISPARTA, TURKEY*

e-mail:oulukut@mmf.sdu.edu.tr *e-mail:scom@mmf.sdu.edu.tr*

Abstract

Merely electric field exposure is often occurred by electric transmission lines, electric appliances without current flow. The aim of this study was to investigate the effects of a 50 Hz electric field on peripheral nerve regeneration in rats. The exposure system was based on parallel-plate-capacitor system. Electric field exposure set-up was established for studies on forty male Sprague-Dawley rats. The rats were randomly divided into four groups each containing 10 rats. Four groups examined variables associated with the method and timing of surgical repair, the arrest of Wallerian degeneration, and the role of electric field in functional recovery. Treatment group1, treatment group 2 and treatment group 3 were subjected to electric fields of 10 kV/m strengths. Control group were subjected to the same procedure, but with the device not activated. The ambient temperature and relative humidity percent of the room housing this facility were maintained at 24 ± 2 °C and 55 ± 5 respectively. Standard poly-carbonate animal cages with PVC lids were kept between the parallel plates producing vertical component of electric field for exposing the animals. The duration of exposure of rat was 1 months. Treatment group1, treatment group 2 and treatment group 3 showed that a vein-graft conduit did not improve functional recovery compared with standard epineurial repair. Also, delayed repair compared favorably with immediate repair.

Key words: Electric field, parallel plate, peripheral nerve regeneration

Introduction

Extremely low frequency (ELF) electric field (EF) and electromagnetic field (EMF) were demonstrated to affect biological systems in vitro and in vivo [World Health Organization, 1984]. Unlike the ionizing radiation and radiofrequency waves, the energy transferred to the biological tissues by the ELF fields is no significant. Some biological processes may be more sensitive than others to ELF EMFs resulting in measurable outcomes.

Weak DC EF was applied to accelerate nerve regeneration following different peripheral nerve injury models [Politis et al., 1988; Kerns et al., 1991; Kerns and Lucchinetti, 1992]. Pulsed electromagnetic field (PEMF), as a non-invasive modality was also effective in enhancing nerve regeneration [Ito and Bassett, 1983; Orgel et al., 1984; Sisken et al., 1989; Walker et al., 1994].

The sinusoidal AC magnetic field was found to accelerate nerve regeneration following a crush injury [Rusovan and Kanje, 1991]. To our knowledge, how ELF EF affects nerve regeneration has not been studied before. Animal studies focused on the magnetic field components, whether they investigate hazards or benefits associated with ELF EMFs. The theoretical background is that the magnetic field is almost unperturbed by tissues as opposed to EFs. Magnetic field is created when electric current flows. EF represents the force that a charge exerts on other charges and a potential difference is sufficient for its presence even when a current does not flow. Pure EFs may have biological effects [Repacholi and Greenebaum, 1999].

Materials and Methods

In this study the experiment was performed on forty young adult, male Sprague–Dawley rats weighing 180–240 g. The study was approved by the Institutional Review for Animal Research Board of SDU and conducted in accordance with the institutional guidelines. The rats were randomly divided into four groups each containing 10 rats. Four groups examined variables associated with the method and timing of surgical repair, the arrest of wallerian degeneration, and the role of electric field in functional recovery. Treatment group1, treatment group 2 and treatment group 3 were subjected to electric fields of 10 kV/m strengths. Control group were subjected to the same procedure, but with the device not activated. The ambient temperature and relative humidity percent of the room housing this facility were maintained at 24 ± 2 °C and 55 ± 5 respectively. Standard poly-carbonate animal cages with PVC lids were kept between the parallel plates producing vertical component of electric field for exposing the animals. The duration of exposure of rat was 1 months.

Surgical Procedure

The animals were anesthetized by intraperitonel injection of ketamine (90 mg/kg) and xylazine (6mg/kg). By using a surgical microscope common peroneal nerve was isolated through a short lateral thigh incision on the left side. Two centimeters proximal to its entrance into the lateral crural compartment, peroneal nerve was crushed twice with a no. 3 jeweler's forceps for 30 s, so that only a transparency of the neural sheath was seen at the injury site.

Electric Field Application Set Up

The theory of EF between the plates of parallel plate capacitors was utilized for EF exposure settings [Lorrain and Corson, 1970]. The setup was schematically illustrated in Figure 1. The EF strength was calculated according to the equation E=V/d where V is electric potential between the plates, d is the distance, and E is the EF intensity in volt/meter. Plates were made of a perfect conductor for free charges to disperse homogenously in order to produce uniform EFs. Zinc plated tin sheets of 2 mm thickness were selected for this purpose. Plates of 50X100 cm in dimension were cut out of them and perfectly flattened. The corners were rounded to get rid of corruptions due to end effect. They were placed upright on wooden stands and positioned parallel to each other. In order not to disturb the field, leads were connected to the center of the plates on their outer sides.

The plates were spaced at 50 cm in distance. Three ungrounded plastic cages were placed inside as seen in Figure 1. Three or four rats were housed in each cage. Cages were in adequate size to ensure free movement of rats and hence homogenous shielding of each other. In addition to weekly cleanups of the plates and cages, the setups were frequently scrutinized for gross soil and wetness that would disturb the homogeneity of EF. The attenuation due to routine soiling could be estimated to cause very small variation in EF. From the equation above, average EF densities between the plates were calculated to be 5000 V/0.5 m=10000 V/m (10 kV/m) in 50 Hz groups. Max 3000 TRMS Multimeter (Chauvin Arnoux, Paris, France) was used for voltage measurements.

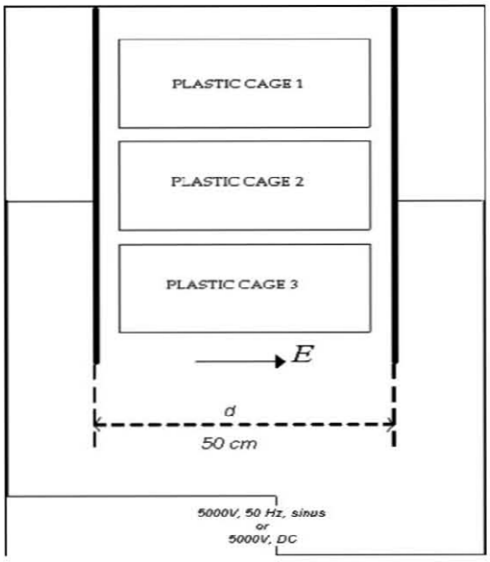


Figure 1. The electric field application set up.

Discussion and Conclusion

International standard commissions (ICNIRP, IEEE) are generally warn about magnetic radiation to public. General consensus that is below 10 kV/m will be harmless. In this study we tried to show that pure electric field was able to affect on a living tissue.

We designed the study to determine whether any changes occur in the rate of nerve regeneration when rats are continuously exposed to strong EFs for 4 weeks following a crush injury. Treatment group1, treatment group 2 and treatment group 3 showed that a vein-graft conduit did not improve functional recovery compared with standard epineurial repair. Also, delayed repair compared favorably with immediate repair. All differences found between the exposure groups of this study were in accordance with lower rates of Wallerian degeneration and nerve regeneration in 50 Hz EF group.

However, their concordance in direction of effect with each other suggests that continuous 50 Hz EF exposure has a weak effect that is detrimental mostly to the rate of early nerve regeneration in a crush injury model. Although the internal EFs induced by 50 Hz EF in this study are estimated to be within the lower limits of endogenous noise. This suggests that electric induction may be required for pure EF effects even though the density of induced fields is not above the endogenous background level.

References

[1] Mustafa Asim Aydin, Selcuk Comlekci, Meltem Ozguner, Gokhan Cesur, Serdar Nasir, Zeynep Dilek Aydin, The influence of continuous exposure to 50 Hz electric field on nerve regeneration in a rat peroneal nerve crush injury model, Bioelectromagnetics, 27:401-413 (2006).

[2] Bassett CA. 1983. Effect of weak, pulsing electromagnetic fields on neural regeneration in the rat. Clin Orthop 181:283–290

[3] Kerns JM, Lucchinetti C. 1992. Electrical field effects on crushed nerve regeneration. Exp Neurol 117:71–80.

[4] Kerns JM, Fakhouri AJ, Weinrib HP, Freeman JA. 1991. Electrical stimulation of nerve regeneration in the rat: The early effects evaluated by a vibrating probe and electron microscopy. Neuroscience 40:93–107.

[5] Lorrain P, Corson D. 1970. Chapter 2: Electrostatic fields. In: Lorrain P, Carson D, editors. Electromagnetic fields and waves. San Fransisco: WH Freeman and Co. pp 40–84.

[6] Politis MJ, ZanakisMF, Albala BJ. 1988. Facilitated regeneration in the rat peripheral nervous system using applied electric fields. J Trauma 28:1375–1381.

[7] Repacholi MH, Greenebaum B. 1999. Interaction of static and extremely low frequency electric and magnetic fields with living systems: Health effects and research needs. Bioelectromagnetics 20:133–160.

[8] Rusovan A, Kanje M. 1991. Stimulation of regeneration of the rat sciatic nerve by 50 Hz sinusoidal magnetic fields. Exp Neurol 112:312–316.

[9] Orgel MG, O'Brien WJ, Murray HM. 1984. Pulsing electromagnetic field therapy in nerve regeneration: An experimental study in the cat. Plast Reconstr Surg 73:173– 183.

[10] Sisken BF, Kanje M, Lundborg G, Herbst E, Kurtz W. 1989. Stimulation of rat sciatic nerve regeneration with pulsed electromagnetic fields. Brain Res 485:309–316.

[11] Walker JL, Evans JM, Resig P, Guarnieri S, Meade P, Sisken BS. 1994. Enhancement of functional recovery following a crush lesion to the rat sciatic nerve by exposure to pulsed electromagnetic fields. Exp Neurol 125:302– 305.

[12] World Health Organization. 1984. Environmental heath criteria 35: Extremely low frequency (ELF) fields. Geneva.

The influence of Pulsed Magnetic Fields (PMF) on the synaptic transmission and on the action potential in the mouse nervous system.

Zaghloul Ahmed[2] and Andrzej Wieraszko [1,2],

[1]Department of Biology/CSI/IBR Center for Developmental Neuroscience, The College of Staten Island, City University of New York, [2] Ph.D. Program in Biology, The Graduate School and University Center of NY, New York.

Abstract

We demonstrated previously that exposure of brain tissue to pulsed magnetic fields (PMF) significantly amplified the magnitude of the evoked potentials. Either increase in the amplitude of the action potential, or amplification of the synaptic efficiency could explain observed results. Further investigation revealed, that Paired Pulse Facilitation (PPF), a form of synaptic plasticity observed in the central nervous system was significantly modified by the exposure to PMFs. Although these results pointed at the synapse, as the site of PMF action, the enhancement of an antidromically evoked potentials, recorded from hippocampal slices implied, that PMF can influence nonsynaptic mechanisms as well. This assumption was supported by PMF-induced amplification of the action potential recorded from isolated, peripheral mouse nerve in vitro. It has been determined, that PMF reduced the axonal threshold, making nerves more excitable. Additional studies demonstrated, that the action of PMF is exerted by modifying the action of ion channels, responsible for synaptic transmission and generation of an action potential. The action of PMF was very specific and related to their frequency.

Introduction.

Our previous investigation revealed that Pulsed Magnetic Fields (PMFs) increased neuronal activity recorded from mouse hippocampal slices (Wieraszko et al., 2005). The enhancement in the activity of the nerve cells was expressed as an increase in the amplitude of electrophysiologically recorded evoked potentials (Wieraszko, 2004), which was correlated with an enhancement of the release of neurotransmitter (glutamate) (Wieraszko et al., 200), and an elevation in the concentration of the second messenger, cAMP (Hogan and Wieraszko, 2004).

The intensity of neuronal activity was measured as the amplitude of the population spike (PS), which represents synchronized firing of the pyramidal neurons **(**Andersen et al., 1971). While the population spike illustrates synaptic activation of neurons, it has to be preceded by the action potential generated non-synaptically. The diagram in Fig 1 shows the sequence of these events. Presynaptic action potential, induced by stimulating electrodes (S), propagates towards the end of the axon and initiates the release of the neurotransmitter (glutamate in our preparation) at the presynaptic terminal (Pre). The neurotransmitter released from the presynaptic part stimulates the postsynaptic part (Post), generating population spike (potential # 3). The same stimulation can also generate the action potential, which will propagate toward the cell body of neuron A initiating antidromically evoked potential # 1. No synaptic transmission is involved in generation of this potential. Therefore, the influence of PMF on both: 1) the presynaptic mechanism of generation of an action potential and, 2) synaptically mediated mechanism of generation of the population spike may contribute to the PMF-induced modifications of the amplitude of the population spike. The purpose of the current research was to evaluate the contribution of the presynaptic and postsynaptic mechanisms in modulation of the population spike by PMF.

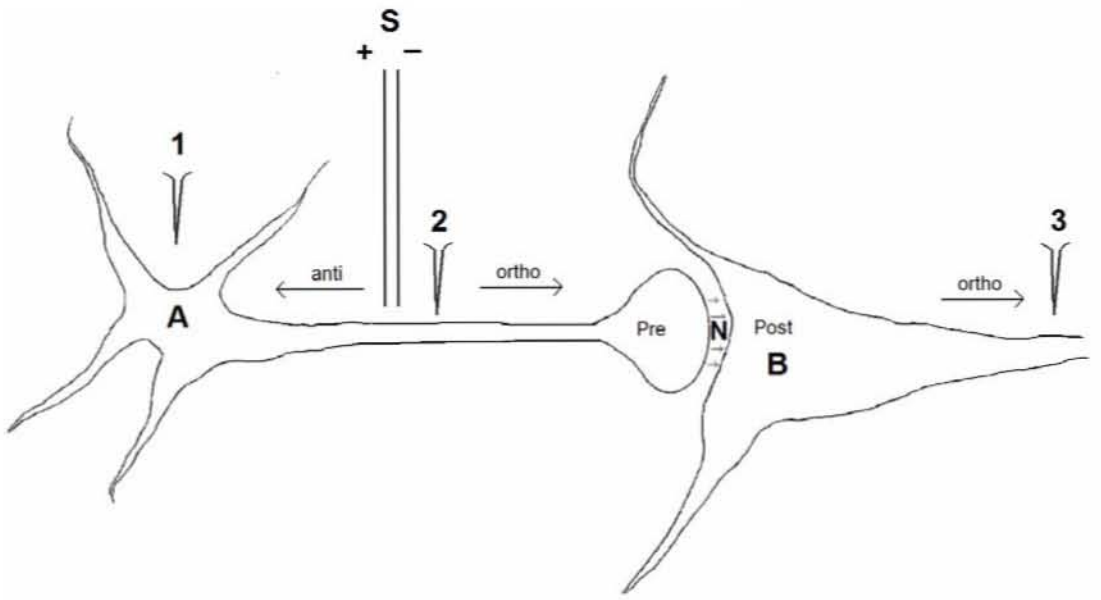


Fig1. The diagram of neuronal activities recorded in the experiments on hippocampal slices. Stimulating electrode (S) initiates the generation and orthodromic propagation of an action potential # 2. This potential reaches the nerve terminal (Pre) stimulating the release of neurotransmitter (N), which activates postsynaptic part initiating generation of the population spike (potential # 3) in neuron B. Thus, the population spike (potential # 3) is generated, as a result of presynaptic and postsynaptic activities. The action potential initiated by stimulating electrode (S) can also propagate towards the cell body of neuron A (antidromic stimulation) generating an action potential # 1. This potential is generated without the involvement of synaptic transmission.

While the mouse hippocampal slices were used to evaluate the involvement of presynaptic and postsynaptic mechanisms, the segments of the mouse sciatic nerve were used to verify the results related to presynaptic component.

Methods

The biological preparation (hippocampal slices, or segments of sciatic nerve) have been incubated in a chamber shown in Fig 2, and exposed to pulsed magnetic fields for 30 minutes. The evoked, neuronal activity of the preparation was followed before, during and after exposure to PMF.

PMF exposure

The pulsed magnetic field (PMF) was generated by DC-powered coils (Trabulsi et al., 1996; Wieraszko, 2004), wound around an acrylic frame, which surrounded the interface-recording chamber. The activation and deactivation of the coils was operated by a programmable timer, which was set at different frequencies to meet the goal of the specific experiment. A plastic tube connected to the building air supply secured the flow of the air indicated by arrows E. The flow of air prevents the water chamber from overheating during electromagnetic field activation (Trabulsi et al., 1996; Wieraszko, 2004) (Fig 2). Regardless of the frequency of the pulsed magnetic field, each pulse has four phases: rising phase (period of coils charging), static magnetic field phase (period of no change; the power supply on), falling phase (period of coils discharging), and then an “off” phase (power supply off), (Fig 3 and 4). The duration of the rising and falling phases (measured as shown in Fig 4) was equal for all frequencies generated by our magnetic field setup; however, the number of these phases is substantially different for different frequencies. Unless specified otherwise, the frequency that was used was 0.16 Hz. The same field was used for hippocampal slices and for sciatic nerve preparation. The one "on" and "off" period was considered as one cycle and the frequency of magnetic field stimulation was expressed as number of these cycles per second (Fig 3). The graph in Fig 3 shows magnetic field pulse recorded on-line for the

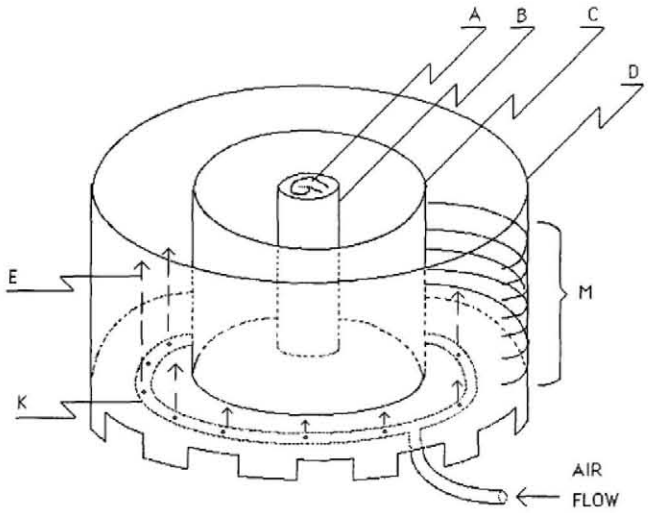


Fig. 2. A diagram of the experimental system. The slice (A) is placed in the chamber (B) that is filled with Ringer's solution and oxygenated with 95%/5% O2/CO2. The water chamber (C) contains the temperature sensor (H) and the oxygenating airflow. The magnetic coil (M) encircled the acrylic frame (D). During the magnetic field application, airflow circulating through a holed tube (K) is turned on, creating an air flow (E) to dissipate any accumulated heat. (According to Wieraszko, 2004).

period of thirty minutes. Neither change in the PMF strength nor shape was observed. A, B and C show on-line PMF recording for 4 minutes in the beginning, middle, and at the end of thirty minute period.

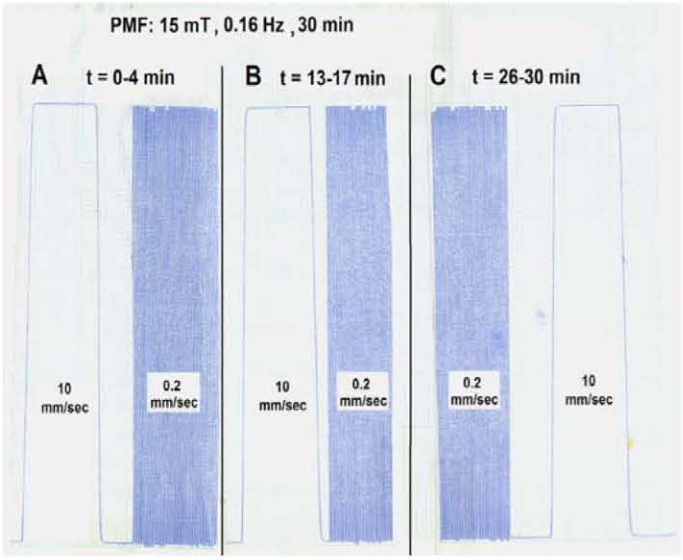


Fig. 3. Thirty minutes of PMF recording. This graph shows - on line - magnetic field pulse recording for the period of 30 minutes that illustrates neither change in the PMF strength nor shape. A, B and C show on-line PMF recording for 4 minutes in the beginning, middle, and at the end of 30 minutes.

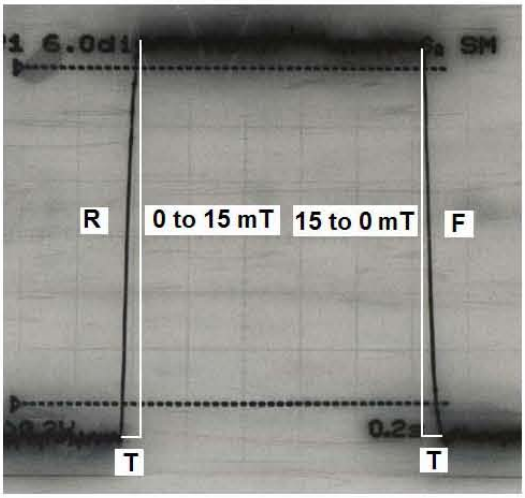


Fig. 4. A photograph of the PMF pulse taken from oscilloscope screen. It shows the rising (R), and falling phases (F). The white vertical lines and horizontal lines (T) were drawn to calculate the slope of the rising and falling phases of magnetic pulse (black trace). The duration of the "on" phase, and the intensity of the field shown on this photograph is 3 sec. and 15 mT, respectively.

Results

A. The influence of PMF on synaptic and nonsynaptic component of neuronal activity tested on hippocampal slices.

The hippocampal slices were prepared from CD-1 strain of mice, as described previously (Wieraszko,

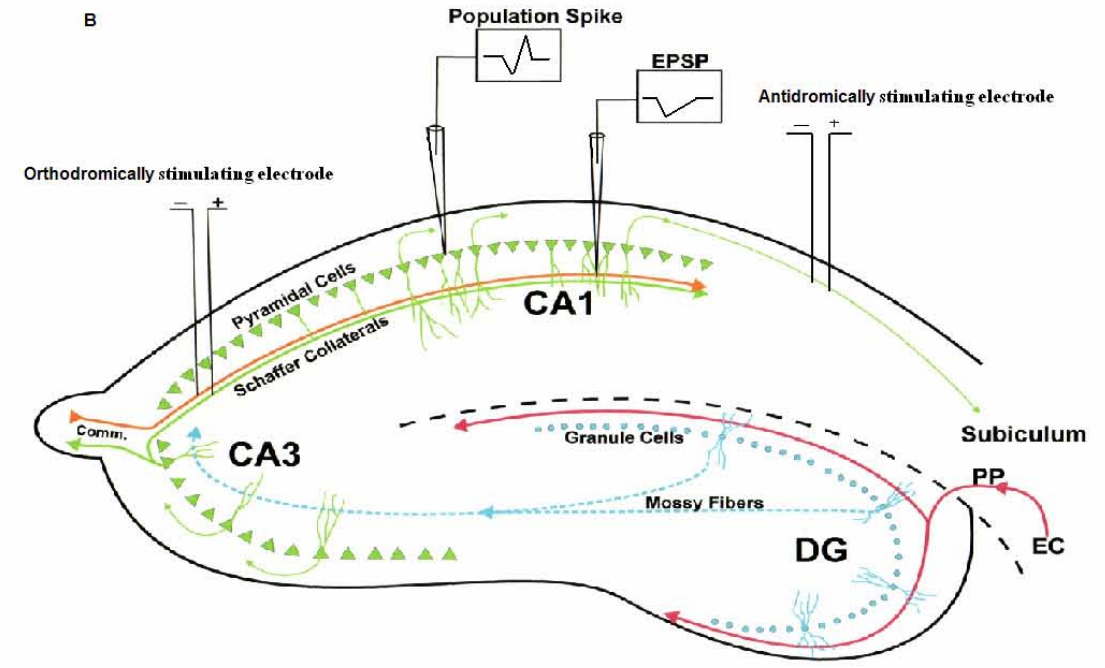


Fig. 5. Hippocampal pathways and recording of their activities. The diagram shows the hippocampal pathways and the location of stimulating and recording electrodes. The electrode stimulating orthodromically is located in CA3 hippocampal subfield. When activated, it evokes the action potential, which propagates towards CA1. This action potential, in turn, synoptically activates CA1 pyramidal neurons, which generate population spike. Pyramidal neurons can be also stimulated nonsynaptically with antidromically stimulating electrode.

1983). The diagram of the cross-section of the hippocampus is depicted in Fig 5. The population spike can be evoked by either orthodromic stimulation of the Schaffer collateral and then recording from the CA1 pyramidal cell layer (this involves synaptic transmission), or by the antidromic stimulation, which is defined as the stimulation of the axonal area of the CA1 and recording from CA1 pyramidal cell layer (it does not involve synaptic transmission). See also Fig 1 for further explanation.

A.1. Effects of PMF on paired pulse facilitation (PPF)

Our previous experiments (Wieraszko, 2004) demonstrated a PMF induced increase in the magnitude of the population spike evoked by single-pulse electrical stimulation applied at the frequency of 0.16 Hz. To analyze this phenomenon further we applied paired-pulse stimulation paradigm, which is considered a good indicator of the changes in the mechanism of orthodromically induced synaptic processes of the neurotransmitter release. Two pulses, separated by the interstimulus interval of 15-55 ms were applied with the frequency of 0.16 Hz to evoke two population spikes. Paired-Pulse Facilitation (PPF) was expressed as an increase in the magnitude of the second population spike as compared to the first one. PPF was calculated as the difference in amplitude between the first population spike (PS1) and the second population spike (PS2). An increase in the second population spike relative to the first will produce higher PPF. The expression of PPF as the difference rather than the ratio has been chosen, since PMF increased both PS1 and PS2 (Fig 6). The experiment was initiated by recording of the PS for 20 minutes prior the exposure to PMF (baseline). The average of the PPF measurements that were calculated from the baseline period was compared to the averages taken from the recordings after the exposure to PMF. The result of ten experiments showed significant increase in PPF after the PMF exposure (n=10, 150 %, p=0.000317, paired sample t test was used). Note, that although the magnitude of both population spikes increased following PMF exposure, the facilitation of the second one exceeded the facilitation of the first (Fig 6).

Statistical analysis revealed, that there was no correlation between initial PPF and the change in the amplification of PPF. Therefore we assumed, that the amplification of PPF was not due to PMF-

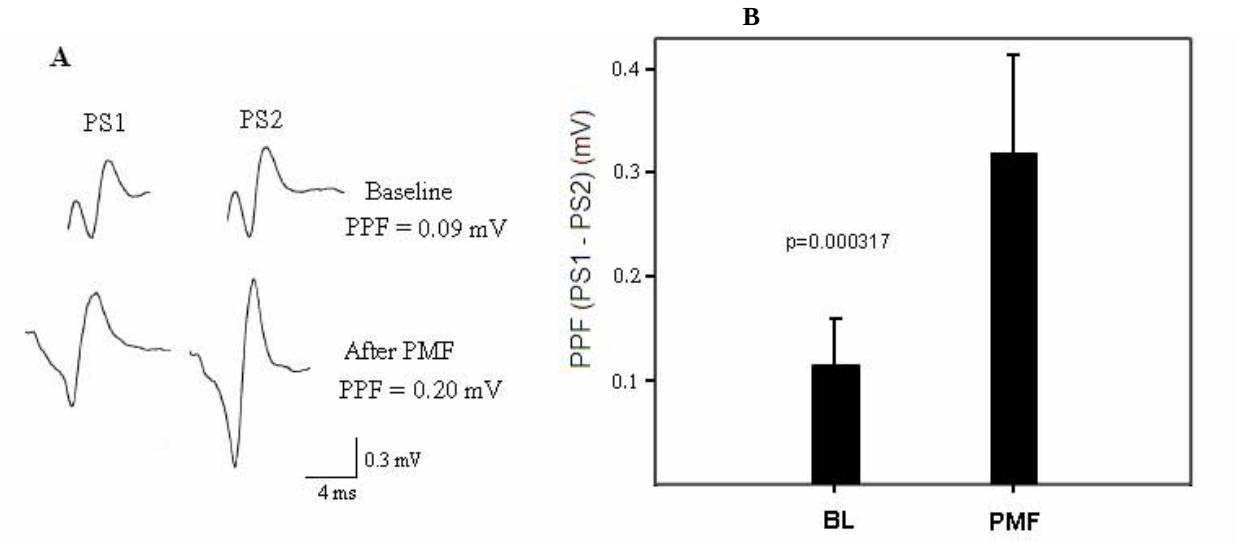


Fig. 6.The influence of PMF on paired pulsed facilitation. A - Potentials marked PS1 and PS2 correspond to the first and second evoked potentials, respectively and were initiated by two consecutive pulses applied with a frequency of 0.16 Hz; inter pulse intervals (IPI) was adjusted accordingly to get the largest PPF (25 – 55 ms). The PPF was calculated as PS2 minus PS1. The upper and lower potentials represent potentials that were recorded during the baseline and after the PMF exposure, respectively. PPF was increased by about 120% after the exposure to PMF. Note, that both PS1 and PS2 increased after exposure. B - the average changes in PPF after the exposure to PMF applied at the frequency of 0.16 Hz (n = 11). The baseline bar (BL) represents the average of PPF from the first 10 - 15 minutes before the application of PMF. The PMF bar represents the average of PPF during maximal effect of PMF amplification. The result of the paired t test is shown in the graph.

induced increase in the number of firing neurons, but due to an increase in the excitability of the same population of neurons, which were active before PMF exposure.

A.2. The effect of PMF on antidromically evoked population spike in the hippocampal slices

To inquire into the mechanisms of PMF, we considered an experimental paradigm that would express the action potential without concomitant involvement from synaptic transmission. Stimulating the hippocampal pyramidal cell layer CA1 with antidromic stimulus (stimulating electrode on the subiculum,

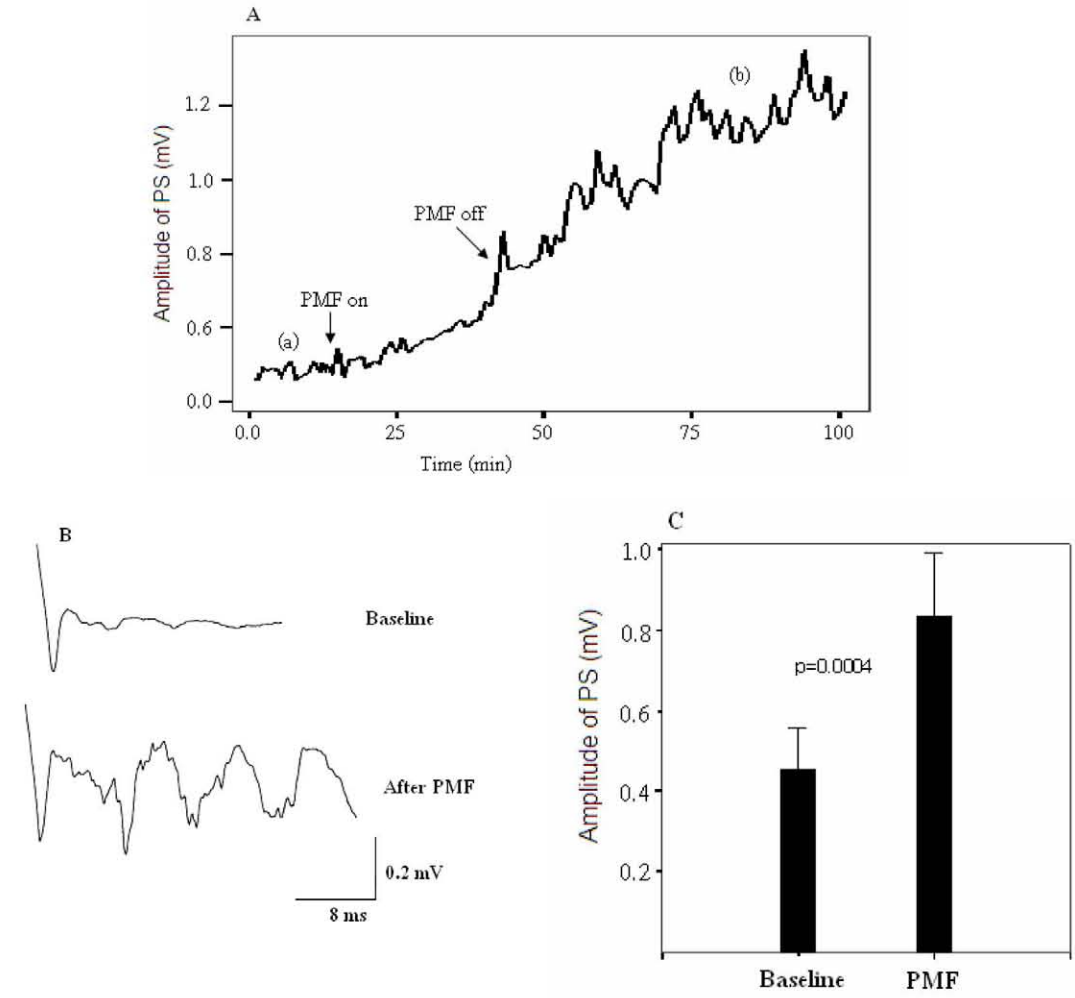


Fig.7. The effect of PMF on the antidromically evoked population spike. The slices were incubated in a calcium free medium and with 2mM kynurenic acid. A – a representative experiment showing the amplitude of the population spikes before (a) and after (b) the application of PMF. B – A waveform that shows the potential amplitude before and after PMF exposure; note the generation of multiple potentials . C – Average results of baseline and at maximal PMF effect (n = 15, p = 0.0004). Paired t test was used.

recording electrode on the pyramidal cell layer CA1) (Fig. 1 and 2) would induce pre-synaptic action potentials only. The addition of kynurenic acid (a blocker of glutamergic receptors) to the slice containing chamber and the omission of calcium would eliminate any contribution of glutamergic synaptic transmission to either the initiation or size of recorded potentials. Fifteen experiments on 15 different slices taken from 5 animals were performed. The potentials were recorded for 20 minutes to create a stable baseline, and then a PMF of 0.16 Hz was turned on for 30 minutes. Averages from the baseline and at the maximal effect of PMF (20 potentials) were compared. The PMF has not only

increased significantly the size of population spikes (n=15, 183.3%, p=0.0004, Fig 7A, B) but also induced multiple firings and seizure like activity (Fig 7 B). There was no correlation between the amplitude of the baseline and the amplitude of the change (the PS amplitude after PMF exposure minus the PS amplitude of baseline) after the exposure to PMF. That means that the effect of PMF was independent of the amplitude of the initial population spike.

B. The influence of PMF on the action potential recorded from the sciatic nerve.

CD-1 strain of mice was used to prepare segments of sciatic nerve. Following decapitation both hind limbs were skinned. The upper thigh muscles were then cut and either the femoral bone was broken or the hip joint was dislocated. The broken limb was pulled away and muscle tissue of the thigh were cut to expose the sciatic nerve from its origin in the vertebral column. The two ends of the sciatic nerve were cut and the nerve was pulled out and placed in the ice-cold Ringer's solution. The nerve was then cut into 4 to 6 mm segments, which were placed in an incubation chamber maintained at 33^{o}C, and constantly oxygenated with a 5%/95% CO_2/ O_2. The individual segment was transferred in turn into a recording chamber. The epineurium (the outermost layer of connective tissue surrounding the entire peripheral nerve) remained intact. The recording electrode was placed inside the epineurium at the end of the cut and the stimulating electrode was placed out side the epineurium at a distance that was varied to obtain the robust compound action potential (CAP) (Fig 8).

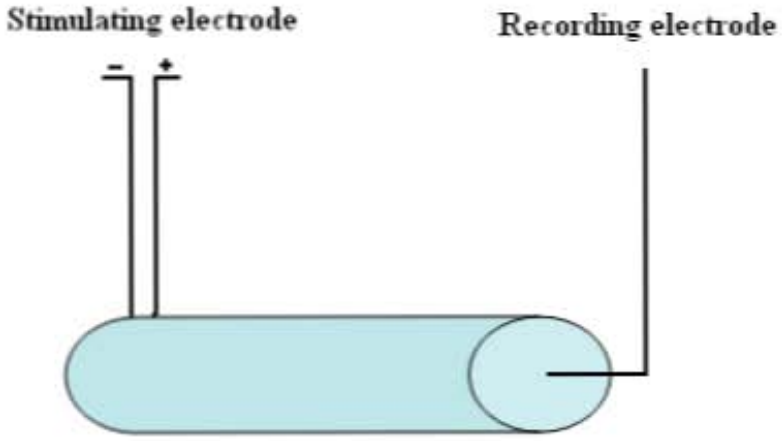


Fig. 8. The placement of the electrodes on a sciatic nerve segment.

B.1. Effects of PMF on compound action potential (CAP)

It can be surmised from the preceding experiments that the PMF effect probably influences the mechanism of action potential through changes in its initiation and propagation. Therefore, we decided to investigate the effect of PMF exposure on the sciatic nerve, which represents simpler preparations without any synaptic connections. The interpretation of the PMF-induced effect could then be circumscribed to the processes responsible for generating, modulating and propagating action potentials.

To investigate the effect of PMF on the compound action potential recorded from the sciatic nerve, 10 experiments were performed. A typical experiment is depicted in Fig 9. The averages of the CAP amplitude recorded in the first 20 minutes (baseline), were compared to the averages of the CAP amplitude recorded 30 minutes after the exposure to PMF. The PMF increased the mean amplitude of the CAP significantly (n=10, 187.1%, p = 0.005, Fig 10). Control experiments revealed, that the amplitude of CAP remained constant for at least 2 hrs, when PMF was not applied. The PMF-induced amplification of the amplitude of the compound action potential occurred independently on electrical stimulation used to induce neuronal activity. When the electrical stimulation was discontinued during PMF exposure, there was still an increase in CAP amplitude (Fig 11).

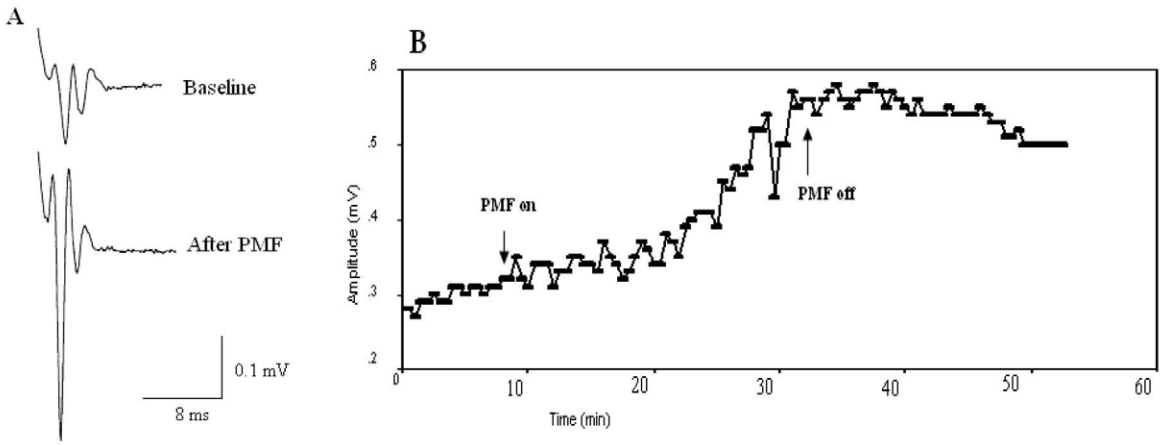


Fig. 9. A representative experiment demonstrating the influence of PMF on CAP. A – The upper and lower potentials represent the CAP before and after PMF exposure, respectively. B – the change in the amplitude of CAP during entire experiment; "PMF on/PMF off" indicates initiation and termination of the magnetic field exposure, respectively.

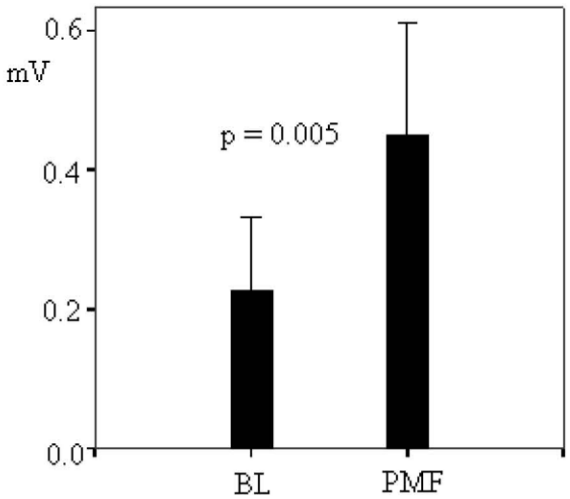


Fig. 10. The influence of PMF on CAP recorded from the sciatic nerve. The bars show the averages of 10 experiments, performed on ten different segments of the sciatic nerve prepared from eight mice. BL refers to the baseline-recording period. The PMF bar represents the recordings at the maximal effect of the PMF. PMF significantly increased the compound action potential (n=10, 187.1%, p = 0.005). Wilcoxon signed ranks test, for 2 related samples was used.

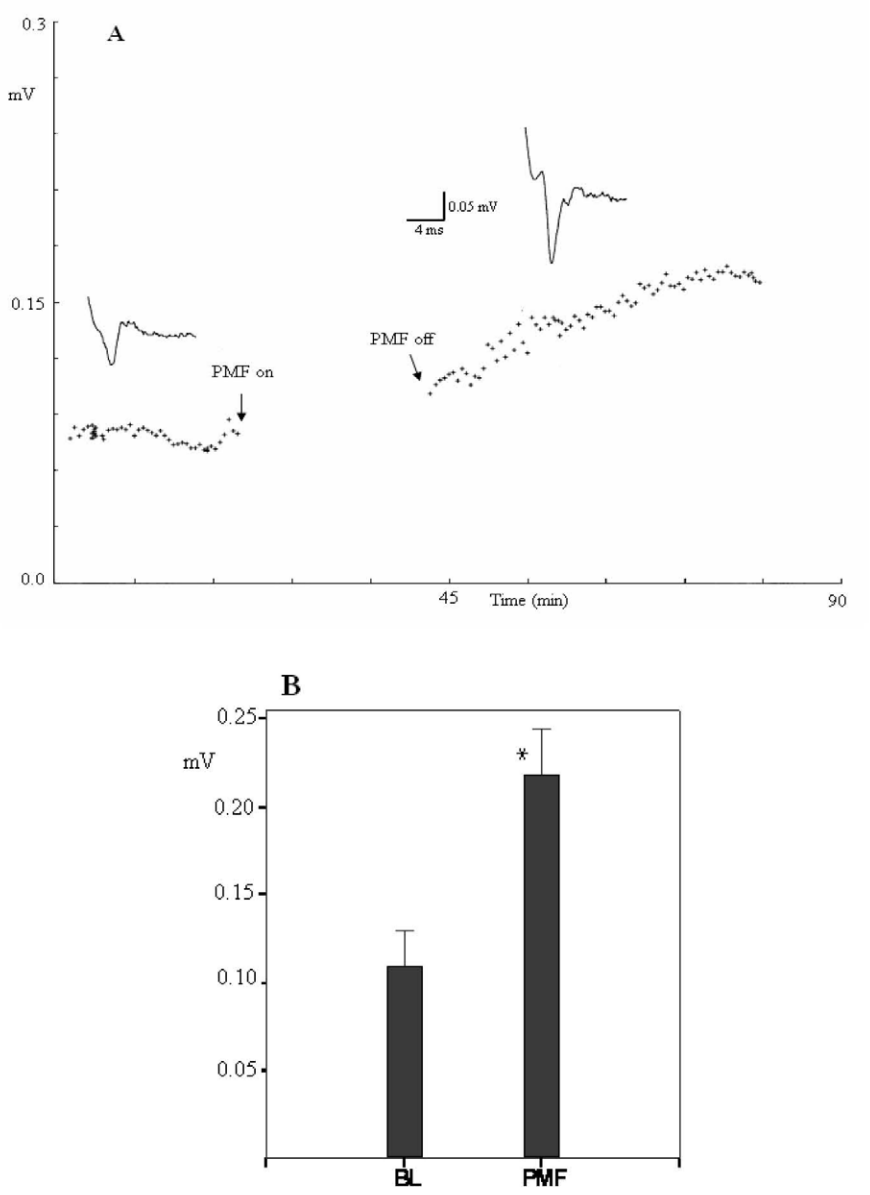


Fig. 11. PMF effect was independent of the concurrent electrical stimulation used to evoke CAP. The recording was followed for 20 minutes and then the electrical stimulation was stopped during the 30 minutes exposure to PMF. After the PMF was turned off, electrical stimulation was resumed and potentials were followed for another 30 minutes. A – An example of a typical experiment: the upper part of the graph represent potentials recorded before and after PMF exposure and the lower part of the graph shows the potential amplitude that was followed throughout the experiment except the period of PMF exposure. Note that during PMF exposure no electrical stimulation was applied and no records of CAP were taken. B – Bars represent the averages that were taken from the baseline period (BL) and at the maximal effect after the PMF exposure (PMF). PMF induced significant increase of the CAP amplitude (n=11, p=0.002, 185.7%, Wilcoxon signed ranks test).

We have also investigated the influence of PMF on the axonal threshold. In most of the experiments, 0.1 V was the lowest strength used to evoke the lowest compound action potential, and for maximal strength one Volt was used. Any stimulus strengths above one Volt were considered supra maximal. During the baseline period of each experiment, one recording was taken at the strength of each stimulus and repeated after the PMF exposure. Note that the same electrical stimulus strength evoked higher CAP amplitude after the PMF exposure. Figure 12 shows that the PMF reduced the threshold

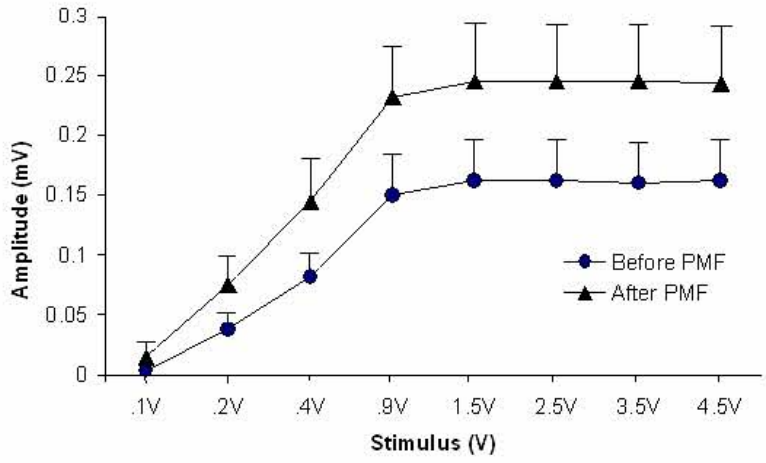


Fig. 12. Effects of PMF on the sciatic nerve threshold. The stimulus strength ranging from 0.1 V to 4.5 V was applied to the sciatic nerve preparation before (● ●) and after (▲ ▲) the exposure to PMF. Eight measurements (one measurement at each value of stimulus strength) were taken from each experiment before PMF exposure (solid circles) and another eight measurements were taken after the PMF exposure (solid triangles). The PMF shifted the threshold curve to the left, which suggests reduction in the axons threshold. That left shift was statistically significant in all stimulus strength values ($p<0.05$, $n=8$) except at 0.1V ($p>0.05$, $n=8$, paired Samples t test). Each point on the graph represents the average of eight experiments.

significantly ($n = 9$, $p<0.05$) in all stimulus strengths except at 0.1 V, where the reduction of the threshold was small and statistically insignificant ($p>0.05$).

B. 2. The effect of PMF on sodium channels

The experiments previously described, suggest that Na^+ and K^+ channels are involved in the mediation of the PMF-induced effect. Therefore the effects of PMF on CAP was studied in the presence of 10nM TTX (a potent sodium channel blocker).

After stable baseline recordings were established, TTX (10nM) was added to the recording chamber. TTX significantly reduced the CAP amplitude ($p = 0.009$, 68.2%, $n = 6$). Fig 13 A and B show a typical experiment and the average of all data, respectively. When the amplitude of the potential stabilized at its minimum value after the addition of TTX (15 - 20 minutes), the PMF was applied for 30 minutes. The depressive effect of TTX was not only eliminated within first 10 minutes of the PMF application, but was reversed to amplification in the later stages of the PMF exposure ($p=0.027$, 80% ± 55%, $n=6$). Figure 13A shows a representative experiment showing the CAP potentials and the change in their amplitudes depicted as the upper and lower parts of the graph, respectively. The bars in figure 13B represent the averages of potentials recorded during three periods of the experiment: 1) baseline (before the addition of TTX and the PMF exposure) marked as (BL); 2) at the maximal of the depressive effect of TTX (TTX) and 3) at the maximal amplification after the PMF exposure (PMF). We have also investigated the effect of the PMF on CAP in the presence of lidocaine, a strong local anesthetic whose action is mediated by the blocking of sodium channel. After stabilization of the potential, lidocaine (150 µM) was added to the recording chamber. It significantly reduced the amplitude of the compound action potential ($p = 0.0005$, $n = 8$). When the amplitude of the potentials stabilized at its minimum value after the addition of lidocaine (15 -20 minutes), the PMF was turned on for thirty minutes. Surprisingly, the

PMF reversed the depressive effect of lidocaine within 7-10 minutes (Fig 14A). The reversal effect of the PMF was significant ($p = 0.0005$, $n = 8$, Fig 14B). Washing away the lidocaine amplified the potential even further ($p = 0.003$, $n = 8$). Figure 14A depicts a typical experiment that shows the potential shape

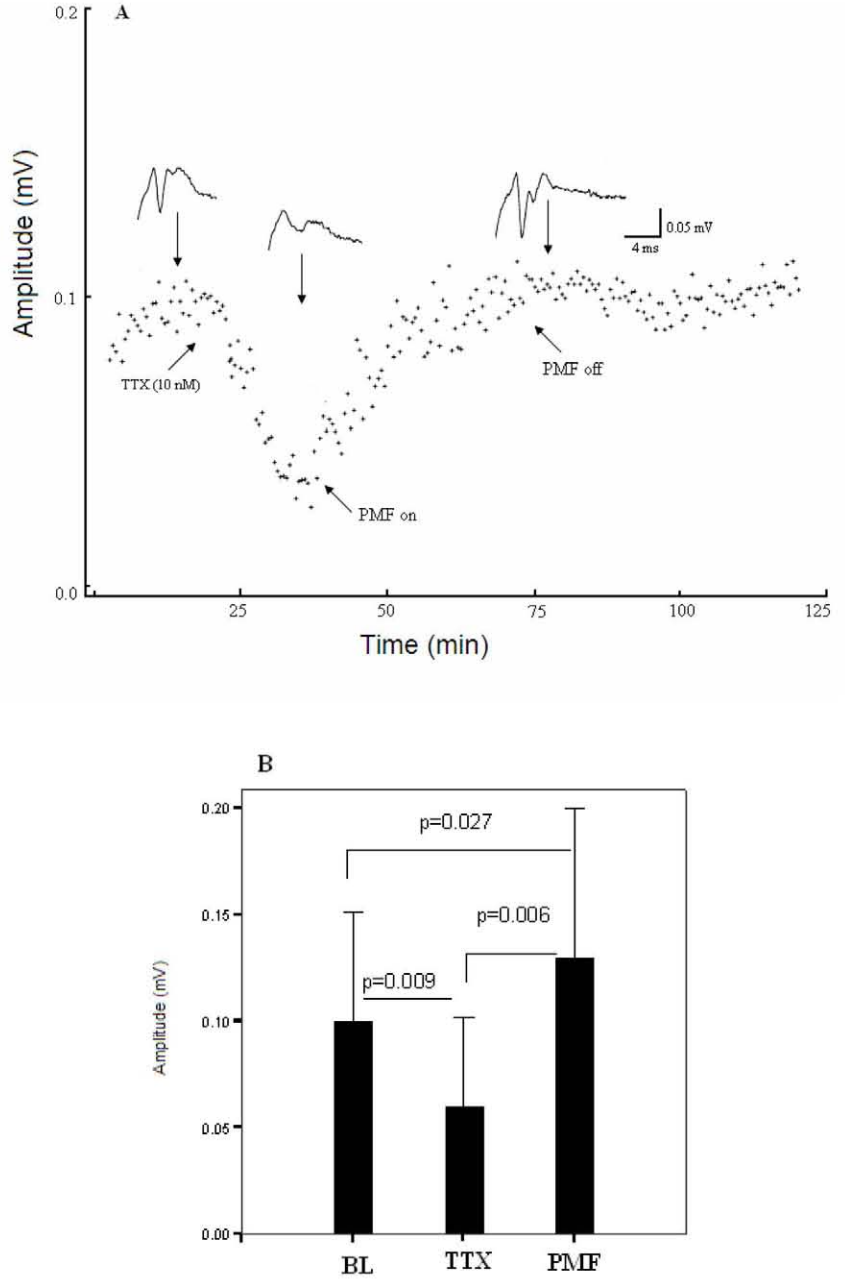


Fig.13. The influence of PMF on TTX-induced depression of CAP. A – A representative experiment. Following 15 minutes of baseline, TTX was added to the recording chamber. TTX reduced the CAP significantly (p=0.009, 68.2%). After the recording in the presence of TTX showed stability, PMF was turned on for 30 minutes. It reversed the TTX-induced depression and in later stage it significantly amplified the potential over the baseline. B - the averages of the potentials recorded during different stages of the experiment: the baseline (BL), after TTX addition (TTX) and after PMF exposure (PMF). PMF significantly reversed the effect of TTX and increased the CAP significantly (p=0.006, 80%, n=6, paired samples t-test).

and amplitude at different periods of the experiment. Bars in Figure 14B represent the average potential for different periods of the experiments.

In control experiments (no PMF) the potential depressed by lidocaine was followed for over an

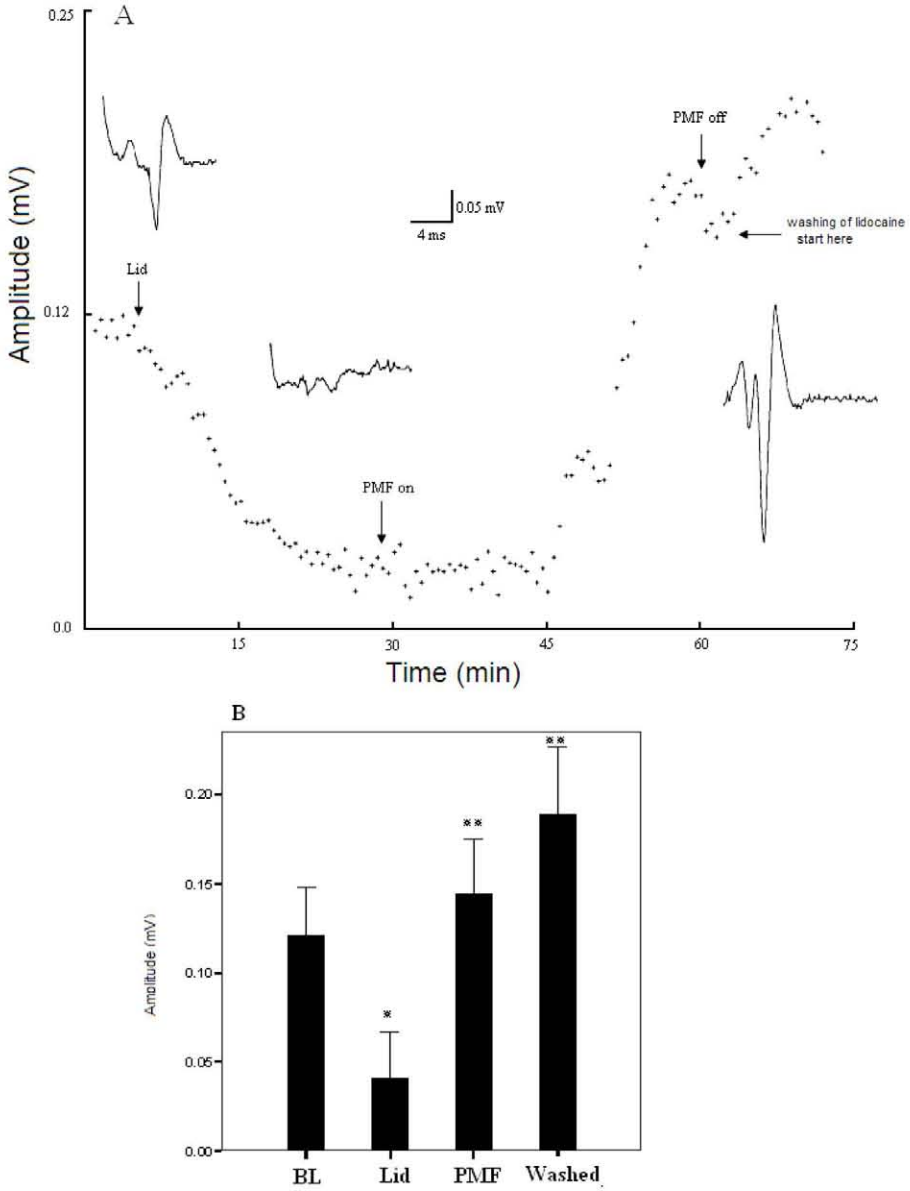


*Fig.14. The influence of PMF on lidocaine-induced depression of CAP. A – A representative experiment demonstrating the depression of CAP by lidocaine (150μM) and the reversal of lidocaine's action by PMF exposure. B – The magnitude of CAP in baseline (BL), after the addition of lidocaine (Lid), after PMF exposure (PMF), and after lidocaine was washed away (Washed). Lidocaine-induced attenuation of CAP (p=0.0005, n=8), was reversed by PMF exposure (p = 0.0005, n = 8, paired t-test). The increase that was induced by PMF exposure was significantly higher than the mean of the CAP of the baseline (p=0.04). Washing of lidocaine away induced additional increase in CAP amplitude, which exceeded the value of the potentials recorded after PMF exposure (p=0.003). *denotes a statistically significant difference (p<0.05) between the baseline and after the addition of lidocaine. **denotes a statistically significant difference (p<0.05) between after PMF and after washing and both baseline and lidocaine.*

hour and no spontaneous recovery was observed, unless the lidocaine was washed away with fresh Ringer's solution (Fig 14B).

The results of experiments with lidocaine and TTX inspired us to investigate the idea, that PMF amplifies the action potential by modifying the gating process of the sodium channel. To verify our assumption we used veratridine, which modifies inactivation gate and induces a persistent activation of the sodium channel (Hille, 2001). In the sciatic nerve preparation veratridine did not change the size of CAP ($n = 10$, $p = 0.619$) but reversed the action of the PMF from facilitation to depression ($p = 0.002$). These results indicate that the PMF potentiated the effect of veratridine probably by facilitating its binding ability.

B.3. The pulsed magnetic field frequency and its effect on CAP.

We have also investigated the influence of magnetic field frequency on the changes in the CAP amplitude. Five frequencies have been selected: 0.5 Hz, 0.16 Hz, 0.07 Hz, 0.03 Hz, 0 Hz (static). The static magnetic field was used to compare the results obtained on sciatic nerve with our previous data on hippocampal slices (Wieraszko, 2000). Interestingly, although the static magnetic field initially reduced the CAP, ($n = 16$, $p = 0.0009$), it induced recovery/amplification of the potential in the later stage of its application ($p = 0.481$, Fig. 15 and 16).Figure 15 shows an example of a typical experiment that represents the amplitude of the potential, and Fig 16 depicts the potential shape at different stages of the experiment**.**

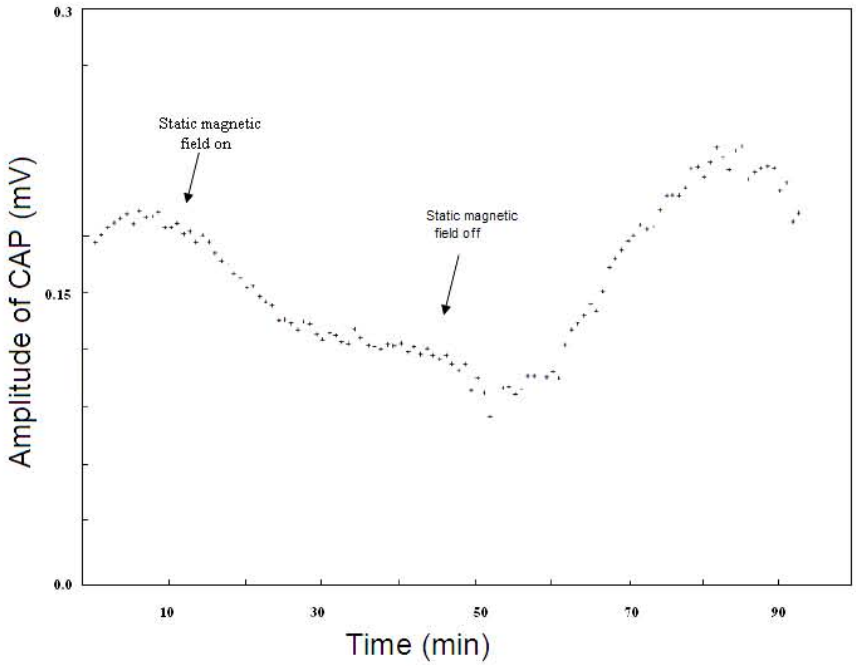


Fig. 15. A representative experiment showing the influence of static magnetic field on CAP recorded from the sciatic nerve. Static magnetic field induced biphasic effect: depression phase during the application of field and recovery/amplification phase after the termination of the field.

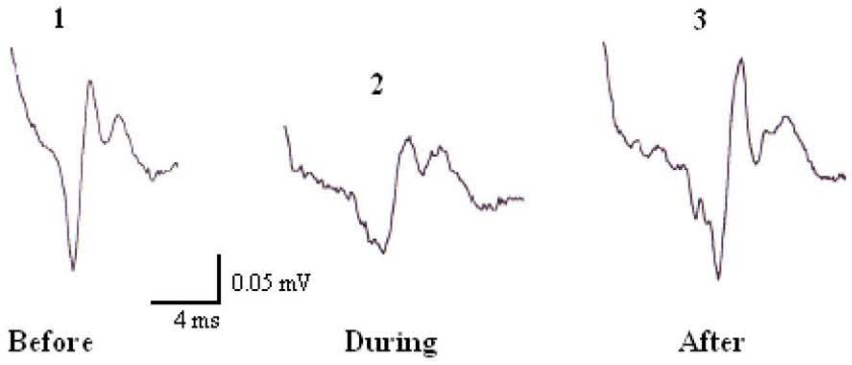


Fig. 16. Three waveforms show the shape and the amplitude of CAP: before (1), during (2), and after (3) exposure to the static magnetic field..

The influence of different frequencies of PMF on the magnitude of CAP is shown in Fig 17.

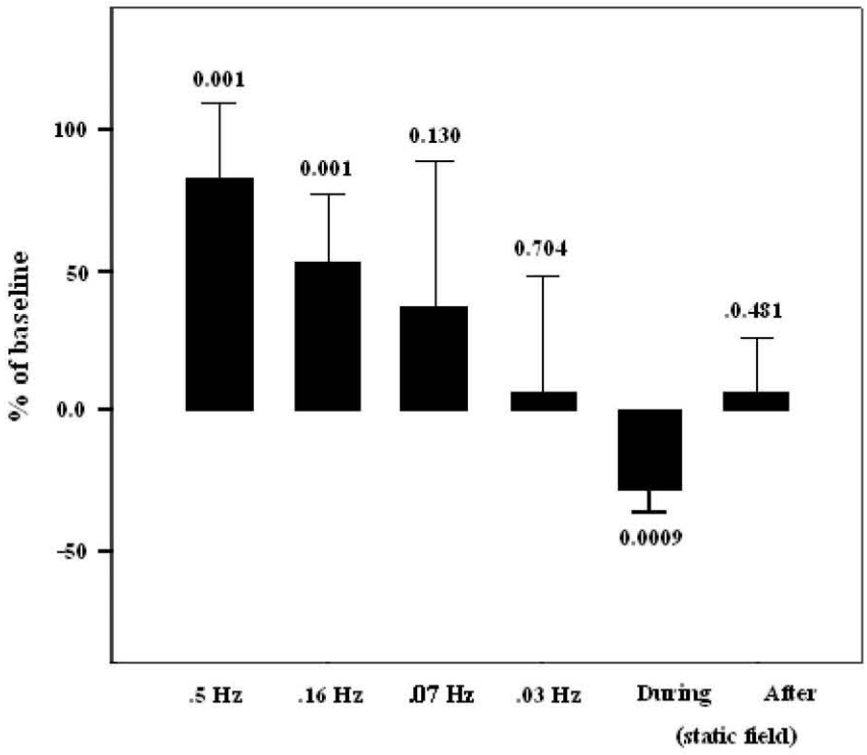


Fig.17. The influence of different frequencies of PMF on CAP recorded from the sciatic nerve. The bars represent the percentage of control calculated as the difference between the average before and after the PMF exposure divided by the average before PMF exposure. The numbers above the bars represent the p value, which was calculated using one sample t test. The difference between groups was statistically significant One way ANOVA was used (F = 7.566, p = 0.0002).

C. Discussion.

Our findings support our previous reports on the effect of PMF on the nervous system (Trabulsi et al., 1996; Wieraszko, 2000; Wieraszko, 2004; Wieraszko, et al., 2004). The effect was frequency-dependent and mediated by synaptic and non-synaptic mechanisms. The enhancement of the paired-pulse facilitation (PPF) implies PMF-induced modulation of presynaptic mechanism, most likely the processes regulating neurotransmitter release. This supports our previous results demonstrating PMF-induced reduction in glutamate uptake (Wieraszko et al., 2005). One can hypothesize, that PMF-induced decrease in Ca^{2+} buffering, amplification of Ca^{2+} release from the internal stores, and/or increase of the influx of Ca^{2+} through calcium channels at the pre-synaptic terminal may be involved in observed effects.

The result from the experiments with antidromic stimulation of the hippocampal slices provided the first clue toward the axonal involvement in the PMF-induced increase in excitability. When synaptic transmission was blocked, the PMF was effectively inducing an increase in the antidromically recorded population spike. Further analysis of the result of these experiments indicated that the population spike amplification was not due to an increase in the number of firing neurons but resulted from an increase in excitability of the same population of neurons. This assumption was further supported by the experiments performed on sciatic nerve. The compound action potential (CAP), recorded from this preparation was permanently amplified following PMF exposure. This amplification was correlated with PMF-induced reduction in the axonal threshold. The plateau of curve illustrating the relationship between CAP amplitude and the strength of the stimulus was similar in the exposed and unexposed preparations. This supports the conclusion that the PMF-induced increase in the CAP amplitude was due to an increase in excitability of the same population of axons and not by the recruitment of new axons.

PMF has been shown not only to reverse the depressive action of TTX and lidocaine, but to amplify the CAP at a later time in the experiment. Apparently, PMF exposure changed the properties of sodium channel reducing its affinity for both ligands. Local anesthesia drugs such as lidocaine can shed more light on how PMF induced hyperexcitability. In the presence of lidocaine sodium channel inactivation is greatly amplified. Hyperpolarization of the cell membrane is needed to relieve this inactivation of the channel (Hille, 2001). Theoretically, lidocaine binds to a site inside the channel pore and its binding is voltage dependent. Since depolarization is needed for the drug to block the channel, it is assumed that lidocaine binds more tightly to an inactivated sodium channel (Hille 2001). These phenomena can explain why the PMF eliminated the lidocaine effect on sodium channels. Hyperpolarization of the cell membrane by PMF initiates following, sequentially occurring events: 1) it opens the inactivated gate more readily; 2) it loosens drug binding; 3) it makes the drug more prone to site dissociation. However, hyperpolarization cannot alone explain all the PMF induced effects mentioned above, and experiments with TTX suggest that PMF exposure induces also changes in the channel protein confirmation. TTX binds to the extracellular site of the sodium channel in a voltage-independent way, blocking stimulated and non-stimulated axons. Since TTX does not react with the channel gating system hyperpolarizing of the cell membrane would not affect the action of TTX. Therefore, the changes in the channel protein conformation, not change in the membrane potential could explain the effect of PMF on TTX-sodium channel interaction.

PMF induced effect was blocked by veratridine. Veratridine reduces the conduction of sodium channel and prevents its inactivation (Hille 2002). The action of veratridine is activity-dependent and it does not affect the activation gate of sodium channels. Veratridine modifies the inactivation gate of sodium channels and the lifetime of that modification is in milliseconds. The reaction of the drug (binding and unbinding) develops from the open state of sodium channel (Hille, 1968; Sutro 1968; Leibowitz et al. 1986; Wang et al. 1990). The dependence of veratridine action on the open state of sodium channel explains the cooperative effect between the PMF and veratridine actions. The PMF increased the rate of activation of sodium channels and that in turn intensified the action of veratridine. Thus, veratridine together with PMF reduced the amplitude of CAP2. Being that PMF did not reverse the action of veratridine, it means that the PMF effect on the shape of the channel protein is specific. If the change in the channel complex is general, it would have affected its affinity to all three antagonists. Instead, the PMF changed the affinity of lidocaine and TTX and reversed their actions, but it did not diminish the affinity for veratridine. Just to the opposite, it intensified its action. This observation points to the probability of the presence of particular sites in the channel complex with different sensitivities to magnetic field exposure.

Although the PMF used in this study is a very specific form of magnetic field spectrum, the findings and their analysis can be applied as a basis for other magnetic field forms biological effects. Magnetic field in general is approved to be beneficial as an adjunct therapy in medicine (see review by Shupak, 2003). The lack of mechanisms of magnetic field action hindered its research toward therapeutics (Rubik, 1997). Here we introduced a mechanistic basis for their effect, which would help and guide clinicians and researchers to the best possible utilization of magnetic field in the treatment of the pathology. A clinical based research could test the effect of PMF on the peripheral nervous system on humans.

Acknowledgements
This research was supported by NIH grant # 1RO1ES110022, PSCCUNY grants # 662850035 and 670890036, and by OMRD Fellowship to CSI/IBR Center for Developmental Neuroscience.

References

Andersen P., Bliss TVP., Skrede KK., (1971). Unit analysis of hippocampal population spike. Exp. Brain Res., 13: 208-221.

Hille, B. (1968). Pharmacological modification of the sodium channel of the frog nerve. J. Gen. Physiol. 51: 199 – 219.

Hille, B. (1968). Charges and potentials at the nerve surface: Divalent ions and PH. J. Gen. Physiol. 51:221 – 236.

Hille, B. (2001). Ion channels of excitable membrane. Third edition, Sinaur Associates, Inc. publishers Sunderland, Massachusetts U.S.A.

Hogan MV, Wieraszko A (2004).An increase in cAMP concentration in mouse hippocampal slices exposed to low-frequency and pulsed magnetic fields. Neurosci. Lett. 366:43-47.

Keynes, R. D., (2002). Studies of multimodal gating of the sodium channel. Sodium channels and neuronal hyper-excitability, published by John Wiley and sons Ltd, pp5-14.

Leibowitz, M. D., J. B.Sutro and B. Hille, (1986). Voltage-dependent gating of veratridine-modified Na channels. J. Gen. Physiol. 87: 25-46.

Rubik, B., (1997). Bioelectromagnetic and the future of medicine. Administrative radiology Journal. 16: 38 – 46.

Semm P, Schneider T, Vollrath L (1980). Effects of an earth-strength magnetic field on electrical activity of pineal cells. Nature, 11: 288(5791):607-8.

Shupak, M. Naomi (2003). Therapeutic uses of pulsed magnetic-field. Radio Science Bulletin, No 307, 9 – 32.

Sutro, J. B. (1986). Kinetics of veratridine action on Na channels of skeletal muscle. J. Gen. Physiol. 87: 1-24.

Trabulsi R, Pawlowski B, Wieraszko A (1996).The influence of steady magnetic fields on the mouse hippocampal evoked potentials in vitro. Brain Res. 728:135-139.

Wang H, Wang X, Scheich H (1996). LTD and LTP induced by transcranial magnetic stimulation in auditory cortex. Neuroreport, 7:521-5.

Wang, G. K., M. Dugas, B. I., Armah and P. Hornerjager, (1990). Sodium chanel comodification with full activator reveals veratridine reaction dynamics. Mol. Pharmacol. 37: 144-148.

Wieraszko A (2000). Dantrolene modulates the influence of steady magnetic fields on hippocampal evoked potentials in vitro. Bioelectromagnetics. 21:175-82.

Wieraszko, A. (2004). Amplification of evoked potentials recorded from mouse hippocampal slices by very low repetition rate pulsed magnetic fields. Bioelectromagnetics 25:537-544.

Wieraszko A., J. Armani, A. Hanna, N. Maqsood, H. Raja, M.V. Hogan (2004) . Changes in neurotransmitter turnover and second messenger levels in brain tissue exposed to magnetic fields. Proc., 3rd Int. Workshop: Biological effects of EMFs, Kos, Greece, pp. 614-632.

Wieraszko, A., Armani, J., Maqsood, N., Raja, H., Philip, S., (2005). Modification of the synaptic glutamate turnover in the hippocampal tissue exposed to low-frequency, pulsed magnetic fields. Brain Res., 1052: 232-235.

Wieraszko A (1983). Uptake of D-[3H] aspartic acid by hippocampal slices: the influence of low and high frequency activation of nerve endings. Brain Res. 259:324-326.

INDIVIDUAL CHANGES IN HUMAN EEG CAUSED BY MODULATED 450 MHz MICROWAVE

RUTH TOMSON[1], MAIE BACHMANN[1], JAAN KALDA[2], MAKSIM SÄKKI[2], JAANUS LASS[1], VIIU TUULIK[1], AND HIIE HINRIKUS[1]

[1]Biomedical Engineering Centre, Tallinn University of Technology

Address: 5 Ehitajate Rd, EE19086 Tallinn, Estonia

[2]Institute of Cybernetics at Tallinn University of Technology

Address: 21 Academy Rd, EE12618 Tallinn, Estonia

Abstract

During resent years our studies have been focused on the effect of modulated low-level microwaves on human EEG rhythms. In this study the experiments with 450 MHz microwave modulated at 40 Hz and 70 Hz frequencies were carried out on a group of 15 volunteers. The field power density at the scalp was 0.16 mW/cm^2. Ten cycles of the exposure (1 min on and 1 min off) with each modulation frequency were applied. The energies of 8 EEG channels FP1, FP2, T3, T4, P3, P4, O1 and O2 were analysed for individuals by two different methods: nonlinear method of scaling analysis for length distribution of low variability periods (LDLVP) and relative changes in EEG energy between segments with and without exposure (*S*-parameter). Statistical analysis of the calculated measures with post-hoc Bonferroni correction by approach with a 0.05 confidence level was applied.

The exposure caused increase of the EEG energy; changes were stronger in temporal and parietal regions and EEG beta rhythms. Statistically significant changes in EEG were detected for 4 subjects (26.7%) with 40 Hz modulation frequency. The rate of multiple chemical sensitivity (between 2 and 10 %) is even lower than sensitivity to microwave.

Keywords: EMF effects, nonionising radiation, microwave radiation, time variability, scaling analysis, spectral analysis, EEG rhythms.

Introduction

The nervous system has been thought to be most sensitive to external electromagnetic field (EMF) since there is a tremendous electrical activity in neural processes. Information processing and transmission in nervous system is based on bioelectromagnetic phenomena. Therefore, can be expected that EMF effects at system level appear most likely in nervous system.

Modulated microwave radiation at non - thermal level of field power density can affect human central nervous system in a sensible way. Except in unhealthy artificial conditions the effect is weak and difficult-to-detect. Reports of possible non-thermal EMF effects are often contradictory and the difficulties in independent repeating of the experimental results cause doubts. Mechanisms behind the effects are still unclear. Several investigators have reported that low-level exposure produces alterations in the EEG signal and brain behavior [1 - 7], while others conclude that exposure to electromagnetic field does not alter resting EEG [8, 9].

In our previous studies the relative changes in the EEG rhythms energy caused by microwave radiation modulated inside the EEG physiological spectrum at frequencies 7 Hz, 14 Hz and 21 Hz were investigated [10]. The conclusion was that the effect produced by microwave radiation has a clear frequency dependence and increases with modulation frequency. The influence of microwave with modulation frequency 217 Hz – technical frequency much higher than the EEG rhythms – has been also reported to produce statistically significant changes in time variability and intensity of the EEG signal for 10-20% of healthy subjects [11].

This study is aimed to evaluate the effect of microwave modulated with intermediate frequencies 40 Hz and 70 Hz. The same exposure conditions utilized in our previous studies were applied. Two methods were selected for EEG analysis: scaling analysis of length distribution of low variability periods (LDLVP) as sensitive to signal time variability [12] and relative change in the EEG energy of segments of the signal with and without exposure as sensitive to the changes in signal level [6].

Method and equipment

Subjects

An experimental study was carried out on a group of volunteers. The group consisted of 15 young persons (aged 21-24): 8 male and 7 female. Their physical and mental condition (tiredness, sleepiness) before the experiment was evaluated by a questionnaire and a clinical interview. All the subjects selected were healthy, without any medical or psychiatric disorders; tired or sleepy people were excluded. After the recordings, they described how they felt during the experiment. The subjects reported neither alertness nor any strain experienced during the recordings.

The experiments were conducted with the understanding and written consent of each subject. The study was conducted in accordance with the Declaration of Helsinki and has been formally approved by the local Medical Research Ethics Committee.

The measurements were performed in a dark laboratory, but no other special conditions were provided. The subjects lay in a relaxed position, with eyes closed and ears blocked during the experiments.

All the subjects were exposed and sham exposed. Only one experimental EEG recording was performed for a subject during a day. The measurements were double blinded. During each test session, the exposed and sham-exposed subjects were randomly assigned. The subjects were not informed of their exposure; however, they were aware of the possibility of being exposed. Subjective factors were also excluded from the computer-performed data analysis: the same algorithms were applied for all the recordings (both for exposed and sham-exposed subjects).

Microwave Exposure

The modulated microwave radiation at non-thermal level of field power density, identical to our previous studies [5, 6, 10, 11, 12], was used. Microwave exposure conditions were the same for all subjects.

The 450 MHz microwave radiation was generated by the Rhode & Swartz (Germany) signal generator model SML02. The RF signal was 100% amplitude modulated by the pulse modulator SML-B3 at 40 or 70Hz frequency (duty cycle 50%). The generator signal was amplified by the Dage Corporation (USA) power amplifier model MSD-2597601. Located in the laboratory, the generator and amplifier were carefully shielded. The 1W EMF output power was guided by a coaxial lead to the 13cm rod antenna NMT450 RA3206 by Allgon Mobile Communication AB, Sweden, located 10 cm from the subject's skin on the left side of the head.

The calculation of the specific absorption rate (SAR) inside the brain was based on the known field power density on skin. The Central Physical Laboratory of the Estonian Health Protection Inspection measured the spatial distribution of the microwave power density by the Fieldmeter C.A 43 Chauvin Arnoux (France) field strength meter. The calibration curves of the field power density dependence on the distance from the radiating antenna were obtained from these measurements taken in the actual conditions of the experiment. During the experiments, the stability of the microwave level was monitored by the IC Engineering (USA) Digi Field C field strength meter.

Estimated from the measured calibration curves, the field power density at the skin was 0.16 mW/cm2. The level of power density was so low that thermal effects were extremely unlikely.

Recording protocols and equipment

The study consisted of three experimental protocols, identical for all subjects. The first protocol was recorded as described below.

First, the reference EEG was recorded over 60 s.

Secondly, modulated microwave radiation was applied. The duration of the exposure was 60 s, and the compensatory pause after the exposure was 60 s. Continuous EEG recordings were made during and 60 s after exposure. The procedure of the cycle was repeated ten times. The microwave exposure was switched on every first 60 s of the cycle. During ten cycles of microwave exposure, the modulation frequency always remained at 40 Hz.

The recording protocol for one subject lasted for 21 min, during which the EEG was continuously recorded.

The second protocol included the same steps, except that the modulation frequency was 70 Hz and the third protocol for the sham-exposure included also the same steps, except that the microwave generator was switched off.

The Cadwell Easy II EEG measurement equipment was used for the EEG recordings. The EEG was recorded by means of 19 electrodes, placed on the subject's head according to the international 10-20-electrode position classification system, with Cz as reference. The EEG recordings were stored on a computer at a sampling frequency of 400 Hz. The recorded EEG signals were examined by an experienced neurologist. Artifacts were detected by visual inspection. The recordings containing multiple artifacts were removed, and the whole recording was repeated.

The pre-processing of the signals was performed in the LabVIEW programming and signal-processing environment. The EEG spectrum 0.5 - 39 Hz was selected for the analysis. The results of the preceding validation of the set-up confirmed the absence of modulation components, caused by parasitic interference between EEG and radio frequency equipment.

Analysis of the EEG based on the LDLVP method

Initially, all the EEG recordings were divided into two sub-signals. The recordings performed with the first and second recording protocol were divided as follows:

- the first subsignal contained all 1 min periods without microwave exposure (all the odd minutes from the initial EEG recording),
- the second subsignal contained all minutes with microwave exposure (all even minutes of the initial EEG recording).

The recordings performed with the sham recording protocol were divided similarly:

- the first sham subsignal contained all the odd minutes,

· the second sham subsignal contained all the even minutes of the initial recording.

The scaling analysis utilizing LDLVP method was applied for two sub-signals.

The LDLVP method has been used and described in details in our previous studies [12 – 14]. Here we provide a brief summary of this method.

First, we define the local variability as the deviation of the current value of the signal from the local average

$$\delta V(t) = V(t) - T^{-1} \int_{-T/2}^{T/2} V(t+\tau) d\tau , \quad (1)$$

where V(t) is the recorded voltage, and the time-window width T is a free (adjustable) parameter. For EEG signals, a reasonable value is provided by T = 60 ms [14].

Secondly, low-variability periods are defined as continuous intervals with

$$\delta V(t) < \delta_0 . \quad (2)$$

Finally, the number of low-variability periods N exceeding length T_0 is plotted against length T_0, see Figure 1.

The value of δ_0 was adjusted for each recording individually, reaching a minimum value so that, for both subsignals, the length of the longest low-variability period was at least 3750 ms.

The hypothesis of this work was that microwave exposure increases EEG variability. Owing to higher variability, there are fewer long low-variability periods. Therefore it is expected that microwave exposure decreases the area of the $T_0(N)$ -curve (see Fig 1), due to faster cut-off at large values of T_0. According to this assumption, the weighted area

$$S_W = \sum_{N=1}^{128} \ln\left(\frac{N}{\max(N-1,1/4)} \right) \ln(T_0) N^{1/2} \quad (3)$$

of the function $T_0 = T_0(N)$ was selected as the non-linear quantitative measure.

Analysis of the EEG based on the *S*-parameter method

Relative changes in the EEG energy between segments with and without exposure *S*-parameter was selected as a measure for detection of the effect on signal intensity.

The analysis method was applied in our previous study [10], except for different comparison intervals. The energies of the different EEG rhythms were analyzed separately. Average energies for segments with and without stimulation were compared. The first 30 s of a 60 s recording segments with and without stimulation were selected as intervals for comparison. The average energy of an arbitrary comparison interval was calculated for the recording segment as follows:

$$s_i = \frac{1}{N} \sum_{r=1}^{N} \left[x(r) \right]^2 \quad (4)$$

where x is the amplitude of the recorded signal and N is the number of samples, during 30 seconds N = 12000. The relative change in the energy of the recording segments with and without stimulation was selected for further analysis. Finally, parameter S was calculated as follows:

$$S = \left(\frac{s_2}{s_1} - 1 \right) \times 100\% \quad (5)$$

where s_1 and s_2 were the average energies inside the comparison intervals without and with stimulation respectively. For sham recordings the same parameter was calculated for comparison intervals as even and odd minutes of the recordings.

At first, the energies of the four basic EEG rhythm frequencies, theta (4 – 7 Hz), alpha (8 – 13 Hz), beta1 (15 – 20 Hz) and beta2 (22 – 38 Hz), were extracted from the total EEG signal (0.5 – 48 Hz) by filtering. The parameter S was calculated separately for the EEG energies of the theta, alpha, beta1 and beta2 rhythms.

Signal processing and calculation of parameters were performed in the LabVIEW programming and signal processing environment.

Statistical analysis

For sham recordings, sub-signals were completely equivalent. The mathematical expectation of the difference in their spectral powers is zero, $\tilde{W}_0 - \tilde{W}_1 = 0$. Next, an estimate of the variance could be obtained as the mean of squared differences:

$$\sigma_f{}^2 = \frac{1}{15}\sum_{n=1}^{15}\left(\tilde{W}_{0nf} - \tilde{W}_{1nf}\right)^2 \quad (6)$$

According to the "zero hypothesis", the EEG recordings of subjects under microwave exposure cannot be distinguished from sham signals. Thus, the "zero hypothesis" implies that $W_0 - W_1 = 0$ and $\left(W_0 - W_1\right)^2 = \left(\tilde{W}_0 - \tilde{W}_1\right)^2$. Consequently, if the zero hypothesis is true, the quantity $x_f = \left(W_{0nf} - W_{1nf}\right)^2 \sigma_f{}^{-2}$ is an *f*-distributed random quantity, the cumulative distribution of which is routinely designated as $F_{1,15}(x_f)$; the indices 1 and 15 stand for the numbers of the degrees of freedom.
Accordingly, the ratio of the computed power difference to the standard deviation of the differences can be used as a quantitative measure, showing how well the zero hypothesis is satisfied; respective *p*-values are obtained by means of the cumulative *f*-distribution:

$$p_f = F_{1,15}\left[\left(W_{0nf} - W_{1nf}\right)^2 \sigma_f{}^{-2}\right] \quad (7)$$

The same technique has been applied to the non-linear quantitative measure (derived from LDLVP), resulting in another two series of *p*-values for recordings at modulation frequency 40 Hz and 70 Hz.

For post hoc analysis the modified Bonferroni correction was applied according to which the smallest p-value is to be multiplied by the number of data points 15, the second smallest is to be multiplied by 15/2=7.5 etc.

Results

The results of LDLVP analysis for a subject are presented in Figure 1. The number of low-variability periods N exceeding the length T_0 is plotted versus the length T_0 for the first and second sub-signal for exposed recording. As can be seen, microwave exposure lowers the curve at the right-hand part of the graph (large values of T_0). Such a change in curve indicates that microwave exposure increases variability of the EEG signal: owing to higher variability there are fewer long low variability periods.

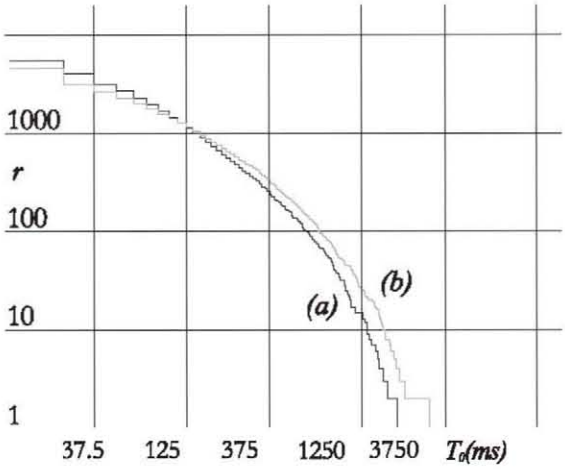


Figure 1. The number of low-variability periods *N* exceeding the length T_0 for a significant subject: black line (a) – second sub-signal of exposed recording (intervals with microwave); grey line (b) – first sub-signal of exposed recording (intervals without microwave).

The results of statistical analysis of the LDLVP quantitative measures for sham and microwave-exposed at modulation frequency 40 and 70 Hz recordings, calculated for each subject, are presented in Table 1. For sham recordings there were no significant results. The ratio of the computed power difference to the standard deviation of differences $\sqrt{x}$ of more than three were considered as significant deviations from the zero hypothesis and are marked in bold. After Bonferroni correction *p*-values not larger than 0.05 were considered as significant deviations from the zero hypothesis and are marked in bold. As can be seen, the analysis resulted in *p*-values lower than 0.05 for 4 cases in the case of microwave exposure at modulation frequency 40 Hz and none for 70 Hz frequency.

Table 1. Calculated using LDLVP method $\sqrt{x}$ and *p*-values as a result of Bonferroni correction for different microwave exposure conditions in P-channels

Frequency band	0.5 – 39 Hz					
	sqrt(x)			*p* - value		
Subject	sham	40 Hz	70 Hz	sham	40 Hz	70 Hz
1	0.07	0.95	1.93	1.000	0.591	0.339
2	-0.11	**-3.02**	-0.77	0.582	**0.025**	0.842
3	1.02	1.30	-0.60	1.000	0.392	0.836
4	0.81	-0.21	-0.60	0.876	0.835	0.760
5	0.67	-0.39	1.68	0.963	0.812	0.403
6	0.81	-0.28	-0.04	0.844	0.838	0.972
7	0.98	-0.63	-0.98	0.837	0.802	0.723
8	-1.23	-1.51	-0.11	0.804	0.315	0.983
9	1.86	**3.69**	0.35	0.715	**0.022**	0.912
10	-0.28	2.49	-0.21	0.769	0.065	0.964
11	0.88	0.46	2.14	1.000	0.816	0.336
12	0.00	**3.09**	-2.74	1.000	**0.029**	0.190
13	-0.04	1.93	1.16	1.000	0.170	0.781
14	-1.30	**-3.69**	0.77	1.000	**0.011**	0.748
15	1.93	0.49	-1.05	1.000	0.857	0.762

The results of the *S* - parameter analysis for the whole group are presented in Figure 2. The graph illustrates the effect of microwave exposure – changes between exposed and not exposed segments of the recordings on different EEG rhythms and for sham, 40 Hz and 70 Hz modulation frequency. As can be seen, microwave exposure causes increase in energy of the EEG beta1 and beta2 rhythms.

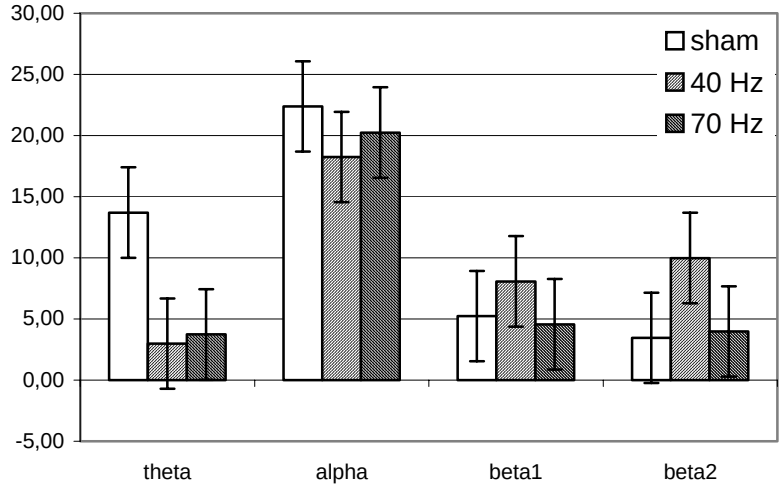


Figure 2. The relative average changes in % (*S* – parameter) of the EEG rhythms total energy of the recording segments with and without microwave exposure in P – channels for the whole group.

The results of statistical analysis of the *S* - parameter are presented in Table 2. For sham recordings there were no significant results. Microwave exposed recordings at modulation frequency 40 Hz have 2 significant values in beta2 region.

Table 2. Calculated *p*-values for different EEG rhythms in P-channels as a result of analysis by post – hoc Bonferroni correction for different microwave exposure conditions

Frequency band	*p*-value											
	Theta			Alpha			Beta1			Beta2		
Subject	sham	40 Hz	70 Hz	sham	40 Hz	70 Hz	sham	40 Hz	70 Hz	sham	40 Hz	70 Hz
1	1.000	1.000	1.000	1.000	1.000	1.000	1.000	0.433	1.000	0.935	1.000	1.000
2	1.000	1.000	1.000	0.612	1.000	1.000	0.902	0.664	1.000	0.780	**0.000**	0.053
3	0.342	1.000	1.000	1.000	1.000	1.000	0.876	1.000	1.000	0.903	0.880	0.671
4	1.000	1.000	1.000	1.000	1.000	1.000	0.983	1.000	1.000	0.875	1.000	0.825
5	1.000	1.000	1.000	1.000	1.000	1.000	0.819	1.000	1.000	0.780	1.000	0.670
6	1.000	1.000	1.000	1.000	1.000	1.000	0.859	1.000	1.000	0.905	1.000	0.543
7	1.000	1.000	1.000	1.000	1.000	1.000	0.780	1.000	1.000	0.781	1.000	0.575
8	1.000	1.000	1.000	1.000	1.000	1.000	0.767	1.000	1.000	1.000	1.000	0.624
9	1.000	1.000	1.000	1.000	1.000	1.000	0.680	1.000	1.000	0.836	0.988	0.573
10	1.000	1.000	0.358	1.000	1.000	1.000	0.837	0.609	1.000	0.800	0.595	0.715
11	0.151	1.000	1.000	1.000	1.000	1.000	1.000	1.000	1.000	1.762	1.000	0.840
12	1.000	1.000	1.000	1.000	1.000	0.066	0.705	1.000	1.000	0.837	1.000	0.818
13	0.548	1.000	1.000	0.077	1.000	1.000	0.794	1.000	1.000	0.757	1.000	0.994
14	1.000	1.000	1.000	1.000	1.000	1.000	1.000	0.383	0.423	0.935	**0.003**	0.690
15	1.000	1.000	1.000	1.000	1.000	1.000	1.000	1.000	0.268	1.000	1.000	0.874

The graphs of changes of the EEG rhythms energy for a significant subject are presented in Fig. 3. In this case increase in the EEG beta2 rhythm energy is more clearly indicated than in Fig. 2 for average changes in the whole group. Effect of 40 Hz modulated microwave is more evident than 70 Hz modulated microwave.

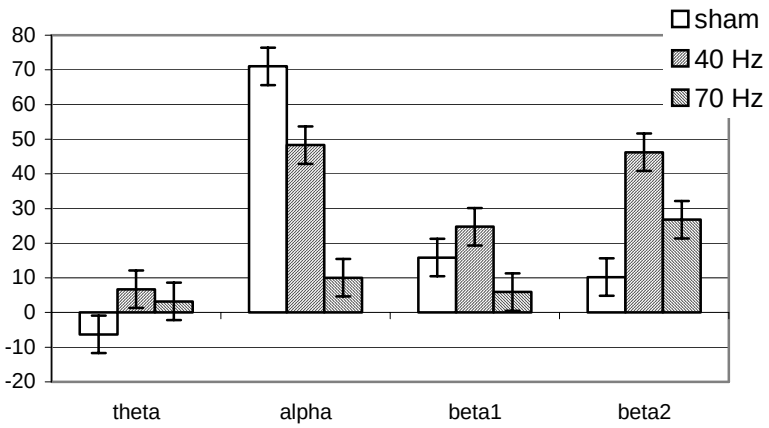


Figure 3. The relative changes (S – parameter in %) of the EEG rhythms total energy in P – channels for a significant subject.

Discussion

As table 1 illustrates, the LDLVP presents the best outcome at modulation frequency 40 Hz, resulting in significant results for 4 subjects. Accordingly, significant effect of exposure to the EEG signal was detected for 26.7 % of subjects. Modulation at frequency 70 Hz was not as effective as 40 Hz; however, it was distinguishable from sham signals, which did not result in any significant deviation.

Considering the direction of influence at modulation frequency 40 Hz, for two subjects under the exposure the computed LDLVP weighted area increased, and for two it decreased. For all subjects, the departure from the sham behavior is statistically reliable. This is somewhat different from what has been observed for the modulation frequency 7 Hz, when the sign of the departure was always negative (corresponding to increased variability) [12]. However, a study at modulation frequency 217 Hz resulted with the outcome, in which for half of the subjects the computed LDLVP weighted area decreased and for another half it decreased [15]. This observation gives us a hint that the physiological effect of the microwave stimulation depends on the modulation frequency (at least there is a difference between the 40, 217 Hz, and the 7 Hz frequencies).

The *S*-parameter measures exceeded the limit of significant deviation from zero hypothesis also at modulation frequency 40 Hz in beta2 frequency band (Table 2), providing 2 significant cases out of 15, that is 13.3 %. There were no significant results at modulation frequency 70 Hz. In an earlier study [10] it was suggested that microwave exposure causes a significant effect when the modulation frequency is higher or comparable with EEG rhythm frequency.

As with both methods, modulation at frequency 70 Hz is not as effective as at 40 Hz. Here we can see that achieved effect is probably concentrated to the lower frequencies. In our previous study with modulation inside the EEG physiological frequencies band the effect has been reported to be more evident at higher modulation frequencies [16]. Possible reason is that 40 Hz is quite close to the EEG physiological frequencies and the switching with brain oscillations more effective.

From those results it is difficult to conclude which measure, LDLVP or *S*-parameter, is more effective and whether the effect of modulation frequencies 40 and 70 Hz appear rather in intensity (*S*-parameter) or time variability (LDLVP) of the EEG signals. The results reported in our previous study with 7 Hz modulated microwave lead to the conclusion that the effect appears in time variability [12], while the next study concerning modulation frequency 217 Hz concluded that the effect is rather in intensity [15].

From Tables 1 and 2, it can be seen that the subjects having significant results overlap. On the other hand, with the LDLVP method, there are 4 significant results compared to 2 with the *S*-parameter. This indicates that microwave stimulation causes different effects for different subjects and there is a need for various methods to detect those effects.

The analysis by the LDLVP method detected the effect of exposure at modulation frequency 40 Hz for 26.7 % of subjects. For instance, the rate of multiple chemical sensitivity (MCS) occurrence is estimated to be between 2 and 10 % in the general population [17]. MCS is characterized by recurrent symptoms involving multiple organ systems and occurring in response to demonstrable exposures to multiple chemically unrelated compounds at doses far below those established to cause harmful effects. Taking this into consideration, LDLVP and *S*-parameter methods demonstrated good sensitivity detecting the effects of microwave stimulation at modulation frequency 40 Hz.

Main trend of changes caused by microwave exposure modulation frequencies was increase of the EEG energy in beta rhythm. Increased beta absolute power was also observed in alcohol-dependent subjects [18].

Conclusion

1. The modulated with 40 Hz 450 MHz microwave exposure caused statistically significant changes in the EEG time variability (26.7% of subjects) and energy variations (13.3% of subjects).

2. Main trend of changes was increase in the EEG beta rhythm energy.

3. The effect is more evident with the modulation frequency closer to the physiological EEG rhythms band.

References

[1] Mann, K., Roschke, J. “Effects of pulsed high-frequency electromagnetic fields on human sleep,” *Neuropsychobiology* 1996, **33**: pp. 41-47

[2] Borbely, A.A., Huber, R., Graf, T., Fuchs, B., Gallmann, E., Acherman, P., “Pulsed high – frequency electromagnetic field affects human sleep and sleep electroencephalogram” *Neurosci. Lett.* 1999, **275**: pp. 207 - 210

[3] Huber, R., Graf, T., Cote, K.A., Wittmann, L., Gallmann, E., Matter, D., Schuderer, J., Kuster, N., Borbely, A.A., Achermann, P. “Exposure to pulsed high-frequency electromagnetic field during waking affects human sleep EEG,” *Neuroreport* 2000; **11**: pp. 3321-3325

[4] Krause, C.M., Sillanmäki, L., Koivisto, M., Häggqvist, A., Saarela, C., Revonsuo, A., Laine, M., Hämäläinen, H. “Effects of electromagnetic field emitted by cellular phones on the EEG during a memory task,” *Neuroreport* 2000; **11**: pp. 761-764.

[5] Lass, J., Tuulik, V., Ferenets, R., Riisalo, R., Hinrikus, H. "Effects of 7Hz-modulated 450 MHz electromagnetic radiation on human performance in visual memory tasks," *Int. J. Radiat. Biol.* 2002; **78**: pp. 937-944
[6] Hinrikus, H., Parts, M., Lass, J. and Tuulik, V.: 2004, Changes in Human EEG Caused by Low – Level Modulated Microwave Stimulation, *Bioelectromagnetics*, **25**: pp. 431 – 440
[7] Curcio, G., Ferrara, M., Moroni, F., D'Inzeo, G., Bertini, M., De Gennaro, L. "Is the brain influenced by a phone call? An EEG study of resting wakefulness" *Neurosci. Res.* 2005, **53**: pp. 265 - 270
[8] Hietanen, M., Kovala, T. , Hamalainen, A.M. "Human brain activity during exposure to radiofrequency fields emitted by cellular phones," *Scand J Work Environ Health* 2000, **26**: pp. 87-92
[9] Krause, C.M., Sillanmäki, L., Koivisto, M., Häggqvist, A., Saarela, C., Revonsuo, A., Laine, M., Hämäläinen, H. "Effects of electromagnetic fields emitted by cellular phones on the electroencephalogram during a visual working memory task," *Int J Radiat Biol* 2000, **76**: pp.1659-1667
[10] Hinrikus, H., Bachmann, M., Tomson, R., Lass, J. "Non-thermal effect of microwave radiation on human brain" *The Environmentalist* 2005, **25**: pp. 187 – 194
[11] Bachmann, M., Kalda, J., Lass, J., Tuulik, V., Hinrikus, H. "Power spectrum distinguishes the effect of microwave stimulation on human EEG at rest" Biological Effects of EMFs 3rd International Workshop, Kos, Greece, 4 – 8 October 2004, pp. 75 – 81
[12] Bachmann, M., Kalda, J., Lass, J., Tuulik, V., Säkki, M., Hinrikus, H. "Non-linear analysis of the electroencephalogram for detecting effects of low-level electromagnetic fields," *Med Biol Eng Comput* 2005; **43**: pp. 142-149
[13] Kalda, J., Säkki, M., Vainu, M., and Laan, M. (2001): 'Zipf's law in human heartbeat dynamics', available: http://arxiv.org/abs/physics/0110075
[14] M. Säkki, J. Kalda, M. Vainu, M. Laan, "The distribution of low-variability periods in human heartbeat dynamics," *Physica A* 2004; **338**: pp. 255-260.
[15] Bachmann, M., Säkki, M., Kalda, J., Lass, J., Tuulik, V., Hinrikus, H. "Effect of 450 MHz microwave modulated with 217 Hz on human EEG in rest" *The Environmentalist* 2005, **25**: pp. 165 – 171
[16] Lass, J., Hinrikus, H., Bachmann, M., Tuulik, V. Microwave radiation has modulation frequency dependent stimulating effect on human EEG rhythms. *Proceedings of the 26th Annual International Conference of the IEEE EMBS* San Francisco, USA, September 1-5, 2004, pp. 4225-4228
[17] Cullen, M.R. "Workers with multiple chemical sensitivities," Occupational medicine: state of the art reviews. Philadelphia: Hanley & Belfus, Inc. 1987; 2: pp. 655-661.
[18] Rangaswamy M, Porjesz B, Chorlian DB, Wang K, Jones KA, Bauer LO, Rohrbaugh J, O'Connor SJ, KuperKuperman S, Reich T, Begleiter H. Beta power in the EEG of alcoholics. *Biol Psychiatry*. 2002 15; 52(8):831-842.

ELECTRIC-FIELD METERS FOR ASSESSING THE EXPOSURE RATIO FROM MULTIPLE RADIO SOURCES AND IMT-2000 CELLULAR BASE STATIONS EMPLOYING THE ISOTROPIC SLEEVE DIPOLE SENSOR AND CODE SELECTIVE RECEIVERS

JUNJI HIGASHIYAMA, KOHJIROH OHSHITA, HIROAKI KOYAMA, YOSHIAKI TARUSAWA, AND SHINJI UEBAYASHI

WIRELESS LABORATORIES, NTT DOCOMO, INC.
3-5 HIKARI-NO-OKA, YOKOSUKA-SHI, KANAGAWA*, 239-8536, *JAPAN

Abstract

This paper proposes novel electric-field (E-field) meters that comprise an isotropic sleeve dipole sensor for a wideband frequency range, code selective receivers, and a GPS receiver.

The sensor achieves isotropy and a wideband frequency range with a high sensitivity level to measure the total exposure ratio from radio sources in the in-situ environment including a scattering domain and where multiple radio sources have different frequencies.

The strength of the E-field from a cellular base station varies dynamically because the transmission power varies depending on the amount of communications traffic. Therefore, for cellular operators, it is important to estimate conservatively the exposure ratio from their base stations at the designed maximum transmission power. A code selective receiver is adopted for conservative estimation of the exposure ratio from the IMT-2000 cellular base stations, which are becoming commonplace worldwide.

The proposed E-field meters can accurately assess the total exposure ratio from 30 MHz to 3 GHz and the profile of the human exposure ratio from IMT-2000 cellular base stations based on in-situ measurement. In addition, we show that the exposure ratio from a typical IMT-2000 cellular base station is less than 1/10000 of the E-field strength reference level given in the ICNIRP guidelines.

Keywords: IMT-2000 cellular system; the ICNIRP guidelines; radio receivers

1. Introduction

When starting the service of a new cellular base station, the E-field strength from the base station must be below the E-field reference level given for the country in which the base station is established. Furthermore, if there are other radio stations around the base station, the electromagnetic environment including the radio waves from the surrounding stations must be evaluated comprehensively. The reference levels for the E-field strength are different for each radio law. However, many radio laws adopt the reference levels given in the ICNIRP guidelines (the ICNIRP reference levels) [1]. The ICNIRP reference levels are different for each radio wave frequency. Therefore, if the E-field strength levels are evaluated in an environment where the radio waves from multiple radio stations have different frequencies, it is important to asses the total exposure ratio considering the difference between the E-field strength levels at each frequency.

For cellular operators, it is important not only to comply with the ICNIRP reference levels, but also to communicate to the general public to enhance public confidence and acceptability for radio frequency (RF) exposure as indicated in the fact sheet issued by the World Health Organization [2]. Therefore, an E-field meter that accurately assesses the total exposure ratio, which is the summation of the squared ratios of the E-field strengths to the ICNIRP reference levels, in the in-situ environment is required.

In order to enhance public confidence and acceptability for RF exposure, it is important to estimate not only the total exposure ratio, but also the profile of the exposure ratio from a cellular base station. The radio waves from cellular base stations include many kinds of digital modulated waves with different frequencies. In addition, the E-field strength from a cellular base station varies dynamically because the transmission power varies depending on the amount of communications traffic. In order to assess the maximum exposure radio from a cellular base station, an assessment of the E-field strength from the base station at the maximum designed transmission power is required. Therefore, the E-field meter that accurately assesses the profile of the exposure

ratio from a cellular base station in the in-situ environment is required to be optimized to the digital modulated waves.

The objective of this paper is to specify, for such an E-field meter and when it is put into service in its operational environment, the methods to assess the value of the total exposure ratio in relevant public-access areas in order to communicate the risk to the general public.

This paper proposes the following two E-field meters.

a) An E-field meter for assessing the total exposure ratio.

b) An E-field meter for assessing the profile of exposure ratio from a cellular base station.

In particular concerning b), the E-field meter for the IMT-2000 cellular system, which is the 3rd generation cellular system and is becoming commonplace worldwide, is proposed.

2. Basic Configuration

a) E-field meter for assessing the total exposure ratio

In order to conform to the ICNIRP reference levels, the total exposure ratio should be less than or equal to one. The total exposure ratio is estimated using (1),

$$e_t^{\,2} = \sum_{i=100\,\mathrm{kHz}}^{1\,\mathrm{MHz}} \left(\frac{E_i}{c} \right)^2 + \sum_{i>1\,\mathrm{MHz}}^{300\,\mathrm{GHz}} \left(\frac{E_i}{E_{L,i}} \right)^2 , \tag{1}$$

where e_t^2 is the total exposure ratio, E_i V/m is the E-field strength at frequency i, and c and $E_{L,i}$ V/m are the ICNIRP reference levels at frequency i.

An E-field meter that measures the strength of the E-fields including those from cellular base stations, FM radio stations, and TV stations, must have a high level of sensitivity throughout a wideband frequency range. In the construction of a wideband E-field sensor, a shorted-dipole element that is shorter than the wavelength is often combined with a diode detector. The detection sensitivity limit of this sensor is approximately 0.1 V/m (100 dBμV/m). However, in order to measure the strength of the E-fields around a cellular base station in the in-situ environment for practical purposes, the detection sensitivity of the E-field sensor must be 1 mV/m (60 dBμV/m).

In addition, in order to measure the E-field strength accurately, the sensor polarization must be set to conform to the target electromagnetic wave polarization. However, in the in-situ environment in which the equipment is surrounded by many reflectors, which is representative of many urban areas, accurate measurement is difficult due to the presence of the scattering domain in the case of measurement using the E-field sensor comprising a shorted dipole. On the other hand, the isotropic E-field sensor enables measurement of the E-field strength without depending on the polarization of the target wave. Therefore, in an in-situ measurement the isotropic E-field sensor must be used.

The target measuring frequency range of the proposed E-field meter is assumed to be from 30 MHz to 3 GHz, which includes the frequencies used by cellular services and many other wireless services. When measuring the strength of the E-field from a cellular base station, as mentioned above, it is practical to have the detection level of 60 dBμV/m. In order to satisfy this requirement, the construction of the proposed E-field sensor is based on a frequency tuning measurement instrument for detection. The relationship between the required sensitivity and antenna factor (AF) for the E-field sensor is given as (2),

$$E_{REQ} = n + SNR + AF_{REQ} + 107 , \tag{2}$$

where E_{REQ} dBμV/m is the required sensitivity level, AF_{REQ} dB/m is the required AF, n dBm is the noise floor of the instrument, and SNR dB is the signal-to-noise ratio (SNR).

If a general spectrum analyzer with the noise floor of -90 dBm for the resolution bandwidth of 100 kHz is adopted as the frequency tuning measurement instrument, in order to achieve the sensitivity of 60 dBμV/m, the AF of 40 dB/m is required for the E-field sensor. In this regard, it is assumed that the E-field sensor can detect the E-field strength, if the SNR is greater than 3 dB.

In order to achieve sensor elements and baluns that exhibit a high sensitivity level across a wideband frequency range, the sensor element design is based on a sleeve dipole and divided sub-elements that correspond to each frequency range. The proposed sensor element comprises a radiator, a sleeve, and a coaxial feeder as shown in Fig. 1.

The radiator comprises multiple cylindrical conductors connected by inductors. The lengths of each conductor are based on a log periodic rule. The inductors function to change the effective length of the radiant region for each frequency because the impedance of the inductors increases with an increase in the frequency. The sleeve is also basically constructed in the same manner as the radiator. However, in the sleeve region, the

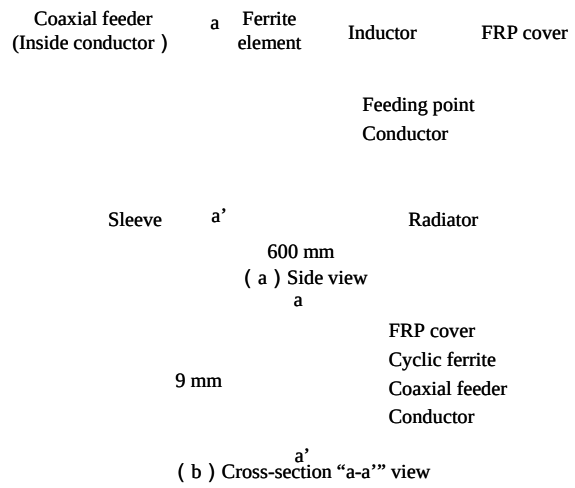


Fig. 1. Construction of proposed sensor element for assessing the total exposure ratio

coaxial feeder is at the center of the conductors, and ferrite elements are inserted between the feeder and the conductors. These ferrite elements provide a sufficient degree of isolation between the feeder and the conductors of the sleeve.

The length of the proposed sensor element including the radiator and sleeve regions is 600 mm, the diameter of the outside conductors is 9 mm, and the entire sensor element is covered with fiber-reinforced plastic (FRP).

Isotropic sensitivity is required for the E-field sensor in the in-situ measurement as mentioned above. Therefore, the proposed E-field senor comprises three sensor elements that cross orthogonally in a three-dimensional Cartesian coordinate system for the isotropic sensitivity.

The proposed E-field meter integrates the proposed wideband 3-axis isotropic E-field sensor above, a switch box for RF signals, a spectrum analyzer, and a notebook PC to control the switch box and spectrum analyzer. A schematic and a photo of the equipment are given in Figs. 2 and 3, respectively.

The spectrum analyzer detects the signal induced at an axis of the proposed E-field sensor. The E-field strength detected by the axis of the proposed sensor is calculated using (3),

$$E_x = P_x + AF_x + L_x + 107\,, \tag{3}$$

where E_x dBμV/m is the E-field strength detected at the x axis, P_x dBm is the received power for the x axis detected by the spectrum analyzer, AF_x dB/m is the AF of the x axis, and L_x dB is the cable loss between the x axis of the sensor and the spectrum analyzer. E_y and E_z are the same as E_x.

The E-field strength of a point of interest is calculated using (4),

$$E = \sqrt{E_x^2 + E_y^2 + E_z^2}\,, \tag{4}$$

where E μV/m is the root mean square of E-field strength of E_x, E_y, and E_z.

The switch box selects the connection to an axis element of the proposed sensor and the spectrum analyzer. The notebook PC controls the switch box and spectrum analyzer, calculates the total exposure ratio using (3), (4), and (1), and shows the frequency spectrum with the ICNIRP reference level and the total exposure ratio.

b) E-field meter for assessing the exposure ratio profile from a IMT-2000 system base station

In order to assess the strength of the E-field from a cellular base station at the maximum designed transmission power, it is effective to utilize characteristics of the transmission power allocated to the control channel. These characteristics are that the transmission power is constant at each cellular base station and that the power is independent of the amount of communications traffic.

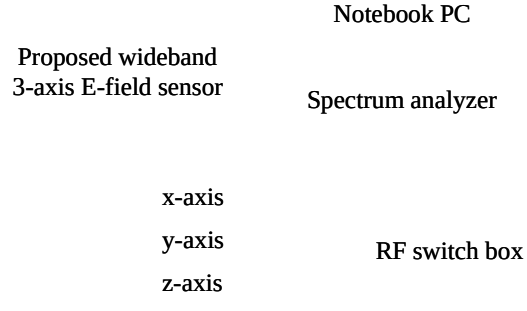


Fig. 2. Construction of proposed E-field meter for assessing the total exposure ratio

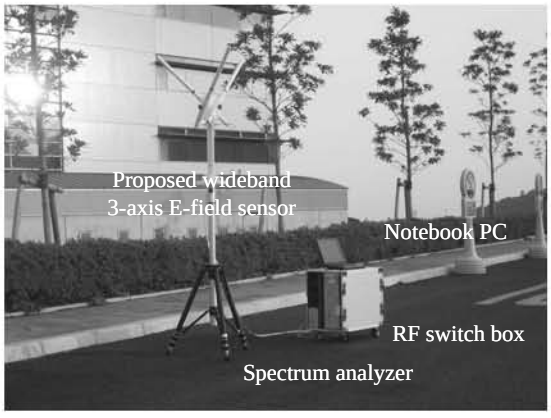


Fig. 3. Proposed E-field meter for assessing the total exposure ratio

The relationship between the total exposure ratio and the exposure ratio from a cellular base station at the designed maximum transmission power is given as (5),

$$e_t^2 = e_{EUT}^2 + e_x^2, \tag{5}$$

where e_t^2 is the total exposure ratio, $e_{EUT}{}^2$ is the exposure ratio from a cellular base station at the designed maximum transmission power, and e_x^2 is the exposure ratio from other radio sources.

In the 2nd generation cellular systems, since the access system is based on the frequency division multiple access (FDMA) system, the strength of the control channel E-field can be adequately measured at the frequency range assigned to the control channel by frequency tuning using a spectrum analyzer. On the other hand, the 3rd generation cellular systems are based on the code division multiple access (CDMA) system. In this system, the frequency spectra of the communication channels overlap. Therefore, in order to measure the E-field strength of the control channel in the wideband code division multiple access (W-CDMA) system, code selective receivers are required. The control channel is called the primary common pilot channel (P-CPICH) in the 3GPP specification [3].

The exposure ratio from W-CDMA system base stations is given as (6) and (7),

$$e_{EUT}^2 = \sum_{i=1}^{N_{EUT}} \left(\frac{E_{rec,i}}{E_{L,i}} \right)^2, \tag{6}$$

$$E_{rec,i}^2 = N_{code} \times E_{P-CPICH}^2, \tag{7}$$

where $e_{EUT}{}^2$ is the exposure ratio from a cellular base station at the designed maximum transmission power, N_{EUT} is the number of radio sources at the W-CDMA system base station, $E_{rec,\,i}$ is the received E-field strength due to *i*-th radio source at W-CDMA system base station, $E_{L,\,i}$ is the ICNIRP reference level at the *i*-th radio frequency, N_{code} is the number of traffic codes, and $E_{P\text{-}CPICH}$ is the E-field strength of the P-CPICH code.

The proposed E-field meter integrates an isotropic E-field sensor comprising the 3-axis dipole elements used in the in-situ measurement, three code selective receivers to detect the W-CDMA system signals, a GPS receiver to detect the geometrical position, and a notebook PC to control the receivers. A schematic and a photo of the equipment are given in Figs. 4 and 5, respectively.

The E-field sensor comprises the 3-axis mutually-perpendicular dipole elements because isotropic sensitivity is required for the E-field sensor in the in-situ measurement as described above. The three code selective receivers correspond to each axis of the isotropic sensor, and detect only the P-CPICH intensity.

The notebook PC controls the code selective receivers and calculates the exposure ratio from the target base station at the designed maximum transmission power. The P-CPICH E-field strength of an interesting point is calculated using (3), (4), and (7). The exposure ratio from a base station at the designed maximum power is calculated using (6). Furthermore, this equation obtains the geometrical position information from the GPS receiver and shows the geometrical profile of the exposure ratio from the target base station.

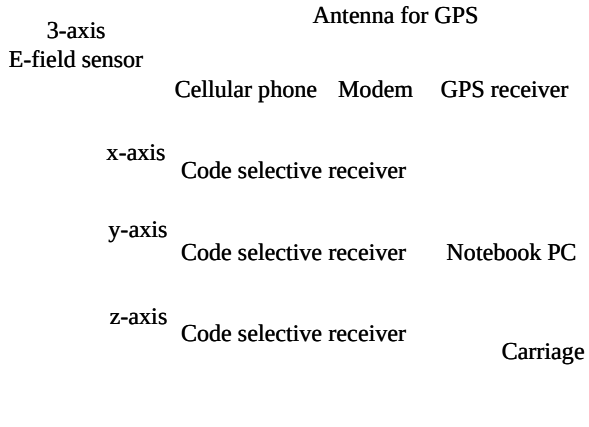


Fig. 4. Construction of proposed E-field meter for assessing the exposure ratio from IMT-2000 system base station

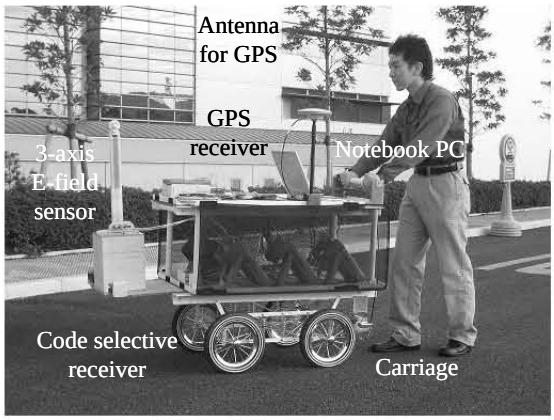


Fig. 5. Proposed E-field meter for assessing the exposure ratio from IMT-2000 system base station

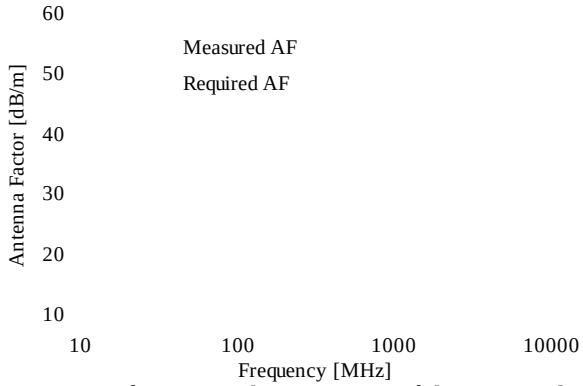


Fig. 6. AF frequency characteristics of the proposed E-field sensor for assessing the total exposure ratio system base station

Table 1. Code Selective Receiver Characteristics for Exposure Ratio from IMT-2000 System Base Station

Item	Value
Frequency Range	2110~2200 MHz
Dynamic Range	-117~-33 dBm
Resolution	0.1 dB
Accuracy	±2 dB
SIR Accuracy	±3 dB
Sampling Interval	10 ms

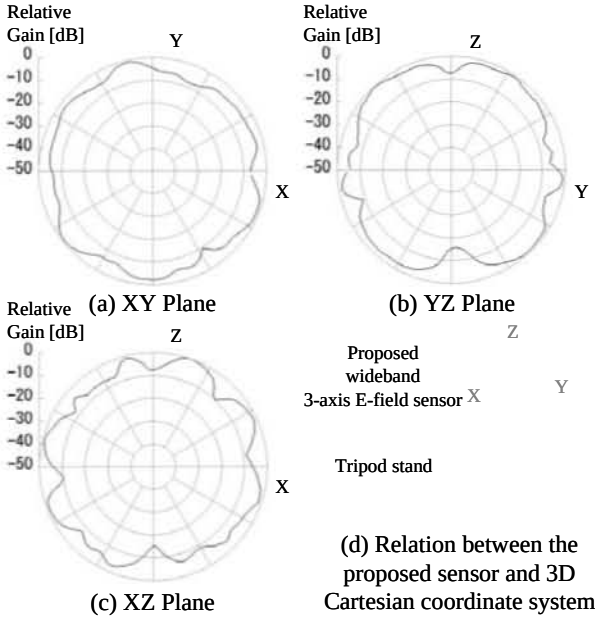


Fig. 7. Isotropic responses of the proposed E-field sensor for assessing the total exposure ratio

3. Characteristics

a) E-field meter for assessing the total exposure ratio

The AF frequency characteristics of the proposed E-field sensor are shown in Fig. 6. The AF is calibrated by using a standard antenna.

The E-field sensor achieves an AF value of 40 dB/m from 30 MHz to 1.7 GHz, and 41 dB/m from 1.7 GHz to 3 GHz.

The isotropic response of the proposed sensor is measured using an SG system (Satimo S. A.). The measurement values at 2 GHz, which is used by W-CDMA systems, are shown in Fig. 7.

Figure 7 shows that the isotropic response of the proposed sensor is within ±5 dB except for below the proposed sensor where there is a tripod stand.

b) E-field meter for assessing the exposure ratio profile from a IMT-2000 system base station

The characteristics of the code selective meter are given in Table 1. For example, at 2 GHz, the AF value of the isotropic sensor in the proposed E-field meter is 45.2 dB/m. Therefore, the proposed E-field meter is estimated to achieve the sensitivity of 0.06 mV/m using (2).

4. Measurement example

a) E-field meter for assessing the total exposure ratio

The total exposure is measured using the proposed E-field meter in an urban area and is shown in Fig. 8.

Figure 8 shows that the proposed E-field meter can assess the exposure ratios from not only cellular base stations, but also other stations such as TV stations. In addition, it shows that the total exposure ratio is approximately 1/5000 (2.08e-2%), and is sufficiently lower than the ICNIRP reference level.

b) E-field meter for assessing the exposure ratio profile from a IMT-2000 system base station

The exposure ratio from a W-CDMA system base station is assessed using the proposed E-field meter. The base station antenna is located in a rural area. The total exposure ratio is assessed approximately every 50 cm from under the antenna to approximately 1.6 km away. The height of the upper end of the antenna attached to a mast is 39.7 m. The total transmission power is 48 W per radio sector. The ICNIRP reference level for the 2-GHz band indicated in the ICNIPR guidelines is 61.4 V/m [1]. The assessed profile for the total exposure ratio is shown in Fig. 9. The figure shows that the maximum value of the total exposure ratio from this base station is approximately 1/10000 of the ICNIRP reference level.

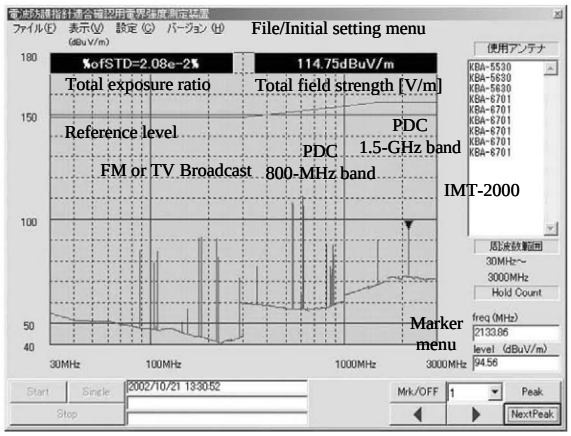


Fig. 8. Measurement example using proposed E-field meter for assessing the total exposure ratio

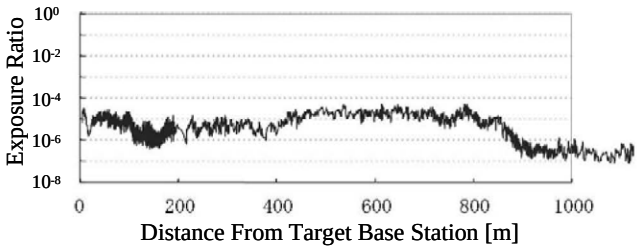


Fig. 9. Measurement example using proposed E-field meter for assessing the exposure ratio from IMT-2000 system base station

5. Summary

The proposed E-field meters achieved the following points.

1) The sensitivity of 1 mV/m was achieved using only one E-field sensor in the frequency range from 30 MHz to 3 GHz, and the total exposure ratio from multiple radio stations was assessed in the frequency range.

2) The E-field meter for assessing the exposure ratio profile from an IMT-2000 system base station comprises code selective receivers was presented, and the exposure ratio profile was assessed.

3) The total exposure ratio is less than 1/5000 of the ICNIRP reference level in an urban area.

4) The maximum value of the exposure ratio profile from a W-CDMA base station is less than 1/10000 of the ICNIRP reference level in a rural area.

References

[1] International Commission on Non-Ionizing Radiation Protection, "Guidelines for limiting exposure to time-varying electric, magnetic, and electromagnetic fields (up to 300 GHz)," April 1998.

[2] World Health Organization, "Electromagnetic fields and public health –Base stations and wireless technologies," Fact sheet N° 304, May 2006.

[3] 3GPP Organization Partners, "3rd Generation Partnership project; Technical Specification Group Radio Access Network; Base Station conformance testing (FDD) (Release 5)," pp. 40-41, 3GPP Organization Partners, June 2005.

THE EFFECT OF HUMAN OPERATOR ON THE MEASUREMENT OF THE ELECTROMAGNETIC FIELD WITH A BROADBAND PROBE

T. SAMARAS, G. TSANIDIS, J. N. SAHALOS

ARISTOTLE UNIVERSITY OF THESSALONIKI
RADIOCOMMUNICATIONS LABORATORY, DEPT. OF PHYSICS,
GR-54124 THESSALONIKI, GREECE

ABSTRACT

In this work we investigated the effect of the human operator body on the measurement of an electric field with a broadband probe. The finite-difference in time-domain technique was used to evaluate the influence. A numerical model of a commercially available probe was created and examined for its operation both within and outside its intended frequency use. Two homogeneous models of the human operator made of dispersive muscle-like material were considered. The first one was with the arm raised above the head at an angle of 45^o with the horizon and the second one was with the arm extended in front of the thorax. Several angles of incidence of the plane wave were simulated and it was shown that the former configuration (arm raised) resulted in more accurate measurements than the latter one. Furthermore, it was established that not only the presence of the human was responsible for the discrepancy of the measured values, but also the input impedance of the probe's dipoles which changed, due to coupling with the human body, thus altering the antenna factor that had been calculated during calibration.

I. INTRODUCTION

In the recent years, the concern, which arose about the possible health hazards of non-ionizing electromagnetic radiation, has led to the introduction of standards or safety guidelines on exposure. In order to compare with the limiting values set in such documents, it is necessary to have a probe that can accurately measure the electric field. There are a lot of factors, which reduce measurement accuracy. The most typical and frequent factors result mainly from the type of antenna used inside the probe, its size, and the mutual coupling between the antenna and the radiation source. Apart from the above, other factors include the detector's dynamic characteristics, the termination of the measurement probe and the deformation of the measured field, which is caused, e.g. by the person performing the measurement.
In the present study, we examine the influence of the human operator on the calibrated characteristics of a field probe and, consequently, on the measurement accuracy. In particular, we investigate what is the effect of the proximity of the human body on the probe's frequency response, its isotropicity and the calculated antenna factor (AF).

II. MATERIALS AND METHODS

Principle of operation of a broadband probe

A broadband probe of the electric field usually consists of a dipole antenna, a non-linear detector, lumped elements, which are used for filtering and shaping, a transmission line and some monitoring instrumentation. The principle of operation of the probe is based on the production of a voltage across the detector at the antenna terminals, when a continuous wave field is applied. This radiofrequency voltage has a dc component proportional to the square of the incident field, due to the non-linear characteristics of the detector. This component is filtered and is conveyed over the transmission line to the monitoring instrumentation. In order to obtain an omnidirectional pattern of the measurement probe, it is necessary to use three mutually perpendicular antennas and to sum their output voltages, so as to result to the output voltage [1].

Numerical model of the broadband probe

The numerical modeling was performed with the use of the finite-difference in time-domain (FDTD) technique. The model of the probe was based on a real product (Narda Model 8760), which operates in the frequency range from 300kHz to 1GHz. The isotropicity of the probe was achieved with three dipoles, which were placed on planar substrates combined to form a beam with the cross section of an equilateral triangle. Each of the orthogonal dipoles formed an angle of 54.74^o with the axis of the beam (Figure 1). These dipoles consisted of a

layer of a perfect electrical conductor with 9cm length, 4cm width and 0.2 mm thickness, printed on a dielectric substrate 1.4mm thick, of which the dielectric constant was assumed to be 3. Across the gap between the two parts of the dipole antenna a lumped element was mounted with resistance 1MΩ, where the induced voltage was measured due to the incident electric field (linear detector). The effective voltage of the measurement probe resulted from the summation of the induced voltages of the three dipoles, after squaring them. This structure was placed inside an empty cup, whose shape was conical. The shaft of the probe was assumed made of dielectric material, with the same dielectric constant 3, and had a radius of 2cm.



(a) (b)

Figure 1: (a) Cross section of the probe (b) Side view of the probe with the dipoles

During the process of calibration, the probe was excited by a plane wave with vertical polarization and field strength of 1V/m. Figure 2 presents the frequency response of the probe in the frequency range from 300kHz to 2.4GHz. The response in the operation range of the probe was almost frequency independent and its flatness was within ±0.75dB. When the frequency was increased beyond the point where the dipole antenna is electrically short ($\beta_o h<0.3$), the response was seen to peak in the vicinity of the frequency for the first resonance of the dipole antenna ($\beta_o h=\pi/2$), which is approximately at 1.6GHz. The curves of Figure 3 indicate that the probe's linearity is very weakly dependent on the frequency in its operation range. The radiation pattern of the probe (not shown here) confirms that isotropy is achieved by the mutually orthogonal configuration of the three dipoles.

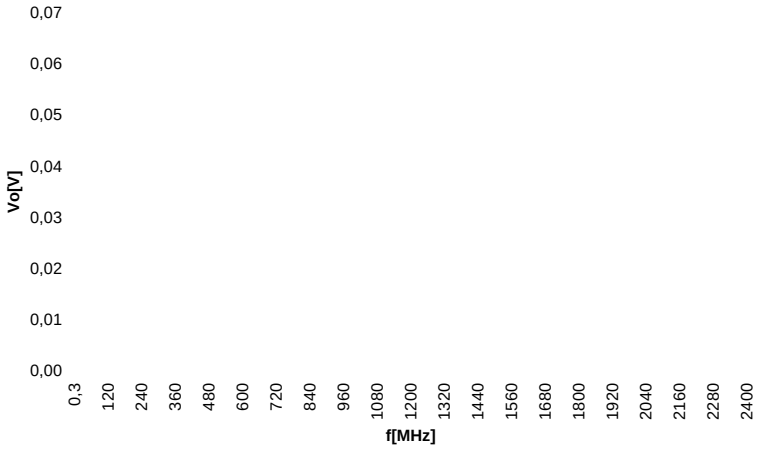


Figure 2. Frequency response of the numerical model of the probe to a plane wave of vertical polarization and electric field strength of 1V/m

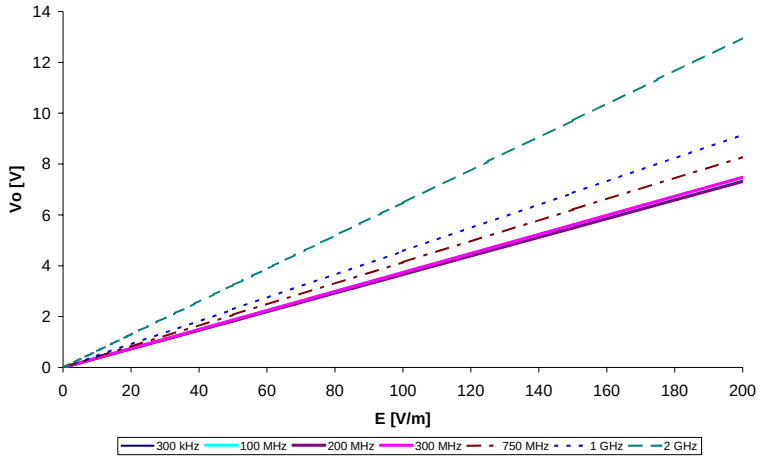


Figure 3. Response of the numerical model of the probe to a plane wave of vertical polarization and varying electric field strength for several frequencies

Through the process of calibration the antenna factor (AF) in dB(1/m) can be determined:

$$AF = 20\log_{10}(\frac{E}{V}) \quad (1)$$

where E is the electric field incident on the antenna and V is the voltage developed across the output of the antenna. Accordingly, an unknown electric field can be determined by the calibrated probe in terms of the measured voltage. Figure 4 shows the calculated AF, which seems to be approximately flat in the operation range, while the range of the first resonance of the dipoles is obvious.

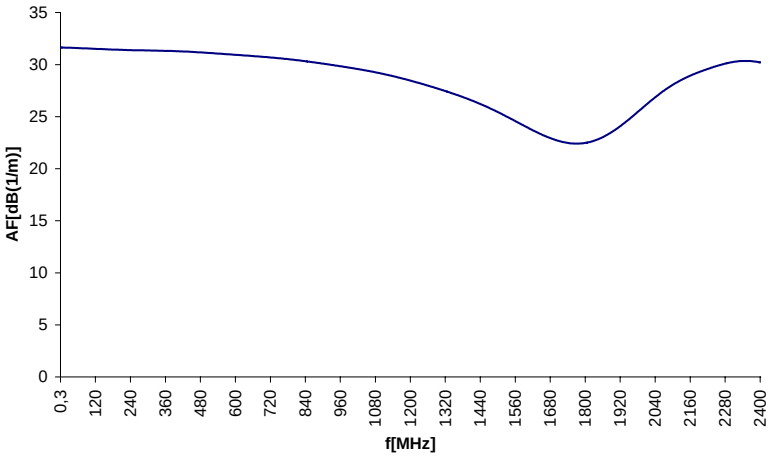
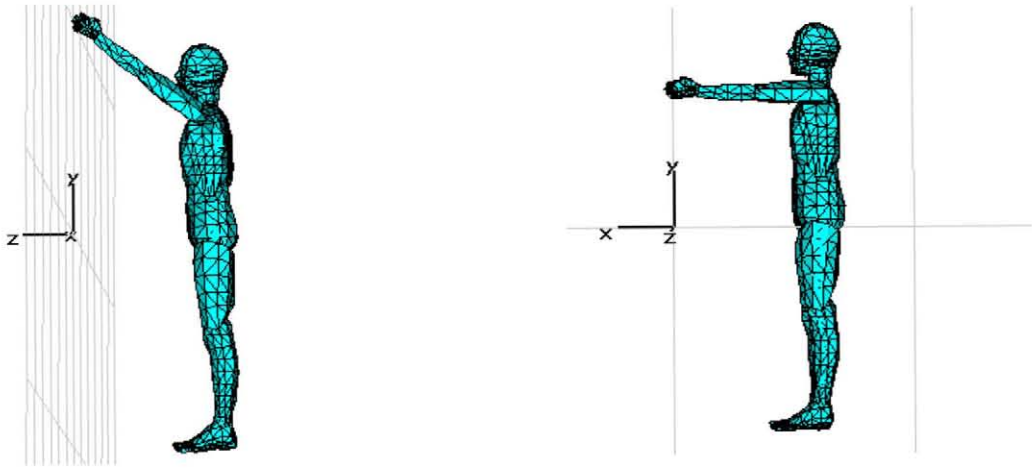


Figure 4. The antenna factor (AF) of a probe calibrated with a plane wave of vertical polarization

Numerical model of the human operator

Our computations assumed a human model of 1.70m height, 0.4625 width and 0.47m depth, which was available on the internet (www.3dcafe.com). The hand of the model was moved with program CtrlView® (www.ctrlview.com) to create two different human models. Figure 5a shows the human model for which the direction of the hand forms a 45^{o} angle with the horizon. For the second model the direction of the hand coincided with the direction of the horizon (Figure 5b). Both models were homogenous and consisted of material corresponding to human muscle. The dielectric properties of the muscle-simulating material were described by a 2nd order Debye model, in order to take into account the frequency dependency of them in the range of 300kHz to 2.4GHz. The constants assumed were ε_{∞}=40, ε_{s1}=3948, ε_{s2}=59.09, τ_1=4.62×10^{-8}s, and τ_2=9.11×10^{-10}s.



(a) (b)

Figure 5: (a) Human model with raised arm (b) Human model with extended arm

III. RESULTS

In the following we discuss the influence of the human body on the frequency response and the isotropicity of the calibrated probe. Figure 6 presents the frequency response of the probe, when the latter was used by the first and second human model respectively and was illuminated by a plane wave similar to that used in the calibration procedure. In both cases the variation with frequency was more intense than when the probe was in free space, a fact which confirms that the presence of the human affects the electromagnetic environment. In the case of the second model (Figure 6b), the influence of the human was more evident, because the measurement was performed in front of the body, which results in the probe being influenced by all the changes of the field caused by the human. In both models alterations were also observed in the isotropicity of the measurement probe, especially in the vertical plane. The second model seems to have affected more the isotropicity of the probe than the first one and especially in the higher frequencies, where the wavelengths became smaller than the model's dimensions.



(a) (b)

Figure 6: Calibration response of the probe in the presence of the human model (a) and (b) of Figure 5.

In the present study we also investigated a series of measurement configurations, in which the probe was held by the human model and was excited by plane waves with different polarizations and from different directions. Initially we simulated the first human model (raised arm) with the probe for a vertically polarized incident plane wave coming from the front of the model. With regard to the accuracy of the measurement, we always compute the percent relative divergence of the measured and the actual field based on:

$$J[\%] = \frac{E_{TRUE} - E_{MEASURED}}{E_{TRUE}} \times 100 \quad (2)$$

Figure 7 demonstrates the deviation as a function of the frequency of the incident wave. It seems that the measured field followed to a satisfactory degree the variations of the actual field in the probe's operation range (300kHz - 1GHz), where the deviation was less than 1.6dB. This divergence of field was caused by the changes of the dipole's input impedance, because of the coupling, which takes place between the human model and the measurement probe. This variation of impedance of the three dipoles is shown in Figure 8, where it can be noticed that there fluctuations in the lower frequencies and a stabilization in the range above 200MHz.

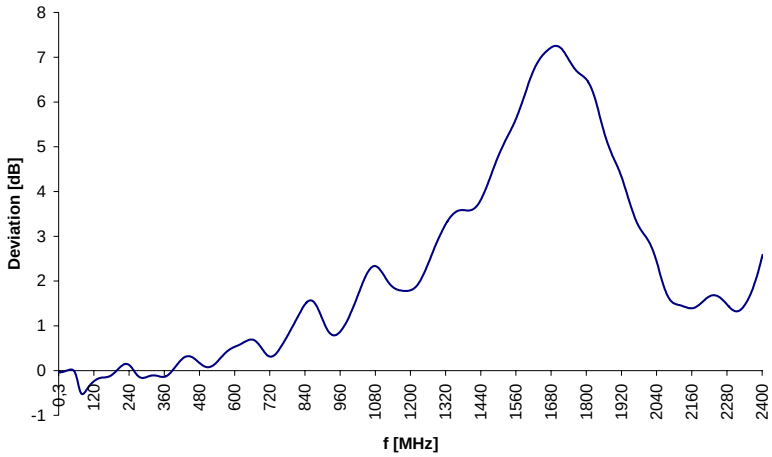


Figure 7. Deviation of the measured electric field from the true electric field for the human model with the raised arm

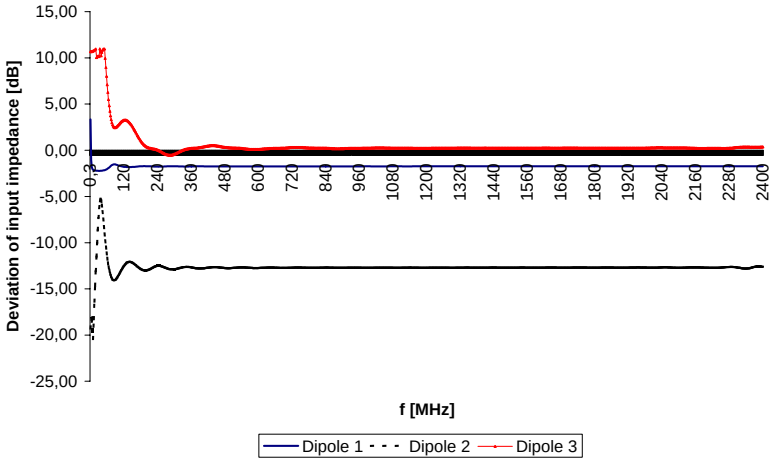


Figure 8. Deviation of the input impedance of the probe's dipoles due to coupling with the human body

In the higher frequency range (above 1 GHz) the difference between the measured and the actual field was greater than in the operation range, not only due to the change of the impedance of the dipoles, but also because of the reduction in the calculated AF, since this is the range of dipole resonance. As a result there was an underestimation of the electric field up to 55%. This means that when the probe is used in an environment of multiple sources, there must be adequate filtering, so that the measurement is not contaminated by fields in the frequency range, where the probe fails to operate correctly.

As a further step, we examined the incidence of the plane wave from various other angles and not only from the front of the model. The different deviation between measured and actual field established that the coupling between human and probe was dependent on the direction of the incident field. Moreover, we simulated a horizontally polarized plane wave irradiating the human operator from the front, showing that coupling also depended on field polarization.

We repeated the above procedure for the second human model (extended arm). Figure 9 shows that this model affected more the accuracy of measurement than the first one, when it was illuminated from the front, because of the fields scattered by the human body. In this case, the deviation of the measured value from the true one reached 4dB. However, for the higher frequencies (> 100MHz), this deviation became less than 2dB, when the field was incident from the back of the human operator.

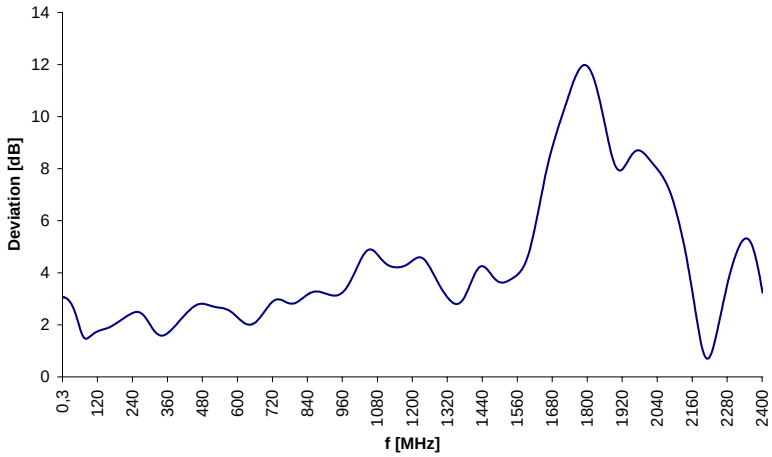


Figure 9. Deviation of the measured electric field from the true electric field for the human model with the extended arm

IV. DISCUSSION - CONCLUSIONS

The use of a probe consisting of three mutually vertical dipoles can be used for the measurement of electric fields only in its operation range. The frequency response of the probe is limited by the dipoles dimensions. The cup or the shaft of the probe do not seem to affect the measurement, as long as they are present in its calibration. However, the presence of the human operator changes the incident electromagnetic field. As a result the probe does not measure the real incident field, but the one developed around the human operator. The deviation is larger when the operator holds the probe with an extended arm in front of him/her and becomes smaller when he/she holds it with an arm raised above his/her head at an angle of 45^{o} with the horizon. This is actually the way of use proposed by the manufacturer and has been confirmed by the simulations conducted in this study. For this configuration, it was found also (not presented here) that the effect of the ground is minimized, since the probe is high above it.

Another source of inaccuracy in the measurement is the change of input impedance of the dipoles, since they couple with the dielectric body of the human operator. This change in impedance leads to a different AF from the one evaluated during the calibration. Therefore, even if the incident field remained unchanged, the probe would still give a wrong field value. The coupling of the probe with the human body depends on the angle of arrival, the frequency and the polarization of the incident field, making the introduction of a correction factor impossible.

REFERENCES

[1] H. I. Bassen and G. S. Smith, “Electric Field Probes – A Review”, *IEEE Trans Antennas Propagat*, vol. 31, no. 5, pp. 710-718, 1983

VARIATION OF RFR VIA APPLIED HUMAN VOICE AND PURE TONE IN DIFFERENT STRENGTHS & FREQUENCIES TO MOBILE PHONE

ELCIN OZGUR, GOKNUR GULER

BIOPHYSICS DEPARTMENT, GAZI UNIVERSITY MEDICAL FACULTY
GAZI UNIVERSITESI TIP FAKULTESI BIYOFIZIK ANABILIM DALI
06510 BESEVLER ANKARA TURKEY
elcinozgur@gazi.edu.tr, gozturk@gazi.edu.tr

Abstract
GSM DCS 1800 mobile phone radiation emitted by Nokia 3210 (0.81 W/kg digital SAR) was measured by electromagnetic radiation meter while speaking into phone by different frequency-strength pure tone and human voices generated sound production device, also in quiet condition in the sound-proof room. The measurements are taken in 2-second-periods as instantaneously during 6 minutes and saved in high configuration computer. Average values of these measurement data were calculated after whole experiment concluded.
In quiet condition, 7.7 V/m external E fields were averaged. Applied pure tone, man and woman voices, between 0-120 dB strength and 125-8000 Hz frequency range made E field values increase approximately as 24 V/m.
It was detected that all types of sound in 60 dB strength and having 3-4 kHz frequencies, daily life speech range are the threshold for mobile phone radiation increment. Statistically insignificant change was observed between quiet condition and below 60 dB range. 60 dB and loader voices in the range of 1-4 kHz frequencies generated nearly the same E field values as 24 V/m.

Introduction
Number of mobile phone users already above 2 billion and it is anticipated that this number will reach to 5 billion next 5 years. Not only basic qualifications such as voice, data and image transfer, but also mobile phones becoming multi terminal devices make the body of consumer grow. Innovations on mobile phone technology are actualized everyday such as models taking picture, recording video, for babies and having options of “push and talk” which teenagers like and use very often. The wide and growing use of cellular phones has also raised questions about the possible health risks associated with Radio Frequency (RF) electromagnetic fields. In order to estimate health risks, cellular phone users have to obtain the relative exposure levels. However, the RF exposure level is very difficult to measure accurately and quantify for all individuals as SAR (Specific Absorption Rate) because exact measurements of SAR in vivo, which has a direct effect on user in relation to the output level of cellular phone, are almost impossible[1]. ICNIRP (International Commission for Non-Ionizing Radiation Protection) prepared guidelines for limiting EMF exposure directly related to adverse health effects caused by EMF radiation by means of coupling with body directly or indirectly. Two classes of guidance are presented as Basic restrictions and Reference levels. Basic restrictions are the restrictions on exposure to time-varying electric, magnetic, and electromagnetic fields that are based directly on established health effects. Depending upon the frequency of the field, the physical quantities used to specify these restrictions are current density (**J**), specific energy absorption rate (SAR), and power density (**S**). Reference levels are provided for practical exposure assessment purposes to determine whether the basic restrictions are likely to be exceeded. Some reference levels are derived from relevant basic restrictions using measurement and/or computational techniques, and some address perception and adverse indirect effects of exposure to EMF. The derived quantities are electric field strength (**E**), magnetic field strength (**H**), magnetic flux density (**B**), power density (**S**), and currents flowing through the limbs (*IL*)[2,3]. In other words, determining of the reference levels gives information about if the basic restrictions are exceeded.
In this study, we measure the cellular phone radiation operating in GSM DCS 1800 MHz by using electromagnetic radiation meter in order to determine the individuals’ exposure levels to inform the quantity of exposure and estimate health risks. Mobile phone, Nokia 3210 with 0,81 W/kg digital SAR value was used.

Measurements were executed while pure silence, and also applying pure tone, man and woman voices, between 0-120 dB strength and 125-8000 Hz frequency range spoken into the mobile phone in a pure silent room.

Materials and Methods

Two identical Nokia 3210 (0.81 W/kg) were chosen as mobile phones for which we obtain the exposure level while speaking into the phone with the human voices in different frequencies and intensities. Also we measured the exposure value when pure tone applied. Pure tone, artificial sound not exist in nature, was generated by audiometer (Interacoustics Clinical Audiometer AC 40) applied to mobile phone microphone as receiver using headphone (SONY). Audiometer operates pure tone in 0-120 dB strength and 125-8000 Hz frequency range. Also, it can modulate average tone of man and woman voices into different frequencies and strengths in the same range. A woman and a man volunteers whose voices are in the average range of frequencies. NARDA EMR 300 and type 8.3 probe were used as radiation measurement device. Measurements were taken for duration of 10 minutes per 2 seconds and the data saved to the computer connected to device via fiber optic cable. The whole data were averaged before statistical analysis.

4 cases as “pure silence”, “pure tone”, “woman voice”, “man voice” are analyzed if measured external E field levels change with respect to type, frequency and intensity of voice.

Result

For Nokia 3210, there is an increase for certain frequencies and strengths in tree of these four cases of which “pure tone”, “woman voice”, “man voice” with respect to “pure silence”($p<0.05$). However, this increase is independent of voice type, namely external E field levels are the same for “pure tone”, “woman voice”, “man voice”.

For 125 Hz, E field is 7,68 V/m same as in pure silence mode in all intensities starting from 0 dB up to 120 dB. For 250 Hz, with the voice of 90 dB, 100 dB and 110 dB intensities speaking into mobile phone changing the external E field level as 23,89 V/m ; 24,26 V/m ; 24,19 V/m respectively. For 500 Hz; changes in E field beginning between of 90 dB and 120 dB the intensities as 24,13 V/m by 90 dB; 24,26 V/m by 100 dB; 24,17 V/m by 110 dB and 24,17 V/m by 120 dB. For 750 Hz; voices between 80 dB-120 dB intensities makes field values as 24,1 V/m; 23,83 V/m; 24,25 V/m; 24,16 V/m and 24,15 V/m respectively. Also, the E field level changed by applying the voice intensity of the same range for 1 kHz as 24,15 V/m; 23,87 V/m; 24,23 V/m; 24,18 V/m and 24,15 V/m . The threshold intensity that change the E field level generated by mobile phone for 1.5 kHz sound is 70 dB. The E field levels for intensities between 70 dB and 120 dB are 24,13 V/m; 24, 13 V/m; 23,9 V/m; 24,18 V/m; 24,15 V/m respectively. Again for voice having 2 kHz frequency and intensities changing from 70 dB to 120 dB, the field values are 24,13 V/m; 24,13 V/m; 24,07 V/m; 24,23 V/m; 24,16 V/m and 24,16 V/m.

Voice in frequency of 3 kHz makes the E field value change if these voices are 60 dB and more strength. For 2 kHz and 60 dB voice makes E field level as 23,81 V/m. and for the other intensity of voices in this frequency which increase the level of mobile phone’s radiation are 24,12 V/m; 24,29 V/m; 24,28 V/m; 24,25 V/m and 24,22 V/m respectively. For 4 kHz also there are the same range of intensity as 60 dB – 120 dB having E field value as 23,95 V/m; 24,13 V/m; 24,13 V/m; 24,43 V/m; 24,41 V/m and 23,73 V/m and 23,55 V/m respectively. In 6 kHz, only 110 dB and 120 dB voices increase the radiation as 24,22 V/m and 24,20 V/m. For 8 kHz voices in all strengths, E field value measured as 7,89 V/m nearly the same as in pure silence mode. Table 1 contains all these data in detail. For this reason, whole data averaged for three types of voices (Table 1, Figure 1-4)

Discussion

The use of mobile phone by adult, young people, children and the elderly has grown rapidly which causes increased concern of public, scientists and experts about the health effects of these phones in the last years. Therefore, the intensive research continues to be carried out in order to find if they cause any possible health risk for humans.

GSM-1800 signals SAR levels ranging from 0.1 to 2 W/kg. Modulations named as GSM-217, GSM-Basic, GSM-DTX or GSM-Talk have SAR values between this range.

GSM-217Hz is GSM signals are amplitude modulated by rectangular pulses with a repetition frequency of 217 Hz and a duty cycle of 1:8 (pulse width 0.576 ms), corresponding to the dominant modulation component of GSM. The ratio between slot average SAR and time average SAR is 8. GSM- Basic is in addition to this basic GSM-217Hz TDMA frame, every 26th frame is idle, which adds an 8 Hz modulation component to the signal . The ratio between slot average SAR and time average SAR is 8.3. The discontinuous transmission mode (DTX) is active during periods without speaking into the phone. To save battery power, the transmission is reduced to 12 frames per intermediate multiframe of 104 frames (compared to 100 frames for GSM Basic). The frame structure of the DTX signal results in 2, 8 and 217 Hz components. The ratio between slot average SAR and time average SAR is 69.3.

GSM-Talk generates temporal changes between GSM-Basic and GSM-DTX and simulates a conversation with an average duration of 97s and 50s for Basic and DTX, respectively. The ratio between slot average SAR and time average SAR is 11.9. Furthermore, arbitrary field on/off intermittence in the range from seconds to hours can be applied [4,5,6].

In this study, Mobile phone Nokia 3210, spoken into the phone, mostly in GSM Basic mode measured externally in order to obtain an opinion about how much user exposure. All in all, we found that the external E field which mobile phone generates while user speaks into phone without cease is triple of the measured value while nobody speaks into phone when conversation is ended for both user.

In Lonn at al. study, the output power for all mobile phone callas managed by GSM operator Telia Mobile was recorded during one week in four defined areas (rural, small urban, suburban and city area) in Sweden [7]. The recording included output power for 900 MHz and the 1800 MHz frequency band. Conclusion of this report is that in rural areas where base stations are sparse, the output power level used by mobile phones are on average considerably higher than in more densely populated areas. So, our experiment was done in pure silent room in the city center where the base stations near and actively operated and in the time period of before primetime (09.00-11.30 AM), prime time(12.00- 13.30 AM) and after prime (14.00-17.00 AM) time of weekdays.

As a result, we found that mobile phone user expose more RF radiation when he / she is talking in the periods out of prime time. In the period called as prime time the external E field value is constant both for silence and speaking into mobile phone.

There is no difference if the voice belonging to woman, man or child on the level of external E field that mobile phone generates. There is threshold level of sound intensity changing mobile phones technology. 50 decibels (dB) the range of whispering is the threshold strength in order to recognize the voice which is speaking into mobile phone Nokia 2100 although 60 dB can be solely threshold for Nokia 3210.

A quantitative assessment of individual exposure to radiofrequency fields epidemiological studies of possible health effects for many reasons.

Table 1: External electric field values (V/m) generated by Nokia 3210 in GSM-Talk modulation with pure tone, woman and man's voices in a sound proof room.

Intensity/ Frequency	**Nokia 3210**			
(dB/Hz)	**Pure Silence**	**Pure Tone**	**Man's Voice**	**Woman's voice**
0 /125	7.68	7.68	7.7	7.68
10 /125	7.68	7.68	7.7	7.68
20 /125	7.68	7.68	7.7	7.68
30 /125	7.68	7.68	7.7	7.68
40 /125	7.68	7.68	7.7	7.68
50 /125	7.68	7.68	7.7	7.68
60 /125	7.68	7.68	7.7	7.68
70 /125	7.68	7.68	7.7	7.68
80/125	7.68	7.68	7.7	7.68
90 /125	7.68	7.68	7.7	7.68
0 /250	7.68	7.69	7.69	7.69
10 /250	7.68	7.69	7.69	7.69
20 /250	7.68	7.69	7.69	7.69
30 /250	7.68	7.69	7.69	7.69
40 /250	7.68	7.69	7.69	7.69
50 /250	7.68	7.69	7.69	7.69
60 /250	7.68	7.69	7.69	7.69
70 /250	7.68	7.69	7.69	7.69
80/250	7.68	7.69	7.69	7.69
90 /250	7.68	23.87	23.9	23.89
100 /250	7.68	24.26	24.27	24.26
110 /250	7.68	24.19	24.2	24.19
0 /500	7.68	7.9	7.9	7.9

10 /500	7.68	7.9	7.9	7.9
20 /500	7.68	7.9	7.9	7.9
30 /500	7.68	7.9	7.9	7.9
40 /500	7.68	7.9	7.9	7.9
50 /500	7.68	7.9	7.9	7.9
60 /500	7.68	7.9	7.9	7.9
70 /500	7.68	7.9	7.9	7.9
80/500	7.68	7.9	7.9	7.9
90 /500	7.68	24.1	24.15	24.13
100 /500	7.68	24.26	24.27	24.26
110 /500	7.68	24.17	24.17	24.17
120 /500	7.68	24.17	24.18	24.17
0 /750	7.68	7.62	7.62	7.62
10 /750	7.68	7.62	7.62	7.62
20 /750	7.68	7.62	7.62	7.62
30 /750	7.68	7.62	7.62	7.62
40 /750	7.68	7.62	7.62	7.62
50 /750	7.68	7.62	7.62	7.62
60 /750	7.68	7.62	7.62	7.62
70 /750	7.68	7.62	7.62	7.62
80/750	7.68	24.1	24.1	24.11
90 /750	7.68	23.85	23.8	23.84
100 /750	7.68	24.25	24.26	24.25
110 /750	7.68	24.15	24.17	24.15
120 /750	7.68	24.15	24.15	24.15
0 /1000	7.68	7.9	7.9	7.9
10 /1000	7.68	7.9	7.9	7.9
20 /1000	7.68	7.9	7.9	7.9
30 /1000	7.68	7.9	7.9	7.9
40 /1000	7.68	7.9	7.9	7.9
50 /1000	7.68	7.9	7.9	7.9
60 /1000	7.68	7.9	7.9	7.9
70 /1000	7.68	7.9	7.9	7.9
80/1000	7.68	24.15	24.13	24.18
90 /1000	7.68	23.85	23.87	23.88
100 /1000	7.68	24.2	24.26	24.24
110 /1000	7.68	24.16	24.2	24.17
120 /1000	7.68	24.16	24.17	24.15
0 /1500	7.68	7.9	7.9	7.9
10 /1500	7.68	7.9	7.9	7.9
20 /1500	7.68	7.9	7.9	7.9
30 /1500	7.68	7.9	7.9	7.9
40 /1500	7.68	7.9	7.9	7.9
50 /1500	7.68	7.9	7.9	7.9
60 /1500	7.68	7.9	7.9	7.9
70 /1500	7.68	24.13	24.1	24.2
80/1500	7.68	24.14	24.1	24.14
90 /1500	7.68	23.85	24	23.85

100 /1500	7.68	24.25	24.2	24.25
110 /1500	7.68	24.15	24.17	24.15
120 /1500	7.68	24.14	24	24.13
0 /2000	7.68	7.96	7.96	7.96
10 / 2000	7.68	7.9	7.9	7.9
20 /2000	7.68	7.96	7.96	7.96
30 /2000	7.68	7.9	7.9	7.9
40 /2000	7.68	7.96	7.96	7.96
50 /2000	7.68	7.9	7.9	7.9
60 /2000	7.68	7.9	7.9	7.9
70 /2000	7.68	24.13	24.14	24.13
80/2000	7.68	24.14	24.12	24.14
90 /2000	7.68	24	24.11	24.1
100 /2000	7.68	24.24	24.2	24.26
110 /2000	7.68	24.17	24.13	24.18
120 /2000	7.68	24.14	24.16	24.19
0 /3000	7.68	7.89	7.89	7.89
10 / 3000	7.68	7.89	7.89	7.89
20 / 3000	7.68	7.89	7.89	7.89
30 / 3000	7.68	7.89	7.89	7.89
40 / 3000	7.68	7.89	7.89	7.89
50 / 3000	7.68	7.89	7.89	7.89
60 / 3000	7.68	23.83	23.8	23.81
70 / 3000	7.68	24.11	24.13	24.1
80/ 3000	7.68	24.11	24.13	24.1
90 / 3000	7.68	24.23	24.33	24.3
100 / 3000	7.68	24.3	24.2	24.33
110 / 3000	7.68	24.2	24.2	24.34
120 / 3000	7.68	24.17	24.17	24.31
0 / 4000	7.68	7.89	7.89	7.89
10/ 4000	7.68	7.89	7.89	7.89
20 /4000	7.68	7.89	7.89	7.89
30 /4000	7.68	7.89	7.89	7.89
40 /4000	7.68	7.89	7.89	7.89
50 /4000	7.68	7.89	7.89	7.89
60 /4000	7.68	24.01	23.91	23.92
70 / 4000	7.68	24.13	24.13	24.13
80/ 4000	7.68	24.13	24.13	24.13
90 / 4000	7.68	24.43	24.43	24.43
100 / 4000	7.68	23.41	23.41	24.41
110 / 4000	7.68	23.59	23.69	23.9
120 / 4000	7.68	23.58	23.59	23.48
0 / 6000	7.68	7.94	7.94	7.94
10/ 6000	7.68	7.94	7.94	7.94
20 / 6000	7.68	7.94	7.94	7.94
30 / 6000	7.68	7.94	7.94	7.94
40 / 6000	7.68	7.94	7.94	7.94
50 / 6000	7.68	7.94	7.94	7.94

60 / 6000	7.68	7.94	7.94	7.94
70 / 6000	7.68	7.94	7.94	7.94
80/ 6000	7.68	7.94	7.94	7.94
90 / 6000	7.68	7.94	7.94	7.94
100 / 6000	7.68	7.94	7.94	7.94
110 / 6000	7.68	24.17	24.26	24.17
120 / 6000	7.68	24.21	24.24	24.16
0 / 8000	7.68	7.89	7.89	7.89
10/ 8000	7.68	7.89	7.89	7.89
20 / 8000	7.68	7.89	7.89	7.89
30 / 8000	7.68	7.89	7.89	7.89
40 / 8000	7.68	7.89	7.89	7.89
50 / 8000	7.68	7.89	7.89	7.89
60 / 8000	7.68	7.89	7.89	7.89
70 / 8000	7.68	7.89	7.89	7.89
80/ 8000	7.68	7.89	7.89	7.89
90 / 8000	7.68	7.89	7.89	7.89
100 / 8000	7.68	7.89	7.89	7.89
110 / 8000	7.68	7.89	7.89	7.89

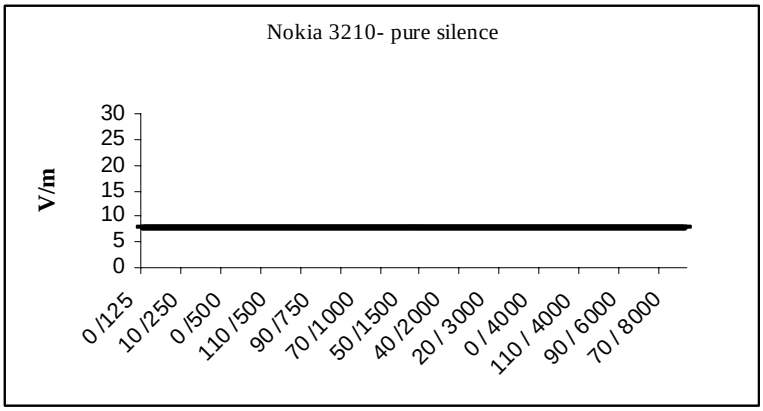


Figure 1: External electric field values (V/m) generated by Nokia 3210 in GSM-Talk modulation in pure silence in a sound proof room

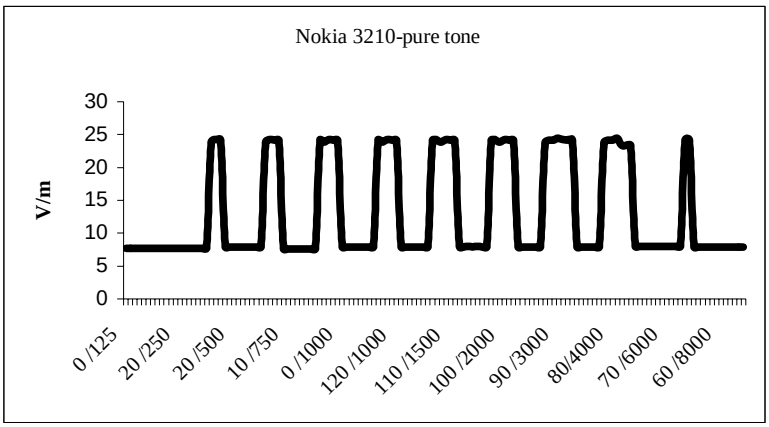


Figure 2: External electric field values (V/m) generated by Nokia 3210 in GSM-Talk modulation with pure tone in a sound proof room.

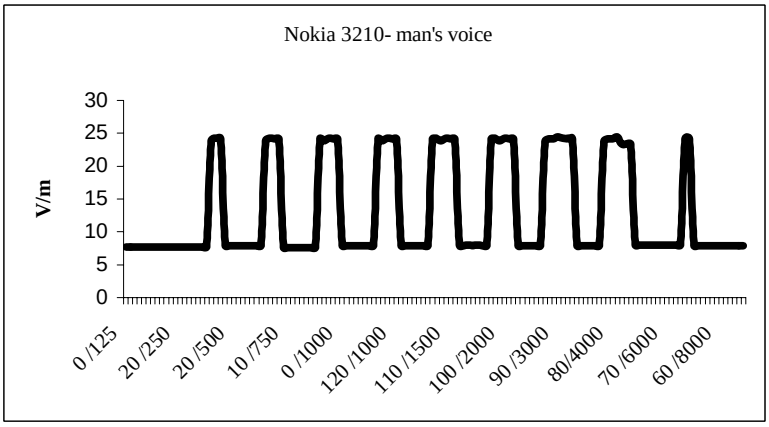


Figure 3: External electric field values (V/m) generated by Nokia 3210 in GSM-Talk modulation with man's voices in a sound proof room.

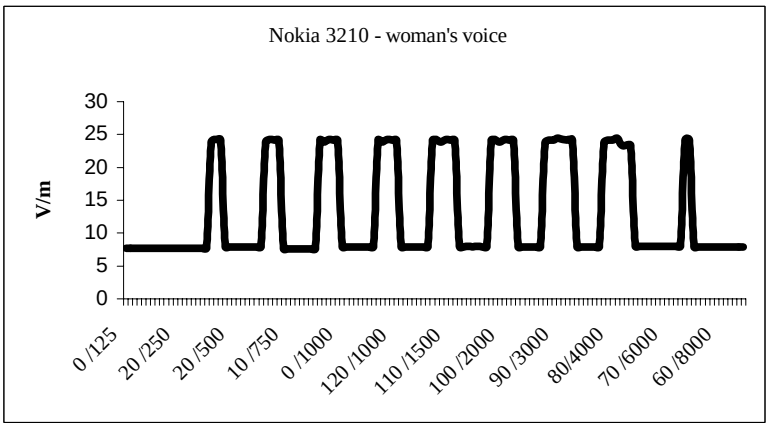


Figure 4: External electric field values (V/m) generated by Nokia 3210 in GSM-Talk modulation with woman's voices in a sound proof room.

References

1) Kim, S.C., Nam, K.C., Kim, D.W. (2005). Estimation of relative exposure levels for cellular phone users using a neural network, Bioelectromagnetics online,DOI 10.1002/bem.20203,www..interscience.wiley.com
2) ICNIRP 1998 Standards: Guidelines for Limiting Exposure to Time Varying Electric and Magnetic Fields (Up to 300 GHz), International Commission on Non-Ionizing Radiation Protection, Health Physics, 74, 494-522, (1998).
3) ICNIRP Health Issues Related to the Use of Hand-Held Radiotelephones and Base Transmitters. Health Physics, 70 , 587 (1996).
4) Capri, M., Scarcella E. ,Bianchi, E., Fumelli, C., Mesirca, P., Agostini, C., Remondini, D., Schuderer, J., Kuster, N., Franceschi, C., Bersani, F. (2004). 1800 MHz radiofrequency (mobile phones, different Global System for Mobile communication modulations) does not affect apoptosis and heat shock protein 70 level in peripheral blood mononuclear cells from young and old donors. *International Journal of Radiation Biology* 80: 389 – 397
5) Wiart, J. Dale, C. Bosisio, A.V. Le Cornec, A. (2000). Analysis of the influence of the power control and discontinuoustransmission on RF exposure with GSM mobile phones, *Electromagnetic Compatibility, IEEE Transactions*, 42, 376-385
6) REFLEX,(2004). Risk Evalution of Potential Environment Hazards From Low Frequency Electromagnetic Field Exposure Using Sensitive in vitro Methods, Final Report, EU Quality of Life and Management of Living Resources, QLK4-CT-1999-01574.
7) Lönn1, S., Forssén1,U., Vecchia,P., Ahlbom1,A. and Feychting, M.(2004). Output power levels from mobile phones in different geographical areas; implications for exposure assessment. *Occupational and Environmental Medicine* 61:769-772

MAGNETIC FIELDS FOR RELIEF OF MYOFASCIAL AND/OR LOW BACK PAIN THROUGH TRIGGER POINTS

Carlton F. Hazlewood, Marko S. Markov

Research Consultants International, Houston, USA, e-mail: carltonh@swbell.net;
Research International, Buffalo USA email: msmarkov@aol.com

Abstract

It is known that a significant fraction of both acute and chronic pain experience is myofacial in nature. This paper address the potential for pain relief to be induced by placing magnets over the trigger points associated with that referred pain. This is even more important in patients with various disabilities and experiencing chronic sacro-iliac and/or low back pain.

It is well recognized that a trigger point is a functional, rather than an anatomical, entity. From the point of view of magnetotherapy it appears to us that the trigger points represent a plausible physiological/tissue "window" and/or pathways which allows magnetic fields to penetrate through physiological barriers and thus returning injured tissues to the homeostatic state. It should be noted that these "tissue windows" represent physiological "entrance points" for eventual exogeneous stimulations, mainly physical by nature, to enter the body.

There is evidence that the application of magnetic field (via permanent magnets) on trigger points is more effective for pain relief as compared to other parts of the body surface. The systemic effects should also be considered when magnetic field effects are discussed. (We first presented this idea at the 2004 meeting in Kos.)

We discuss the mechanisms of action related to ion transport as central to the integrity and proper functioning of nerve excitability and muscle contraction. Any disruption of their normal function would directly and markedly affect human neurosensory and neuromotor performance. Biophysical phenomena associated with modification of ion transport are in the millivolt and picoampere range. Therefore, electrophysiological changes in ion channel functions are among the most sensitive indicators, if not the most sensitive indicator, to detect and quantify physiological effects of electromagnetic fields.

We postulate that in addition to the known effect of magnetic fields on water structure there could be a change in the tensile properties of cartilage, ligaments, and other soft tissue structures which secondarily may relieve tension on arthritic joints or on chronically "inflamed" areas.

Introduction

Increasing interest in alternative and complimentary medicine has attracted the attention of scientists and clinicians to the potential benefit of using various static magnetic fields and EMFs for therapeutic purposes. It is now clear that magnetic fields interact with biological tissues in a way that specific physiological changes occur. Both static and time varying magnetic fields were successfully applied to treat therapeutically resistant problems in the musculoskeletal system (Bassett, 1989 and 1994; Pilla and Markov 1994; Markov 1995; Itoh, et al., 1991; Markov and Pilla 1995; Shupak, 2003; Rosch and Markov, 2004). It is accepted that EMFs provide a practical, exogenous method for inducing cell and tissue modifications that can correct selected pathological sites. The most effective clinical applications of these physical factors are related to bone unification as well as reduction of pain and edema in soft tissues (Bassett 1989; Markov and Pilla 1995). For musculoskeletal injuries and post-surgical, post-traumatic and chronic wounds, magnetic fields are recognized as a modality that contributes to reduction of edema. It is well known that edema reduction can be a major therapeutic instrument in the acceleration of pain and stress relief. Surprisingly, edema reduction has been reported with low amplitude (in the range of 1-50 mT), low frequency (in the range of 1-100 Hz), and pulsed radiofrequency (27.12 MHz) signals applied to the site of injury/pain (Markov and Pilla 1995; Rosch and Markov, 2004).

Static and time-variable electromagnetic fields have been applied with apparent success in the management of pain in a variety of orthopedic conditions, most commonly traumatic bone fractures or surgical osteotomies (Becker and Selden, 1985; Becker, 1990; Miner and Markoll, 1993, Trock *et al.*, 1994; Bassett,1994). Carpenter and Ayrapetyan (1994) and Rosch and Markov (2004) edited books that provide excellent overviews of the biological effects of electric and magnetic fields. It is clear that this is an emerging field in biology and medicine. Attempts are being made to scientifically document the impact of electric and magnetic fields on biological systems.

The remarkable observations that there are no known adverse effects with using permanent magnets or low frequency EMF stimulation, lends support for the therapeutic use of magnetic fields is (Rosch and Markov, 2004). In addition, the large body of scientific publications supports the notion that magnetic therapy may have utility in the treatment of pain (Foley-Nolan et al. 1990 and 1992; Ellis 1993; Trock et al. 1993a, 1993b, and 1994; Markov and Pilla 1995; Vallbona et al. 1997; Sartucci et al. 1997; Sherman et al. 1998). However, it should be noted that despite a number of clinical studies performed world-wide indicating successful use of magnetic fields for treatment of various diseases and pathologies, little is known regarding the effectiveness of magnetic fields in relieving low back pain (LBP).

One of us (CFH) has placed magnets on his body in order to test for pain relief. Placing the magnet on the site of the pain experience led to some relief, but never considered satisfactory, except on rare occasions. Upon seeing a figure from Travell and Simons (1983), in a pain clinic, which schematically showed a trigger point at the mid-thigh area near the groin referring pain to the right knee cap, the idea surfaced, that one could possibly "inter the body magnetically" at the site of the trigger point. If that were the case, would pain relief be experienced? The procedure was completed within one and one half hours—the patellar pain (chronic for CFH) completely dissipated. This experience was shared with another physician-scientist, more elaborate experimental designs were considered and executed. Also, by applying the magnets to trigger points of referred pain, volunteer subjects have been relieved of their pain within twenty to forty minutes (Vallbona *et* al., 1997).

Herein, we discuss the use of static magnetic fields to provide pain relief in specific, and therapy for myofascial problems in general.

Chronic Pain Symptoms

Chronic pain can be defined as pain that persists past the normal time of healing and lasts at least six months. Chronic pain is not only a burden to the individual who must cope with the experience of persistent pain symptoms, but also to the health care system that is often unable to permanently alleviate the suffering experienced by the individual. The experience of chronic pain is a complex mixture of factors that include pathological tissue changes eliciting nociception as well as psychosocial and psychophysiological behaviors elicited by pain. By definition, pain is a subjective phenomenon. Therefore it is well understood that, in order to obtain an accurate assessment of the pain experienced by an individual, a self-report of the pain intensity and symptoms must be considered along with other appropriate medical assessments (Goodman and McGrath 1991).

Even with the rapid, and often successful advances in surgical techniques and non-invasive therapies for the treatment of painful conditions such as low back pain, many individuals suffering from these conditions continue to experience pain after medical interventions have been performed (Mayer and Gatchel 1988). The risk of anesthesia, the length and tolerance of postoperative immobility, and the effects of the biomechanics of the spine have to be considered with respect to possible surgical interventions. Bed rest, anti-inflammatory medications, steroidal injections, and physical therapy programs are often prescribed. In many of these individuals, the incidence of overuse or misuse of medication (Kouyanou et al. 1997) and excessive activity limitation (Haythornthwaite et al. 1991; Vendrig and Lousberg 1997) are not uncommon pain behaviors.

Myofascial pain: chronic pain in a different perspective .

What is myofascial pain? Let us first say some words about "myofascial problem". Physiologist have known for relatively long time that each and everyone of the some 400 skeletal muscles in the human

body are surrounded by connective tissue called fascia. For various reasons myofascial problems could occur at the surface of interaction between muscle and fascia, in many cases caused by an inflammation. The demonstration of the problem that occurs might be the appearance of a localized sensation of pain at a given spot of the body which is manifested also at the body surface as a myofascial trigger point. In many cases the trigger point might be distant from the place at which myofascial problem originated. Such trigger points might be found at different areas over the body and when touched the pain might be aggravated. Further, a myofascial trigger point is defined as a hyperirritable spot, usually within a taut band of skeletal muscle or in the muscle's fascia, that elicits a painful experience upon touch (Travell and Simons, 1983, Vol. 1, p. 3). Myofascial pain syndrome is discussed, in detail, through out the two volume set by Travell and Simons (1983, Volumes 1 and 2) entitled: MYOFASCIAL PAIN AND DYSFUNCTION. As pointed out by Travell and Simons, the word "myofascial" was used, as early as 1940, "…to describe the identification and treatment of trigger areas in muscles of the low back and by 1948, in pectoral muscles" (Vol. 1, p. 10). Janet Travell, in 1952, adopted the term *myofascial*. She observed that during an infraspinatus muscle biopsy, stroking or pinching either the superficial fascia or the contractile tissue of the muscle evoked the referred pain pattern from the muscle" (Travell and Simons, 1983, Vol. 1, p.10). In addition, Travell and Simons record that "*The expressions, 'myofascial pain' and 'myofascial syndrome,' have the advantage that they clearly situate the illness in the muscle or its fascia, and that they have been used consistently to identify TP [trigger point] phenomena…*"

Trigger points.

Trigger points may be latent or active and Travell and Simons (1983) define them as "a focus of hyperirritability in a tissue that, when compressed, is locally tender and, if sufficiently hypersensitive, gives rise to referred pain and tenderness..." Thus, a trigger point is a functional, rather than an anatomical, entity. Nevertheless, the identification of trigger points with its referred pain experience, is relatively easy to identify with the Trigger Point Manual of Travell and Simons. When a trigger point is inactive, it is difficult to identify, yet when the process of activation begins the sensitivity of the trigger point becomes greater and greater to touch—hence, easier to identify. This onset of sensitivity may be referred to as a latent trigger point. Note: an active myofascial trigger point is always associated with pain, while a latent trigger point, is not usually associated pain. The latent trigger point, however, may cause restriction of motion and weakness of the affected muscle. The latent trigger point may persist for years after partial recovery from injury has begun. Acute attacks of pain may exist, since minor overstretching, overuse, or cooling of the muscle may serve to reactivate it (Travell and Simons, 1983). In summary, both latent and active trigger points cause dysfunction, and active trigger points cause pain. Finally, it should be recognized that myofascial trigger points are to be distinguished from those of other tissues such as skin, ligaments and periosteum (Travell and Simons, 1983).

Normal muscles do not contain detectable trigger points. Normal muscles have no taut bands of muscle fibers, are not tender to firm palpation, exhibit no local twitch responses, and do not refer pain in response to applied pressure. Males or females of any age can develop trigger points--particularly sedentary, middle-aged women. Except in later years, women seem somewhat more likely than men to develop myofascial pain syndromes. It appears that women are more likely (rather than men) to seek medical aid for pain of myofascial origin (Travell and Simons, 1983).

Active trigger points are more likely to reside in postural muscles of the neck, shoulder, pelvic girdles, and the muscles of mastication. Again, the upper trapezius, scalenes, sternocleidomastoids, levator scapulae and quadratus lumborum muscles are commonly involved. *Myofascial pain is referred from trigger* points in *specific patterns characteristic of each muscle* (Travell and Simons, 1983). The trigger points, for spontaneous pain, are rarely located in the spatial area of the pain experience. That is, trigger points and the area of the pain experience are spatially displaced. Referred pain of myofascial trigger points usually is described as dull and aching, often deep, with intensity varying from low-grade discomfort to severe and incapacitating. It may occur at rest, or only on motion.

Digital pressure on a given trigger point (or penetrating the trigger point with a needle) elicits referred pain or causes an increase in intensity of that pain. The more hypersensitive the trigger point, the more intense and consistent is the referred pain, and the more extensive and sustained is its distribution. In various myofascial trigger point syndromes, pain is rarely completely symmetrical across the body. At examination, the patient usually complains of pain from the most recently activated trigger point. When this trigger point is eliminated, the pain pattern may shift to that of an earlier trigger point that also must be inactivated. If the initial (or dominant) trigger point is inactivated first, the patient may recover without further treatment. Travell and Simons (1983) point out that Pain referred from myofascial trigger points do not

follow simple segmental patterns, familiar neurological patterns, nor the known patterns for referred pain of visceral origin.

The severity and extent of the referred pain pattern depends on the degree of irritation, and/or inflammation of the trigger point, not on the size of the muscle. Trigger points are activated directly by acute overload, overwork fatigue, direct trauma, and by chilling. Primary myofascial trigger points also develop in muscles subject to excessive repetitive or sustained contractions (overload fatigue). Secondary trigger points are likely to develop in adjacent muscles that are chronically overloaded by spasms. It is well known that active myofascial trigger points vary in irritability from hour-to-hour and from day to day. The amount of stress required to produce myofascial pain is highly variable, compared with other muscular pains, including angina and intermittent claudication, that are due to arterial insufficiency. Trigger-point irritability may be increased *from a latent to an active level by* many factors. The amount of stress needed to activate a latent trigger point and thus cause a clinical pain syndrome depends on the degree of conditioning of the muscle; the greater the exercise tolerance of the muscle, the lower the susceptibility of its trigger points to activation.

Once, knowledge of the referred pain by trigger points was clear, an assumption was made that magnetic fields, applied to trigger points, would reduce or abolish the pain referred by the specific trigger point. The first test of this hypothesis was initiated in pilot study of a small population of subjects with a chronic pain condition known as the Post Polio syndrome. In this clinical setting, the trigger points and their sites of referred pain were well delineated.

Post-polio syndrome.

Overuse of body parts is perhaps the largest cause of myofascial type pain. The magnitude of the population involved with the malady is unknown; however, one well-known group within the broad group of disabilities is the survivors of polio. Within this group is found a sizable number people suffering from both chronic and acute pain: the Post-polio syndrome (PPS). Halstead *et al.* (1985) compiled responses to questionnaires sent in 1985 to polio survivors identified through informal networks. The pain was classified as myofascitis secondary to progressive denervation; and this continues to be reasonable. For example, Trojan and Cashman (2005) point out that "The cause of PPS remains unclear, but is likely due to distal degeneration of enlarged post-poliomyelitis motor units.". Subsequent observations, revealed psychological and social effects that cause changes in both quality of life and in lifestyle (Hollingsworth, *et al*, 2005). In regard to numbers: one of the latest estimates of the size of the population of polio survivors is set at one million. Within that group, the population of people with post-polio syndrome is stated to be on the order of 80% (Elrod et al., 2005) In this project, 75.5% of the patients had muscle pain and 75.4% had joint pain. The types of pain experiences in this group are multiple, including a lot of diffuse muscle and joint pain (Smith and Mabry, 1995). Recovery from the diffuse muscle pain can take many months and requires considerable compliance (Peach and Olejnik, 1991). The joint pain is thought to be due to degenerative arthritis caused by age. Subacute or chronic sacroilitis occurs very often, but many times it is not recognized because other forms of low back pain mask it.

Clinical study of Postpolio Patients. A double blind, randomized clinical trial was conducted in postpolio patients to determine if pain was relieved by application of static magnetic fields applied directly over an identified pain trigger point (Vallbona et al. 1997). The devices used in this study were Bioflex magnets (Magnalex, Inc., Corpus Christi, TX) which have a pattern of concentrically arranged circles of alternating magnet polarity. Depending on the area involved, the device was a disc (40 or 90 mm in size), a credit card-sized pad, or a strip. The magnetic field intensity of the device was rated at 500 Gauss at the device surface for the 40-mm disc and the strips. The 90-mm discs and credit-card pads were rated at 300 Gauss at the surface. Placebo devices were of identical sizes and shapes.

Fifty postpolio patients with muscular or arthritic pain participated in this study. Twenty-nine patients (5 males, 24 females; mean age=51.5 years) were randomly selected to receive treatment with the active magnetized device; 21 patients (6 males, 15 females; mean age=55.9) received treatment with the inactive device. Patients were asked to complete a McGill Pain Questionnaire to provide a subjective evaluation of his or her general pain experience (a validated method for analyzing pain). Only one area of pain was evaluated, even thought multiple sites may have been present. A trigger point associated with the site of pain was grossly elicited first by finger palpation and then by firm application of a blunt object, which in non-painful areas produced a sensation of pressure but no pain. The patient was asked to subjectively grade the pain at the trigger point on a scale from 1 to 10 (with 1 being the least and 10 being

the maximum). The appropriately sized magnetic or placebo device was placed on the area of pain with adhesive tape for 45 minutes. After removal of the device, the patient was asked to assess the intensity of pain again using the McGill Pain Questionnaire. The proportion of patients in the active-device group who reported a pain score decrease greater than the average placebo effect was 76%, compared with 19% in the placebo-device group ($p < .0001$) (Vallbona, *et al.*, 1997).

Chronic Low Back Pain

Low back pain (LBP) represents an important health problem in which medical costs and lost work capacity are major issues. Disorders of the low back are a major cause of disability of people under the age of 45 (Mayer and Gatchel 1988). In fact, work incapacity resulting from LBP has been estimated to vary between 2% and 8% in Western Europe and North America (Nachemson 1992). The medical costs associated with the treatment of low back disorders have been estimated to fluctuate between $4.6 and $60 billion annually in the U.S. (Lee 1994; Miedema et al. 1998).

Static and time-varying EMFs have been applied with apparent success in the management of pain in a variety of orthopedic conditions, most commonly traumatic bone fractures or surgical osteotomies (Bassett 1989). Furthermore, in the domain of osteoarthritis several double blind, placebo-controlled studies demonstrated the efficacy of pulsed EMFs for the relief of pain (Trock et al. 1993a, 1993b, and 1994).

A large body of scientific literature suggests that magnetic therapy my have utility in the treatment of pain (Foley-Nolan et al. 1990 and 1992; Ellis 1993; Trock et al. 1993a, 1993b, and 1994; Markov and Pilla 1995; Vallbona et al. 1997; Sartucci et al. 1997; Sherman et al. 1998). However, it should be noted that despite a number of clinical studies performed world-wide indicating successful use of magnetic fields for treatment of various diseases and pathologies, little is known regarding the effectiveness of magnetic fields in relieving LBP.

In the experimental design, trigger points were identified for the subject's pain experience. Magnets of a specific design were placed over the trigger points responsible for the pain experience. These magnets had been charged to surface field strengths between 300 to 500 Gauss and were disc-shaped. The disc magnets can be kept in place by means of adhesive tape and/or specially made double sided adhesive, which is attached directly to the disc surface. It is clear from initial studies that the application of the magnets to a trigger point can reduce or eliminate (by subjective measure) the pain referred from that trigger point. The mechanisms of the effect of magnetic fields on soft tissues have not been elucidated.

The hypothesis

One of us (MSM) have been studied the biological and clinical effects of magnetic fields for several decades. The hypothesis for "biological windows" have been proposed in 1976 and further developed. This term refers to existing preferred values of magnetic fields that cause significant biological response. It appears that Mother Nature, during evolution, created mechanisms for response at which selected magnetic fields are detected, while living creatures neglected other signals, which could be even stronger (Markov, 1994). The existence of such windows have been proven in studies with various living systems as well as with different systems in human body. Probably we should speak about "biophysical windows" instead of "biological windows". The difference should be that this idea is more related to the physical parameters of the applied endogenous signal rather than to biological characteristics. From a biological point of view, one plausible mechanism could be linked to the idea proposed by Blank (2004), who reported existence of a domain in the heat shock protein HS70 that is responsible for detecting the MF signal.

We are proposing a hypothesis that trigger points represent a real biological "window" or "door" for delivering the magnetic field to the muscles or other body parts that experience pain. Let us make a following model: The part of the body that represents an activated trigger point virtually could open the door for any physical influence. When appropriate magnetic field is applied, like a key for the locker, the door "opens" and allows the magnetic field, virtually to enter the body. Next, via the systemic effect (presented by us at Kos meeting 2003), the signal is delivered to the source of the problem – where irritation, inflammation, or some other pathophysiological disturbances took place. In that part of the body, inflammation may invoke T-lymphocytes for fighting the inflammation. As it was shown, by one of us, at the Rhodes meeting (Nindl et al, 2002) and in our recent publication (Markov et al., 2006), magnetic fields more significantly influence the lymphocytes activated by the disturbances.

This hypothesis might be summarized as follows:

- A trigger point becomes activated due to inflammation at the interface between muscles, and fascia
- If an appropriate magnetic field is applied, the trigger point secures the pathway for the magnetic field
- Via systemic effect, the signal is delivered to the source of inflammation (i.e., the interface between muscle and fascia
- Magnetic fields stimulate those T-lymphocytes that have been activated by inflammation, thus reducing the inflammation and, in turn, bring about pain relief.

We also postulate that, there could be a change in the tensile properties of cartilage, ligaments, and other soft tissue structures, which secondarily may relieve tension on arthritic joints or on chronically "inflamed" areas. Such ideas seem very possible in light of the work of Becker and Selden (1985) and Vallbona, *et* al. (1983). That the magnetic fields interact with the biological “transmission lines” contained within the trigger point area; and, that the “transmission lines” possibly communicate with the inflamed area of the pain experience. Such speculation is consistent with the concept of the systemic effect (Ericsson, *et al.*, 2005) (Markov, *et al.*, 2006).

Continuing with this line of thought, we remind the reader that connective (i.e., the extracellular matrix) has been suggested to be involved in myofascial pain as well as in pain relief. As discussed above, a network of connective tissue surrounds each muscle fiber of a given muscle, all muscle groups (arms, legs, trunk, head, and neck), all nerve fibers, neuromuscular junctions, etc. (Fawcett, 1994, Chapters 5, 10, and 11; Barker, 1974). It has been hypothesized that contraction-relaxation units exist throughout the extracellular matrix of the body (Hazlewood, 2003). It is proposed that shortening of these "units” do induce pain, and relaxation of these "units" do induce pain relief. For myofascial type pain the possibility of the involvement of the connective tissues as a player in various pain syndromes is reasonable.

In conclusion: We realize that the speculations put forth in this presentation may be a little overwhelming. Nevertheless, we ask for your indulgence--please remember, these speculations are intended to provoke both thought and experimentation. Note: We are searching for an explanation of the observation that the probability of pain relief is enhanced when a magnet is placed over a trigger point as opposed to direct placement on the painful area; and, therefore ask the question: Could trigger points serve as a sensitive “tissue window” providing pathways of stimulation to the needed area?

References

Barker, D. 1974 The morphology of muscle receptors. In: Muscle Receptors. By Barker, D., Hunt, C.C., and McIntyre, A.K. Ed. By Hunt, C.C. Springer-Verlag Berlin. 310 pp.

Bassett, C.A.L. 1989. Fundamental and practical aspects of therapeutic uses of pulsed electromagnetic fields (PEMFs). Critical Reviews in Biomedical Engineering. 17:451-529.

Bassett, A. 1994. Therapeutic Uses of Electric and Magnetic Fields in Orthopedics. In: Carpenter, D.O., and Ayrapetyan, S. Biological Effects of Electric and Magnetic Fields--*Beneficial and Harmful effects*. Vol. 2. Academic Press, Inc. pp.13-48.

Becker, R.O**.** 1990. Cross Currents. The perils of electromedicine, the promise of electromedicine. The Putnam Publishing Group, New York, NY

Becker, R.O**.**, and Selden, G. 1985. The Body Electric: Electromagnetism and the Foundation of Life:William Morrow & Company, Inc., New York, p 364.

Blank, M. and Goodman R. 2004. A biological guide for electromagnetic safety: The stress response. Bioelectromagnetics. 25: 642-646

Carpenter, D.O. and Ayrapetyan, S. (Eds.) 1994. Biological Effects of Electric and Magnetic Fields. Vol. 1, *Sources and Mechanisms* and Vol. 2, *Beneficial and Harmful Effects*. Academic Press.

Ellis, W.V. 1993. Pain control using high-intensity pulsed magnetic stimulation. Bioelectromagnetics. 14:553-556.

Elrod, L.M., Jabben, M., Oswald, G., Szirony, G.M. 2005. Vocational Implications of Post-polio syndrome. *Work.*25(2): 155-161.

Environmental Health Criteria 69: Magnetic Fields World Health Organization, Geneva 1987, p 197.

Fawcett, D.W. 1994. Bloom and Fawcett: A Textbook of Histology. Twelfth edition. Chapman & Hall, New York. 964 pp.

Foley-Nolan, D., Barry, C., Coughlan, R.J., O'Connor, P., and Roden, D. 1990. Pulsed high frequency (27MHz) electromagnetic therapy for persistent neck pain. A double blind, placebo-controlled study of 20 patients. *Orthopedics* **13**:445-451

Foley-Nolan, D., Moore, K., Codd, M., Barry, C., O'Connor, P., and Coughlan, R.J. 1992. Low energy high frequency pulsed electromagnetic therapy for acute whiplash injuries. A double blind randomized controlled study. *Scand. J. Rehab. Med.* **24**:51-59.

Glassman, L.S., McGrath, M.H. and Bassett C.A.L. 1986. Effect of external pulsing electromagnetic fields on the healing of soft tissue. Ann. Plast. Surg. 16:287-295.

Grande, D.A., Magee F.P., Weinstein, A.M., and McLeod, B.R. 1990. The effects of low-energy combined AC and DC magnetic fields on articular cartilage metabolism. Annals N.Y. Acad. Sci. 404-407.

Halstead, L.S., Wiechers, D.O., Rossi, C.R. 1985. Late effects of poliomyelitis: A national survey. In: Halstead LS, Wiechers DO (eds): *Late Effects of Poliomyelitis.* Miami, Florida: Symposia Foundation.

Hazlewood, C. F. 2003. Treatment of Post-Polio Pain with a Static Magnetic Field and Some Notions on Mechanism. In: "Magnetotherapy: Potential Therapeutic Benefits and Adverse Effects". Ed. By Michael J. McLean, Stefan Engstrőm and Robert R. Holcomb Floating Gallery Press. pp. 191-207.

Haythornthwaite, J.A., W.J. Sieber, and R.D. Kerns. 1991. Depression and the chronic pain experience. Pain. 46:177-184.

Health and Safety Guide No. 27: Magnetic Fields Health and Safety Guide. World Health Organization. 1989, p 24.

Herman, E., R. Williams, P. Stratford, A. Fargas-Babjak, and M. Trott. 1994. A randomized controlled trial of transcutaneous electrical nerve stimulation (CODETRON) to determine its benefits in a rehabilitation program for acute occupational low back pain. Spine. 19:561-568.

Hollingsworth, L., Diderot, M.J., and Levington, C. 2005 Post-polio Syndrome: Psychological Adjustment to Disability. *Issues Ment. Health Nurs* 23(2): 135-156.

Itoh, M., Montemayor, J.S., Matsumoto, E., Eason, A., Lee, M.H., and Folk, F.S. 1991. Accellerated wound healing of pressure ulcers by pulsed high peak power electromagnetic energy (Diapulse). *Decubitus* **4**:29-34,

Loeser, J.D. 1980. Perspectives on pain. In: Clinical Pharmacology and Therapeutics. P. Turner, ed. University Park Press:Baltimore. pp. 313-316.

Markov, M.S. 1995. Electric current and electromagnetic field effects on soft tissue: Implications for wound healing. Wounds. 7:94-110.

Markov, M.S. and Pilla, A.A. 1995. Electromagnetic field stimulation of soft tissues: pulsed radio frequency treatment of post-operative pain and edema. Wounds. 7:143-151.

Markov, M.S., Hazlewood, C.F., Ericsson, A.D. 2004. Systemic effect – a plausible explanation of the benefit of magnetic field therapy: A hypothesis - 3rd International Workshop on Biological Effects of EMF – Kos, Greece, October 4-8, 2004, 673-682, ISBN 960-233-151-8.

Mayer, T.G. and R.J. Gatchel. 1988. Introduction and overview of the problem. In: Functional Restoration for Spinal Disorders: The Sports Medicine Approach. T.G. Mayer and R.J. Gatchel, eds. Lea & Febiger:Philadelphia, PA. pp. 3-15.

McCray, R.E. and N.J. Patton. 1984. Pain relief at trigger points: a comparison of moist heat and shortwave diathermy. JOSPT. 5:175-178.

Miner, W.K., and Markoll, R. 1993. A Double-Blind Trial of the Clinical Effects of Pulsed Electromagnetic fields in Osteoarthritis. *J. Rheumatol.* 20: 456-460.

Nachemson, A.L. 1992. Newest knowledge of low back pain: a critical look. In: Clinical Orthopaedics and Related Research. M.R. Urist, ed. J.P. Lippincott Co.:Philadelphia. pp. 8-20.

National Research Council (NRC). 1996. Possible Health Effects of Exposure to Residential Electric and Magnetic Fields. Executive Summary. Committee on the Possible Effects of Electromagnetic Fields on Biological Systems, Board on Radiation Effects Research, Commission on Life Sciences, and National Research Council. National Academy Press:Washington, D.C. pp. 1-7.

Nindl, G., Johnson, M.T., Hughes, E.F., Markov, M.S. 2002. Therapeutic electromagnetic field effects on normal and activated Jurkat cells - International Workshop of Biological effects of Electromagnetic fields, Rhodes, Greece, 7-11 October 2002, p.167-173. ISBN # 960-86733-3-X.

Pfingsten, M., J. Hildebrandt, E. Leibing, C. Franz, and P. Saur. 1997. Effectiveness of a multimodal treatment program for chronic low-back pain. Pain. 73:77-85.

Peach, P. and Olejnik, S. 1991. Effect of Treatment and Non-Compliance on Post-Polio Sequelae. *Orthopedics* **14**: 1199-1203.

Pilla, A.A. and Markov, M.S. 1994. Bioeffects of weak electromagnetic fields. Reviews on Environmental Health. 10:155-169.

Rosch P.J. and Markov M.S.(eds.) 2004. Bioelectromagnetic Medicine, Marcel Dekker NY, 850 pp.

Sartucci, F., Bonfiglio, L., Del Seppia, c., Luschi, P., Ghione, S., Murri, L., and Papi, F. 1997. Changes in pain perception and pain-related somatosensory evoked potentials in humans produced by exposure to oscillating magnetic fields. Brain Research. 769:362-366.

Sherman, R.A., Robson, L., and Marden, L.A. 1998. Initial exploration of pulsing electromagnetic fields for treatment of migraine. Headache. 38:208-213.

Shupak N.2003. Therapeutic uses of pulsed magnetic-field exposure: A review. Radio Science Bulletin # 307; 9-32

Travell, J.G. and Simons, D.G. Myofascial Pain and Dysfunction The Trigger Point Manual: Volume 1, The Upper Extremities, published in 1983 and Volume 2, The Lower Extremities, published in 1992. Williams and Wilkins.

Trock, D.H., A.J. Bollet, R.H. Dyer, Jr., L.P. Fielding, W.K. Miner, and R. Markoll. 1993a. A double-blind trial of the clinical effects of pulsed electromagnetic fields in osteoarthritis. J. Rheumatol. 20:456-460.

Trock, D.H., A.J. Bollet, and R. Markoll. 1993b. Treatment of osteoarthritis with pulsed electromagnetic fields. Arthritis and Rheumatism. 36:130-131.

Trock, D.H., Bollet, A.J., and Markoll, R. 1994. The Effect of Pulsed Electromagnetic Fields in the Treatment of Osteoarthritis of the Knee and Cervical Spine. Report of Randomised, Double Blind, Placebo Controlled Trials. *J. Rheumatol.* **21**:1903-1911.

Trojan, D.A., and Cashman, N.R. 2005 Post-poliomyelitis Syndrome. *Muscle Nerve.*31(1): 6-19

Vallbona, C., Hazlewood, C.F. and Jurida G.. 1997. Response of pain to static magnetic fields in postpolio patients: a double-blind pilot study. Arch. Phys. Med. Rehabil. 78:1200-1203.

Varcaccio-Garofalo, G., Carriero, C., Loizzo, M.R., Amoruso, S., and Loizzi, P.. 1995. Analgesic properties of electromagnetic field therapy in patients with chronic pelvic pain. Clin. Exp. Obst. Gyn. 22:350-354.

Vendrig, A.A. and Lousberg, R. 1997. Within-person relationships among pain intensity, mood and physical activity in chronic pain: a naturalistic approach. Pain. 73:71-76.

Wagstaff, P., Wagstaff, S., and Downey, M. 1986. A pilot study to compare the efficacy of continuous and pulsed magnetic energy | short-wave diathermy | on the relief of low back pain. Physiotherapy: 72:563-566.

World Health Organization (WHO). 1987a. Magnetic Fields. United Nations Environment Programme, World Health Organization, and The International Radiation Protection Association. Environmental Health Criteria 69. pp. 25-33, 119-127.

World Health Organization (WHO). 1987b. Magnetic Fields Health and Safety Guide. United Nations Environment Programme, World Health Organization, and The International Radiation Protection Association. Health and Safety Guide No. 27. pp. 7-24.

FLUIDIC MICROSYSTEMS FOR BIOlOGICAL CELL SAMPLE HANDLING AND ANALYSIS

KARAN KALER, YOULAN LI, THIRUKUMARAN T. K.,

COLIN DALTON AND RANJIT PRAKASH

DEPARTMENT OF ELECTRICAL AND COMPUTER ENGINEERING
SCHULICH SCHOOL OF ENGINEERING,
UNIVERSITY OF CALGARY,
2500 UNIVERSITY DRIVE N.W.,
CALGARY, CANADA (T2N-1N4)

Abstract

The ability to manipulate volumes of liquid and their constituent components, such as cells, organelles and their nucleic acids, utilizing very small (microliter) sample volumes provides new and novel opportunities and capabilities in microchip based bio-analysis and detection or lab-on-a-chip based diagnostics. The low sample volume requirements and rapid real-time processing capability enables parallel and multi processing capability without adverse impact on sample degradation.

Our research effort has focused on the development and application of non-invasive cell manipulations and separation techniques to facilitate fraction of diseased and healthy cells on a microchip in a rapid fashion with minimal amount of sample preparation. The cell sample processing capability is provide by electrokinetic based manipulation on-chip by leveraging the phenomena of dielectrophoresis (DEP). We explore the integration of electrokinetic methods for both particle and liquid manipulations utilizing conventional "closed channel" microfluidic structures as well as surface fluidic or "open channel" schemes.

Utilizing closed channel microfluidic structures, we have demonstrated DEP cell separation capability on batch and continuous flow through samples. We have furthermore explored the combined use of liquid and particle DEP to provide alternate means of processing/manipulating micro litre sized liquid droplets containing cells. This cell sample preparation capabilities provided by the integrated DEP and microfluidic, when integrated with other down stream processing components, such as cell lyses, genetic amplification and nucleic acid detection capability, has the potential of providing a complete bio-analysis on a chip. The proposed platform technology is not limited to applications targeted to disease detection; it is equally suitable for the detection of environmental agents and pathogens that have adverse impact on human health, Furthermore, the technology makes available useful small sample handling and analysis capabilities, which can be leveraged to benefit investigations concerning interaction of E.M. fields with biological cells.

1. Introduction

In recent years, as a result of advances in microfabrication methods, materials and process technology and coupled with it's availability to the research community has resulted in many new and novel application of the technology in many diverse areas in addition to the traditional semiconductors and microchip industry [1, 2]. For example the ability to lithographically pattern and etch microscopic scale micro-channels in glass provided a compact footprint for the development of capillary electrophoresis, with improved sample handling, detection and throughput [3]. Furthermore the miniaturization of such devices has made it possible for their infield deployment and handheld operation. Despite the success of such development in fluidic microsystems, a number of issues and obstacles need to be addressed before the technology can be considered reliable and mature enough to be applied successfully in the more critical and demanding arena pf biomedical diagnostics, on a routine basis. Of major concern and a significant challenge in this regard is the availability of suitable on-chip low volume sample preparation and handling methods [4, 5] in additional to suitable sample isolation (valving), pumping, mixing components.

Recent advances in the development and application of A.C. electrokinetics has shown that simultaneous handling and manipulation of very small quantity of fluids and particles, such as cells can be achieved utilizing the traditional closed channel microfluidic and more recently open channel surface microfluidic devices [6]. In the past, A.C. electrokinetic systems leveraging the phenomena of Dielectrophoresis (DEP) have been developed

primarily employing closed fluidic chambers or microfluidic channels and intersections that are interfaced to external fluid pumping and sample injection hardware [7-9]. Such systems, particularly those employing microfluidic channels for cell collection and separation usually require sample preprocessing and are frequently plagued by micro-channel blockage. Such problems need to be overcome in order to successfully commercialize microfluidic cell analysis/sorting devices. The closed channel microfluidic systems are furthermore less amiable to creating complex cell processing structures, due to pressure and flow related problems and the need for extensive valving and flow control devices on-chip and capable of withstanding high operating pressures . In the paper we discuss the utility, application and merits of example "open channel" or surface microfluidics and "closed channel" microfluidic systems for biological cell sample handling and analysis utilizing A.C. electrokinetic approaches.

2. AC electroactuation and manipulation of cells and microfluids by dielectrophoresis (DEP)

Electrical field effect phenomena have been extensively investigated and demonstrated to provide novel ways of manipulating and interrogating individual microscopic sized particles and intact biological cells, immersed in fluid media [10-12]. In this paper we focus on the capabilities and utility of non uniform A.C. (alternating current) electric field effect, referred to as dielectrophoresis (DEP), in providing particle, liquid, droplet actuation at microscopic scales to facilitate the deployment of fluidic microsystems or LOC for the handling and manipulation of cells and subsequently the genetic material of the individually selected or fractionated cell population.

(a) Particle DEP actuation

To illustrate the salient features and basis for particle DEP actuation, consider a microscopic sized spherical shaped particle or object that is immersed or surrounded by another medium and subjected to an externally imposed non uniform electric field. We further assume that the particle and the surrounding medium are characteristically different in terms of the electrical permittivity and conductivity. The time averaged DEP force $\langle \vec{F}_{DEP} \rangle$ acting on a spherical body of radius a, due to a spatially non uniform ac electric field, is summarized as follows [13]:

$$\left\langle \vec{F}_{DEP} \right\rangle = 2\pi\varepsilon_m a^3 \,\mathrm{Re}\left[K_e\right] \nabla E_{rms}^2 \qquad (1)$$

where, $K_e = \dfrac{\varepsilon_p^* - \varepsilon_m^*}{\varepsilon_p^* + 2\varepsilon_m^*}$

In the DEP force expression (Eqn. 1), the quantity $\mathrm{Re}\left[K_e\right]$ refers to the real part of excess polarizability or frequently referred to as the Claussius-Mosotti factor (CMF). The quantities $\varepsilon_p^* = \varepsilon_p - j\frac{\sigma_p}{\omega}$ and $\varepsilon_m^* = \varepsilon_m - j\frac{\sigma_m}{\omega}$ are the complex permittivity of the particle and medium respectively. ε_m , ε_p represent the real dielectric permittivity of the medium and particle σ_m , σ_p refer to the conductivity of the particle; and the medium and $\omega = 2\pi f$ is the radian frequency, where f (Hz).is the applied A.C. electric field frequency. The CMF reflects the polarizability difference the particle and media, and is usually a sensitive function of the applied field frequency. The term ∇E_{rms}^2 is the gradient of the electric field squared.

It is apparent, from Eqn. (1), that the DEP force depends on the particle size (volume), the gradient of electric field squared and the Claussius–Mosotti factor which is frequency dependent. Furthermore, when Re [K_e] > 0, at a particular frequency, the DEP force is positive (+ve DEP) and directed towards the region of increasing field intensity [12]. In contrast, when Re [K_e] < 0, the DEP force is negative (-Ve DEP) and impels the particles to regions of field intensity minimum [14]. The impact of +Ve and –Ve DEP forces acting on particle subjected to nonuniform field, as synthesized by a set of coplanar electrodes, is shown schematically in Figure 1. The +Ve and –Ve DEP effect has the beneficial effect of physically separating or concentrating the particles in regions of field intensity maxima (at the electrode surfaces) and minima (located away from the electrode surfaces).

Most microscopic particles of practical interest, including biological cells, due their structural heterogeneity and differences in the electrical properties of the various ultra structures compared to that of the suspending media may exhibit both +Ve and –Ve DEP behavior in different region of the applied field frequency spectrum [15]. It is due to such characteristic differences in the frequency dependent polarization and the resulting DEP response which enables selective and differential manipulation and physical separation of one or more types of particles or cells in a mixed population suspension.

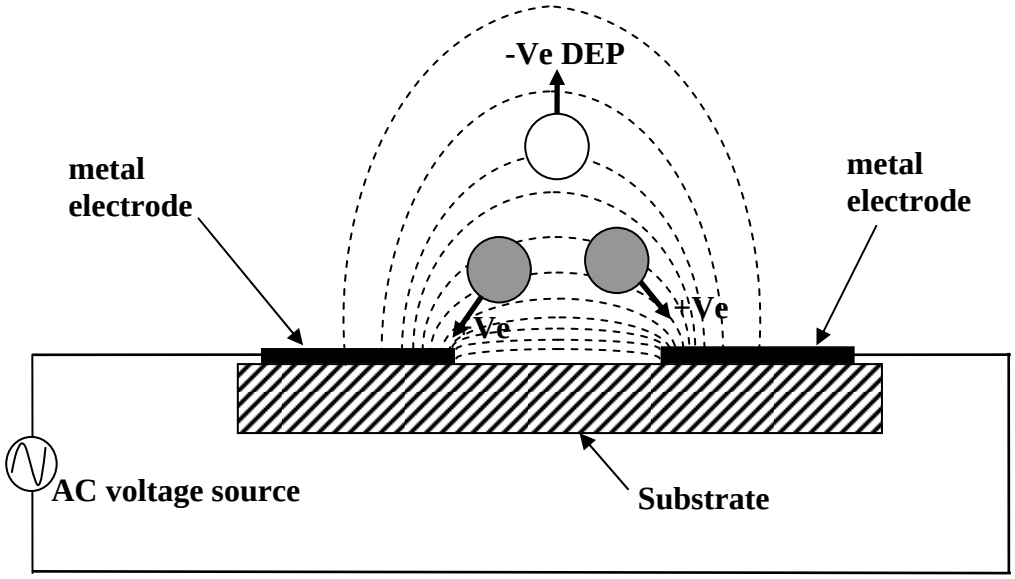


Figure 1. A cross-sectional view of a co-planar electrode geometry, showing the differing +Ve and –Ve DEP forces exerted on particles, induced by a nonuniform AC field, as depicted by the dashed lines the diagram. The shaded particle, experiencing +Ve DEP, are impelled towards and collected at the electrodes, while particle experiencing –Ve DEP body force is impelled upwards into a region of local field intensity minima.

(b) Liquid DEP actuation and droplet dispensing

The utility of the DEP effect is not limited to particulate matter, but maybe made to manifest and exert body forces on aqueous polarizable media [14-16]. The practical and useful utility of the phenomena, especially at the micro scale, enables novels means of handling and manipulating aqueous biological fluid samples, without the need for valving and/or pumping required for isolation, steering and fluid transport in conventional microfluidic systems. Thus, the DEP effect, in addition to serving to electro-actuate microscopic particles and thereby facilitate their manipulation may furthermore be leveraged to enable noninvasive handling and manipulation of microliter volume droplets of aqueous dielectric media on open surfaces. Such open surface manipulation of biological samples circumvents a variety of issues that plague closed channel systems.

The first demonstration of macro scale liquid actuation by DEP was reported by Pillet [16]. By partially immersing two parallel plates in a bath of aqueous dielectric media (oil) and applying an A.C. potential to the plates, he observed that a column of liquid was raised between the plates to a new equilibrium.

More recently, the work of Jones et al [17, 18], Ahmed et al [19] and Kanagasabapathi et al [20] have shown that similar type of controlled actuation of a small quantities of dielectric liquids (oils and low conductivity water), on top of planar surfaces can be achieved by employing a pair of thin coplanar metal electrodes, coated with a thin film dielectric material, of a suitable contact angle (< 70^0), as shown in Figure 2.

For satisfactory operation, liquid that is to be actuated and dispensed is usually introduced as a parent drop at one end on the electrode structure. On application of an AC voltage, typically ~ $230V_{RMS}$ @ 100 kHz, a jet of liquid in the form of finger, confined to the width of the electrodes, protrude from the parent droplet and very rapidly extend to the end of the electrode structure.

The characteristics of this liquid finger formation has been analysed by Jones et al [21]. A reduced-order lumped parameter model was proposed that takes into account liquid surface tension viscous drag, and the DEP force. The resulting expression, describing the DEP force induced on the liquid finger, is as follows [19]:

$$F_{liquid\ DEP} = \frac{(\varepsilon_{liq} - 1)C_d^2 C_{air} V^2}{2(C_d + 2\varepsilon_{liq} C_{air})(C_d + 2C_{air}))} \qquad (2)$$

The liquid DEP force imparted, varies as the square of the applied voltage (V), the permittivity of the liquid (ε_{liq}) and the characteristics of the field in the liquid media, controlled by the electrode structure, dielectric coating and geometry. Upon removal of the voltage, the liquid finger breaks up into one or more smaller sized daughter droplets that are spaced almost uniformly on top of the electrodes. Further refinements in the basic coplanar structure, such a three electrode system, the judicious location of semicircular metal bump areas and their spacing to satisfy the Raleigh jet break criterion have enabled the controlled dispensing of aqueous media (deionized water) in the form multiple identical sub-microliter droplets [19]. These are included in the structure shown Figure 3(a), while figure 3(b) shows the daughter droplets populating the metal bump regions spaced at regular intervals along the coplanar electrode structure.

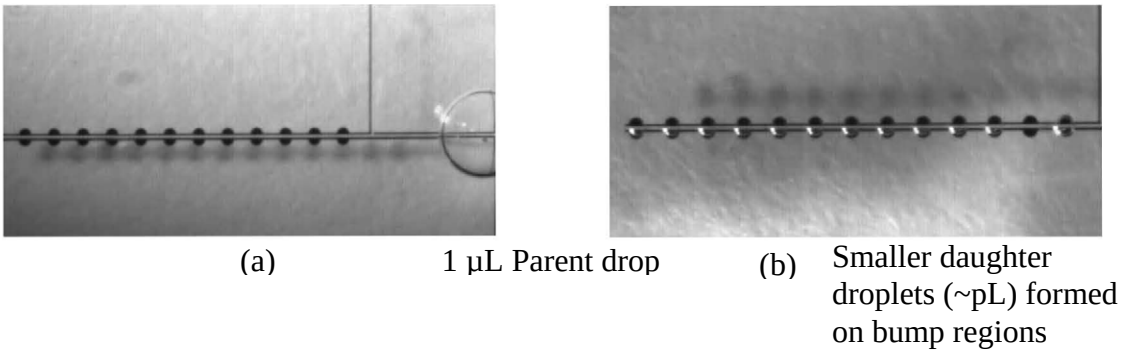


Figure 3. (a) Photographs showing the 3-electrode structure with metal bumps, for improved droplet formation. (b) Successful population of the bump regions with smaller daughter droplets after the applied voltage is removed.

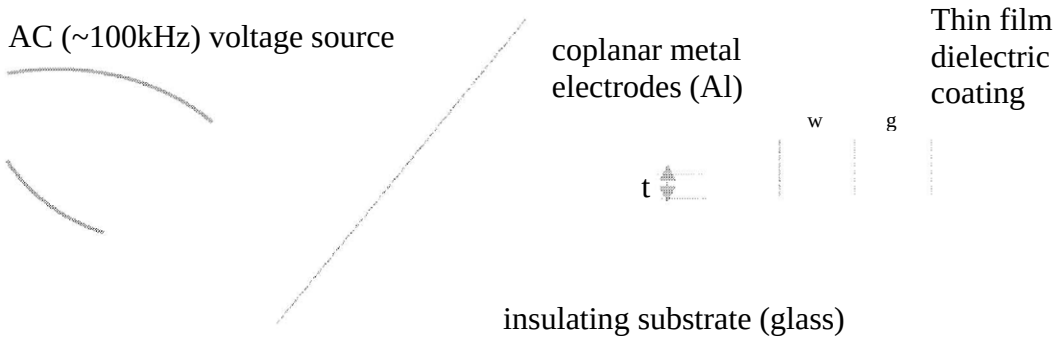


Figure 2. A schematic (a) plan and (b) cross-sectional views of the co-planar electrode geometry, coated with a thin dielectric film, employed for DEP actuating liquid. Nominal dimension of the structure are as follows: t ~ 0.5 µm; w = 30 µm; g = 30 µm.

Thus, successful development and implementation of liquid actuation, droplet formation and transport on open surfaces utilizing liquid DEP, open up a variety of new application in the microfluidics domain concerning the manipulation of minute quantities of fluid sample and it's components. Some such example surface fluidic manipulations are discussed in a later section in this article.

3. Integration of on-chip DEP with microfluidics

Having provided a basis for DEP manipulation of particles and liquid samples, we now turn to its application and utility for lab-on-a chip applications. .In this article we specifically focus on microfluidic devices that integrate DEP for particle/cell handling or processing. The level and extent of the integration effort demanded is very much governed by the application (i.e. application specific). For example, a fully integrated microfluidic device for chip based genetic analysis requires a number of different microfluidic component blocks to facilitate cell manipulation, nucleic acid processing (genetic amplification and separation) and a suitable electro-optical detection system. More specifically a fully integrated platform would include cell sorting and fractionation and /or concentration, cell lysis step to extract the genetic material (DNA, RNA), genetic amplification procedure, such as on-chip PCR and subsequent DNA separation and detection utilizing on-chip capillary electrophoresis.

Thus on-chip sample preparation, including cell separation, is a key and much needed capability that can have a dramatic impact of the overall performance and capabilities of integrated microfluidic chips for bio-analysis and detection. In the past a variety of different techniques methods have been proposed to handle the sample preparation needs, however, many of the proposed approaches, unlike DEP are not readily incorporated on-chip. Here we examine two different approaches, a batch sorting scheme and a continuous DEP based cell fractionation in affecting cell separation in microfluidic channels. A fundamental requirement of all devices that leverage DEP is appropriate synthesis of a nonuniform electric field, which is achieved quite readily using metal electrodes of appropriate dimension, spacing/geometry. However, in order to integrate DEP electrode structures in microfluidic channels, we are limited to the use of planar electrode structures which can be photo lithographically patterned. Furthermore, to facilitate microfabrication, the planar electrodes are limited to locations on the top or bottom sides of the microchannels. The choice of material for the metal electrode material has to be given due consideration. If the channels contents are to be visually inspected or the contents monitored, then it is appropriate to transparent electrodes material such as indium tin oxide (ITO), otherwise either titanium-platinum of chrome-gold electrodes have been shown to suitable and readily deposited and patterned lithographically.
An example of a DEP based microfluidic chip fabricated to make available binary DEP fraction of cells in a continuous fashion [22], is shown in Figure 4.

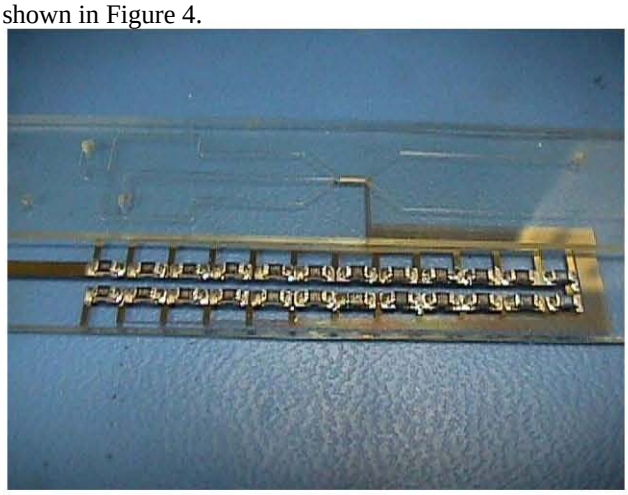


Figure 4 A closed channel microfluidic DEP fractionation chip, showing the microfluidic channels with in-channel microelectrodes for DEP cell sorting

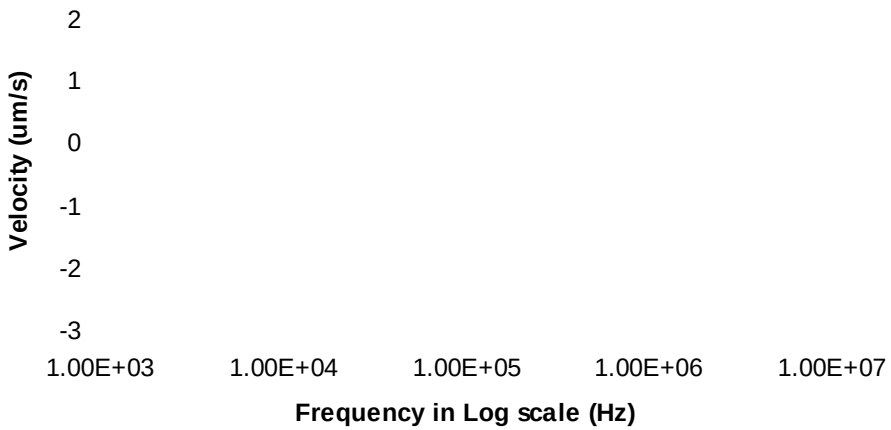


Figure 5. Plot of the DEP velocity spectrum of viable and nonviable yeast cells versus frequency. showing +Ve DEP and –Ve DEP responses [21].

The device is comprised of a cell and sheath injection ports that facilitates the injection of a cell sample into the chamber using off-chip pumping. The dimensions of the sheath flow and cell sample channels are designed to enable hydrodynamic focus of the cell stream under laminar flow. The focused injected cell stream is subjected to a nonuniform isomotive electric field, synthesized by an array of individual biased electrodes. In this isomotive field region cells, depending on their frequency dependent polarizability, may experience positive or negative DEP depending on the frequency of the applied field, and hence are deflected in opposite directions and

normal to the fluid flow. Thus cells experiencing +Ve and –Ve DEP are physically separated and subsequently collected as purer subpopulations downstream. Example DEP spectral of viable and non-viable yeast cell, obtained using the device is shown in Figure 5. The plot reveals that binary fractionation of viable from nonviable yeast cells, suspended in deionized water, and is most efficiently attained over specific regions (10 kHz to 80 kHz and 1 MHz to 5 MHz) of the frequency spectrum. Further integration of the chip, incorporating near-field hybrid attached to the glass substrate facilitates real-time monitoring of cell separation at the outlet ports of the device [23].

An alternative approach to the continuos fraction of cells utilizing DEP is to adopt a batch sorting /separation which is perhaps more suitable in cases where a dilution of the cell sample concentration by the sheath flow as in the continuous separation is not desirable. An example of this batch cell separation device is shown in Figure 6. Unlike the continuous cell sorting device, requiring metallized electrodes on the to and bottom faces of the microfluidic channels, the batch scheme can be readily implemented with an array of electrodes house on a glass substrate while the microchannels enclosing the electrodes are cast in Poly(dimethyl siloxane) (PDMA) and affixed on top of the glass substrate[24]. The use of PDMS polymer for microfluidics, is advantageous as it reduces the time, complexity and cost of prototyping and manufacturing. PDMS is hydrophobic and can easily nucleate air bubbles, however, by exposing the cured PDMS layer to oxygen plasma at a pressure of 0.15 torr renders the surface hydrophilic and makes it compatible for microfluidic handling. The assembled microfluidic DEP device can withstand moderate chamber pressures, typically ~ 30-50 psi.

In such a batch DEP device, a dilute cell suspension is introduced in to the chamber employing pressure driven flow and an AC voltage is applied to the electrode array. Cells experiencing +Ve DEP are collected in the high field regions, while cells experiencing negative DEP are repelled from the electrode surfaces and levitated or trapped in local filed intensity minima (see Figure 7). Since the +Ve DEP cells are strongly held on to the electrode surface and the -Ve DEP cells can be flushed while retaining the cells collected at the electrodes in the chamber. Such batch DEP devices, although simple in design compared to the continuous cell sorting system, finding utility in applications that require concentration of cell sample into a smaller volume.

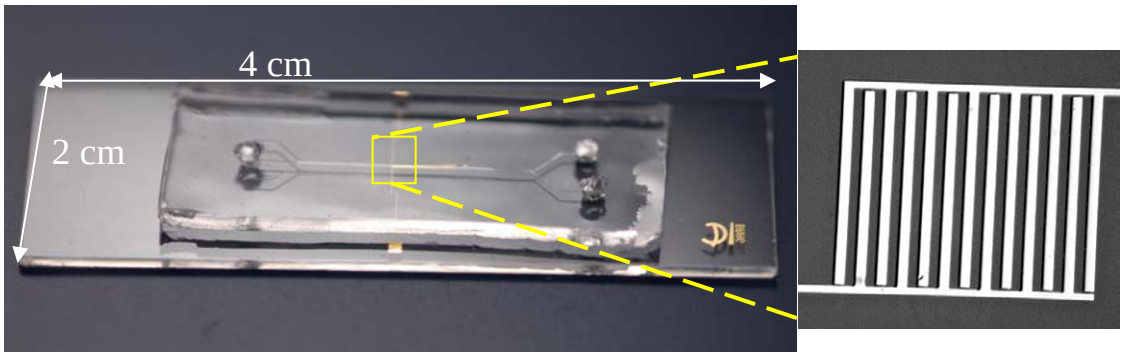
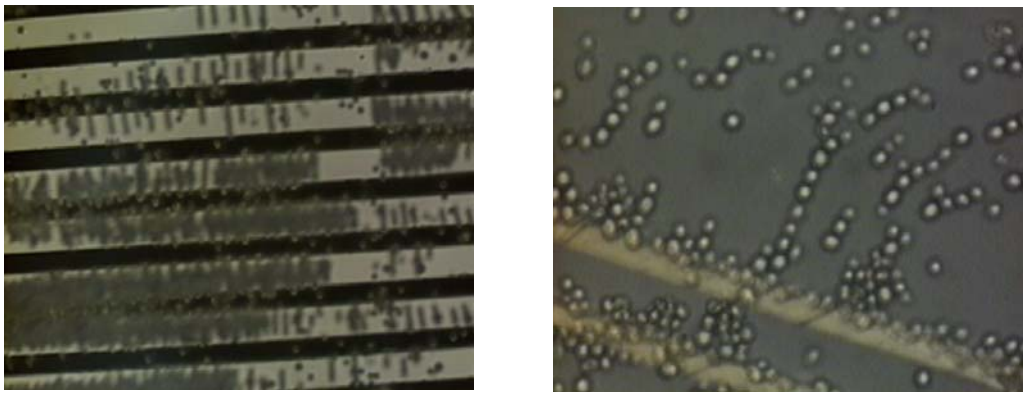


Figure 6. A glass-PDMS microfluidic device for batch DEP cell separation with in-channel planar interdigitated microelectrodes electrodes (electrode width = 20 µm; electrode spacing= 20 µm



(a) (b)

Figure 7 Photographs showing(a) microscopic sized latex beads (10 µm in diameter) suspended in low conductivity media (water) exhibiting –Ve DEP and levitation above the electrode plane and (b) +Ve DEP collection of yeast cells at electrode edges [23].

4. Surface Fluidic Structures for Integrating Liquid and Particle DEP

Conventional microfluidic devices or systems to a large extent are comprised of microfluidic channels, which traditionally are etched in glass or more recently patterned in PDMS or other suitable polymeric substrates. The substrate with the etched channels are then suitably bonded or sealed to another or identical substrate material to form closed microchannel structures. As discussed earlier there are a number of issues concerning the utility and applicability of such devices in the domain of microfluidic when handling or processing of aqueous biological sample containing cells or macromolecules in suspension. Recently, the emergence of Liquid DEP as alternate means of manipulating and processing small quantities, has suggested new and novel schemes of manipulating liquids samples comprised of cell (cell suspensions), macromolecules and/or reagents.

An example surface fluidic structure illustrating the combined manipulation of both liquids and particles (cells) utilizing Liquid and particle DEP phenomena [19] is illustrated in Figure. 8. The microelectrode structure basically combines the liquid actuation and droplet formation station with the particle DEP microelectrode array. The key capabilities of this integrated structure are (1) it's ability to dispense and form droplets of a cell suspension at locations as specified and implemented by the Liquid DEP structure (2) the ability to subject cells suspended in the daughter droplets, formed by liquid actuation, to one or more DEP field frequencies and subsequently convey the sample to another location in the structure. The structure illustrated in Figure 9 was microfabricated integrating different electrode arrangements at the bump regions.

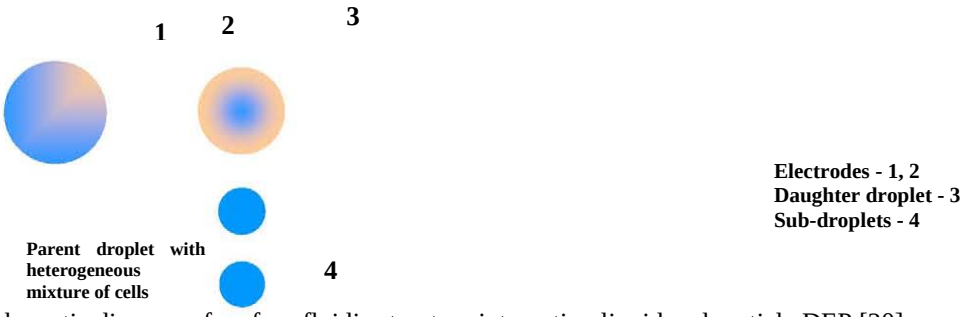


Figure 8. A schematic diagram of surface fluidic structure integrating liquid and particle DEP [20].

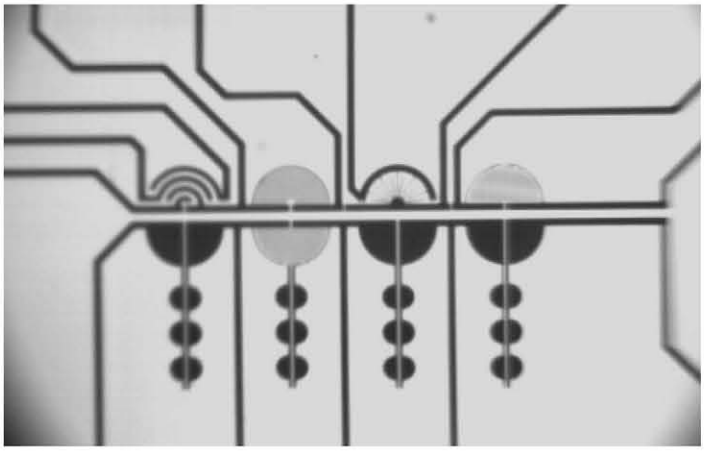
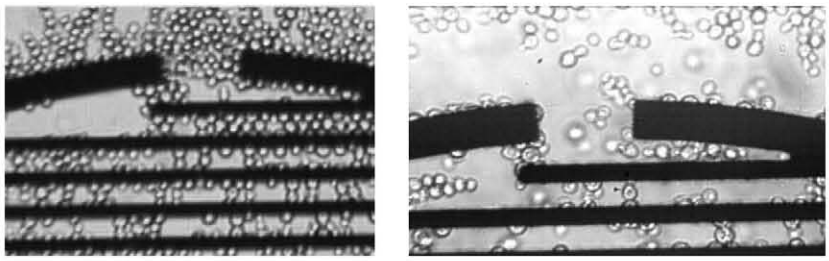


Figure 9. Photograph of the fabricated surface fluidic structure for the combined DEP manipulation of liquid parent droplet and particle within the daughter droplets. Four different electrode arrangements are incorporated in the structure for DEP manipulation of particles.

To verify the particulate DEP effects on open droplets, sample media containing yeast cells (Saccharomyces Cerevisiae) placed directly on the bump region. An AC voltage of 2.47 V_{RMS} was applied at 600 kHz, yeast cells were observed to be pulled towards the electrodes and furthermore forms pearl chain along the periphery of the bump region due to +Ve DEP effect (Fig. 10a). However, at frequencies above 10 MHz, the same cells were repelled from the electrode periphery (-Ve DEP) as in Fig. 10b. Under –Ve DEP conditions, some cells are trapped within the interdigitated electrodes, this phenomenon though not quantified can be attributed to the smaller electrode gaps resulting in very high particle-particle interaction and thereby forming cell-traps. Cells repelled under –Ve DEP conditions were actuated along the electrodes below the bumps, forming picolitre droplets on the lower bumps.

Since liquid actuation, droplet formation and subsequent particle DEP are achieved in rapid fashion, we are

presently engaged in the integration of near-filed optical sensors to detect the presence of a liquid finger, droplets and particle (cell) at suitable locations in the structure.
The combined liquid actuation with droplet formation and muti-frequency DEP examination of cell suspension sample, as well as providing novel opportunities of providing sample preparation, including sorting, analysing and/or separation of cells.

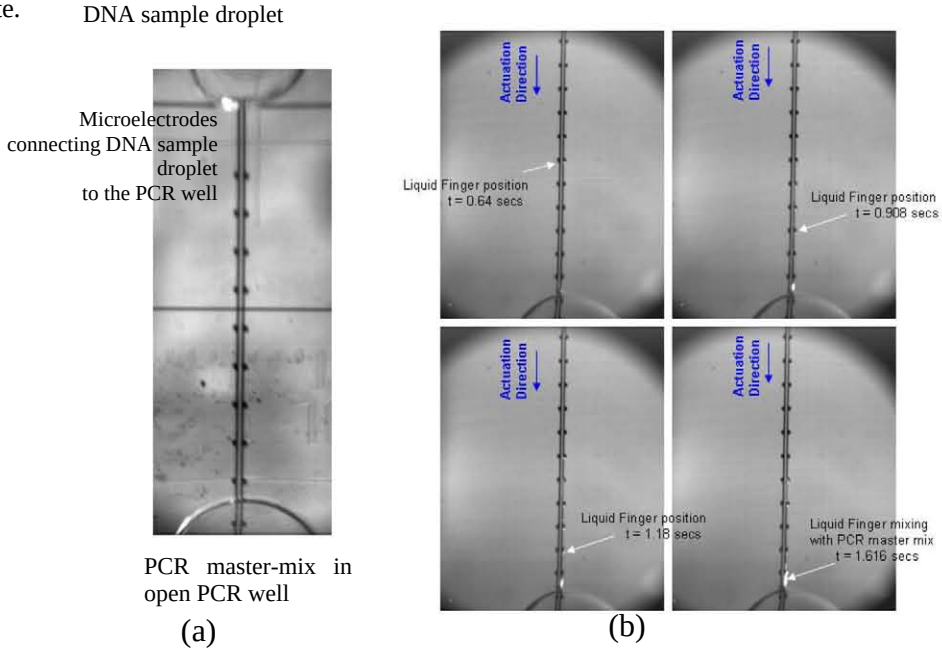


(a) (b)

Figure 10. (a) The +Ve DEP of yeast cells at an applied voltage of 2.47 V_{RMS} and frequency 500 kHz; (b) -Ve DEP of yeast cells at 10 MHz [20].

5. Integration of Liquid/particle DEP with genetic amplification (PCR) and detection

Having demonstrated the particle and liquid handling, we now focus on the integration of other additional liquid handling or processing capabilities necessary to implement genetic amplification utilizing PCR and detection. A fundamental requirement, in addition to thermal cycling, is the mixing of the sample with reagents and buffers. To demonstrated such mixing capabilities we employed DEP liquid actuation to project a finger from the parent droplet housed on top of the coplanar electrodes (see Figure 11) [25]. The electrodes were designed such that they terminated on the edge of a sample well containing PCR mix. The PCR well was coated with Teflon to minimize DNA adsorption and further aided in preventing the liquid in the PCR from forming a finger. Thus once an AC voltage (230V, 100 kHz) was applied to the coplanar electrodes a liquid finger was actuated from the parent drop containing known template DNA and contacted the PCR mix in the well, approximately 10% of the sample DNA was transferred to the PCR well. The chip was then thermal cycled 20 times to amplify the template DNA, transferred by finger actuation into the PCR well. The PCR amplified product was analysed by on-chip capillary electrophoresis to verify the presence of template DNA in the mixed and amplified sample. This is the first demonstration of a microfluidic chip that integrates DEP actuated surface fluidic sample mixing, with conventional closed channel well PCR and CE detection. These finding suggest novel ways of combing the sample preparation afforded by DEP on surfaces with the closed channel amplification and detection on a common substrate.



(a) (b)

Figure 11. (a) Liquid mixing structure, showing sample and PCR drops located at the end of the Liquid DEP actuation structure. (b) Time sequence of liquid finger drawn from the sample drop and mixed with PCR drop in an open PCR well [25].

An alternative approach to the liquid DEP actuated mixing, as illustrated earlier, is to utilize a whole droplet actuation scheme. The actuation of small droplets confined on top of coplanar electrodes is readily achieved by coating the surface of the electrodes with a hydrophobic coating, such as Teflon. The dimensions of the electrodes are based on the droplet volume to be actuated. Unlike the liquid DEP assisted mixing, achieved by employing high frequency fields, whole droplet actuation and transport is achieved at much lower field frequencies [26]. To illustrate whole droplet mixing approach, two drops, one larger (5 µL) than the other (1.5 µL) were placed onto at the ends of a coplanar electrode structure, coated with SU-8 + Teflon film (`thickness ~ 1.6 µm). The contact angle of the water droplets on the Teflon coated surface was 110^0. When an AC voltage (93 V_{RMS} @ 90 Hz) is applied, the smaller (1.5 µL) droplet was conveyed (35.62 mm/sec) towards the larger droplet, located at the opposite other end of the electrode structure. As the droplet is transported along the electrode track, it exhibits small lateral oscillations. A time sequence showing such actuation of the whole droplet is shown in Figure 12. The ability to actuate whole microliter sized droplets and successfully mix them is particularly important when dealing with protein and enzyme samples, which tend to rapidly collapse, due to adsorption when placed on hydrophilic surfaces.

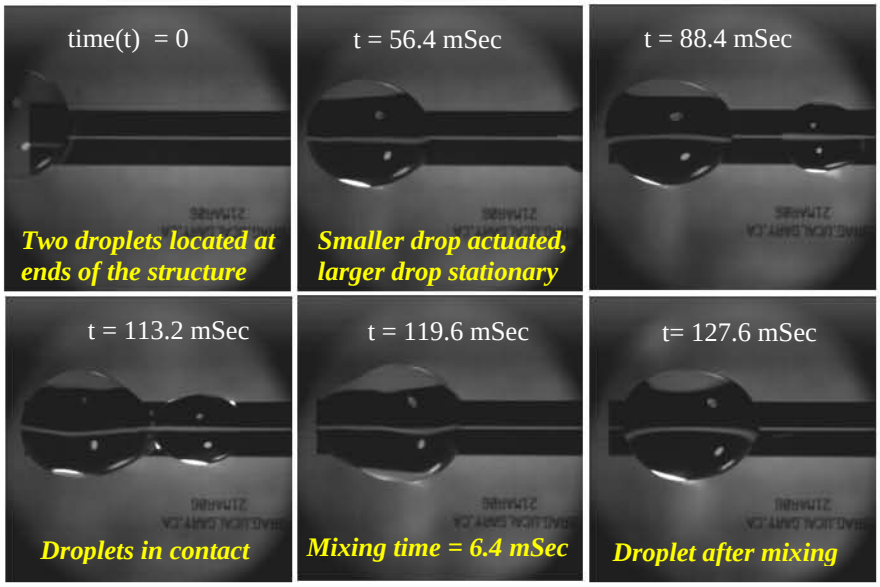


Figure 12. A sequence of photographs, showing the electro-actuation of a µL drop of water. The larger stationary parent drop is mixed with an actuated smaller daughter drop. The details of electrode structure and surface treatment are as follows: Electrode width = 500 µm, Gap = 50µm and Length = 7700 µm; Surface dielectric coating: SU 8-2000.5 + Teflon (~1.6 µm)

6. Conclusion

In this paper we have illustrated both the phenomena of DEP and its practical utility in potential lab-on-chip devices for clinical diagnostic and laboratory applications in the life sciences. These DEP-microfluidic devices provide the on-chip capability of selective and non-invasive manipulation of cells (trapping, levitating, sorting, concentration, purification) in suspension in closed channel microfluidic devices. We have furthermore reviewed new approaches in liquid and particle processing employing DEP forces, generated by co-planar microelectrodes, for combined particle and liquid actuation on top of open surfaces (surface fluidics). This combined liquid/particle processing capability provides unique handling and processing of biological samples in a rapid fashion. We have specifically illustrated this capability in parallel multi-frequency DEP cell fractionation device, which can serve as the front end sample preparation stage of a more complex lab-on-a-chip devices, target for example genetic finger printing and analysis.

7. Acknowledgements

The authors gratefully acknowledge the financial support provide by NSERC, Western Economic Diversification (WED), Canadian Institute for Heath Research (CIHR). We furthermore acknowledge the fabrication support provided by Micralyne Inc and CMC Microsystems, in support of the work presented in this article and the valuable assistance provided by the staff of the U of Alberta Nanofab and the U of Calgary CCIT clean room facility.

References

[1] Kamholz, A.E. (2004) *"Proliferation of microfluidics in literature and intellectual property"*, Lab on a

Chip, **4**(2): pp. 16N-20N.
[2] Kopp, M.U., H.J. Crabtree, and A. Manz (1997) *"Developments in technology and applications of microsystems"*, Current Opinion In Chemical Biology", **1**(3): pp. 410-419.
[3] Manz A., Fettinger J.C., Verpoorte E., Ludi H., Widmer H.M., Harrison D.J. (1991) *"Micomachining of Monocrystalline Silicon and Glass For Chemical-Analysis Systems - A Look Into Next Century Technology Or Just A Fashionable Craze"*, Trac-Trends In Analytical Chemistry **10** (5): pp 144-149.
[4] Koo, J.M. and C. Kleinstreuer (2003) *"Liquid flow in microchannels: experimental observations and computational analyses of microfluidics effects"*, Journal of Micromechanics and Microengineering, 2003. **13**(5): pp. 568-579.
[5] Xuan, X.C. and D.Q. Li (2004) *"Analysis of electrokinetic flow in microfluidic networks"*, Journal of Micromechanics and Microengineering, **14**(2): pp. 290-298.
[6] Hughes, M.P (2002) *"Strategies for dielectrophoretic separation in laboratory-on-a-chip systems.* Electrophoresis, **23**(16): pp. 2569-2582.
[7] Talary, M.S. Burt, J.P.H., Tame, J.A. and Pethig, R.(1996) *"Electromanipulation and separation of cells using travelling electric fields"*, Journal of Physics D-Applied Physics, **29**(8): pp. 2198-2203.
[8] Pethig, R. (1996) *"Dielectrophoresis: Using inhomogeneous AC electrical fields to separate and manipulate cells"*, Critical Reviews in Biotechnology, **16**(4): pp. 331-348.
[9] Li, Y.L. and K. Kaler (2004) *"Dielectrophoretic fluidic cell fractionation system"*, Analytica Chimica Acta, **507**(1): pp. 151-161.
[10] Kaler, K., T.B. Jones, and R. Paul (1995) *"Low-Frequency Micromotions of Dep-Levitated Plant-Protoplasts.1",*. Journal of Colloid and Interface Science, **175**(1): p. 108-117.
[11] Wang, X.B., Yang, J.; H., Y.; Vykoukal, J.; B., F. F.; Gascoyne, P. (2000) *"Cell separation by dielectrophoretic field-flow-fractionation"*. Analytical Chemistry, **72**(4): pp. 832-839.
[12] Rousselet, J., G.H. Markx, and R. Pethig (1998) *"Separation of erythrocytes and latex beads by dielectrophoretic levitation and hyperlayer field-flow fractionation"*, Colloids and Surfaces A-Physicochemical and Engineering Aspects, **140**(1-3): pp. 209-216.
[13] Jones, T. B., 1995 *Electromechanics of particles*, Cambridge University Press.
[14] Pohl, H. A., 1978, *Dielectrophoresis: The behaviour of neutral matter in non-uniform electric fields*, Cambridge University Press.
[15] Kaler K.V.I.S., Xie, J. Jones, T. B. and Paul, R., (1992) *"Dual-frequency dielectrophoretic levitation of canola protoplast"*, J. Biophys. 63 (1), pp. 58-69.
[16] Pellat, H. (1895) *Mesure de la force agissant sur les dielectriques liquides non electrises places dans un champ elitrique"*. C. R. Acad. Sci. Paris, (119): pp. 691-694.
[17] Jones, T.B.(2001) *"Liquid dielectrophoresis on the microscale"*, Journal of Electrostatics, **51**: pp. 290-299.
[18] T. B. Jones M. Gunji, and M. Washizu,, (2001) *"Dielectrophoretic Liquid Actuation and Nanodroplet Formation,"* Journal of Applied Physics, vol. **89**, pp. 1441-1448.
[19] Ahmed, R., Hsu, D., Bailey, C. and Jones, T.B. (2004) *"Dispensing picoliter droplets using dielectrophoretic (DEP) microactuation"*, Microscale Thermophysical Engineering, **8**(3): pp. 271-283.
[20] Thirukumaran T.K., T.B. Jones and KV.I.S. Kaler, *"Droplet-based DEP Microfluidics - High Speed Liquid Actuation on Planar Substrates and Factors Influencing Picolitre Droplet Formation,"* Proceedings of nano2005, vol. 2, pp. 615-622, Sivakasi, India, July 13-15, 2005.
[21] Jones, T.B., *"Dynamics of Dielectrophoretic Liquid Microactuation"*. Proceedings of 4th Int'l Conference on Applied Electrostatics, Dalian, China, 2001.
[22] Youlan Li, Colin Dalton, John Crabtree, Gregory Nilsson and Karan V.I.S. Kaler*, *"Continuous Dielectrophoretic Cell Separation Microfluidic Device"* (manuscript in press).
[23]`Lee Hartley, Karan V.I.S. Kaler, Orly Yadid-Pecht, "Hybrid Integration of an Active Pixel Sensor and Microfluidics for Cytometry on a Chip" TCAS-I Special Issue Smart Sensors (In press).
[24] Thirukumaran T. Kanagasabapathi, Christopher J. Backhouse and Karan V.I.S. Kaler, *"Dielectrophoresis (DEP) of Cells and Microparticle in PDMS Microfluidic Channels"*, Nanotech 2004, Vo1. 1, pp.81-84.
[25] Thirukumaran Kanagasabathi, A. Ranjit Prakash, Karan V.I. S. Kaler, *"Integration of surface microfluidics to closed-channel fluidics for a valveless multi-layer genetic analysis chip"* µTAS 2006, Nov, 2006, Tokyo Japan.(paper accepted).
[26] M. Gunji and M. Washizu,(2005) "Self-propulsion of a water droplet in an electric field," Journal of Physics D-Applied Physics, Vol. 38, pp. 2417-2423.

IN VITRO EXPERIMENTS TO ASSESS ELECTROMAGNETIC FIELDS EXPOSURE EFFECTS FROM RFID READER/WRITER FOR PACEMAKER PATIENTS

S. FUTATSUMORI[1], T. HIKAGE[1], T. NOJIMA[1], B. KOIKE[2], H. FUJIMOTO[3], T. TOYOSHIMA[3]

[1]GRADUATE SCHOOL OF INFORMATION SCIENCE AND TECHNOLOGY, HOKKAIDO UNIVERSITY
KITA 14, NISHI 9, KITA-KU, SAPPORO, HOKKAIDO, 060-0814 JAPAN

[2]JAPAN AUTOMATIC IDENTIFICATION SYSTEMS ASSOCIATION
1-9-5 IWAMOTO-CHO, CHIYODA-KU, TOKYO, 101-0032 JAPAN

[3]MEDTRONIC JAPAN CO., LTD.
SOLID SQUARE WEST TOWER, 580 HORIKAWA-CHO, SAIWAI-KU, KAWASAKI, KANAGAWA, 210-0913 JAPAN

Abstract
Today, the use of implantable cardiac pacemakers has become more widespread and more than 50,000 devices are implanted in Japan per year as of 2005. Implantable cardiac pacemaker patients are excluded from the recommended electromagnetic fields (EMF) level of guidelines such as ICNIRP reference levels. Recently, many communication devices including Radio Frequency Identification (RFID), Electronic Article Surveillance (EAS), and contactless IC cards have been introduced to our daily lives. They are expected to achieve more widespread applications. Accordingly, the assessment of EMF exposure limits for pacemaker patients should be required to complement the EMF safety guidance.
In this paper, electromagnetic interference (EMI) from commercially available RFID reader/writers on implantable cardiac pacemakers and cardioverter-defibrillator (ICD) were investigated. The newly constructed in-vitro experimental test system based upon an Irnich's flat torso phantom was applied. EMI test experiments on 10 types of RFID reader/writers and 13 types of implantable pacemakers and ICDs were conducted. Frequency bands were 125 kHz and HF (13.56 MHz), as well as UHF (950 MHz) and 2.45 GHz. In addition, electromagnetic field distributions of RFID reader/writer antennas were measured in detail. Finally, results of in-vitro EMI test experiments were introduced and characteristics of interferences were discussed.

Introduction
ICNRP guidelines for limiting human exposure were published in 1998 for the purpose of protecting electromagnetic fields (EMF) effects for health [1]. These guidelines include reference levels for occupational and general public exposures. However, these guidelines do not apply to people who wear implantable medial devices. To prevent electromagnetic interference (EMI) on the functions of these devices, it is necessary to find out the conditions which cause malfunctions. A lot of research is being carried out with an increasing in the use of wireless communication devices. In particular, EMI due to mobile phone systems are investigated precisely [2]-[8]. In Japan, guidelines to prevent the EMI is provided and operated under technical report [7].

Radio frequency identification (RFID) technologies are assumed to have widespread application as an automatic recognition method in ubiquitous networks. Scope of the technology includes product management and identification instead of the conventional barcode technology. RFID systems are essential devices to achieve future ICT society.

Several frequency bands, some modulation methods and many types of antenna are employed for RFID systems. For the various types of systems, the effect on implantable cardiac pacemakers and implantable cardiac-defibrillators (ICD) patients should be precisely taken into account. Table. 1 indicates ICNRP reference levels at operating frequency bands of RFID systems. In order to assess the EMI from RFID systems, EMF strengths which cause effects for operations of these devices are required to be examined from experimental and measured results. Then, these threshold field strengths can be compared with the reference levels.

Table 1
ICNRP reference levels for general public exposure to time-varying electric and magnetic fields.
Field strength at RFID operating frequency bands.

Frequency bands	E-field strength (V/m)	H-field strength (A/m)	B-field (μT)
125 kHz	87	5	6.25
HF (13.56 MHz)	28	0.073	0.092
UHF (950 MHz)	42	0.11	0.14
2.45 GHz	61	0.16	0.20

In this paper, in-vitro experiments to assess the electromagnetic field effects due to RFID reader/writers on both pacemakers and ICDs patients are discussed. First, test experiments to obtain EMI characteristics of pacemakers and ICDs are investigated. Combinations of 13 types of implantable devices and 10 types of commercially produced RFID reader/writers are tested using a newly developed test system. Secondly, to obtain the field strength for the estimation of EMI, radio waves from RFID reader/writer antennas are measured precisely. Finally, experimental results are introduced and characteristics of the EMI are discussed.

In vitro electromagnetic interference test experiments

To obtain EMI data and characteristics of RFID reader/writer antennas, test experiments on 10 types of commercially available antennas and 13 types of pacemakers and ICDs are carried out. Tested pacemakers and antennas are shown in Table 2 and Table 3. Pacemakers and ICDs have many operating modes and functions - pacing/sensing polarity, single/dual chamber mode, and antitachycardia functions. The total test mode is 768 modes at different function modes, frequency bands and RFID reader/writer antennas.

The test system is based upon the previously proposed one for the estimation of EMI due to mobile phones described in [2], [3], [5] and [10]. The system is also employed in EMI test experiments reported by Ministry of Internal Affairs and Communications (MIC) of Japan [8] and [9]. The test system consists of a flat human torso phantom, an electrocardiogram (ECG) signal generator/detector, a chart recorder, an oscilloscope, a measurement platform and a RFID reader/writer antenna as shown in Fig. 1, Fig. 2 and Fig. 3.

The torso phantom used in this experiment is some modifications of Irnich's model in the reference described above. Both atrial and ventricular electrode are improved which enables us to separate each chambers' ECG signal levels of more than 20dB. It is therefore taking advantage to examine EMI with low interference by another chambers' signal. In addition, the size of the phantom is slightly different. The tank of the phantom is made of acrylic material and filled with a saline solution (NaCl 1.8g/L). At low frequency, the saline solution provides same electric conductivity 0.2 S/m as human bodies. This means ECG signals between lead wire of a pacemaker and electrodes go through without direct connection. In addition, it is known this concentration of saline solution gives less attenuation constant than actual human body at radio frequency [5]. The torso phantom is suitable for the EMI test experiment, because it allows more conservative results for EMI estimations.

RFID systems are typically operated at the frequency bands - 125 kHz, HF (13.56 MHz), UHF (950 MHz) and 2.45 GHz, as shown in Table 3. Furthermore, these antennas usually have different shapes, locations and radiating fields depending on their purpose, operating frequency bands and their manufacturers. Moreover, positions between a human torso phantom and RFID reader/writer antennas must be determined precisely and be variable. It is required to measure the EMI due to various antennas with accuracy and repeatability. The two-axis sliding measurement platform shown in Fig. 2 enables us to measure RFID antennas moving parallel to the torso phantom (*y*-axis direction), while maintaining the same distance between the phantom and antennas (*x*-axis direction). All parts of this platform are made of dry wood. This system has advantages of high efficiency and data obtained can be reliability assessed.

The number of each RFID system is shown in Table 3. 125 kHz and HF band RFID systems employ amplitude-shift keying (ASK) as modulation method. HF band systems are also compliant with ISO/IEC15693 international standard [11]. In addition, modulation method of UHF band and 2.45 GHz RFID systems are double sideband (DSB) ASK or single sideband (SSB) ASK and frequency hopping spread spectrum (FHSS) or ASK, respectively. EPC Class 1 Generation 2 [12] for UHF band, ARIB STD-T81 [13] or RCR STD-1 [14] for 2.45 GHz are applied as specifications, respectively. In lower frequency bands such as 125 kHz and HF band, an inductive coupling between reader/writer antennas and tags realize their communications. On the other hand, the UHF band and 2.45 GHz systems use electromagnetic waves to communicate with each other. Owing to this dissimilarity, the test procedure introduced in the next section is different.

Table 2
Pacemakers and implantable cardioverter-defibrillators.

Tested devices	Type of chambers	Number of devices
Pacemaker	Single chamber	5
	Dual chamber	5
Implantable Cardioverter-Defibrillator	Single chamber	1
	Dual chamber	2
Total		13

Table 3
RFID reader/writer antennas.

Frequency bands	Modulation methods	Number of antennas
125 kHz	ASK	4
HF (13.56 MHz)	ASK	2
UHF (950 MHz)	DSB-ASK or SSB-ASK	2
2.45 GHz	FHSS or ASK	2
Total		10

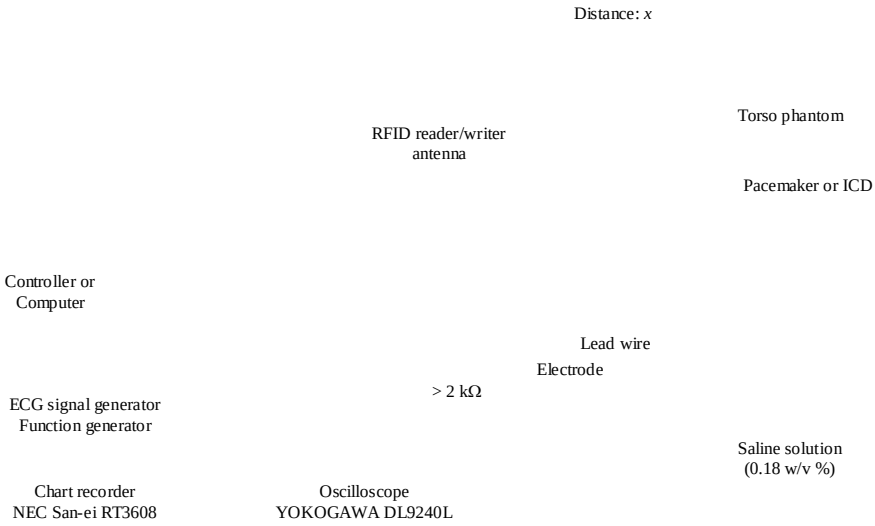


Fig. 1. Configuration of the test system.

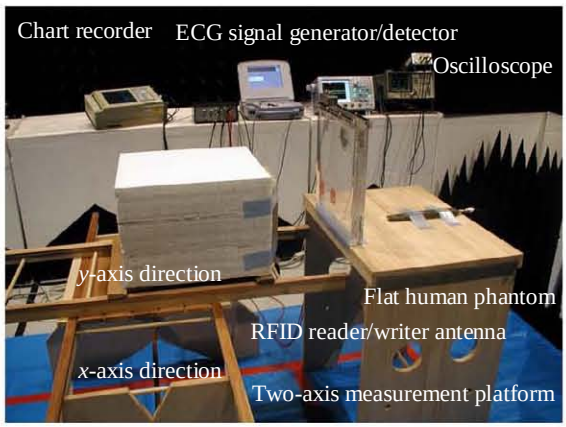


Fig. 2. Overall view of the in-vitro experimental system.

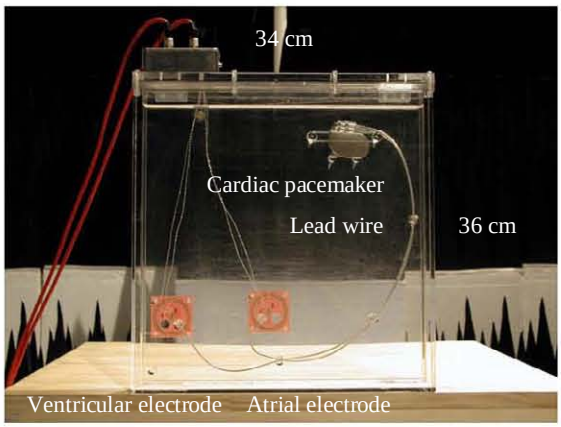


Fig. 3. The human torso phantom.

The in-vitro EMI test experiments procedure is explained as shown in Fig. 4. First of all, in order to obtain most conservative results, both sensitivity and refractory period of pacemakers and ICDs are programmed to maximum sensitivity and minimum time, respectively. Second, configurations of RFID reader/writers are prepared to actual operating mode. The next step depends on frequency bands of RFID reader/writer. EMI of 125 kHz and HF band are assumed to be caused by induced voltage, which follows Faraday's law of induction [4]. Malfunctions may happen when ”an inductor coil” composed of lead wire of pacemakers and ICDs receive changing magnetic field radiated from RFID reader/writer antennas. Because of this mechanism, interferences are examined while the phantom is exposed to changing magnetic field. Antennas are moving in *y*-axis direction (as shown in Fig. 2) and closely attached to the torso phantom. EMI of UHF band and 2.45 GHz band occurs due to direct coupling between antennas and terminals of pacemakers and ICDs [4]. Interference is investigated while the antenna is located at a fixed position and closely attached to the torso phantom.

Then, the ECG signal for each mode is recorded on the paper for 100 seconds. In addition, the distance between antennas and the torso phantom (*x*-axis direction in Fig. 3) is increased when interference occurs. In this case, the maximum interference distance (distance where EMI disappears) is found out and recorded in centimetres. As long as interference exists, sensitivity of pacemakers and ICDs are stepped down to five levels (maximum, 1.0 mV, 2.4 mV, 5.6 mV, minimum) and the maximum interference distance is also recorded. Breakdowns of the EMI test modes and settings are shown in Table 4.

Operating modes of pacemakers and ICDs are VVI mode (the Ventricle chamber is paced, the Ventricle chamber is sensed, and the response to sensing is Inhibited) and AAI mode (the Atrium chamber is paced, the Atrium chamber is sensed, and the response to sensing is Inhibited). In addition, unipolar and bipolar modes are chosen to their sensing/pacing polarity. For each of the operating modes, there are two types of EMI test modes are conducted - one with an injected ECG signal (typical inhibition), and one with no injected ECG signal (typical asynchronous pacing). With ICDs, there are two additional test modes. False Positive mode (one with no injected ECG signal and false detection of fibrillation), and False Negative mode (one with injected ECG signal and false non-detection of fibrillation) are investigated. The EMI test experiments are conducted in a closed, electromagnetic shielded anechoic chamber in Hokkaido University.

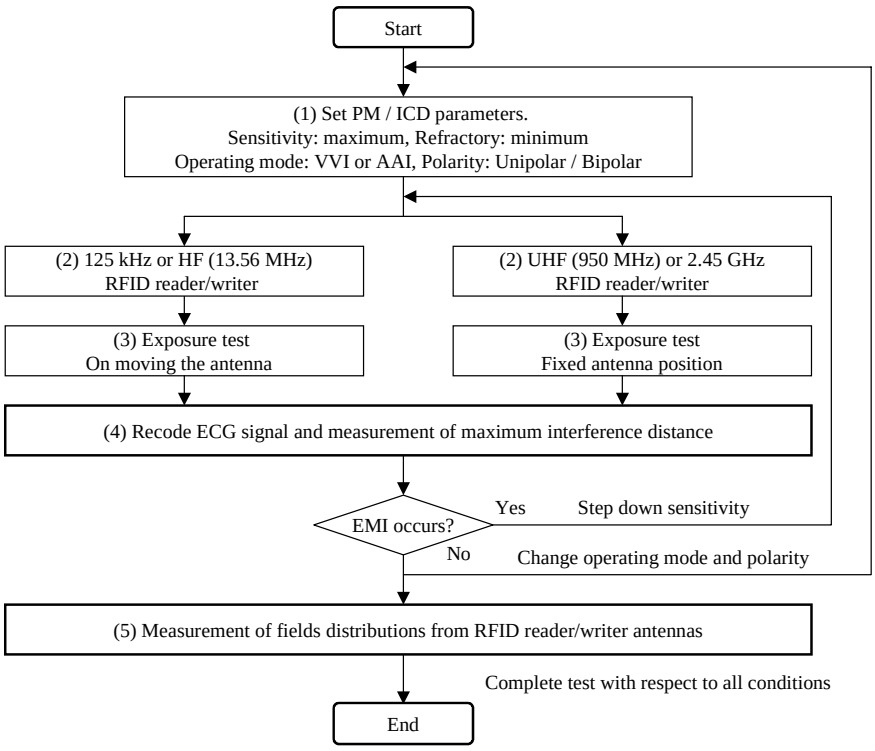


Fig. 4. In-vitro EMI test experiments procedure.

Table 4 EMI test modes and settings.

EMI test modes		Inhibit		Asynchronous		Inhibit		Asynchronous		False Positive	False Negative	Total Modes
PM/ICD Operating modes		VVI		VVI		AAI		AAI		AAI	AAI	
PM/ICD Sensing/Pacing Polarity		UNI	BI	UNI	BI	UNI	BI	UNI	BI	BI	BI	
RFID Reader/writer Frequency Bands	125 kHz	28	40	28	40	32	40	32	40	20	20	320
	HF (13.56 MHz)	14	20	14	20	16	20	16	20	10	10	160
	UHF (950 MHz)	16	20	16	20	12	12	12	12	4	4	128
	2.45 GHz	14	20	14	20	16	20	16	20	10	10	160
Total modes		72	100	72	100	76	92	76	92	44	44	768

PM: Pacemaker, ICD: Implantable cardioverter-defibrillator

UNI: Unipolar, BI: Bipolar

Finally, measurements of field distributions described in the next section are carried out. The measurement area is determined based on the experimental results. In order to find out the correlation between obtained EMI data and field strength, precise measurement is required.

Field distribution measurements of RFID reader/writer

To obtain detailed data to clear up correlations between EMI and EMF strength, field distributions of RFID reader/writers antennas are measured. Both electric and magnetic fields are determined for all RFID reader/writers antennas shown in Table 3. The reason for this is a near field of the antennas is not proportioned to each other. For 125 kHz and HF band, measurement of 729 sample points which include 70 cm × 70 cm × 70 cm (width × height × depth) at 10 cm separation are carried out. In addition to this wide area measurement, we examined more fine separation for the depth direction (*x*-axis direction in Fig. 2). We measure 1029 sample points which include 70 cm × 70 cm × 20 cm (width × height × depth) at 1 cm separation for the depth direction. Figure 6 shows the probe positioners for low frequency bands, which is made of styrene foam. This positioner enables reliable measurement taking the advantages of low reflection or absorption of EMF. Electric field probe EMR-300 (Wandel & Goltermann GmbH, Germany) and magnetic field probe 11941A (Agilent technologies Inc., Palo Alto, CA, USA) are used. For the UHF band and 2.45 GHz, measurements of 3459 sample points are also performed. These measurements include the area of 36 cm × 36 cm × 20 cm (width × height × depth) at 3 cm separation for the width and height direction and at 1cm separation for the depth direction. Electric field probe IXP-050 (IndexSAR Ltd., Newdigate, England) and magnetic field probe 7405-903 (ETS-Lindgren, Cedar Park, TX, USA) are employed.

Figure 6 is a typical 3-dimensional magnetic field radiated from a HF band antenna. In addition, differences of field strength radiated from 4 types of 125 KHz antennas are shown in Fig. 7. This figure indicates 1-dimensitonal magnetic field strengths at the central axis of the antennas. Values of *y*-axis are normalized to the maximum field strength out of 4 types of antennas.

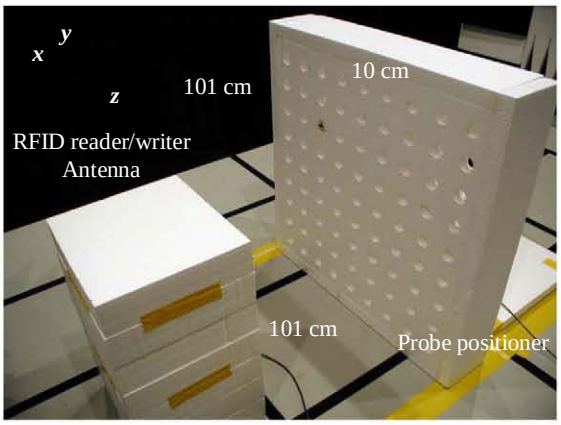


Fig. 5. The probe positioner for low frequency bands. 125 KHz and HF band.

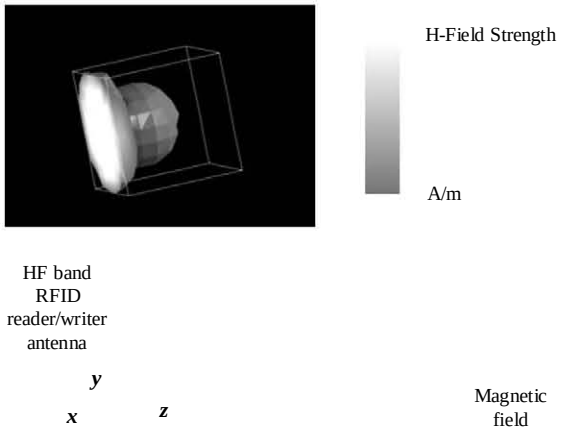


Fig. 6. Typical 3-dimensional magnetic field distribution from a HF band antenna.

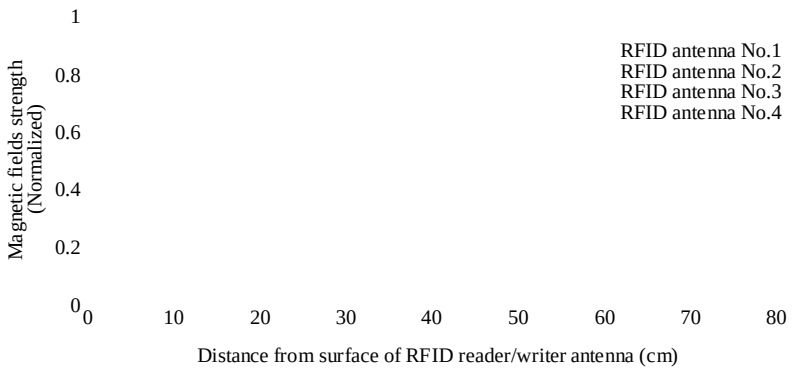


Fig. 7. 1-dimensional magnetic field distributions of 125 KHz RFID reader/writer antennas. Magnetic field strength on the central axis of antennas.

Results & Discussions

First, results of the EMI test experiments are discussed. A total of 768 test modes are used in the experiments. As shown in Fig. 8, 107 modes are affected when pacemakers and ICDs are programmed to maximum sensitivity. Therefore the affected rate is about 14 %. Under these conditions, the maximum interference distance is 15cm. In addition, when the sensitivity is stepped down to minimum sensitivity, the affected mode and rate are 26 modes and about 3 %, respectively. The maximum interference distance of this sensitivity is 11 cm. From this EMI test experiment, when the radio wave from antennas are continuous wave or do not have time-varying envelope curve, no malfunctions happen on pacemakers and ICDs. On the other hand, if they are exposed to changing fields such as pulse modulated wave or changing magnetic field due to movement of antennas, probability of the EMI occurrence is much higher than another condition.

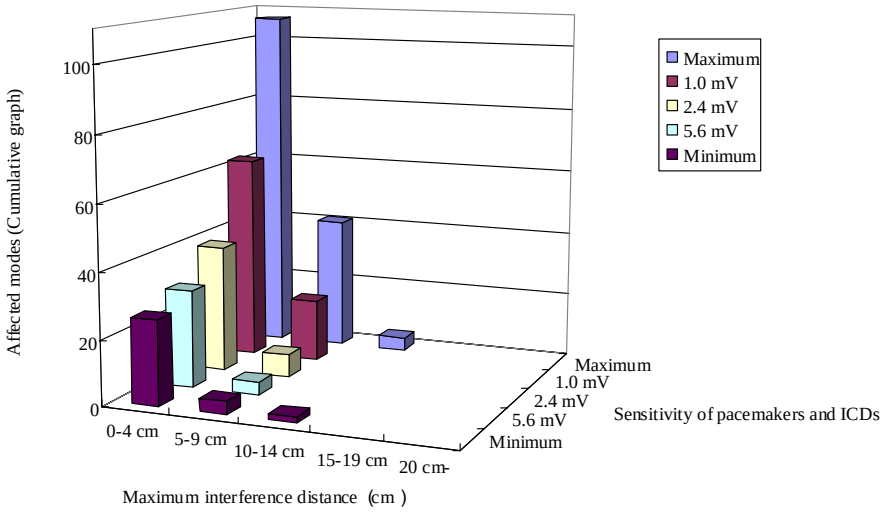


Fig. 8. The results of in-vitro EMI experiments.
Affected modes (Cumulative) and maximum interference distance
depending on sensitivity of pacemakers and ICDs.

Summary

In this paper, to assess the EMF fields' exposure effect from RFID reader/writer antennas, field strengths which cause effects for these implantable devices operations were examined from experimental and measured results. First, EMI due to commercially available RFID reader/writers on pacemakers and ICDs were investigated using newly constructed in-vitro experimental test system. This system was based upon an Irnich's flat torso phantom. In vitro EMI test experiments on 10 types of RFID reader/writers and 13 types of implantable pacemakers and defibrillators were conducted. The frequency bands were 125 kHz, HF (13.56 MHz), UHF (950 MHz) and 2.45 GHz. Secondly, EMF distributions of RFID reader/writer antennas were measured in detail. Finally, results of EMI test experiments were introduced and characteristics of interferences were discussed.

The correlation between the EMI test experiments results and field strength radiated from RFID reader/writers are now being investigated in detail. Further results and discussions are shown in later.

Acknowledgement

The authors would like to thank the members of the Pacemaker Committee of Japan and Japan Automatic Identification Systems Association for their cooperation and support.

References

[1] International Commission on Non-Ionizing Radiation Protection (ICNIRP), "Guidelines for limiting exposure to time-varying electric, magnetic and electromagnetic fields (up to 300 GHz)," Health Phys., vol.74, pp.494-522, 1998.

[2] W. Irnich, L. Batz, R. Muller, and R. Tobisch, "Electromagnetic interference of pacemaker by mobile phones," PACE, vol. 19, pp.1431-1446, Oct. 1996.

[3] V. Barbaro, P. Bartolini, A. Donato, and C. Militello, "Electromagnetic interference of analog cellular telephone with pacemakers," PACE, vol. 19, pp. 1410-1418, Oct. 1996.

[4] T. Toyoshima, M. Tsumura, T. Nojima, and Y. Tarusawa, "Electromagnetic interference of implantable cardiac pacemakers by portable telephones," Japanese journal of cardiac pacing and electrophysiology, vol. 12, no.5, pp. 488-497, 1996.

[5] Y. Tarusawa, K. Ohshita, Y. Suzuki, T. Nojima, and T. Toyoshima, "Experimental estimation of EMI from

cellular base-station antennas on implantable cardiac pacemakers," IEEE Trans. Electromagn. Compat., vol. 47, no. 4, pp.938-950, Nov. 2005.
[6] T. Nojima, and Y. Tarusawa, "A new EMI test method for electronic medical devices exposed to mobile radio wave," IEICE trans. Commun., vol.E88-B, no.1, pp. 11-18, Jan. 2001.
[7] Guidelines on the use of radio communication equipment such as cellular telephones - Safeguards for electric medical equipment, presented at the EMC Conf. Japan, Electromagnetic Medical Equipment Study Group, 1997.
[8] Investigation and research report of electromagnetic interference on medical devices (in Japanese), Ministry of Internal Affairs and Communications (MIC) of Japan, Mar. 2005.
[9] Investigation and research report of electromagnetic interference on medical devices (in Japanese), Ministry of Internal Affairs and Communications (MIC) of Japan, Mar. 2004.
[10] Active Implantable Medical Device - Electromagnetic Compatibility - EMC Test Protocols for Implantable Cardiac Pacemakers and Implantable Defibrillators, AAMI Standard PC69, 1999.
[11] ISO/IEC15693: Identification cards - Contactless integrated circuit(s) cards - Vicinity cards - Part1 : Physical characteristics, International Organization for Standardization, 2000.
[12] EPC Radio-Frequency Identity Protocols Class-1 Generation-2 UHF RFID Protocol for Communications at 860 MHz-960 MHz, Version 1.0.9., EPCglobal, Inc., 2005.
[13] Standard ARIB STD-T81: 2.4GHz-Band RFID Equipment Using Frequency Hopping System for Specified Low Power Radio Station, Association of Radio Industries and Businesses, Japan, 2006.
[14] Standard RCR STD-1: 2.4GHz-Band RFID Equipment for Premises Radio Station, Association of Radio Industries and Businesses, Japan, 2006.

7 HZ ELECTROTHERAPY FOR THE TREATMENT OF SKIN UNDIFFERENTIATED DESEASES

ALBERTO FOLETTI M.D.[1] MARIO LEDDA[2] , EMANUELA ROSOLA[2] , ANTONELLA LISI[2], ENRICO D' EMILIA[4] , SETTIMIO GRIMALDI [2],

[1]Quantech – Milan, Italy
[2]Istituto di Neurobiologia e Medicina Molecolare CNR –Rome, Italy
[4]ISPESL DIPIA Rome Italy

Corresponding Author:
Settimio Grimaldi
Istituto di Neurobiologia e Medicina Molecolare–Consiglio Nazionale delle Ricerche
Via Fosso del Cavaliere 100, 00133 Rome, Italy
Phone 39 06 49934230; Fax 39 0649934231
E-Mail settimio.grimaldi@artov.inmm.cnr.it

Running Title: Effect of electric field on keratinocytes

Key words: NIR, growth differentiation, keratinocytes.

Abstract

Electrotherapy is a treatment method in which an electric stimulus is used to achieve physiological changes in the body.
The specific aim of the present work concerns the effectiveness of low frequency electric fields treatment to modify biochemical properties of human keratinocytes (HaCaT).
Cells exposed to a 7 Hz electric field for one hour (twice daily), showed by Scanning Microscopy modification in shape and morphology; these modifications were also associated to different actin distribution revealed by phalloidin fluorescence analysis.
Indirect immunofluorescence with fluorescent antibodies against involucrin and β catenin, both differentiation and adhesion markers, revealed an increase in involucrin and β catenin expression, supporting that exposure to electric field carries keratinocytes to an upper differentiation level.
Such study confirmed our previous observation and support the hypothesis that 7 Hz electric field, may modify cell biochemistry and interfere in differentiation and cellular adhesion of normal keratinocytes.

INTRODUCTION

In the last twenty years there has been an increasing interest to investigate the possible effect of extremely low frequency (ELF) electric and magnetic fields (Chiabreara 1985, Zhadin 2001) on human health. The experimental approach to the electromagnetic field (EMF) effects on living systems is complicated by various reported non linearities (intensity, frequency and time windows of the fields) and peculiarities (cell type, age, treatment) so that extrapolation or replications among laboratories can hardly be made. The possible mechanisms of the induced effects are still not known, although a number of theoretical models have been proposed (Glaser 1992, Liburdy 1992, Barnes 1996,). This may be partially due to the difficulties in demonstrating reproducible results.
The aim of the present work is to clarify the action's mechanism at cellular level of an electrotherapy procedure performed by an electro-medical device still in clinical use and so easily reproducible in each bio-physical setting like frequency, intensity and exposure's time.
Moreover a second aim of this work is to validate the effectiveness of the current clinical application protocols.
This work concerns the effect of 7 Hz electric field exposure on morphological and biochemical properties of normal human keratinocytes.